DISSERTATION ZUR ERLANGUNG DES DOKTORGRADES
DER FAKULTÄT FÜR CHEMIE UND PHARMAZIE
DER LUDWIG-MAXIMILIANS-UNIVERSITÄT MÜNCHEN

SYNTHESIS AND CHARACTERIZATION OF NEW POLYNITRO COMPOUNDS AND AQUATIC TOXICITY DETERMINATION OF ENERGETIC MATERIALS

Regina Scharf

aus Weilheim i. Obb., Deutschland

2016

ERKLÄRUNG

Diese Dissertation wurde im Sinne von § 7 der Promotionsordnung vom 28. November 2011 von Herrn Prof. Dr. Thomas M. Klapötke betreut.

EIDESSTATTLICHE VERSICHERUNG

Diese Dissertation wurde eigenständig und ohne unerlaubte Hilfe erarbeitet.

München, den 10. November 2016

_____

Regina Scharf

Dissertation eingereicht am

1. Gutachter:	Prof. Dr. Thomas M. Klapötke
2. Gutachter:	Prof. Dr. Konstantin Karaghiosoff
Mündliche Prüfung am	11.10.2016

Für meine Familie

und im Gedenken
an meine Tante
Dr. Anita Schummer
* 17.7.1962
† 25.12.2011

DANKSAGUNG

Zuallererst möchte ich meinem Doktorvater Herrn Prof. Dr. Thomas M. KLAPÖTKE für die tollen, aufregenden und interessanten Jahre danken, die ich in seinem Arbeitskreis verbringen durfte. Danke auch für die interessante Themenstellung, die finanzielle Unterstützung und das uneingeschränkte Vertrauen, das mir entgegengebracht wurde.

Desweiteren gilt mein Dank Herrn Prof. Dr. Konstantin KARAGHIOSOFF für die Übernahme des Zweitgutachtens dieser Dissertation und seiner Unterstützung bei der Auswertung zahlreicher NMR Spektren. Dankeschön auch für den unerschütterlichen Optimismus und die Anekdoten, die an manchen Tagen den Arbeitsalltag aufgelockert haben.

Der Prüfungskommission, bestehend aus Herrn Prof. Dr. Thomas M. KLAPÖTKE, Herrn Prof. Dr. Konstantin KARAGHIOSOFF, Herrn Prof. Dr. Franz BRACHER, Herrn Prof. Dr. Andreas KORNATH, Herrn Prof. Dr. em. Wolfgang BECK und Herrn Prof. Dr. Ingo-Peter LORENZ möchte ich für die Zeit und die Bereitschaft danken sich in dieser zur Verfügung zu stellen.

Ebenfalls danken möchte ich Herrn Dr. Burkhard KRUMM für das schnelle und problemlose Messen von empfindlichen NMR Proben sowie für die Hilfe bei der Auswertung von kniffligen NMR Spektren. Des weiteren möchte ich für die zeitnahe und akribische Korrektur sämtlicher Schriftstücke danken.

Ein großes Dankeschön gebührt auch Herrn Dr. Jörg STIERTORFER, der mir in den letzten Jahren immer wieder mit zahlreichen Ideen und Ratschlägen zur Seite gestanden hat. Auch seine aufmunternde Art und seine teambildenden Maßnahmen im Arbeitskreis, insbesondere die Kochrunde, sollten hierbei erwähnt werden.

Unserer guten Seele im Arbeitskreis, Frau Irene SCHECKENBACH, möchte ich für ihr Organisationstalent und ihre Unterstützung bei allen bürokratischen Angelegenheiten, sowie für die netten und unterhaltsamen Gespräche danken.

Dem gesamten Arbeitskreis möchte ich danken für die stets positive und freundschaftliche Arbeitsatmosphäre. Besonderer Dank gilt dabei meinen Laborkollegen aus D3.100, Dr. Quirin AXTHAMMER, Dr. Richard MOLL, Dr. Carolin PFLÜGER, Dr. Sebastian REST, Dr. Michael WEYRAUTHER als auch den Masterantinnen Cornelia UNGER und Anna WIDERA für die fachlichen und weltanschaulichen Diskussionen sowie für die Motivation, die an manchen Tagen notwendig war, um weiter zu machen.

Im Besonderen möchte ich mich für die tolle Zusammenarbeit und für die Korrekturen dieser Arbeit bei Dr. Quirin AXTHAMMER und Dr. Caronlin PFLÜGER bedanken.

Mein Dank gilt auch dem gesamten X-ray Team, das über die Jahre etliche Kristalle von mir vermessen hat, insbesonder Prof. Dr. Konstantin KARAGHIOSOFF, Dr. Quirin AXTHAMMER, Dr. Alexander DIPPOLD, Dr. Carolin PFLÜGER, Thomas REITH und Norbert SZIMHARDT. Ein besonderer Dank gebührt zudem Dr. Quirin AXTHAMMER für das anschließende Lösen der Kristallstrukturen und die Geduld, auch mir dieses näher zu bringen.

Stefan Huber möchte ich für die unterhaltsamen Stunden danken, die wir gemeinsam bei der Bestimmung der Sensitivitäten verbracht haben.

Ich möchte mich auch bei all meinen Praktikanten bedanken, die durch ihr Engagement und Tatkraft einen erheblichen Beitrag zu dieser Arbeit geleistet haben.

Und nicht zuletzt möchte ich mich bei meiner gesamten Familie, insbesondere bei meinen Eltern FRANZ und ROSMARIE, meinen beiden großartigen Schwestern VERONIKA und ELISABETH und meinem Partner CHRISTIAN (Knuwe), bedanken, die mir während all der Jahre ihre Liebe und unermessliche Unterstützung gegeben und in den richtigen Momenten für den Rückhalt und die notwendige Ablenkung gesorgt haben. Vielen Dank!

TABLE OF CONTENTS

LIST OF SCHEMES

LIST OF FIGURES

LIST OF TABLES

I General Introduction

1 Classification of High-Energy Dense Materials

The term high-energy dense material (HEDM) is coined by the explosives community to describe substances which can attain a high energetic state.[1] In general, HEMs are defined as compounds or mixtures which contain both oxidizer and fuel in a metastable state and deliver their energy by chemical reactions under release of large amounts of gaseous products.[1,2]

The first known energetic material, blackpowder, was accidentally discovered by the Chinese around 200 BC. Blackpowder consists of a mixture of charcoal, sulfur and potassium nitrate and was used as explosive, propellant and in pyrotechnical mixtures in China. However, it took until the 13th to 14th century until blackpowder was finally used for military purposes in Europe.[1,2] A huge progress in the history of explosives was the synthesis of nitroglycerine (NG) by Ascanio Sobrero (1846) and its commercial production invented by Alfred Nobel and his father in 1863.[2] NG was the first compound which combines oxidizer and fuel in just one molecule. This was also the beginning of an enormous growth in the field of HEMs.

Nowadays high-energy dense materials are categorized in three huge classes according to their use: explosives, propellants, and pyrotechnics. Explosives are further subdivided into primary and secondary explosives (Scheme I1.1). Primary explosives are defined as compounds with a very fast transition from combustion or deflagration to detonation

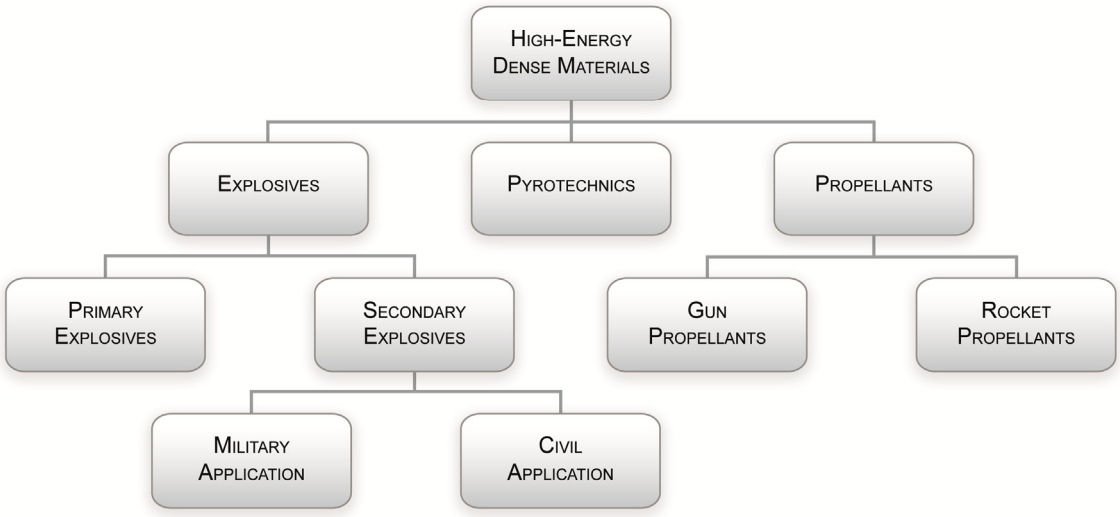

Scheme I1.1 Schematic classification of energetic materials based on their use.

whereupon either a large amount of heat is released or a shock wave is generated which in turn initiates the secondary explosive.[2] In general, primary explosives are very sensitive to impact, friction and heat albeit their sensitivities should be within a useful limit to ensure safe handling and transportation.[3] Until now the most prominent representatives of primary explosives are still mercury fulminate ($Hg(CNO)_2$), lead azide ($Pb(N_3)_2$) and lead styphnate ($Pb(C_6HN_3O_8)$) although activities are driven to develop heavy-metal free replacements.[4]

In contrast to primary explosives, secondary explosives are less sensitive to mechanical stimuli and heat and therefore have to be ignited by the detonation impact of a primary explosive. Secondary explosives are also known as 'high explosives' since performance data like detonation velocity, detonation pressure and heat of explosion are significantly increased compared to primary explosives. According to their application they are grouped in military and civil used secondary explosives. In the 19th century and during World War I and II mainly the high explosives 2,4,6-trinitrotoluene (TNT), pentaerythritol tetranitrate (PETN) and hexogene (RDX) were utilized (Figure I1.1).[2] RDX was developed in 1898 by Georg Friedrich Henning for medical reasons since nitrate esters were known to have vasodilatory effects. It took more than 20 years until RDX was also intensely investigated as military explosive.[5] Nowadays, due to sensitivity issues TNT and PETN are mainly replaced by octogen (HMX) and RDX, which is still used as explosive for military purposes. For civil applications like mining and blasting less sensitive, high thermally stable explosives with a huge blasting power are needed. Nitroglycerin (NG) (Figure I1.2) and hexanitrostilben

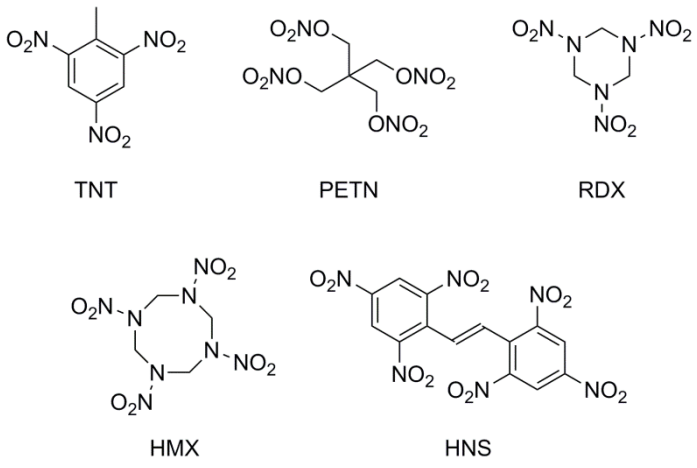

Figure I1.1 Molecular structures of 2,4,6-trinitrotoluene (TNT), pentaerythritol tetranitrate (PETN), hexogene (RDX), octogene (HMX), and hexanitrostilben (HNS).

(HNS) (Figure I1.1) are one of the prominent representatives of this class. To reduce the sensitivity of NG, Alfred Nobel developed a mixture containing three parts NG and one part kieselgur which is still known as dynamite.[2]

Pyrotechnics form the second class of HEMs. In general pyrotechnical compositions are mixtures which contain oxidizer and fuel, as well as an additive. These additives are added to emit bright or colored light, evolve heat or fog or even produce an acoustical signal like howling, whistling and banging.[6] The effects are triggered by non-detonative self-sustaining exothermic reactions. The application of pyrotechnical compositions range from pyrotechnic mixtures in blasting caps or detonators, smoke munitions for military purposes, signal flares to mark specific positions to fireworks. Typical pyrotechnical compositions contain potassium perchlorate or barium chromate as oxidizer and carbon, silicon, boron or a metal like manganese or tungsten as fuel.[2]

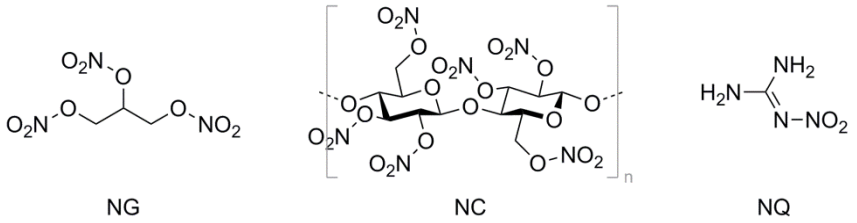

Figure I1.2 Molecular structures of nitroglycerin (NG), nitrocellulose (NC), and nitroguanidine (NQ).

Propellants form the last group in the classification of HEMs. Characteristic for propellants is their controlled and smooth combustion behavior. Unlike explosives propellants do not detonate. During combustion large amounts of hot gases are formed which in turn are used to accelerate projectiles, missiles or rockets. According to their use propellants are distinguished into gun and rocket propellants. The main differences between these two propellants are the increased burning rates and therefore higher pressures generated in the combustion chamber or gun barrel of gun propellants. While gun propellants generate pressures up to 4000 bar in the combustion chamber rocket propellants only reach pressures of 70 bar.[2] Gun propellants are further divided into single-, double- and triple-base propellants. Single-base propellants mainly are comprised of nitrocellulose (NC) and are used in weapons from pistols to artillery weapons. In double-base powders NG and NC are contained in a 1:1 mixture while in triple-base propellants NG, NC and nitroguanidine (NQ) are the major ingredients (Figure I1.2). Allthough triple-base powders show a decreased performance compared to single and double-base powders they are used in large calibre tank and NAVY weapons to prevent erosion and the muzzle flash.[2,7]

2 ROCKET PROPELLANTS

In the last century many efforts have been undertaken to find an ideal propellant for space application. In the beginning of the 20th century the first rocket propellant suggested was a mixture of liquid hydrogen and liquid oxygen but liquid hydrogen was hardly to handle at that time. Therefore, an alternative for liquid hydrogen had to be found like gasoline or methane. After some years of experimental work also liquid oxygen was substituted by dinitrogen tetroxide (N_2O_4) and red fuming nitric acid (RFNA).[8]

Today's propellants are divided in solid and liquid propellants (Scheme I2.1). Liquid propellants are further classified in monopropellants and bipropellants. Monopropellants are mostly liquids consisting of only one compound including both fuel (reducing agent) and oxidizer.[9] When contacted with a catalyst (e.g. shell-405, Ir/Al_2O_3)[10] they react spontaneously. Hot gasses are generated which are used in turn for propulsion. However, since the specific impulses of monopropellants are rather low they are mainly used in small missiles and small satellites.[2] The most commonly used monopropellant nowadays is hydrazine (N_2H_4)[11] although there are many disadvantages like high toxicity and carcinogenicity which in combination with its high vapor pressure, make handling and storage of hydrazine very expensive.[12] Hydrazine and its derivatives like monomethylhydrazine and unsymmetrical dimethylhydrazine are also used as reducing agents in bipropellants. A bipropellant consists of two separately stored liquids, a fuel and an oxidizer, which react hypergolic when contacted with each other. Although these systems are very complex their advantages are their ability to restart as well as their good controllability and high thrusts.[2]

Solid propellants can further be grouped in double-based solid propellants (homogeneous) and composite propellants (heterogeneous).[2] Double-based solid

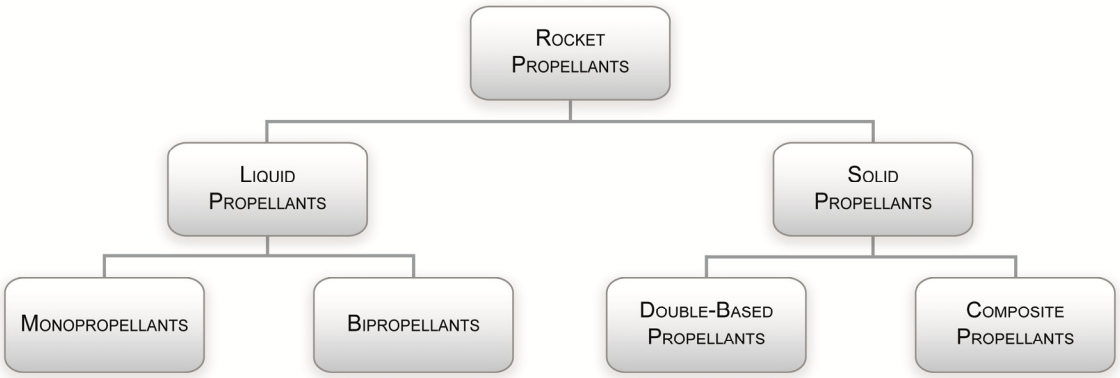

Scheme I2.1 Classification of rocket propellants.

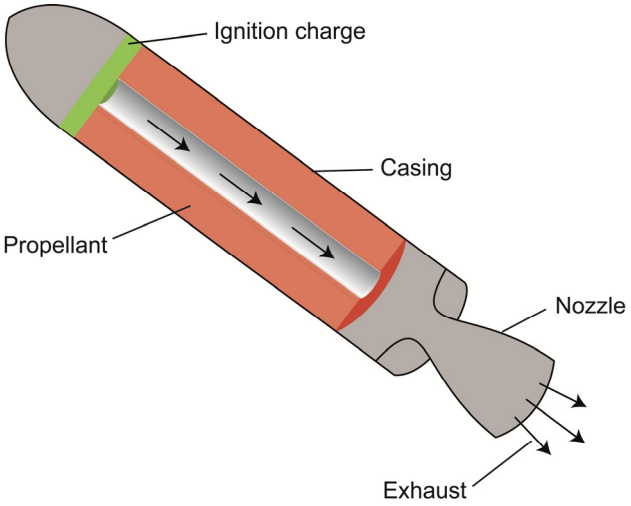

Figure I2.1 Schematic view of a solid propellant rocket engine.

propellants mainly consist of formulations of nitrocellulose and nitroglycerin[13] while composite propellants comprise of an oxidizer, a fuel and an energetic binder and are used in missiles and launch vehicles.[14]

Figure I2.1 shows the schematic setup of a solid propellant rocket engine. The propellant is ignited by the ignition charge whereupon large quantities of rapidly expanding hot gases are produced which eject at high speed through the small opening of the nozzle. According to Newton's third law a thrust is generated in the opposite direction which accelerates the rocket.

For composite propellants almost exclusively ammonium perchlorate (AP) is used as oxidizer while aluminum is the fuel. To increase the mechanical properties of such

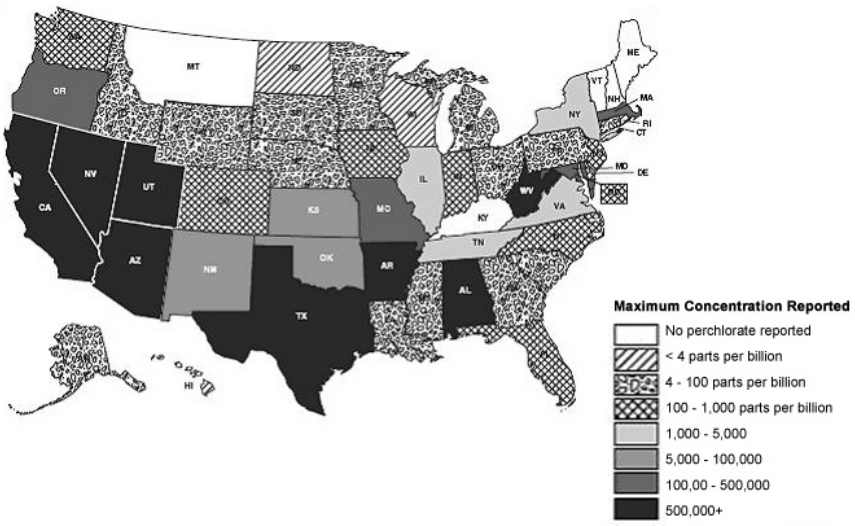

Figure I2.2 Maximum concentrations of the perchlorate anion reported in the US in the ground-water systems.

Figure I2.3 Accidental explosion of AP at PEPCON plant, Henderson, Nevada in 1988 (left). Exhausted hydrochloric acid at the launch of a Scout launch vehicle (right).[15]

composite propellants a binder, mainly hydroxy-terminated polybutadiene (HTPB), is added. The use of AP as oxidizer offers several advantages. AP has a high oxygen balance of +34%, it is completely convertible to gaseous products and stable against mechanical stimuli. Furthermore, the synthesis of AP is convenient by simply reacting ammonia and perchloric acid[16] and it has well known properties with respect to its compatibility and reliability.

However, there are also disadvantages which make it necessary to replace AP. One of the main drawbacks is the environmental concern of AP. AP leaching from discarded motors or repositories seeps into ground-water and contaminates, due to its high solubility and chemical stability, the surface and ground-water systems as shown in Figure I2.2 for the US. Furthermore, mishandling of AP leads to explosions like those in Henderson, Nevada, in 1988 where more than 4.000 t AP spontaneously decomposed (Figure I2.3, left).[17] Additionally to the ground-based impacts there are also atmospheric impacts which have to be considered. Large amounts of toxic hydrogen chloride gases are generated during the combustion of AP which are ejected to the atmosphere and provoke climate change and ozone destruction. The exhausted hydrogen chloride gases also leads to a tactical disadvantage since in the presence of water hydrochloric acid is formed which is easily visible in the atmosphere and reveals the launch position of the missile (Figure I2.3, right).[2,18]

The toxicological effect of AP on the growth and development of vertebrates has to be also considered. Since the diameter of the perchlorate ion is similar to the diameter of the iodide ion it acts as competitive inhibitor of the thyroid gland. As depicted in Scheme I2.2 the iodide uptake is reduced which in turn influences the thyroid's ability to produce hormones and especially affects expectant mothers, fetus and infants.[19]

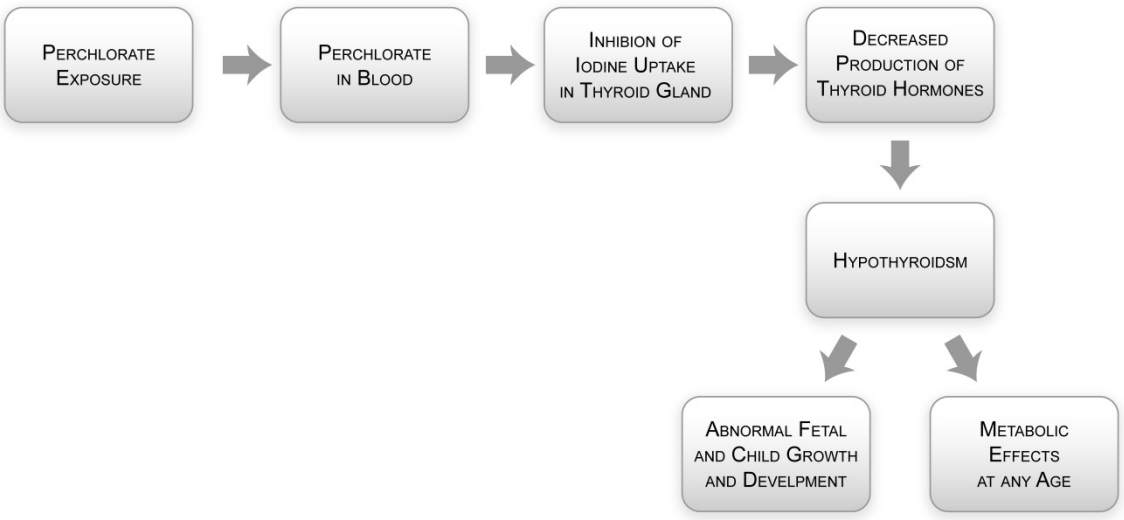

Scheme I2.2 Mode of action of perchlorate in vertebrates.

There are also physical aspects which would suggest searching for an alternative for AP. At temperatures about 150 °C low-temperature thermal decomposition occurs while high-temperature decomposition takes place at temperatures above 300 °C.[20] Moreover, slow cook-off tests showed a decomposition of AP and the formation of acidic side-products, which in turn react with the binder system and causes cracks and cavities in the composite. These leads to variable burning behavior and consequently decrease the performance of the composite propellant.

To overcome these problems AP has to be replaced. This would also reduce the costs and risks associated with transport, storage and cleanup of accidentally released AP.[21] Particularly the costs for ground-water remediation are estimated to be several billion dollars only in the US.[2]

3 High-Energy Dense Oxidizers

Since 1995 much effort has been carried out in order to find an alternative for AP in solid rocket compositions. However, until now there is no substitute with better or comparable properties. For new high-energy dense oxidizers (HEDOs) several requirements have to be fulfilled which are as follows:[2,22]

- high oxygen content (Ω_{CO} > 25%)
- high thermal stability, at least 150 °C
- high density, best close to 2 g cm^{-3}
- sensitivities like PETN (IS 4 J, FS 80 N) or better
- low vapor pressure

- compatibility with fuel and binder
- specific impulse comparable to AP (I_s > 250 s)
- convenient synthesis with minimum number of synthesis steps

For compounds with the empirical formula $C_aH_bN_cO_d$ the oxygen balance Ω assuming the formation of CO_2 is calculated with the following equation[2]

$$\Omega_{CO_2} = \frac{\left[d-(2a)-\left(\frac{b}{2}\right)\right]\times 1600}{M} \quad (1)$$

At higher temperatures CO is formed instead of CO_2 according to the Boudouard equilibrium. The oxygen balance Ω assuming the formation of CO is calculated with the equation

$$\Omega_{CO} = \frac{\left[d-a-\left(\frac{b}{2}\right)\right]\times 1600}{M} \quad (2)$$

whereupon M is the molecular weight of the compound.

The specific impulse I_s is the change in the impulse per mass unit of the propellant in a specified time and is expressed by the formula

$$I_s = \sqrt{\frac{2\,y\,T_c}{(y-1)M}} \quad (3)$$

whereby y is the ratio of the specific heat capacities, R is the gas constant, T_c is the temperature in the combustion chamber and M is the average molecular mass of the formed combustion gases.[2] Typical specific impulses for solid rocket compositions are around 250 s while bipropellants can achieve values of approximately 450 s. For high specific impulses a high temperature in the combustion chamber is important. However, satisfying specific impulses can also be achieved for lower temperatures in the combustion chamber if the average molecular mass of the combustion products is sufficiently low. In this context it is also important to know that an increase of the specific impulse of 20 s would approximately double the maximum payload.[2]

At the moment the currently most promising replacements are phase stabilized ammonium nitrate (AN) and ammonium dinitramide (ADN) (Figure I3.1). Unlike AP, both compounds are halogen-free and therefore produce completely eco-friendly smokeless combustion products. However, their use as propellants in solid rocket compositions is restricted due to several adverse properties. AN suffers from its hygroscopicity, its phase transitions near room temperature which involves also a volume change as well as its low burning rate while ADN already starts to decompose after complete melting at 92 °C.[23]

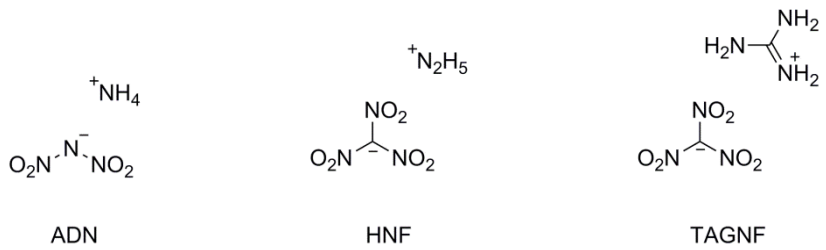

Figure I3.1 Molecular structures of ammonium dinitramide (ADN), hydrazinium nitroformate (HNF) and triaminoguanidinium nitroformate (TAGNF).

The nitroform salts hydrazinium nitroformate (HNF) and triaminoguanidinium nitroformate (TAGNF), as depicted in Figure I3.1, also appear to be promising replacements for AP and therefore are examined thoroughly. Especially HNF show suitable properties as propellant oxidizer with an increased performance compared to commonly used propellants.[24] But similar as before, the application of HNF an TAGNF is also limited by their low thermal stabilities of 128 °C (HNF) and 105 °C (TAGNF) as well as their high sensitivities towards impact and friction.[24,25]

These facts show that further research is absolutely necessary in order to find a suitable replacement for AP.

4 OBJECTIVES

The aim of this thesis is the synthesis and characterization of new environmentally benign molecules which contain a high amount of oxygen. The intention is to use these oxygen-rich compounds as oxidizer in composite propellants in order to replace the common oxidizer ammonium perchlorate (see Chapter 1.2). With regard to their possible future application as high-energy dense oxidizers (HEDOs) they have to achieve several requirements concerning their chemical, physical and energetic properties. To reduce their environmental impact mainly neutral, less water-soluble molecules are investigated instead of salts.

Suitable precursors and building blocks were used to create molecules with a high oxygen content. A general concept of this work is the insertion of moieties containing the trinitromethyl $C(NO_2)_3$ or fluorodinitromethyl $CF(NO_2)_2$ functionalities to various compounds (Figure I4.1). Particularly the 2,2,2-trinitroethyl unit is one of the most

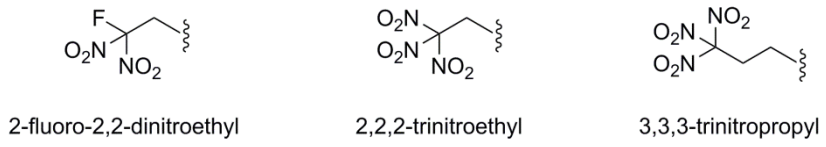

Figure I4.1 Molecular structures of several oxygen-rich moieties.

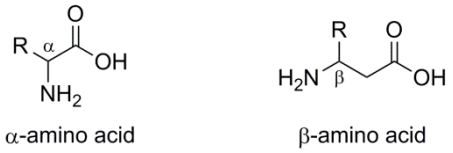

Figure I4.2 Molecular structures of α- and β-amino acids.

important moieties which is frequently introduced to enhance the oxygen content. But also the 3,3,3- trinitropropyl unit is investigated mainly with the aim to increase the stability in comparison to the 2,2,2-trinitroethyl unit.

Amino acids play a crucial role for living organism. They contain an amino group ($-NH_2$), a carboxylic acid (–COOH), and a side-chain R, which is specific for each amino acid. About 500 different proteinogenic and non-proteinogenic amino acids are known each having a particular role in biosynthesis or in processes such as neurotransmitter transport. Due to their nonhazardous character, numerous functionalities and convenient acquisition different α- and β-amino acids (Figure I4.2) are examined as possible starting materials for the synthesis of oxygen-rich compounds.

Since intra- and intermolecular interactions especially between the polynitro moieties influence the chemical and energetic properties of the molecules these are investigated and discussed. Additionally, their physical properties concerning their thermal stabilities and sensitivities towards external stimuli are examined and for future application as HEDO their energetic properties are determined.

An important topic of this work is also the toxicity determination of several known as well as new energetic materials including primary and secondary explosives as well as oxygen-rich compounds by using the luminescent bacteria inhibition test. Since commonly used explosives have shown to be toxic for human, animal or other organisms researchers all over the world try to find alternatives to replace them. The luminescent bacteria inhibition test offers a convenient possibility to compare the toxicity of known and new energetic materials and preliminary estimate their influence on environment. As model organism the marine bacteria *Vibrio fischeri* are used which exhibit a natural bioluminescence. During the toxicity tests of energetic materials the decrease of luminescence is measured and compared to a nontoxic control. The effective concentration is determined at which the luminescence is reduced by half (EC_{50}).

The main part of this thesis is the III RESULTS AND DISCUSSION section which consists of eight chapters. Each chapter is an enclosed research project consisting of an abstract, introduction, discussion of the research results and conclusion as well as an experimental section. Supplementary information for each chapter is enclosed in the Appendix at the end of this work.

5 REFERENCES

[1] J. P. Agrawal, *High Energy Materials Propellants, Explosives and Pyrotechnics*, 1st ed., Wiley-VCH, Weinheim (Germany), **2010**.

[2] T. M. Klapötke, *Chemistry of High-Energy Materials*, 3rd ed., De Gruyter, Berlin (Germany), **2015**.

[3] R. Matyás, J. Pachman, *Primary Explosives*, 1st ed., Springer-Verlag, Berlin (Germany), **2013**.

[4] a) M. H. V. Huynh, M. A. Hiskey, T. J. Meyer, M. Wetzler, *Proc. Natl. Acad. Sci. U. S. A.* **2006**, *103*, 5409–5412; b) T. M. Klapötke, C. M. Sabate, J. M. Welch, *Dalton Trans.* **2008**, 6372–6380; c) G. Geisberger, T. M. Klapötke, J. Stierstorfer, *Eur. J. Inorg. Chem.* **2007**, 4743–4750.

[5] J. Akhavan, *The Chemistry of Explosives*, 2nd. ed., The Royal Society of Chemistry, Cambridge (GB), **2004**.

[6] R. Meyer, J. Köhler, A. Homburg, *Explosives*, 7th ed., Wiley-VCH, Weinheim (Germany), **2015**.

[7] N. Kubota, *Propellants and Explosives*, 1st ed., Wiley-VCH, Weinheim (Germany), **2002**.

[8] J. D. Clark, *Ignition! An Informal History of Liquid Rocket Propellants*, 1st ed., Rutgers University Press, New Jersey (U.S.), **1972**.

[9] K. O. Christe, G. W. Drake **2010**, US7771549B1.

[10] C. Kappenstein, J. P. Joulin, *Adv. Sci. Technol. (Stafa–Zuerich, Switz.)* **2006**, *45*, 2143–2152.

[11] Y. Zhang, J. Shreeve, *Angew. Chem., Int. Ed.* **2011**, *50*, 935–937.

[12] B. Ritz, Y. Zhao, A. Krishnadasan, N. Kennedy, H. Morgenstern, *Epidemiology* **2006**, *17*, 154-161.

[13] a) F. Volk, G. Wunsch, *Propellants, Explos., Pyrotech.* **1985**, *10*, 181–186; b) M. Miszczak, J. Bladek, *Propellants, Explos., Pyrotech.* **1993**, *18*, 29–32.

[14] a) V. A. Arkhipov, A. G. Korotkikh, *Combust. Flame* **2012**, *159*, 409–415; b) H. Shekhar, *Propellants, Explos., Pyrotech.* **2011**, *36*, 356–359; c) M. A. Stephens, E. L. Petersen, R. Carro, D. L. Reid, S. Seal, *Propellants, Explos., Pyrotech.* **2010**, *35*, 143–152.

[15] Credits: NASA.

[16] H. Vogt, J. Balej, J. E. Bennett, P. Wintzer, S. A. Sheikh, P. Gallone, S. Vasudevan, K. Pelin, *Chlorine Oxides and Chlorine Oxygen Acids. Ullmann's Encyclopedia of Industrial Chemistry*, Wiley Online Library, **2000**.

[17] J. W. Reed, *Analysis of the Accidental Explosion at Pepcon, Henderson, Nevada, May 4, 1988*, Sandia National Laboratories, Albuquerque (US), **1988**.

[18] A. Davenas, *Solid Rocket Propulsion Technology*, 1st ed., Pergamon Press, Oxford (UK), **1993**.

[19] a) D. R. Mattie, J. Strawson, J. Zhao, *Perchlorate Toxicity and Risk Assessment*, U.S. Air Force Research, **2006**; b) J. Wolff, *Pharmacol. Rev.* **1998**, *50*, 89–105; c) R. J. Brechner, G. D. Parkhurst, W. O. Humble, M. B. Brown, W. H. Herman, *J. Occup. Environ. Med.* **2000**, *42*, 777–782.

[20] D. Majda, A. Korobov, U. Filek, B. Sulikowski, P. Midgley, D. Vowles, J. Klinowski, *Chem. Phys. Lett.* **2008**, *454*, 233–236.

[21] Green Propulsion: Trends and Perspectives. http://www.aerospace.org/crosslinkmag/summer2011/green-propulsion-trends-and-perspectives/ (accessed July 11, 2016).

[22] Office of Naval Research Home Page. http://www.onr.navy.mil (accessed March 24, 2016).

[23] a) C. Oommen, S. R. Jain, *J. Haz. Mater.* **1999**, *67*, 253–281; b) S. Löbbecke, H. H. Krause, A. Pfeil, *Propellants, Explos., Pyrotech.* **1997**, *22*, 184–188.

[24] H. F. R. Schöyer, A. J. Schnorhk, P. A. O. G. Korting, P. J. van Lit, J. M. Mul, G. M. H. J. L. Gadiot, J. J. Meulenbrugge, *J. Propul. Power* **1995**, *11*, 856–869.

[25] M. Göbel, T. M. Klapötke, *Z. Anorg. Allg. Chem.* **2007**, *633*, 1006–1017.

II Results and Discussion

1 Carbonyl Diisocyanate $CO(NCO)_2$

2 (2-Fluoro-2,2-dinitroethyl)-2,2,2-trinitroethylnitramine

3 Michael Addition of Trinitromethane

4 The 3,3,3-Trinitropropyl Unit

5 Oxalyl Based Energetic Polynitro Derivatives

6 β-Alainine and l-Aspartic Acid

7 *N*-Nitrosarcosine

8 Toxicity Assessment of Energetic Materials

1 Carbonyl Diisocyanate $CO(NCO)_2$

Carbonyl Diisocyanate $CO(NCO)_2$: Synthesis and Structures in Solid State and Gas Phase

Thomas M. Klapötke, Burkhard Krumm, Sebastian Rest, Regina Scharf, Jan Schwabedissen, Hans-Georg Stammler, and Norbert W. Mitzel

as published in

Journal of Physical Chemistry A **2016**, *120*, 4534–4541.

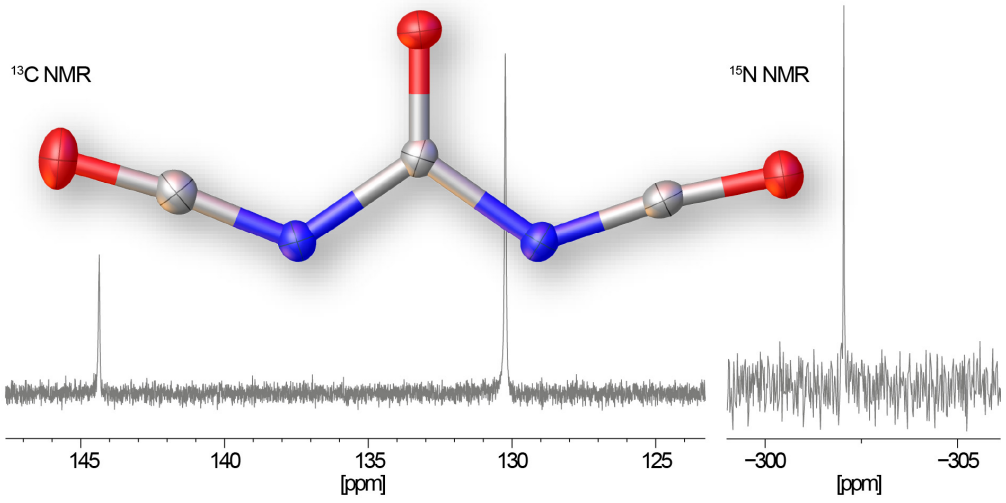

1.1 Abstract

A modified synthesis for carbonyl diisocyanate, $CO(NCO)_2$, starting from trichloroisocyanuric acid and diphosgene is described. In addition to the previously reported ^{13}C NMR resonances, the ^{15}N NMR shift is determined for the first time. The structure in the solid state was determined by X-ray diffraction (XRD) on *in situ* grown crystals, that in the gas phase was experimentally determined by electron diffraction (GED) and for single molecules theoretically by quantumchemical calculations. The structures are compared and discussed with related systems. Quantum-chemical calculations as well as GED and XRD prove *syn–syn* to be the conformation of lowest energy. In quantum-chemical calculations and GED the presence of a *syn–anti* conformer was confirmed and the structure of this conformer was determined.

1.2 Introduction and Synthesis

The chemistry and properties of the well-known carbonic acid H_2CO_3, an essential molecule of life, is still an active topic of research.[1,2] While the free acid is rather unstable, very reactive halides and pseudohalides exist, such as the carbonyl dihalides including the prominent phosgene $COCl_2$, and the dipseudohalides carbonyl diisocyanate $CO(NCO)_2$, diisothiocyanate $CO(NCS)_2$, and the diazide $CO(N_3)_2$. All of these materials have one dominating feature in common: their extreme toxicity and/or hazardousness. Nevertheless, the first two dipseudohalides represent excellent starting materials for further synthetic chemistry.[3–6] Structural studies have been performed for most of the carbonyl halides as well as for the explosive diazide.[7,8] In this contribution, the structure of carbonyl diisocyanate $CO(NCO)_2$ is presented in both solid and gas phase. In addition, a further alternate procedure of synthesis is described. Carbonyl diisocyanate (**1**) was first synthesized in 1966 by thermolysis of trichloroisocyanuric acid, $(ClNCO)_3$.[9] As a side product, nitrogen trichloride was formed, which can explode spontaneously and violently.[10] Because nitrogen trichloride is difficult to remove, an alternate synthesis for **1** was developed by passing carbonyl fluoride or phosgene through a melt of lithium chloride and potassium chloride containing potassium isocyanate.[5,11] These reactions require rather high temperatures above 400 °C and are accompanied by the formation of the mixed halogenocarbonyl isocyanate. A more convenient method for the synthesis of **1** was found in the reaction of trichloroisocyanuric acid with phosgene (Scheme 1.1).[12] The positively

polarized chlorine atom of trichloroisocyanuric acid reacts with the negatively polarized chlorine atom of phosgene under elimination of chlorine. As an intermediate chlorocarbonyl isocyanate is formed, which immediately reacts with further trichloroisocyanuric acid to form **1**.[13,14] Isocyanate **1** has been obtained as a colorless, moisture sensitive liquid. It trimerizes at room temperature, and consequently storage at low temperatures is required.[14]

An alternate synthesis of **1** is accomplished by replacement of phosgene by diphosgene. The use of diphosgene offers several advantages, such as being a liquid at room temperature and thus providing easier handling and storage and being commercially available and stable up to 300 °C.[15–19]

Both reagents, phosgene and diphosgene, furnish **1** in good yields. The treatment of trichloroisocyanuric acid with diphosgene produces small amounts of phosgene and carbon tetrachloride, which are formed due to thermal decomposition of excess diphosgene. All materials can be identified by ^{13}C NMR spectroscopy. The good solubility of **1** in $CDCl_3$ allows the determination of its ^{15}N NMR resonance at −302.0 ppm, which is within the typical region for nitrogen containing heterocumulene type systems.

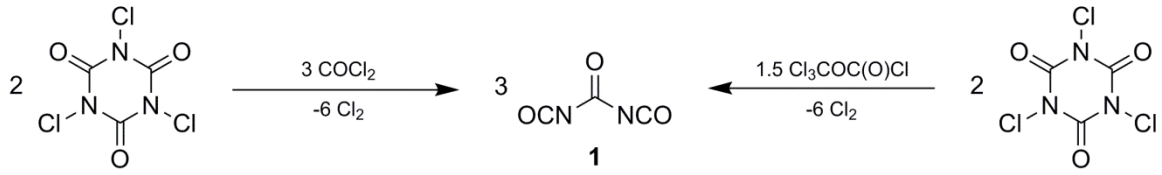

Scheme 1.1 Synthesis of Carbonyl Diisocyanate (**1**) by Reaction of Trichloroisocyanuric Acid with Phosgene and Diphosgene.

1.3 Experimental Section

1.3.1 General Information

Commercially available chemicals were used as supplied. The syntheses and manipulation of air- and moisture-sensitive materials were performed in an inert atmosphere of dry argon (purity 5.0 Air Liquide) using flamedried glass vessels and Schlenk techniques.[20] NMR spectra were recorded with a JEOL Eclipse 400 instrument at 25 °C, and chemical shifts were determined with respect to external standards, Me_4Si (^{13}C, 100.5 MHz) and $MeNO_2$ (^{15}N, 40.6 MHz).

1.3.2 Synthesis of Carbonyl Diisocyanate

(a) Carbonyl diisocyanate (**1**) was prepared according to ref 14; excess amounts of phosgene were removed by recondensation at −20 °C (16 mbar) and **1** was obtained as a pure colorless liquid (55%).

(b) In a flask connected to a distillation apparatus a mixture of trichloroisocyanuric acid (11.6 g, 49.9 mmol) and the highboiling solvent 1-chloro-2-nitrobenzene (37.0 g) was heated to 170 °C. Diphosgene (8.2 g, 41 mmol) was added dropwise under permanent stirring for 1 h. The crude product distilled off and was collected in a receiver cooled to 0 °C. Carbonyl diisocyanate (**1**) was obtained after repeated distillation at ambient pressure (bp 105 °C, oil bath 130 °C) as a colorless liquid (5.0 g, 59%), containing small impurities (approximately 5%) consisting of diphosgene, phosgene, and CCl_4, (the latter two formed by thermal decomposition of diphosgene), identified by ^{13}C NMR spectroscopy.

^{13}C NMR ($CDCl_3$): δ = 144.4 (CO), 130.2 (NCO) ppm. ^{15}N NMR ($CDCl_3$): δ = −302.0 (NCO) ppm.

1.3.3 Quantum-Chemical Calculations

A potential energy surface scan was performed on the MP2 level of theory with the Dunning-type basis set by rotating both isocyanate groups individually around the C–N bond. The resulting three extrema were optimized at different levels of theory using the Gaussian 09 D.01 version.[21] One of the conformers was proven by exhibiting a negative frequency to be a saddle point on the potential energy surface. Frequency calculations and the calculations of numeric cubic force fields were performed at the MP2/cc-pVTZ level of theory. The Natural Bond Orbital (NBO) and Natural Resonance Theory (NRT) analysis was done with the NBO 6.0 package[22] incorporated in the Gaussian 09 D.01 revision.

1.3.4 Gas-Phase Electron Diffraction Experiment

Electron diffraction patterns were recorded on the heavily improved Balzers Eldigraph KD-G2 gas-phase electron diffractometer at Bielefeld University. Experimental details are listed in Table 1.1, instrumental details are reported elsewhere.[23,24]

The electron diffraction patterns were measured on the Fuji BAS-IP MP 2025 imaging plates, which were scanned by using a calibrated Fuji BAS.1800II scanner. The intensity curves (Appendix A1) were obtained by applying the method described earlier.[25] Sector function and electron wavelength were refined[26] using carbon tetrachloride diffraction patterns, recorded in the same experiment as the substance under investigation.

Table 1.1 Details of the Gas-Phase Electron Diffraction Experiment for $CO(NCO)_2$.

Parameters	short detector distance	long detector distance
noozle-to-plate distance, mm	250.0	500.0
accelerating voltage, kV	60	60
fast electron current, μA	1.39	1.37
electron wavelength,[a] Å	0.048733	0.048638
nozzle temperature, K	273	274
Sample pressure,[b] mbar	1.5×10^{-6}	1.6×10^{-6}
residual gas pressure[c], mbar	9.1×10^{-8}	1.3×10^{-7}
exposure time, s	10	10
used *s* range, $Å^{-1}$	9.5–31.9	2.9–15.9
number of inflection points[d]	4	3
R_f factor	4.35	2.54

[a] Determined from CS2 diffraction patterns measured in the same experiment. [b] During the measurement. [c] Between measurements. [d] Number of inflection points on the background lines.

1.3.5 Gas-Phase Electron Diffraction Structural Analysis

The structural analysis was performed using the UNEX program.[27] All refinements were performed using two intensity curves simultaneously (Appendix A1), one from the short and another from the long nozzle-to-detector distance, which were obtained by averaging independent intensity curves measured in one experiment. For the definition of independent geometrical parameters and their groups in the least-squares refinement see Table 1.6. The *syn–syn* conformer was assumed to be of C_{2v} symmetry while the *syn–anti* conformer was modeled to be of C_s symmetry. The differences between values of parameters were kept fixed at the values taken from the MP2/cc-pVTZ calculations. To calculate start values for amplitudes of vibrations and curvilinear corrections used in the gas-phase electron-diffraction refinements, analytical quadratic and numerical cubic force fields were calculated for both *syn–syn* and *syn–anti* conformers employing the MP2/ccpVTZ approximation. The mean square amplitudes and vibrational corrections to the equilibrium structure were calculated with the SHRINK program.[28–31]

1.3.6 X-Ray Crystallography

A suitable crystal of carbonyl diisocyanate was grown from the neat melt by *in situ* crystallization directly on the diffractometer. For this purpose, a solid–liquid equilibrium

Table 1.2 Summary of Crystallographic Data for $CO(NCO)_2$ (**1**).

	1
Chemical formula	$C_3N_2O_3$
M_r	112.05
Crystal system	orthorhombic
Space group	*Pnma* (No. 62)
a (Å)	5.4759(2)
b (Å)	5.5658(2)
c (Å)	14.0998(5)
V (Å^3)	429.73(3)
Z	4
T (K)	99.95(13)
ρ_{calc} (Mg/m^3)	1.732
μ (mm^{-1})	0.159
$2\Theta_{max}$ [°]	60.0
Index range h	$-7 \le h \le 7$
Index range k	$-7 \le k \le 7$
Index range l	$-19 \le l \le 19$
Refl. collect.	13816
Indep. refl.	686
R_{int}	0.0357
Data/restraints/parameters	686/0/49
R_1, $I>2\sigma(I)$ / all data	0.0256/0.0290
wR_2, $I>2\sigma(I)$ / all data	0.0665/0.0687
GoF	1.135
$\rho_{max/min}$ [e Å^{-3}]	0.30/–0.22

was first established at 216.0(1) K close to the melting point. Then all solid except a tiny crystal seed was molten (by using a copper wire as external heating source and microscopic observation) followed by very slowly lowering the temperature, until the whole capillary was filled with a single crystalline specimen. Subsequently it was slowly chilled to 100 K within 3 h. The single crystal of carbonyl diisocyanate (**1**) was measured on an Agilent SuperNova diffractometer using Mo K_α radiation (λ = 0.71073 Å) at 100.0(1) K. Using Olex2,[32] the structure was solved with the Superflip[33] structure solution program using Charge Flipping and refined with the SHELXL[34] refinement package using leastsquares

refinements. All atoms were refined anisotropically. More details are listed in Table 1.2. Data are listed in Table 1.1.

CCDC 1470284 contains the supplementary crystallographic data for this paper. These data can be obtained via www.ccdc.cam.ac.uk/data_request/cif free of charge from The Cambridge Crystallographic Data Centre.

1.4 Results and Discussion

1.4.1 Solid State Structure

A suitable crystal of carbonyl diisocyanate was grown from the neat melt by *in situ* crystallization directly on the X-ray diffractometer. Carbonyl diisocyanate crystallizes in the orthorhombic space group *Pnma* with four molecules per unit cell. The entire molecule occupies the crystallographic mirror plane. Furthermore, it crystallizes isostructurally to the related carbonyl diazide.[8] The molecular structure in the solid state is shown in Figure 1.1.

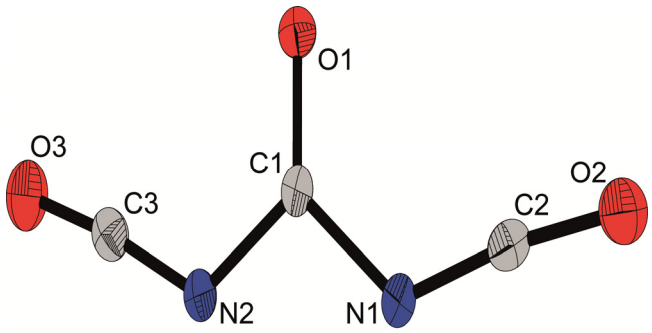

Figure 1.1 Molecular structure of carbonyl diisocyanate (**1**) in the solid state. Displacement ellipsoids are depicted with 50% probability.

The planar molecule adopts nearly C_{2v} symmetry. Both isocyanate groups are oriented *syn* to the carbonyl C=O bond regarding their C–N bonds. Structural parameters of the solid state structure and of comparable other solid state structures are listed in Table 1.3. The carbonyl C=O bond length (1.202(1) Å) is identical to that in the diazide (1.200(6) Å, XRD)[8] within the 3σ range as well as the $C_{carbonyl}$–N distances nearly, which are all in the range from 1.392(1) Å to 1.412(7) Å. On the other hand the C=O bond in urea (carbonyl diamide) is longer by ca. 0.06 Å (1.257(1) Å by XRD[8] or 1.258(1) Å by neutron scattering),[35] whereas the $C_{carbonyl}$–N distance is ca. 0.05 Å shorter (1.338(1) Å respectively 1.349(1) Å). The central ∡(NCN) angle of 109.6(1)° is between those of the diazide (105.6(6)°) and urea (117.0(1)° respectively 117.2(1)°).

Table 1.3 Selected Structural Parameters in the Solid State of **1** and Corresponding Parameters in Carbonyl Diazide and Urea.

Parameters[a]	**$CO(NCO)_2$**	**$CO(N_3)_2$**	**$CO(NH_2)_2$**[b]
$r(CO)_{carbonyl}$	1.202(1)	1.200(6)	1.257(1)
$r(C_1N_1)$	1.392(1)	1.407(8)	1.338(1)
$r(C_1N_2)$	1.399(1)	1.412(7)	1.338(1)
$r(N_1C_2)$	1.227(1)	1.274(7)	
$r(N_2C_3)$	1.226(1)	1.265(7)	
$r(C_2O_2)$	1.150(1)	1.111(7)	
$r(C_3O_3)$	1.150(1)	1.111(7)	
$\measuredangle(N_1C_1N_2)$	109.6(1)	105.5(5)	117.0(1)
$\measuredangle(C_1N_1C_2)$	125.3(1)	111.5(4)	
$\measuredangle(C_1N_2C_3)$	122.7(1)	111.8(4)	
$\measuredangle(N_1C_2O_2)$	172.5(1)	172.1(5)	
$\measuredangle(N_2C_3O_3)$	173.6(1)	172.6(6)	
Intermolecular O···C' contacts (symmetry code) < 3.3 Å			
$O_1\cdots C_2'$ $(1+x, y, z)$	3.006(1)	3.092	
$O_1\cdots C_3'$ $(1-x,1-y,1-z)$	3.011(1)	3.092	
$O_3\cdots C_3'$ $(-0.5+x,0.5-y,1.5-z)$	3.138(1)	3.264	
$O_2\cdots C_2'$ $(0.5+x,0.5-y,0.5-z)$	3.288(1)	3.484	

[a] Distances r in Å, angles $\measuredangle$ in deg. [b] X-ray diffraction at 150 K.

Intermolecular pattern: In the crystal the molecules of carbonyl diisocyanate show two intermolecular O···C distances considerably shorter than the sum of their van der Waals radii (3.2 Å).[36] The shortest one between O1 and C2′ (3.006(1) Å) builds a chain of molecules by translation along the *a*-axis, as shown in Figure 1.2.

These chains occupy one crystallographic mirror plane perpendicular to the *b*-axis and are separated by a distance of 2.783(2) Å (half of the *b*-axis) from the adjacent mirror plane created by a center of inversion resulting in the short O1···C3′ contact of 3.011(1) Å. The relatively high melting temperature of 216(1) K is probably due to the high dipole moment of 1.19 D (MP2/cc-pVTZ). Because of this dipole moment the individual molecules pack in antiparallel chains resulting in dipole moment cancelation, a short distance between the chains and so the formation of layers perpendicular to the *c*-axis as shown in Figure 1.3.

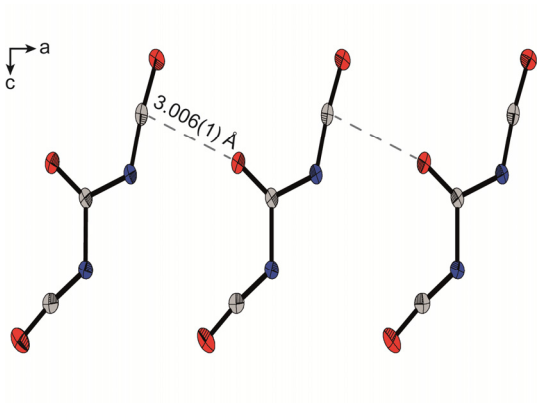

Figure 1.2 View allong the *b*-axis.

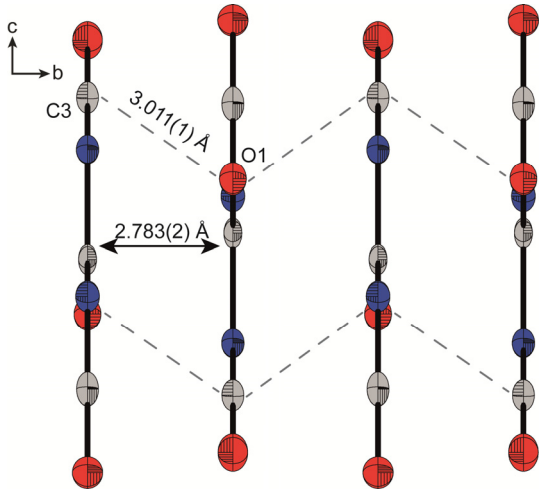

Figure 1.3 View along the *a*-axis showing layers perpendicular to the *c*-axis created by antiparallel chains.

These layers displayed in Figure 1.4 are linked only by weak interactions, the shortest interlayer contact can be found between O3 and C3′ with 3.138(1) Å and nearly accords with the expected sum of the van der Waals radii.

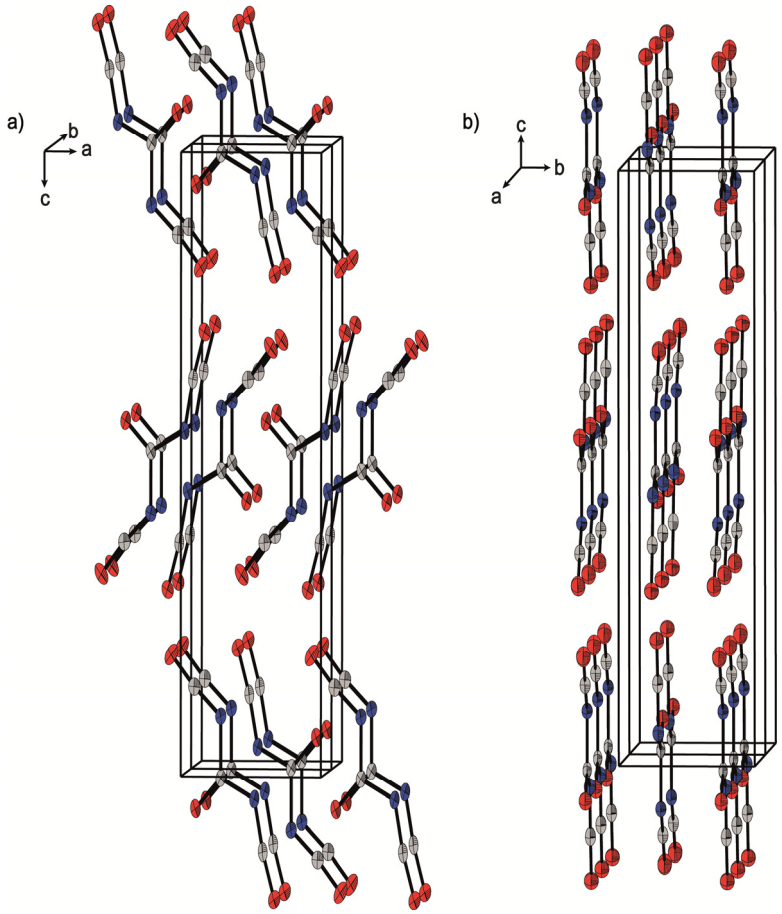

Figure 1.4 Approximate view along the *b*-axis (a) and *a*-axis (b), respectively.

1.4.2 Quantum-Chemical Calculations

A series of quantum-chemical calculations was carried out to estimate the gas-phase composition and structural parameters. At first a potential energy surface (PES) scan was performed rotating the two isocyanate groups individually around the $C_{carbonyl}$–N bond at the MP2 level of ab initio theory[37] with the correlation consistent polarized valence triple ζ basis set.[38] On this potential energy surface three distinguishable extrema were found, which were optimized, and the type of the extrema was checked by frequency calculations at several levels of theory. The two planar conformers *syn–syn* and *anti–syn* are true minima on the PES but the *anti–anti* conformer was proven to be no minimum showing an imaginary frequency. The *anti*/*syn* notation describes the relative orientation of the isocyanate group to the C=O group with respect to the C–N bond. Table 1.4 shows the quantum chemically calculated energy differences and the resulting abundance of the conformers in the gas phase.

Table 1.4 Calculated Relative Differences in Total Energy (ΔE, kcal mol^{-1}), Gibbs Free Energy (ΔG, kcal mol^{-1}) for the *anti–syn* to the *syn–syn* Conformer and the Relative Abundance of the *anti–syn* Conformer in the Gas Phase at 298 K.

Method	ΔE	ΔG	Abundance *anti–syn*
B2PLYP/cc-pVTZ	0.94	0.84	32.5
B3LYP/6-311+G(3d,f)	1.02	0.89	30.5
B3LYP/cc-pVTZ	1.00	0.89	31.0
BP86/6-311+G(3d,f)	0.99	0.84	32.7
BP86/cc-pVTZ	0.98	0.83	33.0
MP2/cc-pVTZ	0.70	0.61	41.5
MPW1PW91/6-311+G(3d,f)	0.97	0.84	32.6
MPW1PW91/cc-pVTZ	0.97	0.84	32.5
PBE0/cc-pvtz	0.96	0.81	33.8

A clear picture is drawn from the calculated differences in the Gibbs free energy and the resulting gas-phase composition. All differences are in the range of 0.81–0.89 kcal mol^{-1} except for the MP2/cc-pVTZ calculation which underestimates the energetic preference of the *syn–syn* conformer. As shown in Table 1.5, the three different conformers (Figure 1.5) exhibit diverse geometrical parameters which can be explained by the theory of NBO.[39,40]

Table 1.5 Calculated Geometrical Parameters on Different Levels of Theory. For Atom Numbering See Figure 1.5.

	PBE0/cc-pVTZ			MP2/cc-pVTZ		
parameters[a]	***syn–syn***	***syn–anti***	***anti–anti***	***syn–syn***	***syn–anti***	***anti–anti***
$r(CO)_{carbonyl}$	1.210	1.205	1.203	1.205	1.200	1.196
$r(C_1N_1)$	1.403	1.419	1.406	1.398	1.415	1.402
$r(C_1N_2)$	1.403	1.399	1.406	1.398	1.395	1.402
$r(N_1C_2)$	1.226	1.228	1.219	1.228	1.230	1.220
$r(N_2C_3)$	1.226	1.227	1.219	1.228	1.227	1.220
$r(C_2O_2)$	1.169	1.168	1.172	1.165	1.164	1.169
$r(C_3O_3)$	1.169	1.169	1.172	1.165	1.165	1.169
$\measuredangle(N_1C_1N_2)$	108.9	112.0	116.3	108.7	111.9	116.3
$\measuredangle(O_1C_1N_1)$	125.5	125.1	121.9	125.6	125.2	121.9
$\measuredangle(O_1C_1N_2)$	125.5	122.9	121.9	125.6	122.9	121.9
$\measuredangle(N_1C_2O_2)$	172.6	172.9	173.3	172.4	172.9	173.1
$\measuredangle(N_2C_3O_3)$	172.6	172.6	173.3	172.4	172.5	173.1

[a] Distances r in Å, angles $\measuredangle$ in deg.

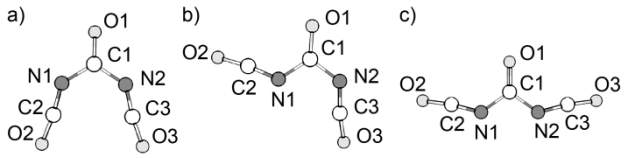

Figure 1.5 Atom numbering of the optimized structures of *anti–anti* (a), *syn–anti* (b) and *syn–syn* conformers (c).

The longest carbonyl C=O bond is found in the *syn–syn* conformer and the shortest in the *anti–anti* one. This is due to the occupancy of the antibonding orbitals of the double bond. The σ* orbital is occupied with 0.028 electrons in the *syn–syn* and by 0.020 electrons in the *anti–anti* conformer. This effect is more pronounced in the π* orbital, where the corresponding orbital of the *syn–syn* conformer is occupied by 0.267 electrons, whereas the analogous orbital in the *anti–anti* conformer is occupied by 0.227 electrons. In the *syn–anti* conformer the C_1N distance to the *syn* isocyanate group is by 0.02 Å longer than the corresponding distance to the *anti* isocyanate group. This structural feature is caused by the donation of electron density from the lone pair $n(N_2)$ of the adjacent isocyanate group into the antibonding $\sigma^*(C_1N_1)$ orbital in the *syn* group and results in an occupancy of 0.105 electrons compared to the occupancy of the σ* orbital of the shorter C_1N_2 bond of 0.089

electrons. This explains the variation of bond lengths to the different isocyanate groups. The shortening of the C–N and the elongation of the C–O bond in the isocyanate fragment of the *anti–anti* conformer manifests itself in the NRT[41–43] structures of the conformers. For each conformer the most contributing resonance structure is the one with a C–N single bond and a C≡O triple bond in one isocyanate group. The contribution of this resonance structure is 20.4% for each structure of the *anti–anti* conformer, 18.4% and 18.0% for the two structures of the *syn–anti* conformer, and 17.4% for each of the structures of the *syn–syn* conformer. Thus, this result is in accordance with the tendency of the bond lengths in the misocyanate group among the three different conformers.

The shortening of the central ∡($N_1C_1N_2$) angle from the *anti–anti* to the *syn–syn* is a common feature with the $F_2NC(O)NCO$[44] (B3LYP/aug-cc-pVTZ) and the $CO(N_3)_2$[8] (B3LYP/6–311+G(3df)). This feature can be explained by a resonance structure occurring within the NRT analysis. For the *syn–syn* conformer a resonance structure weighted with 5.3% is observed where the nitrogen atoms carry opposite charges. Thus, the reason for the shortening might be an electrostatic one.

1.4.3 Gas-Phase Structure

Gas-phase electron diffraction (GED) was used to determine the structure of the free molecule of the carbonyl diisocyanate $CO(NCO)_2$ (**1**) experimentally. The structural analysis was performed using the UNEX program.[27] All refinement steps were performed with two different averaged intensity curves (short and long nozzle-to-detector distance). For the definition of independent structural parameters and their groups in the least-squares refinement, see Table 1.6. The differences of the values of parameters in one group were kept fixed at the calculated values of the MP2/cc-pVTZ level.

To describe the conformational composition in the gas-phase a two conformer model was used in the refinement. The Z-matrix of the *syn–syn* conformer was set up to obey C_{2v} symmetry while the one for the *syn–anti* conformer adopts C_s symmetry. The central angle ∡($N_1C_1N_2$) was refined separately for each conformer. The angles ∡(C–N=C) and ∡(N=C=O) were refined in groups with fixed differences based on the MP2/cc-pVTZ calculations for each conformer giving contributions for the long-range distances among the isocyanate groups of one molecule. Refining the angles ∡(C–N=C) and ∡(N=C=O) independently resulted in chemically unreasonable structural parameters. The final gas-phase composition according to the GED refinement is 66(3)% for the *syn–syn* conformer.

Table 1.6 Structural Parameters from the Gas-Phase Electron Diffraction Refinement.

	syn-syn			syn-anti		
parameters[a]	**r_e, ∢$_e$**	**r_g**	**l**	**r_e, ∢$_e$**	**r_g**	**l**
$r(C_1O_1)$	1.196(1)[1]	1.991(3)	0.0180[7]	1.191(1)[1]	1.194(1)	0.0177[7]
$r(C_1N_1)$	1.392(1)[2]	1.401(1)	0.0272[7]	1.408(1)[2]	1.417(1)	0.0290[7]
$r(C_1N_2)$	1.392(1)[2]	1.401(1)	0.0272[7]	1.389(1)[2]	1.397(1)	0.0271[7]
$r(N_1C_2)$	1.213(1)[1]	1.220(1)	0.0419[7]	1.212(1)[1]	1.259(1)	0.1121[7]
$r(N_2C_3)$	1.213(1)[1]	1.220(1)	0.0419[7]	1.215(1)[1]	1.223(1)	0.0450[7]
$r(C_2O_2)$	1.150(1)[1]	1.191(1)	0.0689[7]	1.149(1)[1]	1.154(1)	0.0150[7]
$r(C_3O_3)$	1.150(1)[1]	1.191(1)	0.0689[7]	1.150(1)[1]	1.155(1)	0.0150[7]
∢$(N_1C_1N_2)$	106.1(3)[3]			110.3(6)[5]		
∢$(C_1N_1C_2)$	125.9(6)[4]			126.3(9)[6]		
∢$(C_1N_2C_3)$	125.9(6)[4]			129.1(9)[6]		
∢$(N_1C_2O_2)$	171.8(6)[4]			174.2(9)[6]		
∢$(N_2C_3O_3)$	171.8(6)[4]			173.8(9)[6]		

[a] Distances r_e and r_g as well as amplitudes l in Å, angles ∢$_e$ in deg. Experimental errors are represented as three standard deviations and are given in parentheses. Superscript numbers 1, 2, ..., 7 represent groups, in which parameters were tied together in least-squares method by fixing differences between their values to values taken from the MP2/cc-pVTZ calculations.

The radial distribution curve Figure 1.6 shows some discrepancy between the modeled and the experimental values in the range of 4.5 Å. In this region the scattering is due to the distances among the isocyanate groups in both conformers. Additionally the *syn–anti* conformer the terms of the $O_{carbonyl}\cdots O_{syn}$ as well as the $N_{syn}\cdots O_{anti}$ and the $C_{anti}\cdots O_{syn}$ occur in this region.

The refined gas-phase structures of both conformers show very similar bond lengths except for the carbonyl isocyanate C–N bond. This bond length differs for the *syn* isocyanate unit between the *syn–syn* conformer and the *syn–anti* conformer by about 0.01 Å. On the other hand the C–N bond length to the isocyanate moiety in the *anti* conformation is even shorter than the analogous distance in the *syn–syn* conformer. The shortening of a C–N bond seems to be caused by the other isocyanate group either being *syn* or *anti* and thus shortening or lengthening the bond. This effect is also observed for ClC(O)NCO[45] where the C–Cl bond is longer in the *anti* conformer (1.757(5) Å) compared to that of the *syn* conformer (1.729(5) Å). Furthermore, this effect is observed in $F_2ClCC(O)NCO$[46] for which the *gauche–syn* conformer has a C–C bond of 1.541(7) Å in length, that is, 0.007(7) Å shorter

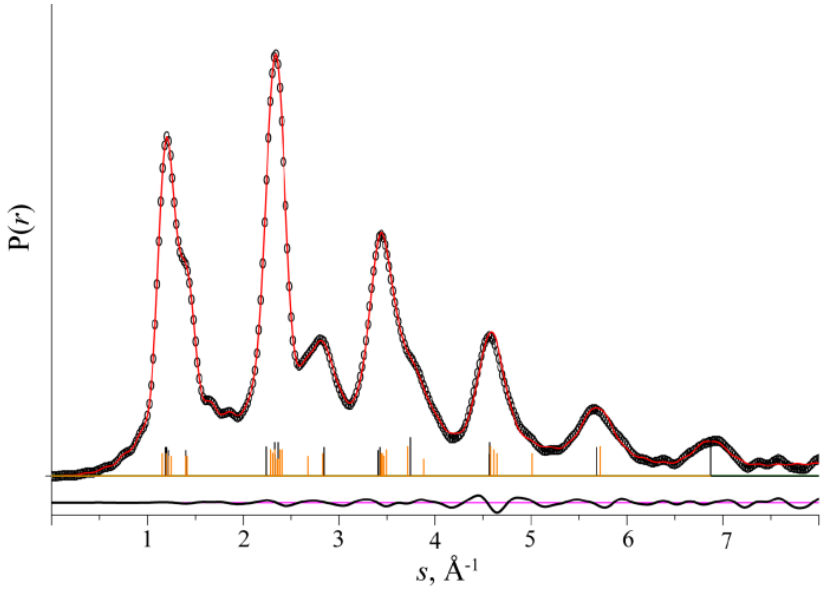

Figure 1.6 Experimental (circles ○) and model (continuous line −) radial distribution functions of $CO(NCO)_2$ (1). The difference curve is shown below. Vertical bars indicate interatomic distances in the model (black, *syn–syn*; orange, *syn–anti*).

than in the *gauche–anti* conformer. Another difference regarding the geometrical parameters occurs in the isocyanate ∡(N=C=O) angle. In a cumulene-type structure, one would expect an angle close to 180° at the central atom but in the present case, angles of 6° (*syn–anti*) and 8° (*syn–syn*) are observed.

The structural parameters obtained for the two conformers of $CO(NCO)_2$ can be compared to the structural parameters of previously examined compounds, FC(O)NCO,[47] ClC(O)NCO,[45] $CH_3C(O)NCO$[48] and $F_2ClCC(O)NCO$.[46] A detailed listing of selected parameters is presented in Table 1.7. Only one of the mentioned examples, $CH_3C(O)NCO$, was found to be composed of a single conformer composition in the gas phase. In contrast to this, FC(O)NCO is found to consist of 75(12)% *syn* conformer, ClC(O)NCO of approximately 75% *syn*, and $F_2ClCC(O)NCO$ shows a conformational mixture in the gas phase with 72(7)% *gauche–syn* contribution. The longest carbonyl C=O bond is observed for ClC(O)NCO with 1.209(16) Å for the *syn* and 1.201(16) Å for the *anti* conformer. The trend for a shorter carbonyl C=O bond in the *anti* conformer is also observed for the case of $F_2ClCC(O)NCO$ and in the present case. Another tendency in the compared structures is the larger central ∡(XCN) angle in the *anti* conformer which differs about 4° in each case. The smallest ∡(XCN) is found in the *syn–syn* conformer of $CO(NCO)_2$ with 106.1(3)° which is 1.5° smaller than the corresponding angle in FC(O)NCO, whereas the largest ∡(XCN) angle is observed for the *anti* conformer of $F_2ClCC(O)NCO$ (116.1(16)°). As expected from the VSEPR model all the listed central ∡(XCN) angles differ and are smaller than 120°. In the gas phase the carbonyl C=O

Table 1.7 Comparison of Structural Parameters of Different Carbonyl-Bonded Isocyanates.[a]

		X	***r*(CO)$_{carb.}$**	***r*(C—N)**	***r*(N=C)**	***r*(C=O)**	**∢(*X*CN)**	**∢(NCO)$_{isocya.}$**	**ref**
$CO(NCO)_2$ (*syn*)	r_e	N	1.196(1)	1.392(1)	1.213(1)	1.150(1)	106.1(3)	171.8(6)	this work
$CO(NCO)_2$ (*anti*/*syn*)	r_e	N	1.191(1)	1.408(1)	1.212(1)	1.149(1)	110.3(6)	174.2(9)	this work
FC(O)NCO (*syn*)	r_a	F	1.192(8)	1.388(4)	1.215(9)	1.154(8)	107.8(8)	174.6(25)	47
ClC(O)NCO (*syn*)	r_a	Cl	1.209(16)	1.391(6)	1.227(23)	1.137(16)	112.5(8)	173.1(23)	45
ClC(O)NCO (*anti*)	r_a	Cl	1.201(16)	1.384(6)	1.218(23)	1.139(16)	115.8(8)	173.4(23)	45
$CH_3C(O)NCO$ (*syn*)	r_a	C	1.199(6)	1.413(7)	1.119(7)	1.159(6)	111.5(4)	173.0[b]	48
$F_2ClCC(O)NCO$ (*syn*)	r_e	C	1.195(1)	1.378(9)	1.218(1)	1.157(1)	112.3(16)	173.1[b]	46
$F_2ClCC(O)ONCO$ (*anti*)	r_e	C	1.192(1)	1.374(9)	1.216(1)	1.158(1)	116.1(16)	172.5[b]	46

[a] Distances r in Å, angles ∢ in deg. [b] Fixed parameters.

bond lengths of the symmetric pseudohalide-carbonyl $CO(CN)_2$ [49] (1.206(4) Å) are longer than that of carbonyl diisocyanate (1.196(1) Å). This fact can be rationalized according to the rule of Bent:[50] an electron withdrawing atom or group receives more p character in its bond to the central atom while bonds to electropositive substituents possess more s character. Hence, the isocyanate groups concentrate more p character of the central carbon atom than the cyanide groups do. Consequently the carbonyl bond of **1** has left less p-orbital contribution in the isocyanate compound and therefore is shorter. Another structural parameter confirming the more electron-withdrawing character of the isocyanate group compared to the cyanide group is the central angle at the carbonyl carbon atom. As the bonds to the isocyanate groups exhibit more p-orbital character, the angle at 106.1(3)° is shorter than the corresponding one in the dicyanide compound at 114.9(6)°.

1.5 Conclusions

An alternate synthesis procedure, as well as thorough structural characterization in the solid and gas phase is described for the diisocyanate of carbonic acid, $CO(NCO)_2$. The new synthetic protocol replaces gaseous phosgene by the easier-to-handle liquid diphosgene. The solid state comprises solely molecules with planar *syn–syn* conformation. This conformer is also dominant in the gas phase (66(3)%), but additionally an *anti–syn* conformer was observed. On this basis the stereoelectronic effects of the conformation could be investigated using the NBO analysis.

1.6 References

[1] Reisenauer, H. P.; Wagner, J. P.; Schreiner, P. R. Gas-Phase Preparation of Carbonic Acid and Its Monomethyl Ester. *Angew. Chem., Int. Ed.* **2014**, *53*, 11766–11771.

[2] Bernard, J.; Seidl, M.; Kohl, I.; Liedl, K. R.; Mayer, E.; Galvez, O.; Grothe, H.; Loerting, T. Spectroscopic Observation of Matrix-isolated Carbonic Acid Trapped from the Gas Phase. *Angew. Chem., Int. Ed.* **2011**, *50*, 1939–1943.

[3] Axthammer, Q. J.; Klapötke, T. M.; Krumm, B.; Moll, R.; Rest, S. F. The Energetic Nitrocarbamate $O_2NN(H)CO[OCH2C(NO_2)_3]$ Derived from Phosgene. *Z. Anorg. Allg. Chem.* **2014**, *640*, 76–83.

[4] Klapötke, T. M.; Krumm, B.; Rest, S. F.; Suceska, M. Polynitro Containing Energetic Materials Based on Carbonyldiisocyanate and 2,2-Dinitropropane-1,3-diol. *Z. Anorg. Allg. Chem.* **2014**, *640*, 84–92.

[5] Jaeckh, C.; Sundermeyer, W. Chemical Reactions in Fused Salts. XV. Synthesis and Reactions of Carbonyl Halides and Pseudohalides. *Chem. Ber.* **1973**, *106*, 1752–1757.

[6] Bunnenberg, R.; Jochims, J. C. Carbonyl Diisothiocyanate. *Chem. Ber.* **1981**, *114*, 2075–2086.

[7] Romano, R. M.; Della Vedova, C. O.; Downs, A. J.; Tobon, Y. A.; Willner, H. New Members of an Old Family: Isolation of IC(O)Cl and IC(O)Br and Evidence for the Formation of Weakly Bound Br···CO. *Inorg. Chem.* **2005**, *44*, 3241–3248.

[8] Zeng, X.; Gerken, M.; Beckers, H.; Willner, H. Synthesis and Characterization of Carbonyl Diazide, $OC(N_3)_2$. *Inorg. Chem.* **2010**, *49*, 9694–9699.

[9] Nachbaur, E. Carbonic Acid Derivatives. II. Preparation and Properties of Carbonyl Isocyanate. *Monatsh. Chem.* **1966**, *97*, 361–367.

[10] Schneider, S.; Gerken, M.; Haiges, R.; Schroer, T.; Boatz, J. A.; Dixon, D. A.; Grant, D. J.; Christe, K. O. Synthesis and Characterization of Silyldichloramines, Their Reactions with F^- Ions, Instability of N_2Cl_2 and NCl_2^-, and Formation of NCl3. *Inorg. Chem.* **2007**, *46*, 93–102.

[11] Verbeek, W.; Sundermeyer, W. Preparation of Carbonyl and Fluorocarbonyl Pseudohalides in Molten Salts. *Angew. Chem., Int. Ed.* **1967**, *6*, 871–872.

[12] Hagemann, H. Carbonyl Diisocyanate. DE2411674A1, 1975.

[13] Hagemann, H. Carbonyl Diisocyanate. DE2408069A1, 1975.

[14] Akteries, B.; Jochims, J. C. Carbonyl Diisocyanate: a New Preparation and Some Reactions. *Chem. Ber.* **1986**, *119*, 83–95.

[15] Hentschel, W. Chlorinated Methyl Formates. *J. Prakt. Chem.* **1887**, *36*, 305–317.

[16] Oya, M.; Katakai, R.; Nakai, H.; Iwakura, Y. Novel Synthesis of N-carboxy-α-amino Acid Anhydride. *Chem. Lett.* **1973**, 1143–1144.

[17] Kurita, K.; Matsumura, T.; Iwakura, Y. Trichloromethyl Chloroformate. Reaction with Amines, Amino Acids, and Amino Alcohols. *J. Org. Chem.* **1976**, *41*, 2070–2071.

[18] Itoh, M.; Hagiwara, D.; Kamiya, T. A New Reagent for Tertbutoxycarbonylation: 2-*Tert*-butoxycarbonyloxy-imino-2-phenylacetonitrile. *Org. Synth.* **1979**, *59*, 95–101.

[19] Kurita, K.; Iwakura, Y. Trichloromethyl Chloroformate as a Phosgene Equivalent: 3-Isocyanatopropanoyl Chloride. *Org. Synth.* **1979**, *59*, 195–201.

[20] Shriver, D. F.; Drezdzon, M. A. *The Manipulation of Air-Sensitive Compounds.* 2nd ed.; John Wiley & Sons: New York, 1986.

[21] Frisch, M. J.; Trucks, G. W.; Schlegel, H. B.; Scuseria, G. E.; Robb, M. A.; Cheeseman, J. R.; G. Scalmani, V. B.; Mennucci, B.; Petersson, G. A.; Nakatsuji, H.; Caricato, M.; Li, X.; Hratchian, H. P.; Izmaylov, A. F.; Bloino, J.; Zheng, G.; Sonnenberg, J. L.; Hada, M.; Ehara, M.; Toyota, K.; Fukuda, R.; Hasegawa, J.; Ishida, M.; Nakajima, T.; Honda, Y.; Kitao, O.; Nakai, H.; Vreven, T.; J. A. Montgomery, J.; Peralta, J. E.; Ogliaro, F.; Bearpark, M.; Heyd, J. J.; Brothers, E.; Kudin, K. N.; Staroverov, V. N.; Kobayashi, R.; Normand, J.; Raghavachari, K.; Rendell, A.; Burant, J. C.; Iyengar, S. S.; Tomasi, J.; Cossi, M.; Rega, N.; Millam, J. M.; Klene, M.; Knox, J. E.; Cross, J. B.; Bakken, V.; Adamo, C.; Jaramillo, J.; Gomperts, R.; Stratmann, R. E.; Yazyev, O.; Austin, A. J.; Cammi, R.; Pomelli, C.; Ochterski, J. W.; Martin, R. L.; Morokuma, K.; Zakrzewski, V. G.; Voth, G. A.; Salvador, P.; Dannenberg, J. J.; Dapprich, S.; Daniels, A. D.; Farkas, Ö.; Foresman, J. B.; Ortiz, J. V.; Cioslowski, J.; Fox, D. J. *Gaussian 09*. Rev. A.02 ed.; Gaussian, Inc.: Wallingford CT, 2009.

[22] Gledding, E. D.; Badenhoop, J. K.; Reed, A. E.; Carpenter, J. E.; Bohmann, J. A.; Morales, C. M.; Landis, C. R.; Weinhold, F. *NBO 6.0*; Theoretical Chemistry Institute, University

of Wisconsin: Wisconsin, 2013; http://nbo6.chem.wisc.edu (accessed March 31, 2016).

[23] Berger, R. J. F.; Hoffmann, M.; Hayes, S. A.; Mitzel, N. W. An Improved Gas Electron Diffractometer - the Instrument, Data Collection, Reduction and Structure Refinement Procedures. *Z. Naturforsch.* **2009**, *64B*, 1259–1268.

[24] Reuter, C. G.; Vishnevskiy, Y. V.; Blomeyer, S.; Mitzel, N. W. Gas Electron Diffraction of Increased Performance Through Optimization of Nozzle, System Design and Digital Control. *Z. Naturforsch.* **2016**, *71B*, 1–13.

[25] Vishnevskiy, Y. V. The Initial Processing of the Gas Electron Diffraction Data: An Improved Method for Obtaining Intensity Curves from Diffraction Patterns. *J. Mol. Struct.* **2007**, *833*, 30–41.

[26] Vishnevskiy, Y. V. The Initial Processing of the Gas Electron Diffraction Data: New Method for Simultaneous Determination of the Sector Function and Electron Wavelength from Gas Standard Data. *J. Mol. Struct.* **2007**, *871*, 24–32.

[27] Vishnevskiy, Y. V. *UNEX*; version 1.6.0 beta; UNEXProg: 2013.

[28] Sipachev, V. A. Calculation of Shrinkage Corrections in Harmonic Approximation. *J. Mol. Struct.: THEOCHEM* **1985**, *22*, 143–151.

[29] Sipachev, V. A. Anharmonic Corrections to Structural Experiment Data. *Struct. Chem.* **2000**, *11*, 167–172.

[30] Sipachev, V. A. Local Centrifugal Distortions Caused by Internal Motions of Molecules. *J. Mol. Struct.* **2001**, *567–568*, 67–72.

[31] Sipachev, V. A. The Use of Quantum-mechanical Third-order Force Constants in Structural Studies. *J. Mol. Struct.* **2004**, *693*, 235–240.

[32] Dolomanov, O. V.; Bourhis, L. J.; Gildea, R. J.; Howard, J. A. K.; Puschmann, H. OLEX2: a Complete Structure Solution, Refinement and Analysis Program. *J. Appl. Crystallogr.* **2009**, *42*, 339–341.

[33] Palatinus, L.; Chapuis, G. SUPERFLIP. A Computer Program for the Solution of Crystal Structures by Charge Flipping in Arbitrary Dimensions. *J. Appl. Crystallogr.* **2007**, *40*, 786–790.

[34] Sheldrick, G. M. A Short History of SHELX. *Acta Crystallogr.* **2008**, *64A*, 112–122.

[35] Swaminathan, S.; Craven, B. M.; McMullan, R. K. The Crystal Structure and Molecular Thermal Motion of Urea at 12, 60 and 123 K from Neutron Diffraction. *Acta Crystallogr.* **1984**, *40B*, 300–306.

[36] Bondi, A. van der Waals Volumes and Radii. *J. Phys. Chem.* **1964**, *68*, 441–451.

[37] Moller, C.; Plesset, M. S. Note on the Approximation Treatment for Many-electron Systems. *Phys. Rev.* **1934**, *46*, 618–622.

[38] Dunning, T. H., Jr. Gaussian Basis Sets for Use in Correlated Molecular Calculations. I. The Atoms Boron Through Neon and Hydrogen. *J. Chem. Phys.* **1989**, *90*, 1007–1023.

[39] Glendening, E. D.; Landis, C. R.; Weinhold, F. NBO 6.0: Natural Bond Orbital Analysis Program. *J. Comput. Chem.* **2013**, *34*, 1429–1437.

[40] Weinhold, F. Natural Bond Orbital Analysis: A Critical Overview of Relationships to Alternative Bonding Perspectives. *J. Comput. Chem.* **2012**, *33*, 2363–2379.

[41] Glendening, E. D.; Weinhold, F. Natural Resonance Theory. I. General Formalism. *J. Comput. Chem.* **1998**, *19*, 593–609.

[42] Glendening, E. D.; Weinhold, F. Natural Resonance Theory. II. Natural Bond Order and Valency. *J. Comput. Chem.* **1998**, *19*, 610–627.

[43] Glendening, E. D.; Badenhoop, J. K.; Weinhold, F. Natural Resonance Theory. III. Chemical Applications. *J. Comput. Chem.* **1998**, *19*, 628–646.

[44] Erben, M. F.; Padro, J. M.; Willner, H.; Della Vedova, C. O. Conformational and Structural Determination of F2NC(O)F and F2NC(O)NCO. A Joint Experimental and Theoretical Study. *J. Phys. Chem.* **2009**, *113A*, 13029–13035.

[45] Mack, H. G.; Oberhammer, H.; Della Védova, C. O. How Reliable are Ab Initio Calculations? Experimental and Theoretical Investigation of the Structure and Conformation of Chlorocarbonyl Isocyanate, ClC(O)NCO. *J. Mol. Struct.: THEOCHEM* **1989**, *59*, 277–288.

[46] Ramos, L. A.; Ulic, S. E.; Romano, R. M.; Vishnevskiy, Y. V.; Berger, R. J. F.; Mitzel, N. W.; Beckers, H.; Willner, H.; Tong, S.; Ge, M.; Della Vedova, C. O. Chlorodifluoroacetyl Isocyanate, $ClF_2CC(O)NCO$: Preparation and Structural and Spectroscopic Studies. *J. Phys. Chem.* **2012**, *116A*, 11586–11595.

[47] Mack, H. G.; Della Védova, C. O.; Willner, H. Structures and Conformations of Carbonyl Isocyanates and Carbonyl Azides. An Experimental and Theoretical Investigation. *J. Mol. Struct.* **1993**, *291*, 197–209.

[48] Mack, H. G.; Oberhammer, H.; Della Védova, C. O. Conformation and Structure of Acetyl Isocyanate, $CH_3C(O)NCO$, from Electron Diffraction and Microwave Data and Ab Initio Calculations. *J. Mol. Struct.* **1992**, *265*, 359–366.

[49] Typke, V.; Dakkouri, M.; Schlumberger, F. The Molecular Structure of Carbonyl Cyanide. *J. Mol. Struct.* **1980**, *62*, 111–120.

[50] Bent, H. A. An Appraisal of Valence-bond Structures and Hybridization in Compounds of the First-row Elements. *Chem. Rev. (Washington, DC, U. S.)* **1961**, *61*, 275–311.

(2-FLUORO-2,2-DINITROETHYL)-2,2,2-TRINITRO-ETHYLNITRAMINE: A POSSIBLE HIGH-ENERGY DENSE OXIDIZER

Thomas M. Klapötke, Burkhard Krumm, Sebastian F. Rest, Martin Reynders, Regina Scharf

as published in

European Journal of Inorganic Chemistry **2013**, 5871–5878.

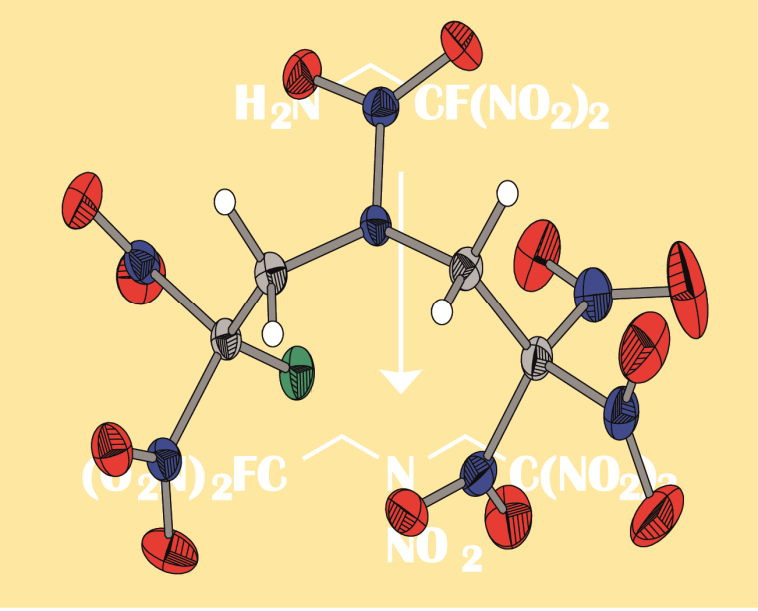

2.1 Abstract

The fluorine-containing polynitro energetic molecule (2-fluoro-2,2-dinitroethyl)-2,2,2-trinitroethylnitramine and the corresponding precursors were synthesized and investigated as potential high-energy dense oxidizers. The compounds have been characterized by using various analytical methods, single crystal X-ray diffraction, vibrational spectroscopy (IR and Raman), multinuclear NMR spectroscopy, elemental analysis, mass spectrometry and differential scanning calorimetry (DSC) measurements. The suitability of the compounds as potential oxidizers in energetic formulations has been investigated. In addition, the heats of formation of the products were calculated with the program package Gaussian 09. Several detonation parameters such as the detonation pressure, velocity, energy and temperature were computed using the EXPLO5 code. Furthermore, the sensitivity towards impact, friction and electrical discharge was determined using the German Federal Institute for Materials Research and Testing (BAM) drop hammer, a friction tester as well as a small-scale electrical discharge device.

2.2 Introduction

Ammonium perchlorate (AP) is a widely used oxidizer in solid-rocket propellants for civil applications. Unfortunately, this readily available and cheap compound comes along with several problems for the environment, such as the formation of large amounts of hydrogen chloride gas during the combustion of a solid rocket composite.[1] Therefore, it is important to drive research towards environmental friendly chlorine free compounds and to provide a large excess of oxygen for the combustion of the used aluminum fuel. Highly nitrated CHNO compounds were found to be useful as high energetic materials because of their good oxygen content.[1a,2]

The performance of solid-rocket boosters depends on the specific impulse as one of the most important parameters. It is proportional to the reciprocal of the molecular weight of the decomposition products M and the temperature inside the combustion chamber T_c during combustion of the composite.[3] An increase of the value for the specific impulse (I_s) by 20 s leads empirically to a doubling of the usual payload.[3a] Therefore, the development of new energetic oxidizers based on CHNO compounds decomposing into small volatile molecules as well as an increase of the temperature of combustion should enhance the specific impulse of modern solid rocket motors.

On the basis of previous investigations, compounds derived from 2-fluoro-2,2-dinitroethylamine and 2,2,2-trinitroethanol might be useful as starting materials for preparing new chlorine free potential high-energy dense oxidizers, which decompose in a more environmental friendly way, even though they contain the halogen fluorine.[1a,2a-c] The chemistry of 2,2,2-trinitroethanol is different to that of other alcohols due to the electron-withdrawing effect of the trinitromethyl group.[4] As a result the basicity of the hydroxyl group is decreased and it behaves acidic (pK_a= 6.1). At pH values above 6, the equilibrium is shifted towards the starting materials nitroform and formaldehyde.[2b,5] The amine 2-fluoro-2,2-dinitroethylamine shows also a decreased basicity due to the electronwithdrawing fluorodinitromethyl functionality (σ* = 4.4).[6] The σ* parameter indicates the influence of a substituent during a reaction through polar (inductive, field, and resonance) effects of organic compounds.[4,7] The most common way for synthesizing new compounds using 2,2,2-trinitroethanol as precursor is a Mannich-type reaction with amine moieties.

A detailed study of the synthesis and characterization of (2-fluoro-2,2-dinitroethyl)-2,2,2-trinitroethylnitramine and precursors is presented in this work. The compounds were investigated as potential high-energetic oxidizers based on the starting material 2-fluoro-2,2-dinitroethylamine, which is known since the 1960ies.[8]

2.3 Results and Discussion

2.3.1 Synthesis

The amine 2-fluoro-2,2-dinitroethylamine (**1**) was synthesized from 2-fluoro-2,2-dinitroethanol with aqueous ammonia (Scheme 2.1).[8a] stephanie.lucha@roche.com After distillation, the amine **1** must be handled very carefully. Therefore, an unexpected sudden deflagration occurs as a neat liquid within several hours at room temperature. Storage of **1** as solution in chloroform is recommended.

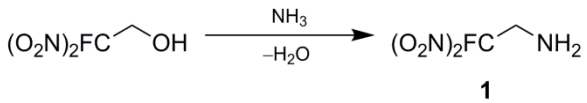

Scheme 2.1 Synthesis of 2-fluoro-2,3-dinitroethylamine (**1**).

The Mannich-type reaction of **1** with 2,2,2-trinitroethanol leads to the mixed secondary amine (2-fluoro-2,2-dinitroethyl)-2,2,2-trinitroethylamine (**2**). The reaction was carried out in chloroform, assisted by the use of molecular sieves (4 Å). Further nitration of compound

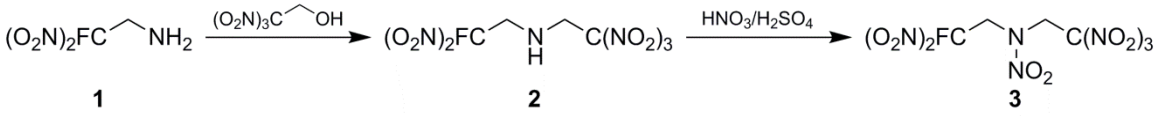

Scheme 2.2 Synthesis of compound **2** and **3** from 2-fluoro-2,2-dinitroethylamine (**1**).

2, using a mixture of nitric and sulfuric acid, gave the corresponding nitramine (2-fluoro-2,2-dinitroethyl)-2,2,2-trinitroethylnitramine (**3**) in good yields (Scheme 2.2).

2.3.2 Mulitnuclear NMR Spectroscopy

The compounds were thoroughly characterized by ^{1}H, ^{13}C{^{1}H}, ^{15}N and ^{19}F NMR spectroscopy. The ^{1}H NMR spectrum of compound **1** revealed the resonance of the CH_2 group as a doublet at δ = 3.92 ppm caused by the coupling with the adjacent fluorine atom ($^{3}J_{F,H}$ = 17.6 Hz). The amino resonance was observed broadened at δ = 1.49 ppm. In the ^{13}C NMR the resonance for the fluorodinitromethyl group was identified as a doublet at δ = 123.0 ppm with a coupling constant of $^{1}J_{C,F}$ = 287.5 Hz. The methylene carbon resonance occurred also as doublet at δ = 44.5 ppm ($^{2}J_{C,F}$ = 19.6 Hz). The amino nitrogen resonance of 2-fluoro-2,2-dinitroethylamine was observed at δ = −377.2 ppm in the ^{15}N NMR spectrum. Additionally, the nitrogen atoms of the nitro groups appeared at δ = −20.8 ppm as a doublet due to the ^{2}J coupling with fluorine ($^{2}J_{15N,F}$ = 15.0 Hz). The ^{19}F NMR spectrum showed a broadened resonance at δ = −111.1 ppm, because of the quadrupolar influence of ^{14}N in the nitro groups.

The ^{1}H NMR spectrum of (2-fluoro-2,2-dinitroethyl)-2,2,2-trinitroethylamine (**2**) showed different resonances for the two methylene groups. The doublet at δ = 4.31 ppm ($^{3}J_{H,H}$ = 7.8 Hz), which was caused by a ^{3}J coupling with the adjacent NH moiety, was assigned to the trinitroethyl group of **2**. The resonance of the CH_2CFC$(NO_2)_2$ moiety appeared as a doublet of doublets at δ = 4.10 ppm owing to an additional $^{3}J_{H,F}$ coupling with coupling constants of $^{3}J_{H,H}$ = 7.3 Hz and $^{3}J_{H,F}$ = 16.6 Hz. The NH resonance was observed as a quintet at δ = 2.55 ppm. In the ^{13}C NMR spectrum the resonance of the trinitromethyl carbon was typically found as a broadened resonance at δ = 126.2 ppm.

The fluorodinitromethyl carbon resonance was found at δ = 121.3 ppm as doublet with a $^{1}J_{C,F}$ coupling constant of 288.3 Hz. As expected, the resonances of the CH_2 moieties were observed as a singlet at δ = 52.5 ppm [CH$_2$C$(NO_2)_3$], and as a doublet at δ = 50.8 ppm [CH$_2$CF$(NO_2)_2$; $^{2}J_{C,F}$ = 19.2 Hz], respectively. The ^{15}N NMR spectrum showed the nitro resonances of two different polynitromethyl moieties as a doublet of multiplets at δ = −22.9 ppm [CF(NO$_2$)$_2$; $^{2}J_{N,F}$ = 14.9 Hz] for the fluorodinitromethyl moiety and the trinitromethyl functionality as a triplet at δ = −32.3 ppm [C(NO$_2$)$_3$; $^{3}J_{N,H}$ = 2.0 Hz]. The amine

resonance appeared as a doublet at δ = −373.0 ppm owing to the direct $^{1}J_{N,H}$ coupling with 83.0 Hz.

The resonances of the two methylene groups in the ^{1}H NMR spectrum of **3** were identified as a singlet at δ = 6.14 ppm for the trinitroethyl moiety and at δ = 5.80 ppm as doublet with a $^{3}J_{H,F}$ coupling constant of 9.5 Hz for the fluorodinitroethyl group. Similar to **2**, at δ = 124.2 ppm a broadened singlet appears in the ^{13}C NMR spectrum for the trinitromethyl carbon and the fluorodinitromethyl carbon was identified as a doublet at δ = 118.6 ppm ($^{1}J_{C,F}$ = 294.0 Hz). The methylene carbon connected to the trinitromethyl moiety was found as a singlet at δ = 55.2 ppm, and a doublet at δ = 55.0 ppm was assigned to the second methylene group adjacent to the fluorodinitromethyl group with a $^{2}J_{C,F}$ coupling constant of 16.1 Hz. The ^{19}F NMR spectrum showed a broadened resonance appearing as triplet at δ = −107.1 ppm. In the ^{15}N NMR spectrum the different polynitro moieties as well as the newly introduced nitramine functionality were detected (Figure 2.1). The resonance at δ = −22.5 ppm was assigned to the nitrogen atoms of the fluorodinitromethyl group. As a result of the $^{3}J_{N,H}$ = 1.7 Hz coupling with the attached methylene hydrogen and an additional $^{2}J_{N,F}$ = 15.2 Hz coupling, this resonance is split into a doublet of triplets. Owing to the $^{3}J_{N,H}$ coupling of 2.0 Hz, the resonance of the C(NO_2)$_3$ moiety was found as a triplet at δ = −33.7 ppm. The nitramine group showed two resonances, a quintet at δ = −33.4 ppm for the nitro group ($^{3}J_{N,H}$ = 3.2 Hz, coupling to four hydrogen atoms of the two methylene groups), and the amine nitrogen resonance was identified as a singlet at δ = −217.2 ppm.

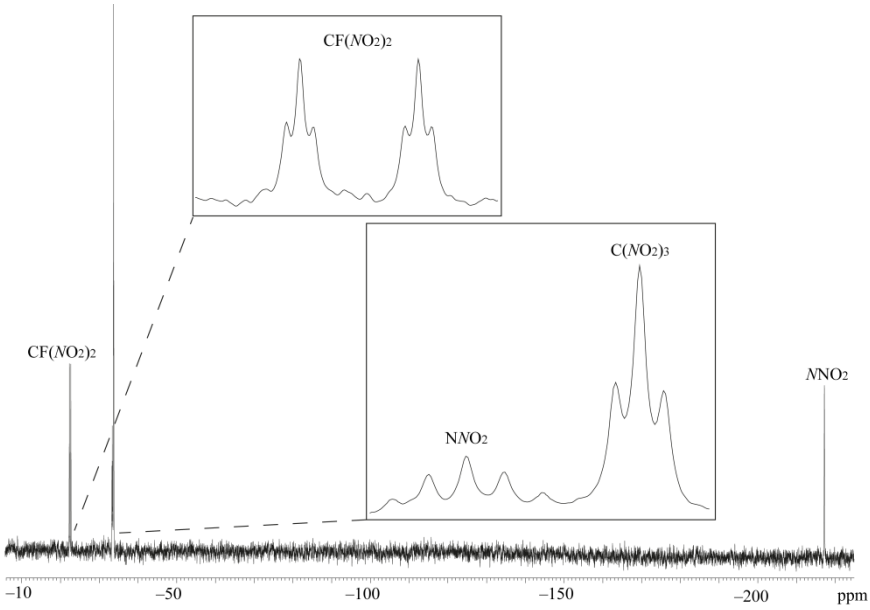

Figure 2.1 ^{15}N NMR spectrum of (2-fluoro-2,2-dinitroethyl)-2,2,2-trinitroethylnitramine (**3**) in [D_6]acetone.

2.3.3 Vibrational Spectroscopy

The vibrational spectra of **1**–**3** showed the characteristic asymmetric stretching vibrations $\nu_{as}(NO_2)$ in the range of 1614–1579 cm^{-1} and the symmetric stretching vibrations $\nu_s(NO_2)$ at 1316–1270 cm^{-1} (Table 2.1). The two different polynitro moieties (trinitromethyl/fluorodinitromethyl moiety) might cause the observed spread of the $\nu_{as}(NO_2)$ vibration energies. For compounds **1** and **2** the N–H stretching vibrations of the amine moieties were observed in the range of 3428–3361 cm^{-1}. The C–N, C–O, C–F and C–C vibrations of **1**–**3** could be observed in the typical ranges for CHFNO compounds, respectively.[9]

Table 2.1 IR and Raman bands of carbonyl and nitro groups for **1**–**3**.

	1		**2**		**3**	
	IR	**Raman**	**IR**	**Raman**	**IR**	**Raman**
ν(NH)	3428 (w) 3364 (w)	3361 (9)	3368 (w)	3368 (4)		
$\nu_{as}(NO_2)$	1581 (vs)	1588 (18)	1579 (vs)	1312 (23) 1601 (22) 1585 (18)	1591 (vs)	1614 (22) 1589 (10) 1566 (5)
$\nu_s(NO_2)$	1281 (m)	1310 (18)	1305 (s) 1245 (m)	1311 (30) 1247 (12)	1316 (m) 1270 (w)	1300 (16) 1271 (44)

Frequencies in cm^{-1}; IR intensities: vs = very strong, s = strong, m = medium, w = weak; Raman intensities at 300 mW in brackets.

2.3.4 X-Ray Diffraction

The compounds **2** and **3** were investigated by low-temperature single-crystal X-ray diffraction. The crystal and structure refinement data of the structure determinations are given in Table 2.2. Suitable single crystals for X-ray diffraction measurements were obtained by slow evaporation of chloroform. The bond lengths and angles of compound **2** and **3** are comparable with previously discussed values for CHNO-compounds containing a trinitromethyl moiety.[3b,10] Additional data on intermolecular interactions of **2**–**3** are given in the Appendix A2.

The molecular structure of (2-fluoro-2,2-dinitroethyl)-2,2,2-trinitroethylamine (**2**) is shown in Figure 2.2. Compound **2** crystallizes in the orthorhombic space group $Pna2_1$ with eight formula units per unit cell and a density of 1.89 g cm^{-1} at 173 K. The average N–O bond lengths of the trinitromethyl and the fluorodinitromethyl moieties are 1.217 Å for the two molecules in the asymmetric unit. For the top molecule, there is a typical propeller-type

Table 2.2 Crystal and structure refinement data for **2** and **3**.

	2	**3**
formula	$C_4H_5FN_6O_{10}$	$C_4H_4FN_7O_{12}$
Formula mass [g mol^{-1}]	316.12	361.11
Temperature [K]	173	173
Crystal size [mm]	0.40 × 0.18 × 0.03	0.20 × 0.06 × 0.02
Crystal description	colorless platelet	colorless needle
Crystal system	orthorhombic	orthorhombic
Space group	$Pna2_1$	$Pna2_1$
a [Å]	18.5686(10)	16.8034(5)
b [Å]	5.9732(4)	6.1707(2)
c [Å]	20.0793(15)	11.8499(4)
β [°]	90	90
V [Å^3]	2227.1(3)	1228.70(7)
Z	8	4
ρ_{calc} [g cm^{-3}]	1.8856(3)	1.9522(1)
μ [mm^{-1}]	0.195	0.204
$F(000)$	1280	728
θ range [°]	4.12–30.00	4.21–30.07
index ranges	$-19 \le h \le 26$	$-23 \le h \le 23$
	$-7 \le k \le 8$	$-8 \le k \le 8$
	$-28 \le l \le 27$	$-16 \le l \le 16$
Reflections collected	14438	15575
Reflections observed	6265	3599
Reflections unique	5149	3119
$R1$, $wR2$ (2σ data)	0.0410, 0.0856	0.0346, 0.0719
$R1$, $wR2$ (all data)	0.0576, 0.0952	0.0450, 0.0778
max. / min. transmission	1.00000/0.89677	1.00000/0.93078
Data/restraints/parameters	6265/1/387	3599/0/217
GoF on F^2	1.042	1.030
Largest diff. peak/hole [e Å^{-3}]	0.310/–0.253	0.332/–0.317

orientation of the trinitromethyl moiety with C2–C1–N–O torsion angles between 31.0(3)°and 51.7(3)°. The bottom molecule shows a comparable structure of the trinitromethyl moiety with a contrary sense of rotation [C6–C5–N–O: –55.8(3)° to –35.5(3)°]. The orientation of the fluorodinitromethyl moieties also indicates a propeller-like structure.[9c] The C–C–N–O torsion angles of these four nitro groups [26.2(3)°/ –27.5(3)°/–36.7(3)°/65.9(3)°] are within the typical range for a propeller like structure of polynitromethyl moieties (23–67°).[9c] Several weak intermolecular improper hydrogen bonds might be a reason for the quite high density of **2**.

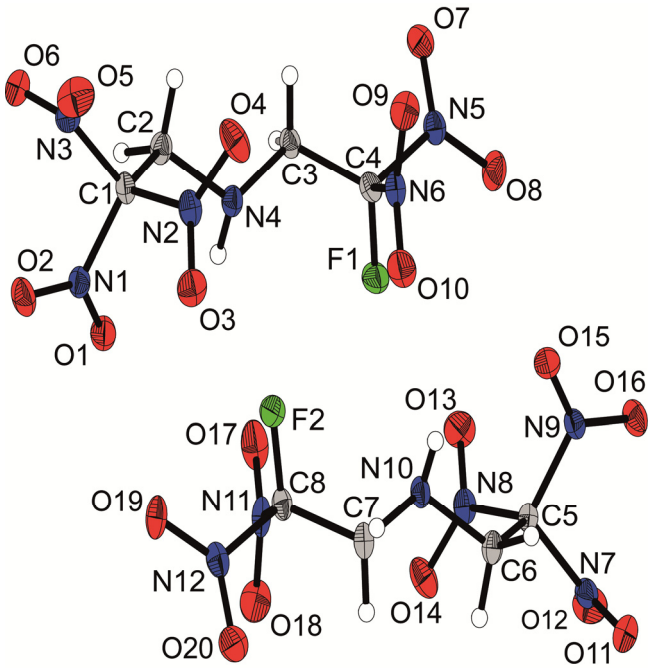

Figure 2.2 Molecular structure of amine (2-fluoro-2,2-dinitroethyl)-2,2,2-trinitroethylamine (**2**). Thermal ellipsoids are shown at the 50% probability level. Selected distances [Å] and angles [°]: C1–C2 1.522(3), C2–N4 1.455(3), C3–N4 1 459(3), C3–C4 1.510(3), C4–F1 1.325(2), C1–$(NO_2)_{avg.}$ 1.520, C4–$(NO_2)_{avg.}$ 1.537, C5–C6 1.523(3), C6–N10 1.460(3), C7–N10 1 454(3), C7–C8 1.506(3), C8–F2 1.328(3), C5–$(NO_2)_{avg.}$ 1.518(3), C8–$(NO_2)_{avg.}$ 1.536, C2–N4–C3 113.1(2), C3–C4–F1 113.2(2), C6–N10–C7 113.8(2), C7–C8–F2 113.3(2), C2–C1–N1–O1 31.0(3), C2–C1–N2–O4 50.9(2), C2–C1–N3–O6 51.7(3), C3–C4–N5–O7 26.2(3), C3–C4–N6–O9 –64.9(2), C6–C5–N7–O11 –35.5(3), C6–C5–N8–O14 –55.8(2), C6–C5–N9–O15 –36.7(3), C7–C8–N11–O18 65.9(3), C7–C8–N12–O20 –27.5(3).

(2-Fluoro-2,2-dinitroethyl)-2,2,2-trinitroethylnitramine (**3**) also crystallizes in the orthorhombic space group *Pna*2_1 with four formula units in the unit cell (Figure 2.3). The density at 173 K was calculated with 1.95 g cm^{-1}. The average N–O bond length of the trinitromethyl moiety is 1.209 Å. The trinitromethyl moiety displays a molecular geometry with a propeller-type orientation of the nitro groups connected to C1.[9c] The twisted orientation is energetically favorable and leads to several N···O-dipolar interactions between the geminal NO_2 groups (range of 2.56–2.62 Å), which are considerably shorter than the

sum of the van der waals radii for nitrogen and oxygen (ca. 2.9 Å).[9c] The shorter distances are caused by the fact that such twisting of the nitro groups reduces the intramolecular electrostatic repulsion between the oxygen atoms, while at the same time optimizing the attractive N···O interactions between the geminal NO_2 groups.[9c] The average fluorodinitromethyl moiety C1F1$(NO_2)_2$ N–O bond length [1.214(4) Å] is comparable to that of the trinitromethyl group. The C2–C1–N–O torsion angles [–37.6(2)°/38.9(2)°] are also in the typical range (23–67°) of a propeller-type orientation of the nitro groups attached.[9c] At 1.226(3) Å, the averaged N–O distance of the nitramine moiety is slightly longer than the previously described polynitro groups. This might be caused by some shared π-electron density between the N–N bond and the N–O bonds of the nitramine moiety.[9c] The C3–N3–N4–O dihedral angles (–20.7°/1.3°) are in the typical range for cyclic nitramines like hexogen (RDX).[11] The C–F distance with 1.324(3) Å is comparable with a C–F single bond and typical for a fluorodinitromethyl moiety.[12]

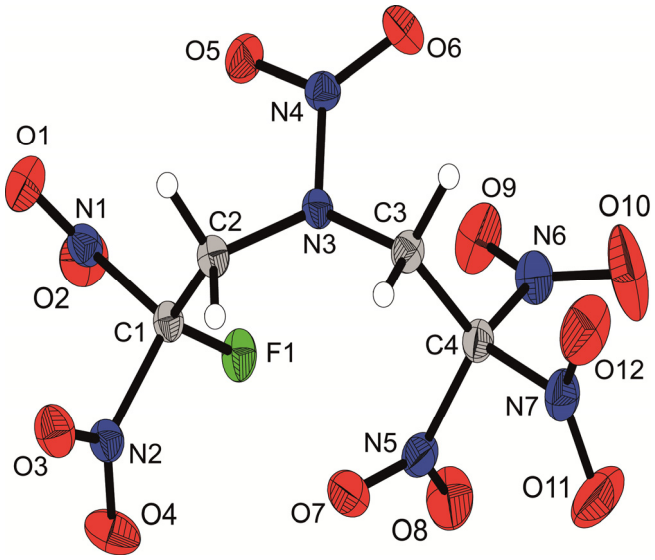

Figure 2.3 Molecular structure of (2-fluoro-2,2-dinitroethyl)-2,2,2-trinitroethylnitramine **3**. Thermal ellipsoids are shown at the 50% probability level. Selected distances [Å] and angles [°]: C1–C2 1.534(2), C1–F1 1.324(2), C1–$(NO_2)_{avg.}$ 1.544, C2–N3 1.457(2), N3–N4 1.383(2), N3–C3 1.454(2), C3–C4 1.529(2), C4–$(NO_2)_{avg.}$ 1.530, C2–C1–F1 114.3(1), C2–N3–N4 115.3(1), O6–N4–N3 118.2(1), C2–C1–N1–O1 –37.6(2), C2–C1–N2–O3 38.9(4), C2–N3–N4–O5 –20.7(2), C3–N3–N4–O6 1.3(2), C3–C4–N5–O7 –33.8(2), C3–C4–N6–O9 –64.2(2), C3–C4–N7–O12 –26.4(2).

2.3.5 Thermal and Energetic Properties

The compounds **2** and **3** are stable when exposed to air and moisture. As indicated earlier, amine **1** decomposes violently within hours as neat compound at ambient temperature. Thermal stabilities for **1**–**3** were investigated with various DSC measurements (heating rate: 5 °C min^{-1}). The melting point of compound **1** was determined roughly at –11 °C.

Decomposition starts at 80 °C. The melting points were rising from 37 °C for **2** to 87 °C for **3**. Decomposition becomes significant for compound **2** at 121 °C and 162 °C for **3**. The investigated physical and chemical properties are shown in Table 2.3.

The sensitivities towards impact, friction and electrostatic discharge for **2** and **3** were determined experimentally according to standards of the Federal Institute for Materials Research and Testing (BAM)[13] and the results are displayed in Table 2.4. The compounds **2** and **3** showed comparable impact sensitivity values with 6 J for **2** and 5 J for **3**, respectively. The friction sensitivity was determined with 360 N for compound **2**. Nitration to **3** decreased the stability towards friction to 144 N. Amine **1** was omitted from the determination of the sensitivities owing to its instability as neat liquid.

Table 2.3 Physical and chemical properties of **1**–**3**.

	1	**2**	**3**
Formula	$C_2H_4FN_3O_4$	$C_4H_5FN_6O_{10}$	$C_4H_4FN_7O_{12}$
MW [g mol^{-1}]	153.07	316.12	361.11
T_m [°C][a]	–11	37	82
T_d [°C][b]	80	121	162
N [%][c]	27.45	26.59	27.15
$N + O$ [%][d]	69.26	77.20	80.32
Ω_{CO} [%][e]	5.2	20.2	28.8
Ω_{CO2} [%][f]	–15.7	0	11.1
ρ [g cm^{-3}][g]	1.80	1.79	1.85
$-\Delta U°_f$ [kJ kg^{-1}][h]	1631.8	821.7	575.9
$-\Delta H°_f$ [kJ mol^{-1}][i]	264.7	287.0	238.8

[a] Melting (T_m) point from DSC measurement carried out at a heating rate of 5 °C min^{-1}. [b] Decomposition (T_d) point from DSC measurement carried out at a heating rate of 5 °C min^{-1}. [c] Nitrogen content. [d] Combined nitrogen and oxygen content. [e] Oxygen balance assuming the formation of CO. The oxygen balance of ammonium perchlorate is 34.0% [f] Oxygen balance assuming the formation of CO_2. [g] Experimental density from pycnometer measurement. [h] Calculated energy of formation at 298 K. [i] Calculated heat of formation at 298 K.

Predictions of the detonation parameters using the EXPLO5 code[14] were performed based on heats of formations calculated ab initio using the Gaussian 09 program package[15] at the CBS-4M level of theory. Energetic parameters are attributed to the density of the corresponding compound at ambient temperature. The resulting heats of detonation (Q_v), detonation temperatures (T), pressures (p) and velocities (D) for **1**–**3** are shown in the Table 2.4. The densities needed for the estimation of the detonation parameters with the EXPLO5 code[14] were derived from experimental determinations *via* pycnometer measurements for **2** and **3**. The calculated detonation velocities of **2** (8719 m s^{-1}) and **3**

(8673 m s^{-1}) are in the range of the known value for RDX (8750 m s^{-1}), and therefore both compounds might be useful as high-performing oxygen rich energetic materials.[16] The thermal stability rises from 80 °C (compound **1**) through 121 °C (compound **2**) to 162 °C for compound **3**.

The specific impulses of the compounds **1**–**3** were calculated for compositions of 70% oxidizer, 16% aluminum, 6% polybutadiene acrylic acid, 6% polybutadiene acrylonitrile and 2% bisphenol-A ether modeled on rocket-motor compositions for solid-rocket boosters used by the NASA Space Shuttle program.[17] These impulses were compared with the calculated impulse of AP in an analogous composition. The chosen mixture with AP as oxidizer provides a specific impulse of 258 sec. The impulses for **1**–**3** were increasing with increasing oxygen content (249–266 s). Nitramine **3** shows a superior specific impulse of 266 s relative to an analogous mixture with AP as oxidizer. The lesser oxygen balance of the compounds **1**–**3**, according to AP, also leads to a decreased oxygen balance for the calculated formulations that varies between –64.94% and –46.21%. A similar composition with AP as oxidizer has an oxygen balance of –30.1%.

Table 2.4 Predicted detonation and combustion parameters (using the EXPLO5 code) and sensitivity data for **1**–**3**.

	1	**2**	**3**
$-Q_v$ [kJ kg^{-1}]	5136	5733	5210
T_{ex} [K][a]	3535	4310	4104
V_0 [L kg^{-1}][b]	750	752	748
p [kbar][c]	315	368	354
D [m s^{-1}][d]	8496	8719	8637
Impact [J][e]	n.d.	6	5
Friction [N][e]	n.d.	360	144
ESD [J][f]	n.d.	0.1	0.1
Grain size [μm][g]	liquid	< 100	< 100
Thermal shock[h]	burns	burns	burns
I_s [s][i]	249	257	266
Ω_{comp} [%][j]	–64.94	–53.96	–46.21

[a] Temperature of the explosion gases. [b] Volume of the explosion gases (assuming only gaseous products). [c] Detonation pressure. [d] Detonation velocity. [e] Impact and friction sensitivities according to standard BAM methods.[13] n.d. = not determined. [f] Sensitivity towards electrostatic discharge. n.d. = not determined. [g] Grain size of the samples used for sensitivity tests. [h] Response to fast heating in the "flame test". [i] Specific impulse for compositions with 70% oxidizer, 16% aluminum, 6% polybutadiene acrylic acid, 6% polybutadiene acrylonitrile and 2% bisphenol-A ether at 70.0 bar chamber pressure using the EXPLO5 code[14]. The specific impulse for similar composition with ammonium perchlorate (I_s(AP) = 258 s, Ω_{comp}(AP)= –30.13%) has been calculated. [j] Oxygen balance for the composition used for combustion calculations.

2.4 Conclusion

Two new energetic polynitro compounds containing a fluorodinitromethyl moiety derived from 2-fluoro-2,2-dinitroethylamine (**1**) with a high positive oxygen balance were synthesized and characterized using multinuclear NMR, vibrational spectroscopy, elemental analysis and mass spectrometry and single-crystal X-ray crystallography. The single-crystal X-ray structures revealed a typical propeller like orientation of the trinitromethyl moiety for both the secondary amine **2** and the nitramine **3**. A rather high crystal density for **3** was found with 1.95 g cm^{-3}, which is comparable with hexogen (RDX).[1b] The calculated detonation velocities of **2** (8719 m s^{-1}) and **3** (8673 m s^{-1}) are slightly below the literature known value for RDX (8750 m s^{-1}).[16] The thermal stability rises from 80 °C (compound **1**) through 121 °C (compound **2**) to 162 °C for compound **3**. The sensitivities of **2**–**3** with 6 J for **2** and 5 J for **3** are slightly less than pentaerythritol tetranitrate (PETN), which is a basic requirement for new compounds to be meant as potential high energy dense oxidizers.[1b,3a] Surprisingly, compound **2** turned out to be insensitive towards friction. With respect to a possible application as high-energy dense oxidizer in solid rocket boosters, the specific impulses (I_s) of **1**–**3** were calculated in formulations with fuel, oxidizer & additives. Compound **3** in particular turned out to be a quite promising oxidizer with a superior specific impulse of 266 s relative to similar formulations with ammonium perchlorate (AP) [I_s(AP) = 258 s] and acceptable sensitivities as a neat compound. Apart from the high specific impulse of **3**, compound **2** showed a comparable value to an AP composite. This promising result makes secondary amine **2** interesting as potential precursor for further reactions in the course of developing new potential high-energy dense oxidizers.

2.5 Experimental Section

General Procedures

The syntheses and manipulation of air- and moisture-sensitive materials were performed in an inert atmosphere of dry argon (purity 5.0 Air Liquide) using flame-dried glass vessels and Schlenk techniques.[18] Commercial available chemicals (all Sigma Aldrich) were used as received. 2,2,2-Trinitroethanol and 2-fluoro-2,2-dinitroethanol were prepared according to literature known procedures.[2b,2c,8a,10c,19]

Raman spectra were recorded with a Bruker FT-Raman MultiRAM Spectrometer equipped with a Klaastech DENICAFC LC-3/40 laser source at 300mW laser power; infrared spectra were measured with a Perkin–Elmer Spectrum BX-FTIR spectrometer equipped

with a Smiths DuraSamplIR II ATR device. All spectra were recorded at ambient temperature as neat samples. Densities were determined at ambient temperature using a Quantachrome Ultrapyc1200e gas pycnometer equipped with helium (5.6 Air Liquide). NMR spectra were recorded with a JEOL Eclipse 400 instrument and chemical shifts were determined with respect to external Me_4Si (^1H, 399.8 MHz; ^{13}C, 100.5 MHz), $MeNO_2$ (^{15}N, 40.6 MHz) and CCl_3F (376.5 MHz). Mass spectrometric data were obtained with a JEOL MStation JMS 700 spectrometer (DEI+/DCI+). Analyses of C/H/N were performed with an Elementar Vario EL Analyzer. Melting points were measured with a Perkin-Elmer Pyris6 DSC using a heating rate of 5 °C min^{-1} and checked by a Büchi Melting Point B-540 apparatus; they are not corrected. The sensitivity data were performed using a BAM drophammer and a BAM friction tester.[13]

Computational Details

All ab initio calculations were carried out using the Gaussian 09 (Revision B.03) program package[15b] and visualized by GaussView 5.08.[15a] Structure optimizations and frequency analyses were performed with Becke's B3 three parameter hybrid functional using the LYP correlation functional (B3LYP). For C, H, N and O a correlation consistent polarized double-zeta basis set was used (cc-pVDZ). The structures were optimized without symmetry constraints and the energy is corrected with the zero point vibrational energy.[20]

The enthalpies (H°) and free energies (G°) were calculated and finally corrected to a temperature of 298 K using the complete basis set method (CBS-4M) on the basis of ab initio optimized structures or X-ray diffraction data to obtain accurate values.[20a] The CBS models use the known asymptotic convergence of a pair of natural orbital expressions to extrapolate from calculations using a finite basis set to the estimated complete basis set limit. CBS-4 starts with a HF/3-21G(d) structure optimization, which is the initial guess for the following self-consistent field (SCF) calculation as a base energy and a final MP2/6-31+G calculation with a CBS extrapolation to correct the energy in second order. The used reparametrized CBS-4M method additionally implements a MP4(SDQ)/6-31+(d,p) calculation to approximate higher order contributions and also includes some additional empirical corrections.[20b,20c] The enthalpies of the gas-phase species were estimated according to the atomization energy method.[20a,21]

All calculations affecting the detonation parameters were carried out using the program package EXPLO5 V6.01.[14,22] The detonation parameters were calculated at the CJ point with the aid of the steady-state detonation model using a modified Becker-Kistiakowski-Wilson equation of state for modeling the system. The CJ point is found from the Hugoniot curve of the system by its first derivative.[22,23] The main detonation products for the calculations of

the energetic parameters were assumed with N_2, H_2O, CO_2 and HF for a CHFNO-compound. In addition, compounds with a positive oxygen balance provide O_2 as combustion product. The specific impulses were also calculated with the EXPLO5 program, assuming an isobaric combustion of a composition of 70% oxidizer, 16% aluminum as fuel, 6% polybutadiene acrylic acid, 6% polybutadiene acrylonitrile as binder and 2% bisphenol-A as epoxy curing agent.[17] A chamber pressure of 70.0 bar and an ambient pressure of 1.0 bar with frozen expansion conditions were estimated for the calculations.

X-ray Crystallography

For all compounds, an Oxford Xcalibur3 diffractometer with a CCD area detector was employed for data collection using Mo-K_α radiation (λ = 0.71073 Å). The structures were solved by direct methods (SIR97)[24] and refined by full-matrix least-squares on F^2 (SHELXL).[25] All non-hydrogen atoms were refined anisotropically. The hydrogen atoms were located in a difference Fourier map and placed with a C–H distance of 0.99 Å for CH_2 groups. ORTEP plots are shown with thermal ellipsoids at the 50% probability level.

CCDC-946430 (for **2**) and CCDC-946431 (for **3**) contains the supplementary crystallographic data for this paper. These data can be obtained free of charge from the Cambridge Crystallographic Data Centre *via* www.ccdc.cam.ac.uk/data_request/cif.

Synthesis

CAUTION! All high-nitrogen- and -oxygen-containing compounds are potentially explosive energetic materials. In particular, 2-fluoro-2,2-dinitroethylamine (**1**) was proven to be a dangerous unstable material, when handled as neat compound. Especially with this compound, this necessitates additional meticulous safety precautions (earthed equipment, Kevlar gloves, Kevlar sleeves, face shield, leather coat, and ear plugs). In addition, 2,2,2-trinitroethanol and 2-fluoro-2,2-dinitroethylamine show significant degrees of toxicity,[26] including own recent results.[27] Particular care should be exercised in handling of those materials and derivatives.

2-Fluoro-2,2-dinitroethylamine (**1**)

Prepared according to the literature.[8a,28].

DSC (5 °C min^{-1}, onset): T_m = approx. –11 °C, T_{dec} = 80 °C. ^{1}H NMR ($CDCl_3$) δ = 3.92 [d, 2H, CH_2CF(NO_2)$_2$, $^3J_{H,F}$ = 17.6 Hz], 1.49 (s, br, 2H, NH_2) ppm. ^{13}C{^{1}H} NMR ($CDCl_3$) δ = 123.0 [d, *C*F(NO_2)$_2$, $^1J_{C,F}$ = 287.5 Hz], 44.5 [d, *C*H_2CF(NO_2)$_3$, $^2J_{C,F}$ = 19.6 Hz] ppm. ^{15}N{^{1}H} NMR ($CDCl_3$) δ = –20.77 [d, CF(*N*O_2)$_2$, $^2J_{N,F}$ = 15.0 Hz], –377.20 (s, *N*H_2) ppm. ^{19}F NMR ($CDCl_3$) δ = –111.1 [br. s, C*F*(NO_2)$_2$] ppm. IR (ATR) ν = 3428 (w), 3364 (w), 2916 (w), 1581 (vs), 1434 (w), 1318

(m), 1281 (m), 1193 (w), 1088 (w), 1052 (w), 990 (w), 849 (w), 786 (m), 686 (w) cm^{-1}. Raman (300 mW) ν = 3361 (9), 3003 (15), 2942 (33), 2860 (4), 2202 (3), 1588 (18), 1436 (13), 1310 (18), 1190 (4), 978 (5), 852 (100), 564 (7), 504 (7), 418 (18), 381 (56), 320 (7), 282 (8) cm^{-1}. MS (DEI^+): m/z (%) = 154 (1) $[M + H]^+$, 106 (1) $[M + H - NO_2]^+$, 61 (1) $[M^+ - 2\ NO_2]$. Elemental analysis $C_2H_4FN_3O_4$ (153.07): calcd. C 15.69, H 2.63, N 27.45; found: C 15.82, H 2.59, N 227.35

2-Fluoro-2,2-dinitroethyl 2,2,2-trinitroethylamine (**2**)

2,2,2-Trinitroethanol (0.59 g, 3.2 mmol) and 2-fluoro-2,2-dinitroethylamine (0.50 g, 3.2 mmol) were diluted in chloroform (10 mL) under argon. Molecular sieves (4 Å, 0.5 g) were added and the reaction mixture was stirred at ambient temperature for 24 h. The reaction mixture was filtered, and the volatile materials were removed under vacuum yielding **2** as slightly orange colored oil. The crude product was recrystallized in chloroform giving colorless crystals of **2** (0.81 g, 78%).

DSC (5 °C min^{-1}, onset): T_m = 37 °C, T_{dec} = 121 °C. ^{1}H NMR ($CDCl_3$) δ = 4.31 [d, 2H, C*H*$_2$C(NO_2)$_3$, $^3J_{H,H}$ = 7.8 Hz], 4.10 [dd, 2H, C*H*$_2$CF(NO_2)$_2$, $^3J_{H,H}$ = 7.3 Hz, $^3J_{H,F}$ = 16.6 Hz], 2.55 [qi, 1H, N*H*] ppm. ^{13}C{^{1}H} NMR ($CDCl_3$) δ = 126.2 [br., *C*(NO_2)$_3$], 121.3 [d, *C*F(NO_2)$_2$, $^1J_{C,F}$ = 288.3 Hz], 52.5 [*C*H$_2$C(NO_2)$_3$], 50.8 [d, *C*H$_2$CF(NO_2)$_3$, $^2J_{C,F}$ = 19.2 Hz] ppm. ^{15}N NMR ($CDCl_3$) δ = –22.9 [dm, CF*N*O$_2$)$_2$, $^2J_{N,F}$ = 14.9 Hz], –32.3 [t, C(*N*O$_2$)$_3$, $^3J_{N,H}$ = 2.0 Hz], –373.0 (d, *N*H, $^1J_{N,H}$ = 83.0 Hz) ppm. ^{19}F NMR ($CDCl_3$): δ = –109.6 [br. t, C*F*(NO_2)$_2$, $^3J_{F,H}$ = 15.6 Hz] ppm. IR (ATR) ν = 3368 (w), 2933 (w), 2895 (w), 1579 (vs), 1479 (m), 1443 (m), 1403 (w), 1371 (w), 1358 (w), 1338 (w), 1305 (s), 1243 (m), 1154 (m), 1138 (m), 1063 (w), 999 (w), 981 (w), 879 (w), 857 (w), 850 (m), 799 (m), 780 (m), 757 (m), 725 (m), 667 (w) cm^{-1}. Raman (300 mW) ν = 3368 (4), 3024 (10), 3012 (11), 2983 (16), 2937 (74), 2886 (6), 1612 (23), 1601 (22), 1585 (18), 1483 (4), 1447 (18), 1405 (12), 1373 (20), 1359 (53), 1311 (30), 1247 (12), 1148 (11), 1037 (10), 995 (7), 911 (11), 881 (9), 859 (100), 851 (27), 809 (4), 783 (5), 763 (7), 668 (5), 642 (9), 576 (9), 523 (15), 471 (8), 440 (20), 421 (48), 399 (49), 381 (65), 368 (47), 330 (26), 281 (20), 263 (35), 210 (36) cm^{-1}. MS (DEI^+): m/z (%) = 316.1 (1) $[M^+]$, 269 (1) $[M^+ - HNO_2]$, 224 (1) $[M^+ - 2\ NO_2]$, 193 (29) $[NHCH_2C(NO_2)_3]^+$, 166 (29) $[NHCH_2CF(NO_2)_2]^+$, 115 $[C_4H_4FN_2O]^+$, 147 (29) $[NHCH_2C(NO_2)_2]^+$, 85 $[C_4H_4FN]^+$, 46 (100) $[NO_2]^+$, 30 (100) $[NO]^+$. Elemental analysis $C_4H_5FN_6O_{10}$ (316.12): calcd. C 15.20, H 1.59, N 26.59; found: C 15.50, H 1.61, N 26.29. IS: 6 J; FS: 360 N; ESD: 0.1 J; grain size: < 100 µm.

2-Fluoro-2,2-dinitroethyl 2,2,2-trinitroethylnitramine (**3**)

Compound **2** (0.68 g, 2.2 mmol) was added slowly into a mixture consisting of sulfuric acid (96%, 4 mL) and nitric acid (100%, 2 mL) at 0 °C. The reaction mixture was stirred at ambient temperature for 4 h and poured onto a large excess of ice (200 g). The colorless precipitate was filtered, washed with water and dried in vacuo to obtain a colorless powder of **3** (0.59 g, 76%). Alternatively, crude **2** (yellow oil) is sufficient and can be used for the nitration without loss of product.

DSC (5 °C min^{-1}, onset): T_m = 85 °C, T_{dec} = 165 °C. ^{1}H NMR ([D$_6$]acetone) δ = 6.14 [s, 2H, C*H*$_2$C(NO$_2$)$_3$], 5.80 [d, 2H, C$_2$CF(NO$_2$)$_2$, $^3J_{H,F}$ = 9.5 Hz] ppm. ^{13}C{^{1}H} NMR ([D$_6$]acetone) δ = 124.2 [s, *C*(NO$_2$)$_3$], 118.6 [d, *C*F(NO$_2$)$_2$, $^1J_{C,F}$ = 294.0 Hz], 55.2 [s, *C*H$_2$C(NO$_2$)$_3$], 55.0 [d, *C*H$_2$CF(NO$_2$)$_3$, $^2J_{C,F}$ = 16.1 Hz] ppm. ^{15}N NMR ([D$_6$]acetone) δ = –22.5 [dt, CF(*N*O$_2$)$_2$, $^2J_{N,F}$ = 15.2 Hz, $^3J_{N,H}$ =1.7 Hz], –33.4 [q, N*N*O$_2$, $^3J_{N,H}$ = 3.2 Hz], –33.7 [t, C(*N*O$_2$)$_3$, $^3J_{N,H}$ = 2.0 Hz], –217.2 (s, *N*NO$_2$) ppm. ^{19}F NMR ([D$_6$]acetone) δ =–107.1 [t, C*F*(NO$_2$)$_2$, $^3J_{F,H}$ = 9.1 Hz] ppm. IR (ATR) ν = 3371 (vw), 2965 (vw), 2926 (vw), 1707 (w), 1591 (vs), 1492 (vw), 1465 (w), 1444 (vw), 1359 (w), 1316 (s), 1270 (w), 1229 (w), 1182 (vw), 1052 (vs), 949 (vw), 905 (w), 849 (m), 800 (s), 763 (w), 737 (m), 701 (vw), 686 (w) cm^{-1}. Raman (300 mW) ν = 3024 (24), 2978 (53), 1614 (24), 1589 (10), 1566 (5), 1439 (5), 1407 (6), 1391 (14), 1358 (50), 1340 (15), 1300 (16), 1271 (44), 1228 (3), 1128 (3), 1058 (4), 1002 (2), 978 (11), 878 (3), 868 (15), 854 (100), 804 (2), 784 (5), 755 (2), 723 (4), 626 (10), 545 (12), 442 (8), 425 (18), 402 (31), 388 (17), 369 (11), 341 (9), 324 (49), 247 (14), 221 (11), 209 (6) cm^{-1}. MS (DEI$^+$): m/z (%) = 361 (1) [M$^+$], 269 (1) [M$^+$ – 2 NO$_2$], 211 (1) [M$^+$ – C(NO$_2$)$_3$], 118 (29) [CH$_2$C(NO$_2$)$_2$]$^+$, 46 (100) [NO$_2$]$^+$. Elemental analysis C$_4$H$_4$FN$_7$O$_{12}$ (361.11): calcd. C 13.30, H 1.12, N 27.15; found: C 13.40, H 1.20, N 26.3. IS: 5 J; FS: 192 N; ESD: 0.1 J; grain size: < 100 µm.

2.6 References

[1] a) T. M. Klapötke, S. F. Rest, *New Trends Res. Energ. Mater. Proc. Semin*., 13th **2010**, Pt. 2, 642–651; b) J. P. Agrawal, *High Energy Materials Propellants, Explosives and Pyrotechnics*, 1st ed., Wiley-VCH, Weinheim, Germany, **2010**.

[2] a) M. E. Hill, US3306939, **1967**; b) M. Göbel, T. M. Klapötke, *Adv. Funct. Mater.* **2009**, *19*, 347–365; c) T. M. Klapötke, B. Krumm, R. Moll, *Chem. Eur. J.* **2013**, *19*, 12113–12123; d) T. M. Klapötke, B. Krumm, R. Moll, S. F. Rest, *Spectroscopic and structural studies of nitro substituted fluoro-methanes and ethanes*, 20th International Symposium on Fluorine Chemistry (ISFC), Kyoto, Japan, **2012**; e) T. M. Klapötke, B.

Krumm, R. Moll, S. F. Rest, W. Schnick, M. Seibald, *J. Fluorine Chem.* **2013**, DOI: 10.1016/j.jfluchem.2013.06.019.

[3] a) T. M. Klapötke, *Chemistry of High-Energy Materials*, 2nd Ed., de Gruyter, Berlin, **2012**; b) T. M. Klapötke, B. Krumm, R. Moll, S. F. Rest, *Z. Anorg. Allg. Chem.* **2011**, *637*, 2103–2110.

[4] J. Hine, J. W. Bailey, *J. Org. Chem.* **1961**, *26*, 2098–2099.

[5] T. N. Hall, *Tetrahedron* **1963**, *19*, 115–120.

[6] H. G. Adolph, *J. Org. Chem.* **1975**, *40*, 2626-2630.

[7] a) C. K. Ingold, *J. Chem. Soc. (Resumed)* **1930**, 1032-1039; b) L. A. Kaplan, H. B. Pickard, *J. Org. Chem.* **1970**, *35*, 2044-2045.

[8] a) H. G. Adolph, M. J. Kamlet, *J. Org. Chem.* **1969**, *34*, 45–50; b) L. V. Kustova, Y. I. Rubtsov, E. P. Kirpichev, L. T. Eremenko, R. G. Gafurov, A. G. Korepin, *Zh. Fiz. Khim.* **1976**, *50*, 1903–1904.

[9] a) A. B. Sheremetev, I. L. Yudin, *Mendeleev Commun*. **2005**, *15*, 204–205; b) G. Socrates, *Infrared and Raman Characteristic Group Frequencies: Tables and Charts*, 3rd ed., Wiley, Chichester, UK, **2004**; c) Y. Oyumi, T. B. Brill, A. L. Rheingold, *J. Phys. Chem.* **1985**, *89*, 4824–4828.

[10] a) M. Göbel, B. H. Tchitchanov, J. S. Murray, P. Politzer, T. M. Klapötke, *Nat. Chem.* **2009**, *1*, 229–235; b) M. Göbel, T. M. Klapötke, *Z. Anorg. Allg. Chem.* **2007**, *633*, 1006–1017; c) M. Göbel, T. M. Klapötke, *Acta Crystallogr. Sect. C* **2007**, *63*, o562–o564; d) M. Göbel, T. M. Klapötke, P. Mayer, *Z. Anorg. Allg. Chem.* **2006**, *632*, 1043–1050; e) S. K. Bhattacharjee, H. L. Ammon, *Acta Crystallogr. Sect. B* **1982**, *38*, 2503–2505.

[11] a) D. I. A. Millar, I. D. H. Oswald, C. Barry, D. J. Francis, W. G. Marshall, C. R. Pulham, A. S. Cumming, *Chem. Commun.* **2010**, *46*, 5662-5664; b) C. S. Choi, *Acta Crystallogr. Sect. B* **1972**, *28*, 2857–2862.

[12] a) H. L. Ammon, S. K. Bhattacharjee, *Acta Crystallogr. Sect. B* **1982**, *38*, 2718–2721; b) H. L. Ammon, S. K. Bhattacharjee, S. R. Hall, B. Skelton, *Acta Crystallogr. Sect. C* **1983**, *39*, 1565–1568; c) H. L. Ammon, S. K. Bhattacharjee, *Acta Crystallogr. Sect. C* **1984**, *40*, 487–490.

[13] Laying down test methods pursuant to Regulation (EC) No 1907/2006 of the European Parliament and of the Council on the Evaluation, Authorisation and Restriction of Chemicals (REACH), ABl. L 142, **2008**.

[14] M. Sućeska, *EXPLO5 V6.01*, Brodarski Institute, Zagreb, Croatia, **2012**.

[15] a) R. Dennington, T. Keith, J. Millam, GaussView, Version 5, Semichem Inc., Shawnee Mission KS, **2009**; b) M. J. Frisch, G. W. Trucks, H. B. Schlegel, G. E. Scuseria, M. A. Robb, J. R. Cheeseman, J. A. Montgomery Jr., T. Vreven, K. N. Kudin, J. C. Burant, J. M.

Millam, S. S. Iyengar, J. Tomasi, V. Barone, B. Mennucci, M. Cossi, G. Scalmani, N. Rega, G. A. Petersson, H. Nakatsuji, M. Hada, M. Ehara, K. Toyota, R. Fukuda, J. Hasegawa, M. Ishida, T. Nakajima, Y. Honda, O. Kitao, H. Nakai, M. Klene, X. Li, J. E. Knox, H. P. Hratchian, J. B. Cross, V. Bakken, C. Adamo, J. Jaramillo, R. Gomperts, R. E. Stratmann, O. Yazyev, A. J. Austin, R. Cammi, C. Pomelli, J. W. Ochterski, P. Y. Ayala, K. Morokuma, G. A. Voth, P. Salvador, J. J. Dannenberg, V. G. Zakrzewski, S. Dapprich, A. D. Daniels, M. C. Strain, O. Farkas, D. K. Malick, A. D. Rabuck, K. Raghavachari, J. B. Foresman, J. V. Ortiz, Q. Cui, A. G. Baboul, S. Clifford, J. Cioslowski, B. B. Stefanov, G. Liu, A. Liashenko, P. Piskorz, I. Komaromi, R. L. Martin, D. J. Fox, T. Keith, M. A. Al-Laham, C. Y. Peng, A. Nanayakkara, M. Challacombe, P. M. W. Gill, B. Johnson, W. Chen, M. W. Wong, C. Gonzalez, J. A. Pople, *Gaussian 09*, Rev. B.03, Gaussian, Inc., Wallingford CT, **2003**.

[16] P. W. Cooper, *Explosives Engineering*, 1st ed., Wiley-VCH, New York, **1996**.

[17] a) NASA, Space Shuttle News Reference, 2–20–22–21, http://de.scribd.com/doc/17005716/NASA-Space-Shuttle-News-Reference-1981; b) NASA, press release: STS-122 The Voyage of Columbus, 2008, 82–84, http://www.nasa.gov/pdf/203212main_sts122_presskit2.pdf.

[18] D. F. Shriver, M. A. Drezdzon, *The Manipulation of Air-Sensitive Compounds*, 2nd ed., Wiley, New York, **1986**.

[19] a) H. Feuer, T. Kucera, *J. Org. Chem.* **1960**, *25*, 2069–2070; b) V. Grakauskas, A. M. Guest, *J. Org. Chem.* **1978**, *43*, 3485–3488; c) H. Adolph, *J. Org. Chem.* **1972**, *37*, 747–751; d) N. S. Marans, R. P. Zelinski, *J. Am. Chem. Soc.* **1950**, *72*, 5329–5330.

[20] a) T. M. Klapötke, J. Stierstorfer, Phys. *Chem. Chem. Phys.* **2008**, *10*, 4340–4346; b) J. J. A. Montgomery, M. J. Frisch, J. W. Ochterski, G. A. Petersson, *J. Chem. Phys.* **2000**, *112*, 6532–6542; c) J. W. Ochterski, G. A. Petersson, J. J. A. Montgomery, *J. Chem. Phys.* **1996**, *104*, 2598–2619.

[21] a) E. F. C. Byrd, B. M. Rice, *J. Phys. Chem. A* **2005**, *110*, 1005–1013; b) B. M. Rice, S. V. Pai, J. Hare, *Combust. Flame* **1999**, *118*, 445–458; c) L. A. Curtiss, K. Raghavachari, P. C. Redfern, J. A. Pople, *J. Chem. Phys.* **1997**, *106*, 1063–1079.

[22] M. Sućeska, *Propellants, Explos. Pyrotech.* **1991**, *16*, 197–202.

[23] T. M. Klapötke, B. Krumm, F. X. Steemann, K. D. Umland, *Z. Anorg. Allg. Chem.* **2010**, *636*, 2343–2346.

[24] a) A. Altomare, M. C. Burla, M. Camalli, G. L. Cascarano, C. Giacovazzo, A. Guagliardi, A. G. G. Moliterni, G. Polidori, R. Spagna, *J. Appl. Crystallogr.* **1999**, *32*, 115–119; b) A. Altomare, G. Cascarano, C. Giacovazzo, A. Guagliardi, A. G. G. Moliterni, M. C. Burla, G. Polidori, M. Camalli, R. Spagna, *SIR97*, **1997**.

[25] a) A. L. Spek, *Acta Crystallogr. Sect. D* **2009**, *65*, 148–155; b) G. M. Sheldrick, *Acta Crystallogr. Sect. A 2008*, *64*, 112–122; c) L. J. Farrugia, *J. Appl. Crystallogr.* **1999**, *32*, 837–838; d) G. M. Sheldrick, *SHELX-97*, University of Göttingen, Göttingen (Germany), **1997**.

[26] a) A. L. Fridman, O. B. Kremleva, V. S. Zalesov, Z. V. Platonova, F. A. Gabitov, L. A. Rubinshtein, A. N. Plaksina, *Pharm. Chem. J.* **1977**, *11*, 64–67; b) M. B. Frankel, G. L.; Grant, L. R.; Kistner, R. L.; Lecce, J. V.; Wilson, E. R.; Woolery, D. O. I., *Process studies on nitroform and related compounds*, Final report for period January 30, **1984** – March 31, **1987**, UCRL-15908, Rockwell International Corp., Rocketdyne Division, Canoga Park, CA (USA), **1987**, 1–66.

[27] R. Scharf, T. M. Klapötke, Private communication, LMU Munich September **2012**.

[28] M. B. Frankel, G. L. Rowley, US3544630A, **1970**.

CONVENIENT SYNTHESIS OF NEW ENERGETIC POLYNITRO MATERIALS INCLUDING $(NO_2)_3CCH_2CH_2NH_3$-SALTS VIA MICHAEL ADDITION OF TRINITROMETHANE

Quirin J. Axthammer, Thomas M. Klapötke, Burkhard Krumm, Regina Scharf and Cornelia C. Unger

as published in

Dalton Transactions **2016**, DOI: 10.1039/c6dt03779h.

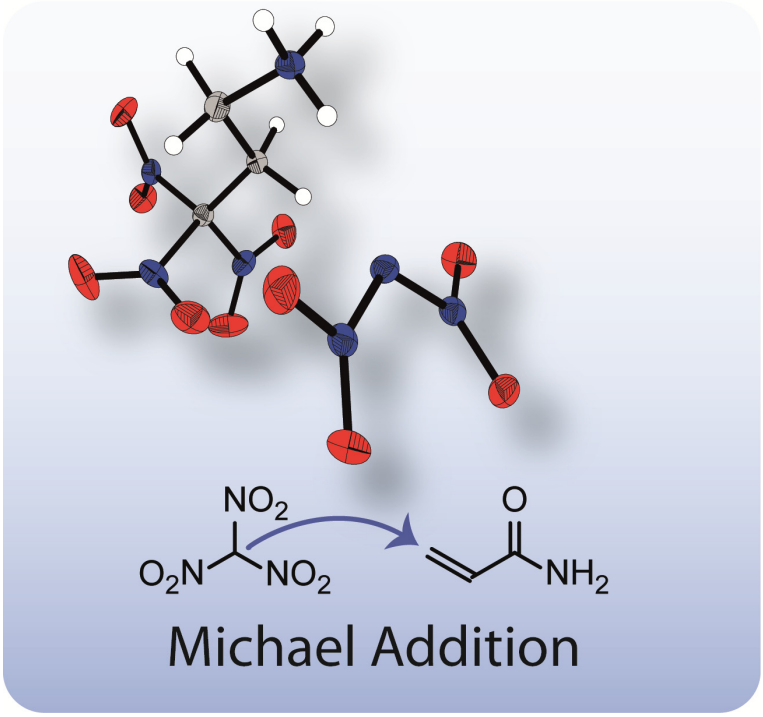

3.1 Abstract

The nucleophilic Michael addition of nitroform with acrylamide creates a variety of energetic products. Several interesting compounds with a trinitromethyl group were synthesized, among them salts containing the trinitropropylammonium cation, $[(NO_2)_3CCH_2CH_2NH_3]X$. Owing to their positive oxygen balance, the suitability of these compounds as potential high-energy dense oxidizers (HEDOs) in energetic formulations was investigated and discussed. Furthermore, numerous important and reactive compounds for the continuing synthesis of molecules with a high oxygen balance are presented. All compounds were fully characterized, including multinuclear NMR spectroscopy, vibrational analysis (IR, Raman), elemental analysis, as well as single crystal X-ray diffraction. Thermal stabilities were studied using differential scanning calorimetry and sensitivity data against friction, impact and electrostatic discharge were collected. The energies of formation were calculated using Gaussian 09 and energetic properties, such as the specific impulse and detonation velocity, were predicted with the EXPLO5 (V6.02) computer code.

3.2 Introduction

The trinitromethane (nitroform) unit is an important building block in the chemistry of high-energy materials, especially in the field of high-energy dense oxidizers (HEDOs).[1] This trinitromethane unit can easily be introduced by a nucleophilic addition on electron deficient α,β-unsaturated starting materials. The so-called Michael addition is one of the most important carbon–carbon bond forming reactions in synthetic organic chemistry. Michael donors are substrates with acidic protons which therefore are capable of forming carbanions. This includes anions from nitroform, fluorodinitromethane, primary nitroalkanes, and secondary nitroalkanes.[2] The electron deficient alkene in this nucleophilic addition is called the Michael acceptor and includes a wide range of α,β-unsaturated ketones, aldehydes, carboxylic acids, esters, amides and cyanides.[3] One such example is reported in the nucleophilic addition of some polynitroalkanes to acrolein oxime.[4]

In this contribution nitroform and the readily available acrylamide are used to build several new oxygen-rich molecules as well as energetic salts containing the $(NO_2)_3CCH_2CH_2NH_3$-cation.

3.3 Results and Discussion

3.3.1 Synthesis

Earlier investigations showed, that with tetranitromethane and various acrylamides, mostly mixtures of 3-nitroisoxazoles and Michael addition products were formed.[5] However, the reaction of acrylamide with nitroform resulted exclusively in the formation of the Michael addition product 4,4,4-trinitrobutanamide (**1**). A similar synthesis of **1** has been reported earlier.[6] However, in the herein presented advanced synthesis **1** was obtained without the use of further chemicals, as mentioned in literature procedures from readily available chemicals (Scheme 3.1).[6a,7] A further advantage is the faster conversion without heating, as well as increased yields from 63% to 97%. Due to the almost quantitative conversion of acrylamide, pure **1** without further purification was obtained. The acid 4,4,4-trinitrobutanoic acid (**2**) was prepared by hydrolysis of the amide **1** in aqueous concentrated hydrochloric acid. The crude material was recrystallized from chloroform to obtain a pure product in 80% yield. Due to their straightforward synthesis with high yields compounds **1** and **2** are excellent starting materials for various compounds containing the trinitromethyl moiety.[8] The acid **2** was converted to the corresponding carbonyl chloride by refluxing in excess thionyl chloride (Method A). The reaction time should be longer than 20 hours to ensure complete conversion to the acid chloride and to prevent the formation of the acid anhydride.[9] 4,4,4-Trinitrobutanoyl chloride (**3**) was isolated in 88% yield. A more convenient synthesis for the carbonyl chloride **3** is the conversion of acid **2** with a stoichiometric amount of oxalyl chloride and DMF as catalyst (Method B). Compound **3** was

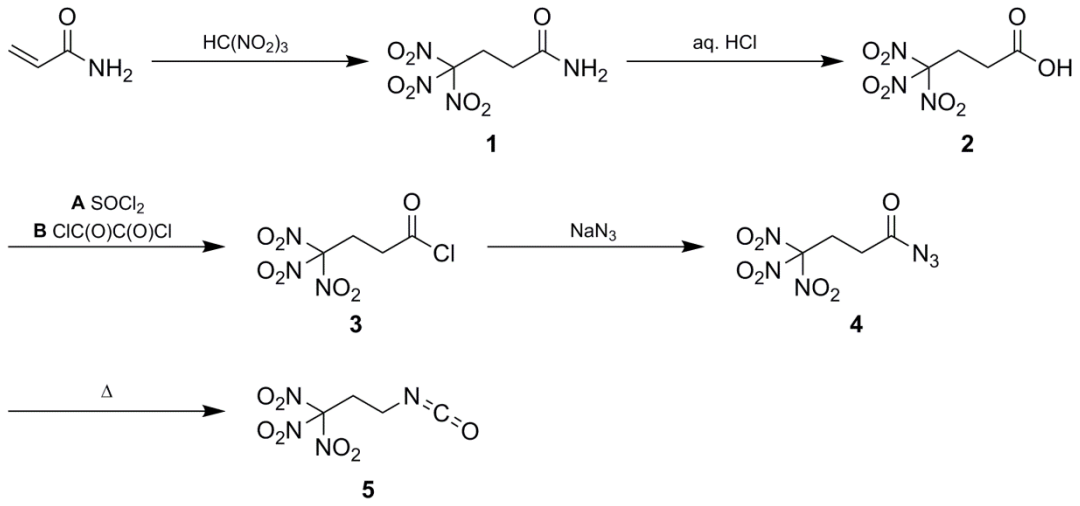

Scheme 3.1 Synthesis of 1,1,1-trinitropropan-3-isocyanate (**5**) starting from acrylamid and trinitromethane.

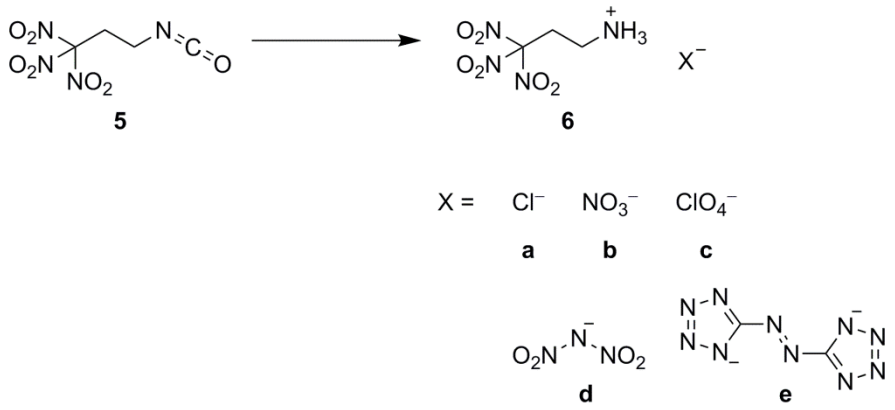

Scheme 3.2 Synthesis of salts of 3,3,3-trinitropropan-1-ammonium (**6**).

obtained in 96% yield while the reaction time was reduced to 4 h. Reaction of compound **3** with sodium azide at ambient temperature yielded the carbonyl azide 4,4,4-trinitrobutanoyl azide (**4**). To obtain the azide **4** as pure colourless solid, the reaction temperature has to be kept below 30 °C during the whole synthesis and work-up procedure. Due to its high sensitivity, extreme care is required when working with this compound. Heating the azide **4** in an organic inert solvent causes the conversion to 1,1,1-trinitropropan-3-isocyanate (**5**) via a Curtius rearrangement. A much safer way for the synthesis of **5** is the subsequent in situ conversion of **4** to the isocyanate **5** without isolation of the very sensitive azide **4**. The isocyanate **5** is a useful precursor for the synthesis of several energetic carbamates, ureas, amines and salts.[8–10] The chloride and nitrate salts **6a** and **6b** of the 3,3,3-trinitropropyl-1-ammonium cation were obtained by controlled hydrolysis of **5** in diluted mineral acid (Scheme 3.2).[11] The perchlorate, dinitramide and 5,5′-azobistetrazolate salts **6c**–**e** were synthesized by metathesis of the chloride salt **6a** with the corresponding silver and potassium salts, respectively (Scheme 3.2). The salt formation of **6** proceeds in high yields around 90%. The nitrate salt **6b**, perchlorate salt **6c** and dinitramide salt **6d** are air and moisture stable and exhibit high positive oxygen balances Ω_{CO} of +15.6% (**6b**), +21.7% (**6c**), and +20.7% (**6d**).

An interesting combination of Michael addition with Mannich condensation is the one-pot reaction of acrylamide (1 eq.), nitroform (2 eq.) and formaldehylde (1 eq.) to give 4,4,4-trinitro-*N*-(2,2,2-trinitroethyl)butanamide (**7**) (Scheme 3.3).[12]

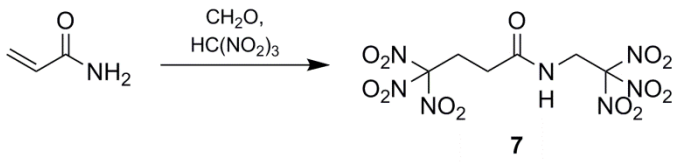

Scheme 3.3 Synthesis of 4,4,4-trinitro-*N*-(2,2,2-trinitroethyl)butanamide (**7**).

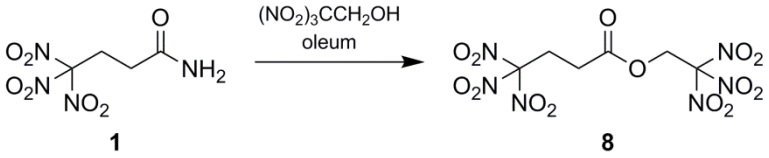

Scheme 3.4 Synthesis of 2,2,2-trinitroethyl-4,4,4-trinitrobutanoate (**8**).

An oxygen rich molecule was also prepared by the esterification of the amide **1** with the alcohol 2,2,2-trinitroethanol. The reaction was performed in oleum (30% SO_3) as strong dehydrating agent.[13] After recrystallization from water/methanol the ester 2,2,2-trinitroethyl-4,4,4-trinitrobutanoate (**8**) was obtained as pure colorless solid (Scheme 3.4).

3.3.2 Multinuclear NMR Spectroscopy

All compounds were thoroughly characterized by ^{1}H, ^{13}C and ^{14}N NMR spectroscopy. In the ^{1}H NMR spectra the two neighboring CH_2 groups are within the range of 3.90 to 2.52 ppm. The methylene unit next to the trinitromethyl moiety is mostly shifted to higher field compared to the CH_2 groups next to a nitrogen or oxygen atom. The vicinal coupling constants of the hydrogen atoms in the ethylene group are not equivalent due to the rotation around the C–C bond, which causes an AA′XX′ spin system.[14] The resonances of the CH_2 moiety of the trinitroethyl group is observed at lower field (4.96 ppm (**7**) and 5.20 ppm (**8**)) compared to the trinitropropyl group.

In the ^{13}C NMR spectra the carbon resonances of the two CH_2 groups of the trinitropropyl part are very variable and are found in the range of 40.5 to 27.6 ppm. The carbon resonances of the trinitromethyl moieties are observed as a broadened signals. Those of the trinitropropyl unit are located at around 128 ppm whereas the resonances of the trinitroethyl unit of compounds **7** and **8** are slightly upfield shifted to approximately 126 ppm.

In the ^{14}N NMR spectra the resonances for the nitro groups of the trinitromethyl moieties are all quite sharp and found in the range of −13 to −31 ppm. For the ammonium moieties of the salts **6a–e** resonances are observed around −355 ppm.

3.3.3 Vibrational Spectroscopy

All compounds were also characterized by IR and Raman spectroscopy. The most characteristic frequencies in the compounds are the carbonyl and nitro groups. The characteristic ν(C=O) stretching vibration is located in a large range from 1785 to 1676 cm^{-1}. It is observed that the carbonyl stretching bands are shifted to higher wave numbers in molecules when they are connected to electron-withdrawing moieties. The

maxima is the acid chloride **3** where the ν(C=O) is located at 1785 cm^{-1}, while for the two amides **1** and **7** signals at 1695 and 1676 cm^{-1} are observed. For the trinitromethyl units both the antisymmetric $\nu_{as}(NO_2)$ in the range of 1604–1582 cm^{-1} and the symmetric stretching vibrations $\nu_s(NO_2)$ at 1303–1288 cm^{-1} are observed. The antisymmetric stretching vibration of the azide moiety of compound **4** is found as characteristic strong signal at 2148 cm^{-1}.

3.3.4 Single Crystal Structure Analysis

Single crystals suitable for X-ray diffraction measurements were obtained by crystallization at ambient temperature from water (**1**, **2**, **6a**, **6b**, and **6d**), from neat material (**4**) or from chloroform (**8**). A full list of the crystallographic refinement parameters and structure data can be found in Appendix A3.

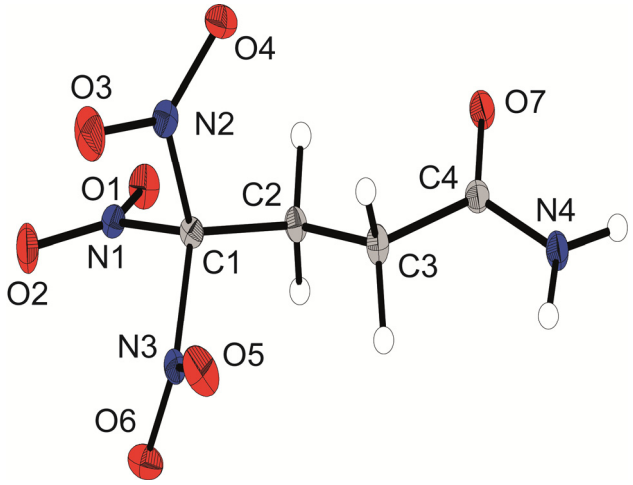

Figure 3.1 X-ray molecular structure of 4,4,4-trinitrobutanamide (**1**). Selected atom distances (Å) and angles (deg.): C1–C2 1.502(2), C1–N1 1.540(2), C1–N2 1.538(2), C1–N3 1.521(1), C2–C3 1.524(2), C3–C4 1.522(2), C4–N4 1.332(2), C4–O7 1.237(1), N1–O1 1.211(1), N4–H5 0.89(2), N4–H6–0.87(1), C2–C1–N2 114.15(9), C2–C1–N1 112.09(9), C2–C1–N3 110.49(9), H6–N4–C4–C3 −178(1), H5–N4–C4–O7 −177(1), N4–C4–C3–C2 −157.3(1), C3–C2–C1–N1 −175.87(9).

The amide **1** crystallizes in the triclinic space group *P*–1 with one molecule as asymmetric unit. The density is 1.835 g cm^{-3} and the molecular structure is shown in Figure 3.1. The geometry of the structure has some very typical characteristics of trinitromethyl compounds.[1b,c,8] The C–N bond lengths in the trinitromethyl moiety are in the range of 1.54 Å, which is significantly longer than a regular C–N bond (1.47 Å) and results from steric repulsion of the proportionally large nitro groups.[1c] As expected, the amide unit is nearly planar and shows a shortened C–N bond.

The acid **2** crystallizes in the monoclinic space group $P2_1/n$ and is shown in Figure 3.2. The quite low density of 1.720 g cm^{-3} can be explained by the strong hydrogen bonds which

are formed between two carboxyl moieties with a donor acceptor distance of 2.632 Å (O8–H8···O7).[15] In this structure another characteristic structure feature, the propeller-like arrangement of the trinitromethyl group could be observed. The three nitro groups are organized around the carbon in a propeller-like geometry to optimize the non-bonded N···O intramolecular attractions (N2···O2, O5···N1, N3···O4). This results in an intramolecular interaction between the partial positive charged nitrogen and the negative charged oxygen in the nitro group. These N···O attractions are found with distances in the range of 2.55 Å, which are much shorter than the sum of the van der Waals radii of nitrogen and oxygen (3.07 Å).[1c, 16]

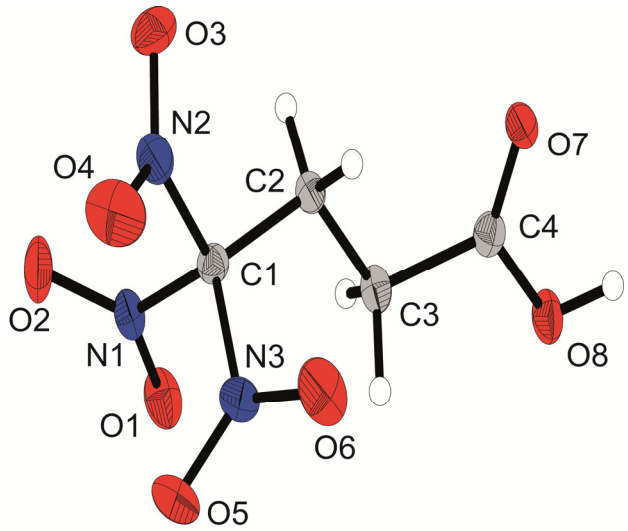

Figure 3.2 X-ray molecular structure of 4,4,4-trinitrobutanoic acid (**2**). Selected atom distances (Å) and angles (deg.): C1–N1 1.523(2), C2–C3 1.528(2), C3–C4 1.509(2), C3–H3 0.99(2), C4–O7 1.218(2), C4–O8 1.311(2), N1–O1 1.216(1), O8–H5 0.86(2), C2–C1–N1 115.2(1), H5–O8–C4–C3 −175(1), O8–C4–C3–C2 179.0(1), C4–C3–C2–C1 −158.4(1), C3–C2–C1–N2 178.3(1), N2–O2 2.557(2), O5–N1 2.571(1), N3–O4 2.550(2).

The carbonyl azide **4** crystallizes in the triclinic space group *P*−1 with one molecule as an asymmetric unit and shows the propeller-like geometry of the trinitromethyl group. The molecular structure is shown in Figure 3.3. The azide, the carbonyl and the carbon backbone inclusively, shows a nearly planar arrangement which is shown by the torsion angle of 1.2(2)° (N5–N4–C4–O7). Typical for carbonyl azides is the slight bending of the azide moiety with an angle of 174.2°. The N4–N5 and N5–N6 bond lengths (1.273(3) and 1.121(3) Å, respectively) are comparable with those in other carbonyl azides.[17]

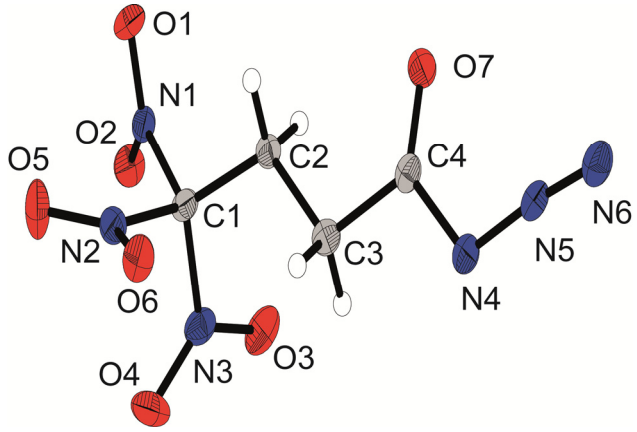

Figure 3.3 X-ray molecular structure of 4,4,4-trinitrobutanoyl azide (**4**). Selected atom distances (Å) and angles (deg.): C1–C2 1.512(2), C1–N1 1.532(2), C2–C3 1.528(3), C3–C4 1.503(2), C4–N4 1.409(2), C4–O7 1.205(2), N4–N5 1.273(2), N5–N6 1.112(2), C2–C1–N3 114.4(1), C4–N4–N5 111.5(1), N4–N5–N6 174.2(2), N6–N5–N4–C4 –176(1), N5–N4–C4–O7 1.2(2), N4–C4–C3–C2 –175.0(1), C4–C3–C2–C1 178.0(1), O2–N2 2.573(2), N1–O5 2.577(2), O4–N3 2.541(1).

The chloride salt **6a** crystallizes as a monohydrate in the triclinic space group *P*–1 and a density of 1.733 g cm^{-3}. The asymmetric unit is shown in Figure 3.4. The conformation of the C1, C2, C3 and N4 atoms is almost perfectly staggered. The extended structure involves secondary interactions in terms of classical intermolecular N–H···O hydrogen bonds and unusual so-called non-classical hydrogen bonds of the type C–H···O; the majority are classified as quite strong.[15]

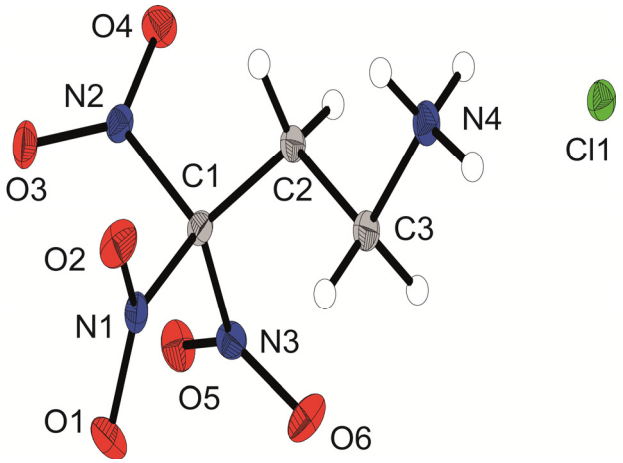

Figure 3.4 X-ray molecular structure of 3,3,3-trinitropropan-1-ammonium chloride (**6a**). Selected atom distances (Å) and angles (deg.): C1–C2 1.507(2), C1–N1 1.522(2), C2–C3 1.533(2), C3–N4 1.491(2), N1–O1 1.217(1), N4–H6 0.89(2), N4–H7 0.88(2), N4–H8 0.88(2), C2–C1–N3 114.5(1), C3–N4–H7 111(1), C3–N4–H8 107(1), C3–N4–H6 109(1), H7–N4–C3–C2 –178(1), N4–C3–C2–C1 –160.1(1), O5–N2 2.582(2), O1–N3 2.555(2), N1–O3 2.545(2).

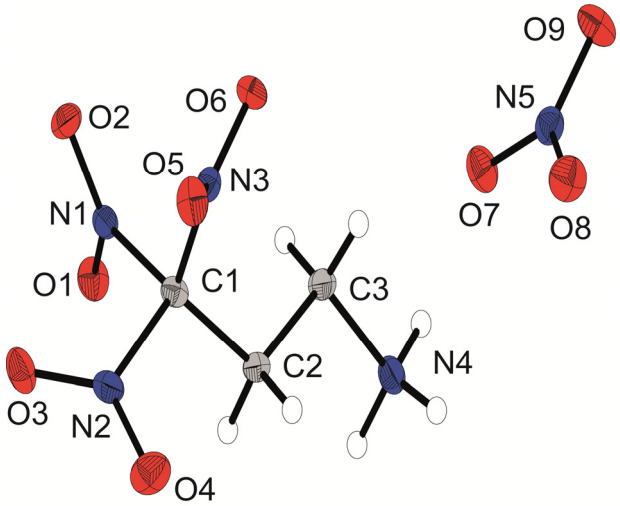

Figure 3.5 X-ray molecular structure of 3,3,3-trinitropropan-1-ammonium nitrate (**6b**). Selected atom distances (Å) and angles (deg.): C1–C2 1.512(2), C1–N1 1.529(2), C2–C3 1.526(2), C3–N4 1.492(2), N1–O1 1.223(2), N5–O7 1.269(2), N5–O8 1.233(2), N5–O9 1.266(2), N4–C3–C2–C1 −173.7(1), C3–C2–C1–N2 175.8(1), H6–N4–C3–C2 170(1), O8–N5–O7–O9 179.7(3), O5–N2 2.581(2), O2–N3 2.587(2), N1–O3 2.530(2).

The nitrate salt **6b** crystallizes in the orthorhombic space group $P2_12_12_1$ with a density of 1.804 g cm^{-3}. The asymmetric unit consists of one anion and cation and is illustrated in Figure 3.5. The protonated form of the 3,3,3-trinitropropan-1-amine shows the same structure characteristics as the hydrochloric salt **6a**.

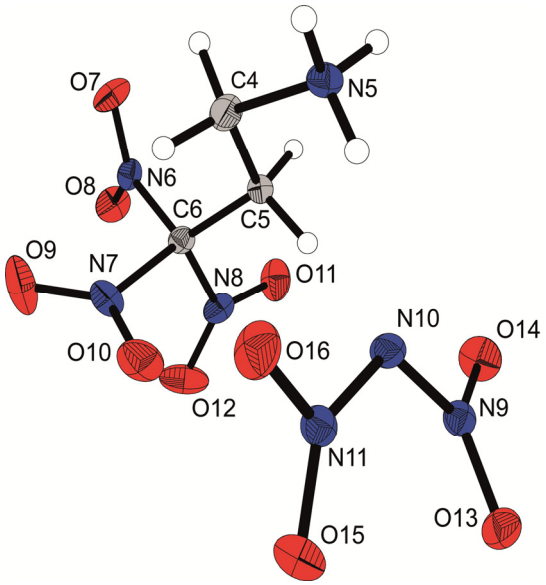

Figure 3.6 X-ray molecular structure of 3,3,3-trinitropropan-1-ammonium dinitramide (**6d**). Selected atom distances (Å) and angles (deg.): O7–N6 1.216(2), O8–N6 1.209(2), N5–C4 1.484(2), N6–C6 1.529(3), N7–C6 1.523(2), N8–C6 1.528(2), C4–C5 1.530(2), C5–C6 1.505(2), O13–N9 1.220(2), O14–N9 1.239(2), O15–N11 1.233(2), O16–N11 1.243(2), N9–N10 1.380(2), N10–N11 1.357(2), O13–N9–N10 124.2(1), O14–N9–N10 111.7(1), N9–N10–N11 115.4(1), O15–N11–N10 124.7(1), O16–N11–N10 112.8(1), O13–N9–N10–N11 -20.8(2).

The molecular structure of the dinitramide salt **6d** is shown in Figure 3.6. Compound **6d** crystallizes in the monoclinic space group *P*–1 with two anions and two cations as asymmetric unit and a density of 1.872 g cm^{-3}. The 3,3,3-trinitropropan-1-ammonium cation shows similar structural features as the ionic structures discussed before. The nitro groups of the dinitramide moiety are slightly twisted out of plane with torsion angles about 20°. The N–N bond lengths with an average distance of 1.37 Å are also slightly shorter than common N–N single bonds.

The ester **8** crystallizes in the monoclinic space group $P2_1/n$ with four formula units per unit cell. The asymmetric unit consists of one molecule and is displayed in Figure 3.7. The average of the N–O and C–NO_2 bond lengths of the trinitromethyl units are all in the same range of 1.21 Å in N–O and 1.52 Å in C–NO_2 whereas no distinction between the ethyl and propyl moiety is visible. Also both trinitromethyl groups show independently the propeller-like orientation of the nitro groups. Also the carbon-carbon bonds are virtually identical within a range of 1.50 to 1.52 Å. Although no classical hydrogen bonds are found in the crystal structure a high density of 1.869 g cm^{-3} was observed. However, non-classical hydrogen bonds of the type C–H···O are detected, whereas the majority is classified as quite strong.[15]

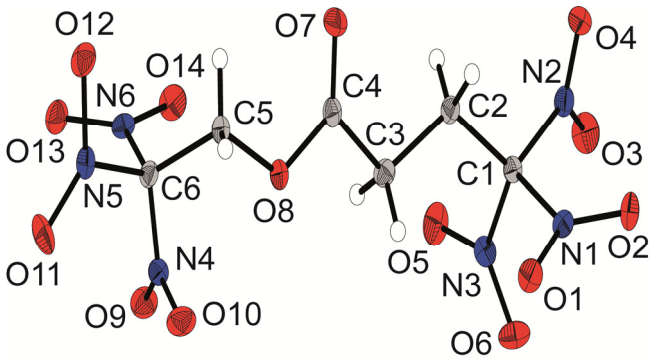

Figure 3.7 X-ray molecular structure of 2,2,2-trinitroethyl-4,4,4-trinitrobutanoate (**8**). Selected atom distances (Å) and angles (deg.): C1–C2 1.515(2), C1–N1 1.528(2), C2–C3 1.514(2), C3–C4 1.497(2), C4–O7 1.200(2), C4–O8 1.363(2), C5–C6 1.520(2), C5–O8 1.424(2), C6–N4 1.525(2), N1–O1 1.222(1), N4–O9 1.213(2), N2–C1–C2–C3 161.5(1), C1–C2–C3–C4 169.4(1), C3–C4–O8–C5 −175.6(1), C4–O8–C5–C6 131.7(1), O8–C5–C6–N5 160.2(1), N3–O3 2.558(2), O6–N1 2.567(2), N2–O2 2.534(1), N4–O11 2.608(2), N5–O13 2.583(2), O9–N6 2.557(1).

3.3.5 Thermal Stabilities and Energetic Properties

Compounds **1**, **2**, **6a**–**e**, **7**, and **8** are stable when exposed to air and moisture. The azide **4** has to be handled very carefully, owning to its high sensitivity towards heat. Reactions of the isocyanate **5** must be carried out with strict exclusion of moisture. Furthermore it should be stored frozen and is not longtime stable, due to rapid polymerization. The thermal stabilities

of all compounds were investigated by performing various DSC measurements with a heating rate of 5 °C min^{-1}. The temperatures at which melting and decomposition occurred, are shown in Table 3.1 together with other physical properties. A remarkably high decomposition point of 178 °C was observed for compound **6a**, likely owing to its stability to form strong hydrogen bonds through the salt structure. Moreover, compounds **7** and **8** (both 155 °C) showed satisfying decomposition points for applications as high-energy dense oxidizers based on CHNO compounds. The sensitivities of compounds **2**–**8** towards impact, friction, and electrostatic discharge were experimentally determined according to the NATO Standardization Agreements;[18] the results are displayed in Table 3.1. All compounds, with exception of the azide **4**, the dinitramide salt **6d**, and the 5,5'-azobistetrazolate salt **6e** showed moderate impact and friction sensitivities.[19] For the amide **1** as well as the nitrate salt **6b** impact sensitivities of 6 J are found, which are in the range of the well-known explosive Hexogen (RDX).

Predictions of the detonation and combustion parameters by using the EXPLO5 V6.02[20] code have been performed based on the heats of formations which were obtained from ab initio calculations. The energetic parameters were calculated with the room temperature densities, which were measured experimentally by gas pycnometer. The resulted heats of detonation Q_v, detonation temperatures T_{ex}, detonation pressures p, and detonation velocities V_{det} for compounds **1**, **2**, **4**, and **6**–**8** are shown in Table 3.2. The dinitramide salt **6d** has the highest detonation parameters with a detonation velocity V_{det} of 9282 m s^{-1} and a detonation pressure of 372 kbar. Compound **6d** is therefore in the range of the high energetic military explosive RDX (8838 m s^{-1}).[20]

The specific impulses I_{sp} of compounds **1**, **2**, **4**, and **6**–**8** were calculated for the neat compounds, for compositions with different amounts of aluminum as fuel, and additional with binder and are also listed in Table 3.2 (further values are summarized in the Appendix A3). These impulses were compared with the calculated impulses of ammonium perchlorate (AP) in an analogous composition. The chosen mixture with AP as an oxidizer provided a specific impulse of 261 s. All compounds show good properties, especially when calculated without binder. The value for the specific impulse of the 5,5'-azobistetrazolate salt **6e** exceeds all others; for the neat compound it is calculated to 271 s, with an admixture of 10% aluminum as fuel 282 s could be achieved (see Appendix A3). For the nitrate and dinitramide salts **6b** and **6d** remarkable high specific impulses of 278 s were reached in compositions containing 85% oxidizer and 15% fuel. In composites containing oxidizer, fuel and binder the specific impulses decrease slightly. The best specific impulse is obtained for the dinitramide salt **6d** with a calculated value of 275 s in a

Table 3.1 Physical properties of the compounds **1**, **2**, **4**, **6a–e**, **7**, and **8** in comparison to AP.

	1	**2**	**4**	**6a**	**6b**	**6c**	**6d**	**6e**	**7**	**8**	**AP**
formula	$C_4H_6N_4O_7$	$C_4H_5N_3O_8$	$C_4H_4N_6O_7$	$C_3H_7N_4O_6Cl$	$C_3H_7N_5O_9$	$C_3H_7N_4O_{10}Cl$	$C_3H_7N_7O_{10}$	$C_8H_{14}N_{18}O_{12}$	$C_6H_6N_6O_{14}$	$C_6H_7N_7O_{13}$	NH_4ClO_4
MW [g mol^{-1}]	222.11	223.10	248.11	230.56	257.12	294.56	301.13	554.31	385.16	386.14	117.49
Density RT [a]	1.78	1.67	1.71	1.76	1.77	1.97	1.84	1.67	1.83	1.84	1.95
T_m [°C][b]	93	55	22	161	135	-	-	-	92	150	-
T_{dec} [°C][c]	120	176	85	178	138	164	112	120	155	155	240
IS [J][d]	6	40	2	20	6	2.5	2	2	30	10	15
FS [N][e]	360	324	144	>360	120	16	30	54	240	240	>360
ESD [J][f]	0.50	0.30	0.10	0.40	0.20	0.08	0.40	0.60	0.10	0.20	>1.50
N [%][g]	25.2	18.8	33.9	24.3	27.2	19.0	32.6	54.6	21.8	25.5	11.9
O [%][h]	50.4	57.4	45.1	41.6	56.0	54.3	53.1	26.7	58.0	54.0	54.5
N + *O* [%][i]	75.6	76.2	79.0	65.9	83.2	73.3	85.7	81.3	79.8	79.5	66.4
Ω_{CO} [%][j]	0.0	+10.1	+6.5	0.0	+15.6	+21.7	+18.6	−11.1	+20.7	+14.5	+34.6
Ω_{CO2} [%][j]	−28.1	−17.9	−19.4	−2.4	−3.1	+5.4	+2.7	−33.4	−4.1	−10.4	+34.6
$\Delta H°_f$ [kJ mol^{-1}][k]	−326	−506	54	−96	−169	−119	32	972	−466	−330	−296
$\Delta U°_f$ [kJ kg^{-1}] [l]	−1374	−2178	301	−318	−554	−312	205	1851	−1124	−770	−2433

[a] Densities at RT measured by gas pycnometer. [b] Onset melting T_m and [c] onset decomposition point T_{dec} from DSC measurement carried out at a heating rate of 5 °C min^{-1}. [d] Impact sensitivity. [e] Friction sensitivity. [f] Sensitivity toward electrostatic discharge. [g] Nitrogen content. [h] Oxygen content. [i] Sum of nitrogen and oxygen content. [j] Oxygen balance assuming the formation of CO and the formation of [j] CO_2 at the combustion. [k] Enthalpy and [l] energy of formation calculated by the CBS-4M method using Gaussian 09.

Table 3.2 Calculated detonation and combustion parameters of compound **1**, **2**, **4**, **6a**–**e**, **7**, and **8** (using EXPLO5 V6.02)[19a] in comparison to AP.

	1	**2**	**4**	**6a**	**6b**	**6c**	**6d**	**6e**	**7**	**8**	**AP**
formula	$C_4H_6N_4O_7$	$C_4H_5N_3O_8$	$C_4H_4N_6O_7$	$C_3H_7N_4O_6Cl$	$C_3H_7N_5O_9$	$C_3H_7N_4O_{10}Cl$	$C_3H_7N_7O_{10}$	$C_8H_{14}N_{18}O_{12}$	$C_6H_6N_6O_{14}$	$C_6H_7N_7O_{13}$	NH_4ClO_4
Q_v [kJ kg^{-1}][a]	−4956	−4786	−5607	−5281	−6697	−6250	−6671	−6212	−6121	−5820	−1422
T_{ex} [K][b]	3383	3505	4071	3793	4319	4309	4382	4141	4277	4009	1735
V_0 [L kg^{-1}][c]	733	731	759	744	821	787	828	814	719	718	885
P_{CJ} [kbar][d]	292	246	291	282	335	390	372	299	324	335	158
V_{det} [m s^{-1}][e]	8187	7624	8259	8019	8913	9096	9282	8541	8616	8628	6368
I_{sp} [s][f]	238	241	261	255	274	265	274	271	258	262	157
I_{sp} [s] (5% Al)[g]	248	248	266	261	276	268	276	278	261	264	198
I_{sp} [s] (10% Al)[g]	256	253	269	267	277	270	277	282	262	266	224
I_{sp} [s] (15% Al)[g]	261	256	270	269	278	270	278	276	263	267	235
I_{sp} [s] (20% Al)[g]	262	258	265	267	276	270	277	270	263	267	244
I_{sp} [s] (25% Al)[g]	251	256	252	265	275	269	276	258	262	264	247
I_{sp} [s] (5% Al, 14% binder)[h]	216	215	237	230	258	264	266	249	242	239	250
I_{sp} [s] (10% Al, 14% binder) [h]	232	229	248	243	264	269	272	256	251	248	257
I_{sp} [s] (15% Al, 14% binder) [h]	244	241	247	247	270	272	275	254	255	253	261

[a] Heat of detonation. [b] Detonation temperature. [c] Volume of gaseous products. [d] Detonation pressure. [e] Detonation velocity calculated by using the EXPLO5 (Version 6.02) program package.[19a] [f] Specific impulse of the neat compound using the EXPLO5 (Version 6.02) program package (70.0 bar chamber pressure, initial temperature 3700 K, ambient pressure 1.0 bar, equilibrium expansion conditions).[19a] [g] Specific impulse for compositions with different amounts of aluminum using the EXPLO5 (Version 6.02) program package (70.0 bar chamber pressure, initial temperature 3700 K, ambient pressure 1.0 bar, equilibrium expansion conditions).[19a]. [h] Specific impulse for compositions with different amounts of oxidizer/compound and aluminum, and 14% binder (6% polybutadiene acrylic acid, 6% polybutadiene acrylonitrile and 2% bisphenol A ether) using the EXPLO5 (Version 6.02) program package (70.0 bar chamber pressure, initial temperature 3700 K, ambient pressure 1.0 bar, equilibrium expansion conditions).[19a].

composite propellant consisting of 15% aluminum and 14% binder. However, also the specific impulses of the nitrate and perchlorate salts **6b** and **6c** with values of 270 (**6b**) and 272 s (**6c**) exceed the specific impulse of the standard optimized mixture of AP (261 s).

3.4 Conclusion

Based on the Michael addition of nitroform several energetic polynitro compounds with a positive oxygen balance were synthesized. Although several synthesis steps are needed for most compounds presented herein only common commercially available chemicals are used and syntheses proceed in high yields. All of the compounds were comprehensively characterized. Several salts containing the 3,3,3-trinitropropylammonium cation were investigated in terms of their energetic properties. Excellent detonation parameters were found for the 3,3,3-trinitropropylammonium dinitramide **6d** with a detonation velocity of 9282 m s^{-1} and a detonation pressure of 372 kbar. These values are significantly higher than those of TNT, RDX, and PETN.[21] With respect to an application as high-energy dense oxidizer in composite solid rocket propellants, the best value was obtained for the corresponding 5,5′-bisazotetrazolate salt **6e**; in a mixture comprised of 90% oxidizer and 10% fuel a calculated specific impulse of 282 s was reached. In composites consisting of oxidizer, fuel and binder best values were obtained for the nitrate salt 6b (270 s), the perchlorate salt 6c (272 s) and the dinitramide salt 6d (275 s). All of these exceed the specific impulse of AP in a similar composition (261 s). However, the perchlorate salt **6c**, the dinitramide salt **6d**, and the 5,5′-bisazotetrazolate salt **6e** show low thermal stabilities and/or high sensitivities to external stimuli, and therefore likely will be less considered for practical use.

3.5 Experimental Section

General Information

Chemicals were were used as supplied (Sigma-Aldrich, Fluka, Acros Organics). Raman spectra were recorded in a glass tube with a Bruker MultiRAM FT-Raman spectrometer with Nd:YAG laser excitation up to 1000 mW (at 1064 nm) in the range between 400 and 4000 cm^{-1}. Infrared spectra were measured with a Perkin–Elmer Spectrum BX-FTIR spectrometer equipped with a Smiths DuraSamplIR II ATR device. All spectra were recorded at ambient (20 °C) temperature. NMR spectra were recorded with a JEOL Eclipse 400 instrument and chemical shifts were determined with respect to external standards Me_4Si

(^{1}H, 399.8 MHz; ^{13}C, 100.5 MHz), $MeNO_2$ (^{14}N, 28.9 MHz; ^{15}N 40.6 MHz), and 1.0 M aqueous NaCl (^{35}Cl, 39.2 MHz). Mass spectrometric data were obtained with a JEOL MStation JMS 700 spectrometer (DCI+, DEI+). Analysis of C/H/N were performed with an Elemental Vario EL Analyzer. Melting and decomposition points were measured with a Perkin-Elmer Pyris6 DSC and an OZM Research DTA 552-Ex with a heating rate of 5 °C min^{-1} in a temperature range of 15 to 400 °C and checked by a Büchi Melting Point B-540 apparatus (not corrected).

X-ray Crystallography

The low-temperature single-crystal X-ray diffraction of compounds **1**, **2**, **4**, **6a**, **6b**, **6d**, and **8** were performed on an Oxford XCalibur3 diffractometer equipped with a Spellman generator (voltage 50 kV, current 40 mA) and a KappaCCD detector operating with MoKα radiation (λ =0.7107 Å). Data collection was performed using the CRYSALIS CCD software.[22] The data reduction was carried out using the CRYSALIS RED software.[23] The solution of the structure was performed by direct methods (SIR97)[24] and refined by full-matrix least-squares on F2 (SHELXL)[25] implemented in the WINGX software package [26] and finally checked with the PLATON software[27]. All non-hydrogen atoms were refined anisotropically. The hydrogen atom positions were located in a difference Fourier map. ORTEP plots are shown with thermal ellipsoids at the 50% probability level. Crystallographic data (excluding structure factors) for the structures reported in this paper have been deposited at the Cambridge Crystallographic Data Centre 1506284–1506290 (**1**, **2**, **4**, **6a**, **6b**, **6d**, and **8**). Additional crystallographic data and structure refinement parameters are listed in the Appendix A3.

Computational Details

All ab initio calculations were carried out using the program package Gaussian 09 (Rev. A.03) [28] and visualized by GaussView 5.08. [29]. The initial geometries of the structures were taken from the corresponding, experimentally determined crystal structures. Structure optimizations and frequency analyses were performed with Becke's B3 three parameter hybrid functional using the LYP correlation functional (B3LYP). For C, H, N and O a correlation consistent polarized double-ξ basis set was used (cc-pVDZ). The structures were optimized with symmetry constraints and the energy is corrected with the zero point vibrational energy.[30] The enthalpies (*H*) and free energies (*G*) were calculated using the complete basis set (CBS) method in order to obtain accurate values. The CBS models use the known asymptotic convergence of pair natural orbital expressions to extrapolate from calculations using a finite basis set to the estimated complete basis set limit. CBS-4 starts with a HF/3-21G(d) geometry optimization, which is the initial guess for the following SCF calculation as a base energy and a final MP2/6-31+G calculation with a CBS extrapolation to

correct the energy in second order. The used CBS-4M method additionally implements a MP4(SDQ)/6-31+(d,p) calculation to approximate higher order contributions and also includes some additional empirical corrections.[31] The enthalpies of the gas-phase species were estimated according to the atomization energy method.[32] The liquid (solid) state energies of formation ($\Delta H_f°$) were estimated by subtracting the gas-phase enthalpies with the corresponding enthalpy of vaporization (sublimation) obtained by Trouton's rule.[33] All calculations affecting the detonation parameters were carried out using the program package EXPLO5 V6.02 (EOS BKWG-S).[20] The detonation parameters were calculated at the Chapman–Jouguet (CJ) point with the aid of the steady-state detonation model using a modified Becker-Kistiakowski-Wilson equation of state for modeling the system. The CJ point is found from the Hugoniot curve of the system by its first derivative. The specific impulses I_{sp} were also calculated with the program package EXPLO5 V6.02 program, assuming an isobaric combustion of a composition of an oxidizer, aluminum as fuel, 6% polybutadiene acrylic acid, 6% polybutadiene acrylonitrile as binder and 2% bisphenol A as epoxy curing agent.[20a] A chamber pressure of 70.0 bar, an initial temperature of 3300 K and an ambient pressure of 1.0 bar with equilibrium expansion conditions were estimated for the calculations.

Synthesis

CAUTION! All prepared compounds are energetic materials with sensitivity toward heat, impact, and friction. No hazards occurred during the preparation and manipulation. However, additional proper protective precautions (face shield, leather coat, earthed equipment and shoes, Kevlar® gloves, and ear plugs) should be used when undertaking work with these compounds.

4,4,4-Trinitrobutanamide (**1**)

An aqueous solution of nitroform (30%, 22.6 g, 45 mmol) was cooled in an ice-bath and acrylamide (3.2 g, 45 mmol) was added. The mixture was stirred 10 minutes at this temperature and 5 h at ambient temperature. The formed precipitate was filtered off and washed several times with cold ethanol and diethyl ether. After drying on air pure 4,4,4-trinitrobutanamide (**1**) was obtained as colorless solid in 97% yield.

DSC (5 °C min^{-1}): 93 °C (mp.), 120 °C (dec.). IR (ATR): ν = 3475 (m), 3368 (w), 3310 (w), 3192 (w), 3010 (w), 2948 (w), 2360 (w), 2340 (w), 1695 (m), 1595 (s), 1567 (vs), 1418 (m), 1364 (w), 1344 (m), 1311 (m), 1299 (m), 1288 (s), 1217 (w), 1155 (w), 1116 (w), 878 (w), 856 (w), 816 (m), 798 (s), 776 (w), 747 (w), 637 (w) cm^{-1}. Raman (500 mW): ν = 3009 (41), 2969 (24), 2938 (78), 1679 (17), 1615 (29), 1599 (43), 1575 (11), 1433 (16), 1417 (43),

1367 (43), 1348 (26), 1307 (31), 1125 (24), 1066 (13),1055 (14), 967 (13), 904 (12), 881 (43), 858 (60), 811 (20), 546 (18), 441 (71), 390 (100), 364 (73), 312 (69), 274 (17), 208 (66) cm^{-1}. ^{1}H NMR ([D_6]DMSO) δ = 7.48 (s, 1H, NH_2), 7.09 (s, 1H, NH_2), 3.59 (m, 2H, CH_2C(NO_2)$_3$), 2.52 (m, 2H, OCCH_2) ppm. ^{13}C NMR ([D_6]DMSO) δ = 170.7 (CO), 131.7 (C(NO_2)$_3$), 29.1 ($C$$H_2$), 29.0 ($C$$H_2$) ppm. ^{14}N NMR ([D_6]DMSO) δ = −28 (C(NO_2)$_3$) ppm. MS (DEI+) m/e: 223.2 [(M+H)$^+$]. Elemental analysis $C_4H_6N_4O_7$ (222.11): calc. C 21.63, H 2.72, N 25.22%; found C 21.65, H 2.65, N 25.05%. IS: 6 J (grain size 250–500 µm). FS: 360 N (grain size 250–500 µm). ESD: >0.5 J (grain size 250–500 µm).

4,4,4-Trinitrobutanoic acid (**2**)

4,4,4-Trinitrobutanamide (**1**) (2.0 g, 9.0 mmol) was added to concentrated hydrochloric acid (37%, 8 mL) and refluxed for 4 hours. The oily layer which formed solidified after standing overnight at 4 °C. The solid was filtered off and recrystallized from chloroform. After drying in the desiccator 4,4,4-trinitrobutanoic acid (**2**) was obtain as pure colorless product in 70% yield.

DSC (5 °C min^{-1}): 55 °C (mp.), 167 °C (dec.). IR: (ATR): ν = 3006 (w), 2958 (w), 2880 (w), 2730 (w), 2651 (w), 2527 (w), 1709 (s), 1587 (vs), 1440 (m), 1425 (m), 1312 (s), 1297 (s), 1237 (s), 1153 (m), 1070 (m), 928 (m), 906 (m), 816 (s), 798 (vs), 665 (m). cm^{-1}. Raman (500 mW): ν = 3006 (8), 2987 (11), 2956 (89), 1652 (10), 1605 (33), 1454 (9), 1418 (46), 1380 (25), 1359 (22), 1312 (31), 1226 (8), 1154 (13), 1071 (21), 982 (21), 908 (42), 857 (101), 802 (8), 655 (11), 628 (9), 546 (7), 484 (11), 412 (56), 402 (58), 377 (91), 313 (35), 275 (9) cm^{-1}. ^{1}H NMR ([D_6]acetone) δ = 3.71 (m, 2H, CH_2C(NO_2)$_3$), 2.89 (m, 2H, OCCH_2) ppm. ^{13}C NMR ([D_6]acetone) δ = 170.4 (CO), 126.3 (C(NO_2)$_3$), 29.2 ($C$$H_2$), 27.6 ($C$$H_2$) ppm. ^{14}N NMR ([D_6]acetone) δ = −29 (C(NO_2)$_3$) ppm. MS (DCI+) m/e: 224.1 [(M+H)$^+$]. Elemental analysis $C_4H_5N_3O_8$ (223.10): calc. C 21.53, H 2.26, N 18.83%; found C 21.39, H 2.24, N 18.70%. IS: 40 J (grain size 250–500 µm). friction tester: 324 N (grain size 250–500 µm). ESD: >0.5 J (grain size 250–500 µm).

4,4,4-Trinitrobutanoyl chloride (**3**)

Method A:

A mixture of 4,4,4-trinitrobutanoic acid (**2**) (6.7 g, 30.0 mmol) and thionyl chloride (16.7 mL, 200 mol) was stirred at room temperature for one hour. After this the reaction mixture was refluxed for 24 hours under exclusion of moisture. The excess of thionyl chloride was removed and the remaining oil was distilled yielding 4,4,4-trinitrobutanoyl chloride as colorless pure product (88%).

Method B:

Oxalyl chloride (326 mg, 2.6 mmol) and a catalytical amount of DMF were added to a suspension of 4,4,4-trinitrobutanoic acid (**2**) (500 mg, 2.2 mmol) in chloroform (10 mL). The reaction mixture was stirred under exclusion of moisture at ambient temperature for 40 min and was refluxed for 3 h. The solvent was removed under reduced pressure yielding 4,4,4-trinitrobutanoyl chloride (**3**) in 96% yield as pure colorless oil.

IR: (ATR): ν = 2997 (w), 2957 (w), 2892 (w), 1785 (s), 1585 (vs), 1425 (m), 1411 (w), 1356 (w), 1294 (s), 1216 (w), 1153 (w), 1062 (w), 996 (m), 943 (s), 857 (m), 799 (s), 780 (s), 693 (m) cm^{-1}. Raman (400 mW): ν = 2950 (51), 1792 (16), 1608 (25), 1414 (24), 1381 (22), 1358 (35), 1304 (30), 1224 (11), 1155 (15), 1065 (26), 998 (13), 948 (15), 905 (17), 858 (102), 784 (21), 694 (19), 635 (17), 532 (20), 456 (58), 396 (44), 374 (65), 275 (50), 233 (31) cm^{-1}. ^{1}H NMR ($CDCl_3$) δ = 3.38 (m, 4H, OCCH_2, CH_2C$(NO_2)_3$) ppm. ^{13}C NMR ($CDCl_3$) δ = 171.1 (*C*O), 127.9 (*C*$(NO_2)_3$), 40.5 (OC*C*H_2), 29.4 (*C*$H_2(NO_2)_3$) ppm. ^{14}N NMR ($CDCl_3$) δ = −31 (C(*N*$O_2)_3$) ppm. MS (DEI+) m/e: 206.1 [(M−Cl)$^+$]. Elemental analysis $C_4H_4N_3O_7Cl$ (241.54): calc. C 19.89, H 1.67, N 17.40%; found C 19.75, H 1.68, N, 17.80%.

4,4,4-Trinitrobutanoyl azide (**4**)

To a solution of sodium azide (0.31 g, 4.8 mmol) in water (2 mL) a solution of 4,4,4-trinitrobutanoyl chloride (**3**) (0.59 g, 2.4 mmol) in acetone (1 mL) was added slowly at 4 °C. After the addition the solution was stirred at 0 °C for two hours. The reaction mixture was extracted with chloroform (3 × 20 mL). The combined organic phases were washed with ice-water (20 mL), an ice-cold sodium bisulfate solution (5%, 20 mL), ice-water (2 × 20 mL) and brine (20 mL). The extracts were dried over magnesium sulfate and the organic solvent was removed at temperatures below 20 °C. The remaining oil solidified in the refrigerator over-night and 4,4,4-trinitrobutanoyl azide (**4**) was obtained as pure colorless solid in 66% yield.

DSC (5 °C min^{-1}): 22 °C (mp.), 85 °C (dec.). IR: (ATR): ν = 3000 (w), 2956 (w), 2893 (w), 2148 (s), 1711 (s), 1585 (vs), 1427 (m), 1359 (m), 1296 (s), 1153 (vs), 1098 (s), 1047 (s), 967 (w), 908 (w), 855 (s), 800 (vs), 704 (m) cm^{-1}. Raman (500 mW): ν = 2947 (71), 2156 (26), 2147 (26), 1716 (22), 1608 (26), 1419 (26), 1360 (36), 1305 (30), 1151 (9), 1101 (16), 1050 (14), 968 (12), 910 (31), 857 (101), 788 (10), 669 (26), 543 (9), 502 (29), 373 (69), 279 (39), 262 (36) cm^{-1}. ^{1}H NMR ($CDCl_3$) δ = 3.38 (m, 2H, CH_2C$(NO_2)_3$), 2.78 (m, 2H, OCCH_2) ppm. ^{13}C NMR ($CDCl_3$) δ = 176.2 (*C*O), 128.6 (*C*$(NO_2)_3$), 30.6 (*C*H_2), 29.3 (*C*H_2) ppm. ^{14}N NMR ($CDCl_3$) δ = −30 (C(*N*$O_2)_3$), −136 (N_β), −147 (N_γ) ppm. Elemental analysis $C_4H_4N_6O_7$ (248.11): calc. C 19.36, H 1.62, N 33.87%; found C 19.89, H 1.65, N 33.54%. IS: 2 J (grain size 250–500 µm). FS: 144 N (grain size 250–500 µm). ESD 0.3 J (grain size 250–500 µm).

1,1,1-Trinitropropan-3-isocyanate (**5**)

To a solution of sodium azide (0.31 g, 4.8 mmol) in water (2 mL) a solution of 4,4,4-trinitrobutanoyl chloride (**3**) (0.59 g, 2.4 mmol) in acetone (1 mL) was added slowly at 4 °C. After the addition the solution was stirred at 0 °C for two hours. The reaction mixture was extracted with chloroform (3 × 20 mL). The combined organic phases were washed with ice-water (20 mL), an ice-cold sodium bisulfate solution (5%, 20 mL), ice-water (2 × 20 mL) and brine (20 mL). The extracts were dried over magnesium sulfate. The solution was slowly heated up to 55 °C and kept at this temperature until no more nitrogen evolved (2 h). The organic solvent was removed to obtain 1,1,1-trinitropropan-3-isocyanate (**5**) as colorless liquid in 68% yield.

Raman (500 mW): ν = 2953 (70), 2156 (13), 2147 (13), 1718 (11), 1610 (24), 1451 (18), 1421 (22), 1363 (37), 1304 (30), 1100 (10), 1051 (13), 914 (20), 887 (12), 856 (100), 811 (10), 535 (10), 502 (16), 460 (10), 375 (68), 305 (17), 279 (22), 254 (20) cm^{-1}. ^{1}H NMR ($CDCl_3$) δ = 3.90 (m, 2H, CH_2), 3.32 (m, 2H, CH_2) ppm. ^{13}C NMR ($CDCl_3$) δ = 127.4 ($C(NO_2)_3$), 123.6 (NCO), 37.4 (CH_2), 35.0 (CH_2) ppm. ^{14}N NMR ($CDCl_3$) δ = −31 ($C(NO_2)_3$), −360 (NCO) ppm. Elemental analysis $C_4H_4N_4O_7$ (220.10): calc. C 21.83, H 1.83, N 25.46%; found C 21.31, H 1.80, N 26.07%.

3,3,3-Trinitropropan-1-ammonium chloride (**6a**)

1,1,1-Trinitropropan-3-isocyanate (**5**) (1.10 g, 5.0 mmol) was refluxed in hydrochloric acid (6 M, 10 mL) for five hours. The solution was concentrated to dryness and the colorless solid was washed with 1,2-dichloromethane. 3,3,3-Trinitropropan-1-ammonium chloride (**6a**) was yielded as colorless solid in 90% yield.

DSC (5 °C min^{-1}): 161 °C (mp.), 178 °C (dec.). IR: (ATR): ν = 2974 (m), 2884 (m), 2660 (w), 2497 (w), 2305 (w), 1989 (w), 1588 (vs), 1501 (m), 1483 (m), 1458 (m), 1417 (w), 1365 (w), 1292 (s), 1160 (m), 1062 (w), 1032 (w), 995 (w), 931 (w), 911 (w), 855 (w), 846 (w), 836 (w), 796 (s), 768 (w), 734 (w) cm^{-1}. RAMAN (300 mW): ν = 3068 (11), 3022 (18), 2998 (40), 2976 (58), 2938 (68), 2913 (25), 2904 (24), 2878 (18), 2859 (44), 2804 (12), 2083 (7), 1610 (37), 1580 (8), 1548 (17), 1491 (10), 1478 (9), 1460 (17), 1423 (21), 1396 (7), 1367 (39), 1300 (33), 1168 (19), 1119 (6), 1065 (8), 1031 (9), 999 (15), 970 (9), 931 (8), 901 (16), 858 (100), 802 (8), 654 (6), 633 (7), 569 (9), 516 (6), 457 (9), 402 (50), 374 (56), 341 (29), 302 (7) cm^{-1}. ^{1}H NMR ([D_6]DMSO) δ = 8.63 (br, 3H, NH_3), 3.82 (m, 2H, CH_2), 3.19 (m, 2H, CH_2) ppm. ^{13}C NMR ([D_6]DMSO) δ = 128.8 ($C(NO_2)_3$), 33.4 (CH_2), 30.3 (CH_2) ppm. ^{14}N NMR ([D_6]DMSO) δ = −31 (NO_2), −356 (NH_3) ppm. Elemental analysis $C_3H_9N_4O_7$ (230.56):

calc. C 15.63, H 3.06, N 24.30%; found C 16.09, H 3.06, N 24.30%. IS: 20 J (grain size 100–250 µm). FS: 360 N (grain size 100–250 µm). ESD >0.5 J (grain size 100–250 µm).

3,3,3-Trinitropropan-1-ammonium nitrate (**6b**)

1,1,1-Trinitropropan-3-isocyanate (**5**) (1.10 g, 5.0 mmol) was refluxed in nitric acid (6 M, 10 mL) for five hours. The solution was concentrated to dryness to give a yellow powder. Recrystallization from ethyl acetate yielded 3,3,3-trinitropropan-1-ammonium nitrate (**6b**) as colorless solid in 89% yield.

DSC (5 °C min^{-1}): 135 °C (mp.), 138 °C (dec.). IR: (ATR): ν = 3120 (m), 3070 (m), 3032 (m), 2977 (m), 2889 (m), 2840 (m), 2763 (w), 2716 (w), 2666 (w), 2588 (w), 2503 (w), 1604 (s), 1506 (w), 1479 (w), 1460 (m), 1425 (w), 1303 (m), 1040 (w), 996 (w), 972 (w), 934 (w), 875 (w), 850 (w), 806 (m), 799 (w), 766 (w), 735 (w), 680 (w) cm^{-1}. RAMAN (1000 mW): ν = 3037 (12), 2984 (47), 3948 (64), 2913 (12), 2859 (52), 2836 (5), 2817 (6), 2083 (11), 2028 (5), 1609 (25), 1465 (13), 1424 (22), 1373 (38), 1305 (27), 1186 (10), 1155 (9), 1035 (99), 1010 (10), 935 (7), 908 (15), 859 (102), 800 (7), 727 (9), 711 (6), 661 (5), 630 (8), 563 (9), 538 (7), 419 (41), 404 (44), 378 (50), 340 (24), 306 (10) cm^{-1}. ^{1}H NMR ([D$_6$]DMSO) δ = 8.10 (br, 3H, NH_3), 3.71 (m, 2H, CH_2), 3.24 (m, 2H, CH_2) ppm. ^{13}C NMR ([D$_6$]DMSO) δ = 128.8 (C(NO$_2$)$_3$), 33.5 (CH$_2$), 30.6 (CH$_2$) ppm. ^{14}N NMR ([D$_6$]DMSO) δ = –4 (NO$_3^-$), –30 (NO$_2$), –359 (NH$_3$) ppm. Elemental analysis $C_3H_7N_5O_9$ (257.12): calc. C 14.01, H 2.74, N 27.24%; found C 13.89, H 2.76, N 27.01%. IS: 6 J (grain size 250–500 µm). FS: 120 N (grain size 250–500 µm). ESD 0.3 J (grain size 250–500 µm).

3,3,3-Trinitropropan-1-ammonium perchlorate (**6c**)

To a solution of 3,3,3-trinitropropan-1-ammonium chloride (**6a**) (196 mg, 0.9 mmol) in water (10 mL) was added at 0 °C under exclusion of light a solution of silver perchlorate monohydrate (190 mg, 0.9 mmol) in water (10 mL). The reaction mixture was stirred 1.5 h at 0 °C. The precipitated silver chloride was filtered off, washed with cold water and the filtrate was evaporated to dryness. 3,3,3-Trinitropropan-1-ammonium perchlorate (**6c**) was obtained as colorless solid in 90% yield.

DSC (5 °C min^{-1}): 164 °C (dec.). IR: (ATR): ν = 3259 (w), 3227 (w), 3168 (w), 2992 (w), 2888 (w), 2361 (w), 2333 (w), 1596 (s), 1513 (w), 1501 (w), 1478 (m), 1430 (w), 1368 (w), 1293 (m), 1152 (m), 1067 (vs), 980 (m), 941 (w), 893 (w), 855 (w), 798 (s), 749 (w), 667 (w) cm^{-1}. RAMAN (1000 mW): ν = 3258 (7), 3241 (6), 3214 (6), 3189 (5), 3143 (5), 3133 (6), 3119 (5), 3067 (4), 3028 (9), 2994 (17), 2960 (29), 2821 (6), 1863 (5), 1601 (39), 1467

(10), 1431 (18), 1370 (25), 1356 (15), 1343 (9), 1302 (21), 1162 (16), 1115 (8), 1078 (12), 1019 (17), 982 (14), 942 (101), 858 (88), 803 (10), 664 (5), 634 (5), 628 (25), 563 (13), 467 (25), 453 (22), 417 (38), 405 (38), 382 (49), 341 (32), 300 (8) cm^{-1}. ^{1}H NMR ([D_6]DMSO) δ = 8.03 (br, 3H, NH_3), 3.70 (m, 2H, CH_2), 3.23 (m, 2H, CH_2) ppm. ^{13}C NMR ([D_6]DMSO) δ = 128.8 ($C(NO_2)_3$), 33.5 (CH_2), 30.4 (CH_2) ppm. ^{14}N NMR ([D_6]DMSO) δ = –31 (NO_2), –356 (NH_3) ppm. ^{35}Cl NMR ([D_4]methanol) = −1011 (ClO_4^-) ppm. Elemental analysis $C_3H_7N_4O_6Cl$ (294.56): calc. C 12.23, H 2.40, N 19.02%; found C 12.25, H 2.57, N 18.44%. IS: 2.5 J (grain size <100 µm). FS: 16 N (grain size <100 µm). ESD 0.08 J (grain size <100 µm).

3,3,3-Trinitropropan-1-ammonium dinitramide (**6d**)

To a solution of 3,3,3-trinitropropan-1-ammonium chloride (**6a**) (350 mg, 1.5 mmol) in water (10 mL) was added at 0 °C under exclusion of light a solution of silver dinitramide (320 mg, 1.5 mmol) in water (10 mL). The reaction mixture was stirred 1.5 h at 0 °C. The precipitated silver chloride was filtered off, washed with cold water and the filtrate was evaporated to dryness. 3,3,3-Trinitropropan-1-ammonium dinitramide (**6d**) was obtained as colorless solid in 96% yield.

DSC (5 °C min^{-1}): 112 °C (dec.). IR: (ATR): ν = 3285 (w), 3047 (w), 2981 (m), 2947 (m), 2662 (w), 1989 (w), 1588 (vs), 1520 (m), 1502 (m), 1478 (w), 1448 (m), 1412 (w), 1365 (w), 1295 (m), 1231 (w), 1183 (s), 1160 (s), 1026 (s), 986 (w), 947 (w), 898 (w), 855 (w), 827 (w), 798 (s), 761 (m), 755 (m), 743 (w), 734 (w), 722 (w) cm^{-1}. RAMAN (1000 mW): ν = 3236 (5), 3228 (4), 3208 (4), 3046 (9), 2984 (24), 2948 (30), 2859 (20), 2818 (4), 1609 (19), 1522 (6), 1484 (7), 1469 (9), 1440 (12), 1419 (10), 1368 (40), 1334 (100), 1313 (30), 1300 (21), 1183 (13), 1162 (11), 1143 (22), 1053 (16), 1027 (21), 984 (17), 950 (10), 919 (6), 899 (10), 858 (88), 826 (75), 805 (6), 759 (14), 748 (10), 647 (6), 559 (11), 488 (23), 403 (39), 377 (52), 341 (45), 298 (16), 209 (7) cm^{-1}. ^{1}H NMR ([D_4]methanol) δ = 8.31 (br, 3H, NH_3), 3.72 (m, 2H, CH_2), 3.43 (m, 2H, CH_2) ppm. ^{13}C NMR ([D_4]methanol) δ = 129.6 ($C(NO_2)_3$), 35.4 (CH_2), 32.3 (CH_2) ppm. ^{15}N NMR ([D_4]methanol) δ = −12.6 (N(NO_2)), –30.2 (NO_2), –352.0 (NH_3) ppm. Elemental analysis $C_3H_7N_7O_{10}$ (301.13): calc. C 11.97, H 2.34, N 32.56%; found C 12.00, H 2.41, N 31.27%. IS: 2 J (grain size <100 µm). FS: 30 N (grain size <100 µm). ESD 0.45 J (grain size <100 µm).

3,3,3-Trinitropropan-1-ammonium 5,5'-azobistetrazolate (**6e**)

A solution of 3,3,3-trinitropropylammonium chloride (233 mg, 1.0 mmol) in water (10 mL) was added to a solution of potassium 5,5'-azobistetrazolate (123 mg, 0.5 mmol) in water (2 mL) at 0 °C. Immediately a yellow precipitate was formed. The reaction mixture was

stirred 1 h at 0 °C. The precipitate was filtered off, washed with water and dried to yield 49% of 3,3,3-trinitropropan-1-ammonium 5,5'-azobistetrazolate (**6e**) as yellow solid.

DSC (5 °C min^{-1}): 120 °C (dec.). IR: (ATR): ν = 2934 (w), 2757 (w), 2675 (w), 2623 (w), 2512 (w), 2084 (w), 1632 (w), 1603 (s), 1590 (s), 1517 (w), 1458 (w), 1424 (w), 1414 (w), 1394 (w), 1369 (w), 1312 (w), 1297 (w), 1185 (w), 1174 (m), 1148 (w), 1080 (w), 1051 (w), 1042 (w), 1010 (w), 903 (w), 856 (w), 806 (s), 796 (s), 774 (w), 756 (w), 738 (m), 667 (s) cm^{-1}. RAMAN (500 mW): ν = 2935 (2), 1484 (48), 1423 (4), 1390 (100), 1195 (2), 1086 (10), 1058 (40), 927 (8), 857 (3), 341 (2) cm^{-1}. ^{1}H NMR ([D_4]methanol) δ = 3.76 (m, 2H, CH_2), 3.48 (m, 2H, CH_2) ppm. ^{13}C NMR ([D_4]methanol) δ = 171.9 ($C$$N_4$), 128.3 ($C$($NO_2$)$_3$), 34.0 ($C$$H_2$), 31.1 ($C$$H_2$) ppm. ^{14}N NMR ([$D_4$]methanol) δ = −19 (CN_4)), −30 ($N$$O_2$), −352 ($N$$H_3$) ppm. Elemental analysis $C_8H_{14}N_{18}O_{12}$ (554.31): calc. C 17.33, H 2.55, N 45.48%; found C 17.48, H 2.49, N 45.28%. IS: 2 J (grain size <100 µm). FS: 54 N (grain size <100 µm). ESD 0.6 J (grain size <100 µm).

4,4,4-Trinitro-*N*-(2,2,2-trinitroethyl)butanamide (**7**)

To a saturated solution of barium hydroxide in water (10 mL) was added acrylamide (1.30 g, 18.2 mmol) and aqueous formaldehyde (37%, 1.50 g, 18.2 mmol) and stirred for 20 minutes. The solution was treated with solid carbon dioxide (5 g) and the precipitated barium carbonate was filtered off. To the filtrate was added an aqueous nitroform solution (30%, 18.3 g, 36.4 mmol), stirred for 20 minutes and refluxed for further 30 minutes. The reaction mixture was cooled in an ice-water bath and the formed precipitate was filtered off. The yellow powder was recrystallized two times from a mixture of methanol/water, to yield 3.93 g (56%) of colorless pure product.

DSC (5 °C min^{-1}): 150 °C (mp.), 155 °C (dec.). IR: (ATR): ν = 3304 (w), 3071 (w), 3011 (w), 2960 (w), 2892 (w), 1676 (m), 1589 (vs), 1543 (s), 1418 (w), 1363 (w), 1299 (s), 1236 (w), 1217 (w), 1155 (w), 1115 (w), 1092 (w), 1050 (w), 935 (w), 854 (m), 803 (s). Raman (400 mW): ν = 3006 (19), 2957 (39), 1677 (18), 1605 (29), 1421 (24), 1365 (28), 1337 (20), 1305 (36), 1117 (14), 1058 (13), 936 (15), 913 (13), 857 (102), 545 (18), 412 (46), 394 (47), 377 (68), 278 (29) cm^{-1}. ^{1}H NMR (CD_3CN) δ = 7.21 (s, 1H, NH), 4.96 (d, 2H, ^{3}J = 6.8 Hz, CH_2NH), 3.47 (m, 2H, CH_2C(NO_2)$_3$), 2.70 (m, 2H, OCCH_2) ppm. ^{13}C NMR (CD_3CN) δ = 169.9 (CO), 131.4 (C(NO_2)$_3$), 127.5 (NHC$H_2$$C$($NO_2$)$_3$), 42.2 (NH$C$$H_2$), 28.8 ($C$$H_2$), 28.6 ($C$$H_2$) ppm. ^{14}N NMR ($CD_3CN$) δ = −29 (C($N$$O_2$)$_3$), −32 (NHC$H_2$C($N$$O_2$)$_3$) ppm. MS (DCI+) m/e: 386.2 [(M+H)$^+$]. Elemental analysis $C_6H_7N_7O_{13}$ (385.16): calc. C 18.71, H 1.83, N 25.46%; found C 18.83, H 1.81, N 25.49%. IS: 10 J (grain size <100 µm). FS: 240 N (grain size <100 µm). ESD 0.2 J (grain size 100 µm).

2,2,2-Trinitroethyl 4,4,4-trinitrobutanoate (**8**)

To a mixture of fuming sulfuric acid (30% SO_3, 4 mL) and concentrated sulfuric acid (8 mL) was added 4,4,4-trinitrobutanoic acid (**2**) (1.7 g, 7.8 mmol) in small portions with cooling to 4°C and stirred until complete solution. 2,2,2-Trinitroethanol (1.53 g, 7.8 mmol) dissolved in water (0.5 mL) was added very carefully to the reaction mixture at 4 °C and stirred for further 12 hours at room temperature. The reaction was quenched with ice-water (5 mL) and the colorless precipitate was filtered off. The product was washed three times with water (20 mL) and dried to obtain 1.20 g (40%) of pure product.

DSC (5 °C min^{-1}): 92 °C (mp.), 155 °C (dec.). IR: (ATR): ν = 3007 (w), 2964 (w), 2895 (w), 1761 (s), 1582 (vs), 1441 (w), 1430 (m), 1419 (w), 1400 (w), 1379 (w), 1363 (w), 1299 (s), 1222 (w), 1169 (s), 1100 (w), 1086 (m), 1037 (w), 1015 (w), 913 (w), 873 (w), 855 (m), 799 (vs), 780 (m), 759 (w), 744 (w), 730 (w), 689 (w), 655 (w) cm^{-1}. Raman (500 mW): ν = 3009 (12), 2987 (21), 2953 (49), 1762 (18), 1609 (36), 1442 (10), 1419 (27), 1401 (129, 1364 (38), 1302 (36), 1263 (10), 1154 (9), 1086 (18), 1038 (10), 1015 (13), 972 (8), 915 (21), 873 (13), 857 (105), 798 (11), 781 (9), 744 (6), 647 (11), 539 (17), 487 (11), 404 (70), 373 (95), 341 (13), 326 (12), 269 (28), 232 (21) cm^{-1}. ^{1}H NMR ($CDCl_3$) δ = 5.44 (s, 2H, OCH_2), 3.43 (m, 2H, CH_2C$(NO_2)_3$), 2.90 (m, 2H, OCCH_2) ppm. ^{13}C NMR ($CDCl_3$) δ = 167.4 (CO), 128.2 ($C(NO_2)_3$), 122.5 (OC$H_2C(NO_2)_3$) 61.3 (OCCH$_2$), 29.3 (CH$_2$), 28.0 (CH$_2$) ppm. ^{14}N NMR ($CDCl_3$) δ = −31 (C($NO_2)_3$), −35 (C($NO_2)_3$) ppm. MS (DCI+) m/e: 387.1 [(M+H)$^+$]. EA ($C_6H_6N_6O_{14}$, 386.14): calc.: C 18.66, H 1.57, N 21.76%; found: C 18.92, H 1.59, N 21.46%. IS: 30 J (grain size <100 µm). FS: 240 N (grain size <100 µm). ESD 0.1 J (grain size 100 µm).

3.6 References

[1] a) T. M. Klapötke, *Chemistry of High-Energy Materials*, de Gruyter, Berlin, 2nd edn, 2012; b) Q. J. Axthammer, B. Krumm and T. M. Klapötke, J. Org. Chem., 2015, **80**, 6329–6335; c) Q. J. Axthammer, T. M. Klapötke, B. Krumm, R. Moll and S. F. Rest, Z. Anorg. Allg. Chem., 2014, **640**, 76–83.

[2] a) M. Göbel, T. M. Klapötke, P. Mayer, *Z. Anorg. Allg. Chem.* 2006, **632**, 1043–1050; b) M. Göbel, T. M. Klapötke, *Adv. Funct. Mater.* 2009, **19**, 347–365; c) M. Göbel, T. M. Klapötke, *Z. Anorg. Allg. Chem.* 2007, **633**, 1006–1017.

[3] J. P. Agrawal, *High Energy Materials*, Wiley-VCH, Weinheim, Germany, 1st edn, 2010.

[4] A. D. Nikolaeva, I. L. Tsentsiper, V. S. Perekhod'ko, *Izv.Vyssh. Uchebn. Zaved., Khim. Khim. Tekhnol.*, 1980, **23**, 152–156.

[5] a) Y. A. Volkova, E. B. Averina, Y. K. Grishin, P. Bruheim, T. S. Kuznetsova, N. S. Zefirov, *J. Org. Chem.*, 2010, **75**, 3047–3052; b) Y. A. Volkova, O. A. Ivanova, E. M. Budynina, E. B. Averina, T. S. Kuznetsova and N. S. Zefirov, *Russ. Chem. Bull.*, 2008, **57**, 2034–2035.

[6] a) M. J. Kamlet, J. C. Dacons, J. C. Hoffsommer, *J. Org. Chem.* 1961, **26**, 4881–4886; b) I. J. Schaffner, *US* 3051743, 1962.

[7] D. J. Glover, J. C. Dacons, D. V. Sickman, M. E. Hill, M. J. Kamlet, *US* 3125606, 1964.

[8] Q. J. Axthammer, B. Krumm, T. M. Klapötke, R. Scharf, *Chem. – Eur. J.* 2015, **21**, 16229–16239.

[9] M. H. Gold, M. B. Frankel, G. B. Linden, K. Klager, *J. Org. Chem.* 1962, **27**, 334–336.

[10] a) M. B. Frankel, *Tetrahedron* 1963, **19**, 213-217.

[11] M. B. Frankel, *US* 2978509, 1961.

[12] a) H. Feuer, U. E. Lynch-Hart, *J. Org. Chem.* 1961, **26**, 391–394; b) H. Feuer, U. E. Lynch-Hart, *J. Org. Chem.* 1961, **26**, 587–589; c) I. J. Schaffner, *US* 3038009, 1962.

[13] a) R. H. Saunders, *US* 2996537, 1961; b) M. E. Hill, *US* 3230247, 1966.

[14] S. Bienz, L. Bigler, T. Fox, M. Hesse, H. Meier, B. Zeeh, *Spektroskopische Methoden in der Organischen Chemie*, Thieme, Stuttgart, 8th edn, 2014.

[15] T. Steiner, *Angew. Chem., Int. Ed.*, 2002, **41**, 48–76.

[16] T. M. Klapötke, B. Krumm, R. Moll, S. F. Rest, Y. V. Vishnevskiy, C. Reuter, H.-G. Stammler, N. W. Mitzel, *Chem. – Eur. J.* 2014, **20**, 12962–12973.

[17] a) T. M. Klapötke, B. Krumm, R. Scharf, *Eur. J. Inorg. Chem.* 2016, 3086–3093; b) A. Wolter-Steingrube, B. E. C. Bugenhagen, C. Herrmann, J. Heck, *Eur. J. Inorg. Chem.* 2014, 4115–4122; c) A. Baumann, A. Erbacher, C. Evangelisti, T. M. Klapötke, B. Krumm, S. F. Rest, M. Reynders, V. Sproll, *Chem. – Eur. J.* 2013, **19**, 15627–15638; d) G. C. Hsu, L. M. Singer, D. B. Cordes, M. Findlater, *Acta Crystallogr.* 2013, **69E**, 1298; e) J. Lapic, A. Pezerovic, M. Cetina, S. Djakovic, V. Rapic, *J. Mol. Struct.* 2011, **990**, 209–216; f) G. Laus, V. Kahlenberg, K. Wurst, S. Nerdinger, H. Schottenberger, *Z. Naturforsch.* 2011, **66B**, 479–486; g) D. Siebler, C. Forster, T. Gasi, K. Heinze, *Organometallics* 2011, **30**, 313–327; h) L. Parkanyi, G. Besenyei, *J. Mol. Struct.* 2004, **691**, 97–106; i) F. M. Menger, J. Bian, V. A. Azov, *Angew. Chem., Int. Ed.* 2002, **41**, 2581–2584; j) Y. Jiao, E. Valente, S. T. Garner, X. Wang, H. Yu, *Tetrahedron Lett.* 2002, **43**, 5879–5881.

[18] a) NATO, Standardization Agreement 4487 (STANAG 4487), Explosives, Friction Sensitivity Tests, 2002; b) NATO, Standardization Agreement 4489 (STANAG 4489), Explosives, Impact Sensitivity Tests, 1999.

[19] *Test methods according to the UN Manual of Test and Criteria, Recommendations on the Transport of Dangerous Goods*, United Nations Publication, New York, Geneva, 4th revised edn, 2003, Impact: Insensitive > 40 J, less sensitive ≥ 35 J, sensitive ≥ 4 J, very sensitive ≤ 3 J; Friction: Insensitive > 360 N, less sensitive = 360 N, sensitive < 360 N > 80 N, very sensitive ≤ 80 N, extremely sensitive ≤ 10 N.

[20] a) M. Sućeska, *EXPLO5 V.6.02*, Zagreb (Croatia), 2013; b) M. Sućeska, *Propellants, Explos., Pyrotech.* 1991, **16**, 197–202.

[21] R. Meyer, J. Köhler, A. Homburg, *Explosives*, Wiley-VCH, Weinheim (Germany), 7th edn, 2015.

[22] *CrysAlis CCD*, Version 1.171.35. (*release 16-05-2011 CrysAlis 171.Net*), Oxford Diffraction Ltd., Abingdon, Oxford (U. K.), 2011.

[23] *CrysAlis RED*, Version 1.171.35.11 (*release 16-05-2011 CrysAlis 171.NET*), Oxford Diffraction Ltd., Abingdon, Oxford (U. K.), 2011.

[24] A. Altomare, M. C. Burla, M. Camalli, G. L. Cascarano, C. Giacovazzo, A. Guagliardi, A. G. G. Moliterni, G. Polidori, R. Spagna, *J. Appl. Crystallogr.* 1999, **32**, 115–119.

[25] a) G. M. Sheldrick, *SHELX-97, Programs for Crystal Structure Determination*, 1997; b) G. M. Sheldrick, *Acta Crystallogr., Sect. A: Found. Crystallogr.* 2008, **64A**, 112–122.

[26] L. Farrugia, *J. Appl. Crystallogr.* 1999, **32**, 837–838.

[27] A. Spek, *Acta Crystallogr.* 2009, **65D**, 148–155.

[28] M. J. Frisch, G. W. Trucks, H. B. Schlegel, G. E. Scuseria, M. A. Robb, J. R. Cheeseman, V. B. G. Scalmani, B. Mennucci, G. A. Petersson, H. Nakatsuji, M. Caricato, X. Li, H. P. Hratchian, A. F. Izmaylov, J. Bloino, G. Zheng, J. L. Sonnenberg, M. Hada, M. Ehara, K. Toyota, R. Fukuda, J. Hasegawa, M. Ishida, T. Nakajima, Y. Honda, O. Kitao, H. Nakai, T. Vreven, J. J. A. Montgomery, J. E. Peralta, F. Ogliaro, M. Bearpark, J. J. Heyd, E. Brothers, K. N. Kudin, V. N. Staroverov, R. Kobayashi, J. Normand, K. Raghavachari, A. Rendell, J. C. Burant, S. S. Iyengar, J. Tomasi, M. Cossi, N. Rega, J. M. Millam, M. Klene, J. E. Knox, J. B. Cross, V. Bakken, C. Adamo, J. Jaramillo, R. Gomperts, R. E. Stratmann, O. Yazyev, A. J. Austin, R. Cammi, C. Pomelli, J. W. Ochterski, R. L. Martin, K. Morokuma, V. G. Zakrzewski, G. A. Voth, P. Salvador, J. J. Dannenberg, S. Dapprich, A. D. Daniels, Ö. Farkas, J. B. Foresman, J. V. Ortiz, J. Cioslowski, D. J. Fox, *Gaussian 09*, Gaussian, Inc., Wallingford CT (US), Rev. A.02 edn, 2009.

[29] R. D. Dennington, T. A. Keith, J. M. Millam, *GaussView*, Semichem, Inc., Wallingford CT Ver. 5.08 edn, 2009.

[30] J. A. Montgomery, M. J. Frisch, J. W. Ochterski, G. A. Petersson, *J. Chem. Phys.* 2000, **112**, 6532–6542.

[31] J. W. Ochterski, G. A. Petersson, J. A. Montgomery, *J. Chem. Phys.* 1996, **104**, 2598–2619.

[32] E. F. C. Byrd, B. M. Rice, *J. Phys. Chem.* 2005, **110**, 1005–1013.

[33] a) F. Trouton, *Philos. Mag.* 1884, **18**, 54–57; b) M. S. Westwell, M. S. Searle, D. J. Wales, D. H. Williams, *J. Am. Chem. Soc.* 1995, **117**, 5013–5015.

A STUDY OF THE 3,3,3-TRINITROPROPYL UNIT AS A POTENTIAL ENERGETIC BUILDING BLOCK

Quirin J. Axthammer, Burkhard Krumm, Thomas M. Klapötke, and Regina Scharf

as published in

Chemistry – A European Journal **2015**, *21*, 16229–16239.

In memory of Professor Dr. mult. Heinrich Nöth

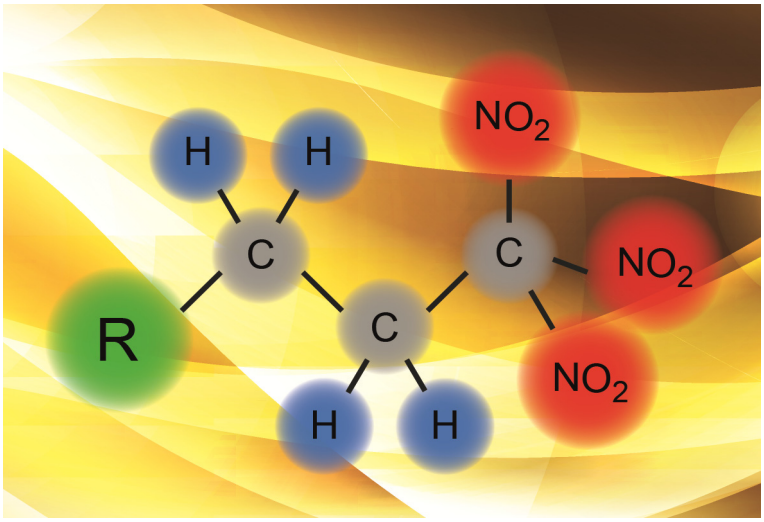

4.1 Abstract

Compared with the well-established 2,2,2-trinitroethyl group in the chemistry of energetic materials, the 3,3,3-trinitropropyl group is less investigated regarding its chemical and energetic properties. Thus, investigations on the syntheses of several compounds containing the 3,3,3-trinitropropyl group were performed and their properties compared with the 2,2,2-trinitroethyl group. All materials were thoroughly characterized, including single-crystal X-ray diffraction studies. The thermal stabilities were examined using differential thermal analysis (DSC) and the sensitivities towards impact, friction, and electrostatic discharge were tested using a drop hammer, a friction tester, and an electrical discharge device. The energies of formation were calculated and several detonation parameters such as the velocity of detonation and the propulsion performance were estimated with the program package EXPLO5.

4.2 Introduction

The 2,2,2-trinitroethyl group is a central building block in the synthesis of energetic materials, especially in the subgroup of high-energy dense oxidizers (HEDOs). This unit can readily be obtained by reacting trinitromethane and formaldehyde in a Henry reaction or by a Mannich condensation of an amine, formaldehyde, and trinitromethane.[1] Many compounds with this moiety have been synthesized and characterized in the recent years.[2,3] Unfortunately, the trinitroethyl moiety is unstable towards bases and nucleophiles and decomposes into their precursors.[4] In contrast, the 3,3,3-trinitropropyl moiety shows a higher chemical stability because such reverse Henry or Mannich reactions are not possible.[5] A disadvantage of the 3,3,3-trinitropropyl group is its quite complex synthesis and the lower oxygen content.[6] Although some compounds with a 3,3,3-trinitropropyl moiety have been reported, nothing is known about the energetic properties, the molecular structure, and the stability of such materials.

High-energy dense oxidizers (HEDOs) are energetic compounds that are based on CHNO and release the excess of included oxygen when ignited.[1b] These oxidizers are, in addition to further components such as binders and fuel, the main part (>70%) in solid rocket propellants.[7] The released oxygen reacts with the fuel, such as carbon backbones or aluminum, and produces plenty of hot gases, which are used for the impulsion of rockets.[8] Presently, ammonium perchlorate (AP), with a high oxygen content and a low price, is the

most commonly used oxidizer in composite propellants. Unfortunately, the combustion of AP releases large amounts of toxic gases such as hydrogen chloride, which causes environmental problems.[9] In addition, use of AP causes pollution of the groundwater in large areas throughout the world.[10] There is also proof that the perchlorate anion has negative health effects, particularly on the hormonal balance of humans and amphibians.[11] For these reasons, new halogen-free propellants with high performance and good stability are desirable.

4.3 Results and Discussion

4.3.1 Synthesis

The central precursor for this work (Scheme 4.1) is the reactive isocyanate 1,1,1-trinitropropan-3-isocyanate (**1**), which is available from a multistep synthesis, starting from a Michael addition of trinitromethane with acrylamide.[12] The salt 3,3,3-trinitropropan-1-amine hydrochloride (**2**) was obtained by controlled hydrolysis of **1** in hydrochloric acid. The amine was further converted into the corresponding alcohol 3,3,3-trinitropropanol (**3**) by a Sandmeyer-type reaction.[13] In this reaction, a diazonium salt is generated by in situ formed nitrous acid, which is subsequently displaced by a nucleophilic substitution with water. The urea derivative **4** is obtained by the reaction of two molecules of **1** by partial hydrolysis.[6b] For the synthesis of bis(3,3,3-trinitropropyl) oxalamide (**5**), the free amine generated from the hydrochloride salt **2** was reacted with oxalyl chloride.[14] The oxalate derivative bis(3,3,3-trinitropropyl) oxalate (**6**) was synthesized by the reaction of oxalyl chloride and the alcohol **3**. The conversion of the alcohol into 3,3,3-trinitropropyl carbamate (**7**) was first mentioned in the 1990s and was realized by a two-step synthesis. At that time, phosgene was reacted with **3** to form the chloroformate, which was further converted with aqueous ammonia to obtain the carbamate **7**.[15] Now, a one-step synthesis was achieved by using the reagent chlorosulfonyl isocyanate (CSI). The advantages of CSI are much shorter reaction times, easier handling of the starting materials, and trouble-free work up.[16] The carbamate **7** was obtained as a colorless, pure product in higher yield compared with the previous route.[15] The nitration of **7** resulted in the 3,3,3-trinitropropyl nitrocarbamate (**8**), which was performed in a mixture of concentrated sulfuric and nitric acid.[3c, 16c] Mannich condensations between an organic nitro compound, an aldehyde, and an amine are very useful reactions.[17] The condensation of the amine **2** with formaldehyde and trinitromethane produced the secondary amine 3,3,3-trinitropropyl-*N*-(2,2,2-trinitroethyl)

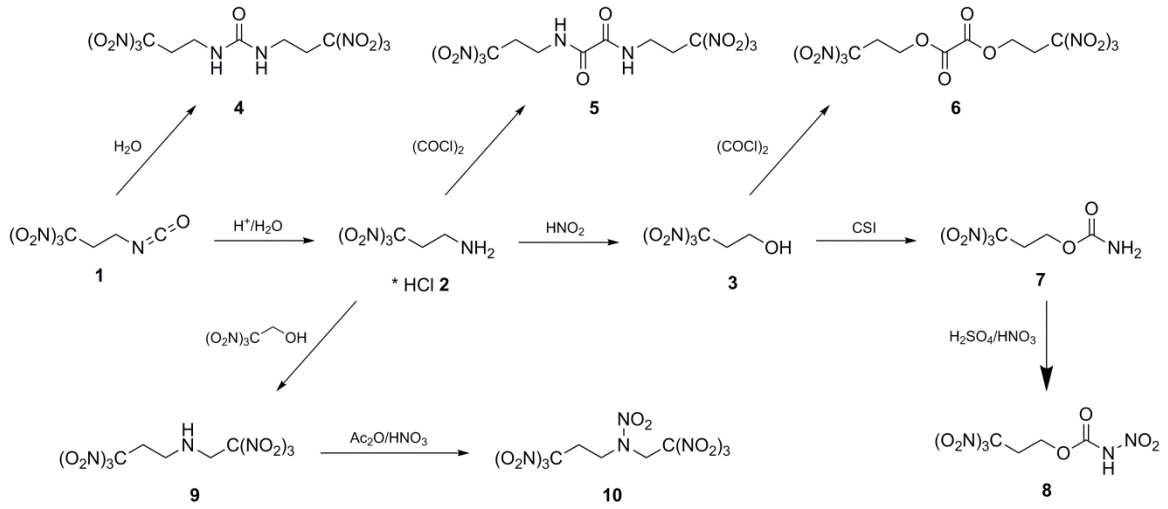

Scheme 4.1 Overview of 3,3,3-trinitropropyl-based compounds.

propan-1-amine (**9**) as a solid with a limited stability.[6a] Upon nitration of **9** in a mixture of acetic anhydride and anhydrous nitric acid, the highly energetic nitramine, *N*-(2,2,2-trinitroethyl)-*N*-(3,3,3-trinitropropyl) nitramine (**10**) was obtained.[6a] The nitramine **10** is air and moisture stable, has an oxygen and nitrogen content of 84%, and has a very high oxygen balance Ω_{CO} of +23.9 %.

4.3.2 NMR Spectroscopy

The ^{1}H, ^{13}C and ^{14}N NMR spectra were recorded in $CDCl_3$ (**1**, **3**, **4**, **9**), [D_3]acetonitrile (**2**, **9**), and [D_6]acetone (**5**–**8**). In the ^{1}H NMR spectra, the two CH_2 groups are within the range 4.84–3.14 ppm. The methylene unit next to the trinitromethyl moiety is shifted to higher field values compared with the CH_2 groups next to nitrogen or oxygen. The vicinal coupling constants of the hydrogen atoms in the ethylene group are not equal owing to the rotation around the C–C bond, causing a AA'XX' spin system.[18]

In the ^{13}C NMR spectra, the carbon resonances of the two CH_2 groups are found near 58 and 33 ppm. As expected, the same effect as in the proton NMR spectra is also observed in the ^{13}C NMR. The carbon resonances next to the trinitromethyl unit are always upfield shifted compared with those connected to the electron-withdrawing elements nitrogen and oxygen. The carbon resonance of the trinitromethyl moiety is observed as a broadened signal; in the case of 3,3,3-trinitropropyl, it is always located around 130 ppm. By comparing this signal with that of the 2,2,2-trinitroethyl unit in **9** and **10**, a significant upfield shift to approximately 125 ppm occurs; and the two groups can thus, be clearly distinguished.

In the ^{14}N NMR spectra, the resonances for the nitro groups of the trinitromethyl moieties are all quite sharp and found in the range of −29 to −32 ppm. For the nitramine **10**,

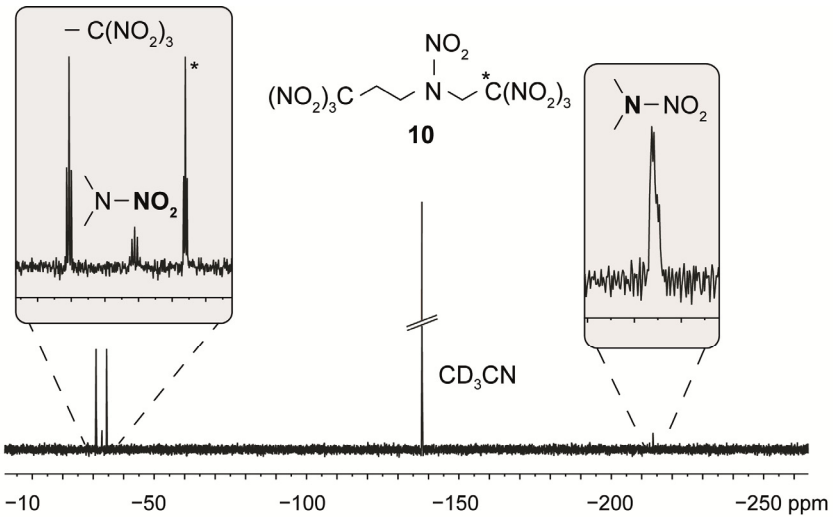

Figure 4.1 ^{15}N NMR spectrum of *N*-(2,2,2-trinitroethyl)-*N*-(3,3,3-trinitropropyl)-nitramine (**10**) in CD_3CN.

a typical ^{15}N NMR spectrum is shown in Figure 4.1, with full assignment of all nitrogen atoms. The nitrogen resonances of the trinitromethyl moieties were observed at −31.0 ppm for the 3,3,3-trinitropropyl unit and at −34.5 ppm for the 2,2,2-trinitroethyl unit. For both resonances, a triplet caused by coupling with the two neighboring methylene hydrogen atoms is present, with coupling constants of $^3J(^{15}N,^1H)$ = 2.8 Hz and $^3J(^{15}N,^1H)$ = 1.9 Hz.

The two nitrogen resonances of the nitramine moiety are observed as multiplets, as expected. The nitro group is located between the two triplets of the trinitromethyl groups at −32.9 ppm, and that of the amine, upfield at −213.7 ppm.

4.3.3 Vibrational Spectroscopy

All compounds were also characterized by their molecular vibration frequencies by IR and Raman spectroscopy. The most characteristic frequencies in the compounds are those of the carbonyl and nitro groups, which are summarized in Table 4.1. For the trinitromethyl units, both the asymmetric $\nu_{as}(NO_2)$ in the range 1600–1581 cm^{-1} and the symmetric stretching vibrations $\nu_s(NO_2)$ at 1285–1307 cm^{-1} are observed. For **8** and **10**, additional NNO_2 groups are included and also additional $\nu_{as}(NO_2)$ and $\nu_s(NO_2)$ vibrations appear at slightly higher wavenumbers.[19] Furthermore, the $\nu_{as}(NO_2)$ vibration is shifted to higher wavenumbers when connected to electron-withdrawing moieties; such as the carboxylate moiety in **6** (1600 cm^{-1}) compared with the carbamate moiety in **7** (1583 cm^{-1}). The same effect influences the C=O stretching vibrations ν(C=O). An example is the urea derivative **4**, where the ν(C=O) is located at 1642 cm^{-1}, whereas in the carbamate **7** (1704 cm^{-1}) and in the nitrocarbamate **8** (1758 cm^{-1}) significant shifts to higher energies are observed.

Table 4.1 Selected IR and Raman bands for **3**–**10**.[a]

	1		**2**		**3**		**4**	
	IR	**Raman**	**IR**	**Raman**	**IR**	**Raman**	**IR**	**Raman**
ν(CO)	-	-	-	-	-	-	1642 (m)	1644 (12)
$\nu_{as}(NO_2)$	1586 (s)	1610 (24)	1597 (s)	1606 (45)	1581 (s)	1608 (19)	1587 (m)	1593 (28)
$\nu_{s}(NO_2)$	1298 (m)	1304 (30)	1303 (m)	1312 (26)	1296 (s)	1306 (25)	1298 (m)	1309 (33)

	5		**6**		**7**		**8**	
	IR	**Raman**	**IR**	**Raman**	**IR**	**Raman**	**IR**	**Raman**
ν(CO)	1659 (m)	1694 (41)	1764 (m)	1769 (51)	1704 (m)	1699 (15)	1758 (m)	1760 (41)
$\nu_{as}(NO_2)$	1583 (s)	1607 (22)	1600 (s)	1615 (25)	1583 (s)	1617 (36)	1590 (s)	1617 (32)
$\nu_{as}(NO_2)$	1297 (m)	1299 (40)	1296 (m)	1292 (29)	1298 (m)	1299 (25)	1291 (m)	1307 (30) 1290 (31)

	9		**10**	
	IR	**Raman**	**IR**	**Raman**
ν(CO)	-	-	-	-
$\nu_{as}(NO_2)$	1581 (s)	1604 (21)	1599 (s) 1555 (s)	1613 (35)
$\nu_{as}(NO_2)$	1302 (s)	1309 (27)	1285 (s) 1268 (s)	1294 (23) 1270 (25)

[a] Frequencies in cm^{-1}; IR intensities: vs = very strong, s = strong, m = medium, w = weak; Raman intensities in brackets.

4.3.4 Single-Crystal X-Ray Diffraction

Single-crystals suitable for X-ray diffraction studies were obtained by crystallization at room temperature from dichloromethane (**6**, **8**, **10**), chloroform (**9**), or acetonitrile (**5**, **7**). A full list of the crystallographic refinement parameters and structural data for compounds **4**–**10** is shown in Appendix A4. To our knowledge, no molecular structure with a 3,3,3-trinitropropyl moiety is presently known.

The urea compound **4** crystallizes in the orthorhombic space group *Pccn* in a large unit cell containing twelve molecules. The asymmetric unit consists of one and a half molecules. The full molecule is shown in Figure 4.2. The C–N bond lengths in the trinitromethyl moiety are in the range of 1.53 Å, which is significantly longer than a regular C–N bond (1.47 Å) and results from steric repulsion from the three relatively large nitro groups around one carbon

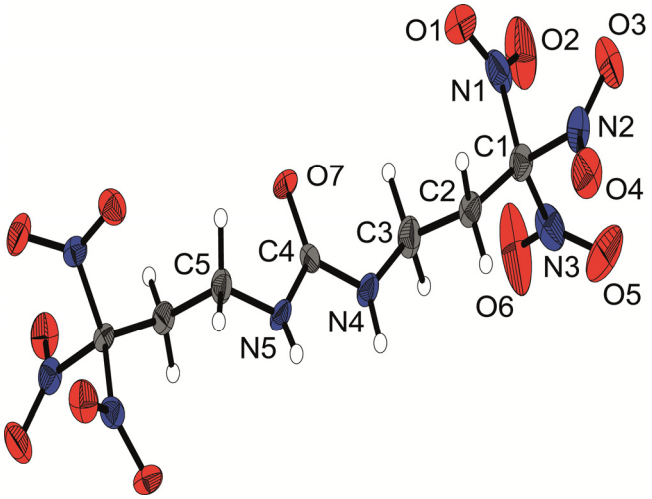

Figure 4.2 Molecular structure of bis(3,3,3-trinitropropyl) urea (**4**). Selected bond lengths [Å] and angles [°]: C1–C2 1.49 5(7), C1–N1 1.519(6), C1–N2 1.539(6), C1–N3 1.526(6), C2–C3 1.535(7), C3–N4 1.447(7), C4–N4 1.352(7), C4–N5 1.343(7), C4–O7 1.233(5); C5–N5–C4 123.0(5), O7–C4–N4 121.9(5), C4–N4–H5 120(4), H5–N4–C3 118(4), C3–N4–C4–O7 –6.5(8), H5–N4–C4–O7 –175(5), O7–C4–N5–C5 3.3(8).

atom.[3c] The three nitro groups are organized around the carbon in a propeller-like geometry to optimize the non-bonded N···O intramolecular attractions. This results in an intramolecular interaction between the partially positively charged nitrogen atom and the negatively charged oxygen atom in the nitro groups.[3c]

These N···O attractions are found to have distances in the range 2.41–2.63 Å, which are much shorter than the sum of the van der Waals radii of nitrogen and oxygen (3.07 Å).[3c, 20] This steric arrangement of the nitro groups was also observed in the half molecule of the asymmetric unit, which is completed by a proper two-fold rotation axis. Furthermore, a disorder of the trinitromethyl group is observed. Two different positions can be identified with a nearly equivalent proportion. In the disorder, the nitro groups always share an oxygen atom that is fully occupied, whereas the other oxygen atom and the nitrogen atom are independent (Appendix A4, Figure A4.1).

Another consequence of the trinitromethyl group's presence, with the quite strong electron-withdrawing effect of the nitro groups, is the reduced bond length of the neighboring carbon–carbon bond (C1–C2 1.485 Å).[2] As expected, the urea unit is nearly planar and shows typical bond geometry.

The oxalamide **5** and the oxalate **6** both crystallize in the monoclinic space group $P2_1/c$ and show the propeller-like steric geometry of the trinitromethyl group. In **5**, the asymmetric unit consists of two half independent molecules that are almost equal. An inversion center in the center of the carbon–carbon bond of the oxalamide moiety completes the molecule (Figure 4.3). The length of this bond (1.54 Å) is rather long for a sp_2

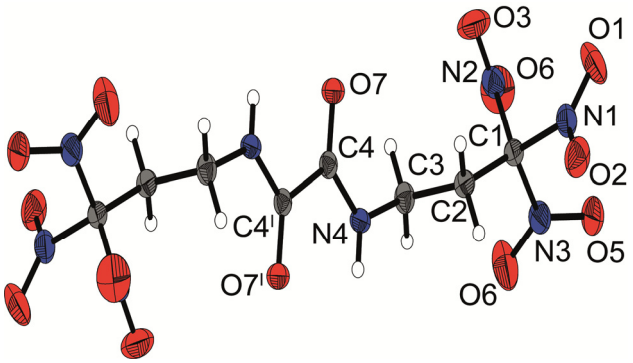

Figure 4.3 Molecular structure of bis(3,3,3-trinitropropyl) oxalamide (**5**). Selected bond lengths [Å] and angles [°]: C2–C1 1.506(2), C3–C2 1.531(3), C4–C4' 1.538(2), N4–C3 1.449(2), N4–C4 1.320(2); C3–N4–C4 121.8(2), H5–N4–C4 120(1), O7–C4–N4 125.0(2), O7–C4–C4 121.6(1), N4–C4–C4 113.4(1), C3–N4–C4–C4 178.3(1), N4–C4–C4–N4 –180.0(2), H5–N4–C4–O7 172(2).

carbon bond, but is common for an oxalamide structure.[21] The same was observed in the structure of oxalate **6** (Figure 4.4). The unique unit is here only one half of the molecule. The 3,3,3-trinitropropyl arm is nipped of to the oxygen O2 atom of the oxalate unit. This causes an additional N···O intramolecular attraction between the partially positively charged nitrogen N3 and O2, which is confirmed by the short distance (2.80 Å).

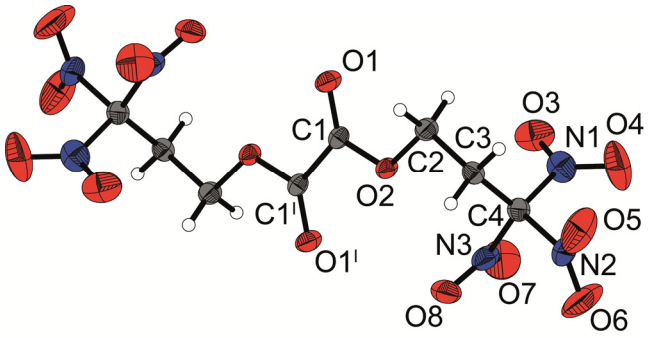

Figure 4.4 Molecular structure of bis(3,3,3-trinitropropyl) oxalate (**6**). Selected bond lengths [Å] and angles [°]: C1–O1 1.198(2), C1–O2 1.325(2), C1–C1' 1.540(2), C2–C3 1.513(2), C2–O2 1.454(2), C3–C4 1.504(2), N2–O4 2.535(2), N1–O7 2.632(2), N3–O6 2.554(2), N3–O2 2.800(2); O1–C1–O2 126.2(1), C3–C2–O2 107.6(1), O1–C1–O2–C2 4.0(2), C1–O2–C2–C3 173.3(1).

The carbamate **7** crystallizes in the orthorhombic space group *Pbca* with eight molecules in the unit cell and one molecule as the asymmetric unit (Figure 4.5). The carbamate moiety, the C2 carbon atom inclusive, shows a nearly planar arrangement. The bond lengths of the C1–N1 (1.33 Å) and the two N1–H bonds (0.85 and 0.86 Å) in the carbamate part are shortened, which is typical for such moieties.[3c] The conformations of the substituents at C2, C3, and C4 are all almost perfectly staggered. The extended structure involves secondary interactions in terms of classical intermolecular N–H···O hydrogen bonding and unusual hydrogen bonding with carbon as donor (C–H···O) (for further information, see Appendix

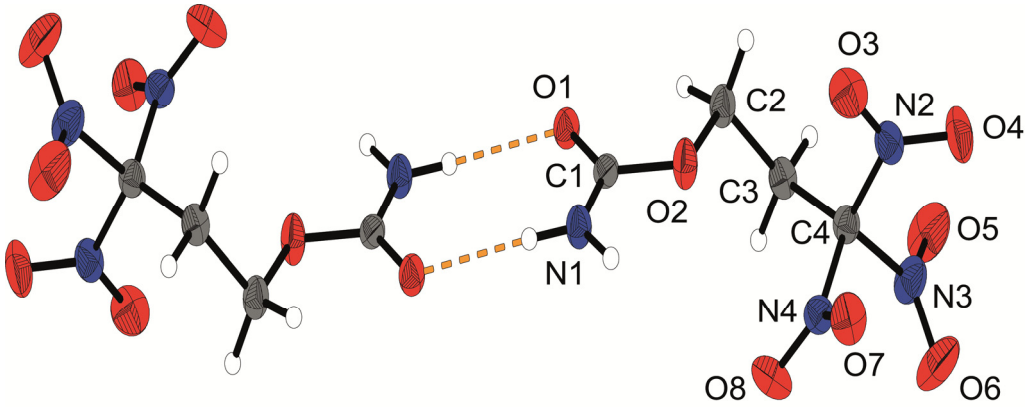

Figure 4.5 Molecular structure of two molecules of 3,3,3-trinitropropyl carbamate (**7**). Selected bond lengths [Å] and angles [°]: C1–N1 1.325(2), C1–O1 1.224(1), C1–O2 1.355(1), C2–C3 1.515(2), C2–O2 1.440(2), C3–C4 1.510(2), N1–H1 0.86(1), N1–H2 0.85(2), O2–N4 2.946(1), N4–O6 2.526(1), O7–N2 2.565(1), O3–N3 2.541(2); N1–C1–O1 125.9(1), N1–C1–O2 111.3(1), O1–C1–O2 122.7(1), C3–C2–O2 109.6(1), C2–C3–C4 117.4(1), H2–N1–C1–O1 –175(1), N1–C1–O2–C2 –179.1(1).

A4). The carbamate unit forms a nearly perfect planar eightmembered ring with another unit (Figure 4.5).

The crystal growing, data collection, solution and refinement of the 3,3,3-trinitropropyl nitrocarbamate (**8**) was difficult, as illustrated by the quite high refinement values. The data collection also had to be performed at ambient temperature owing to a phase transition at lower temperature. This is particularly interesting, as the related compound, 2,2,2-trinitroethyl nitrocarbamate, shows the same behavior.[3c] Compound **8** crystallizes in the orthorhombic space group *Pccn* with one molecule as an asymmetric unit (Figure 4.6). The nitrocarbamate moiety is in a perfect plane that includes the carbon atom C2. The N1–N2 bond length of the nitramine is 1.37 Å, which indicates a significant double bond character,

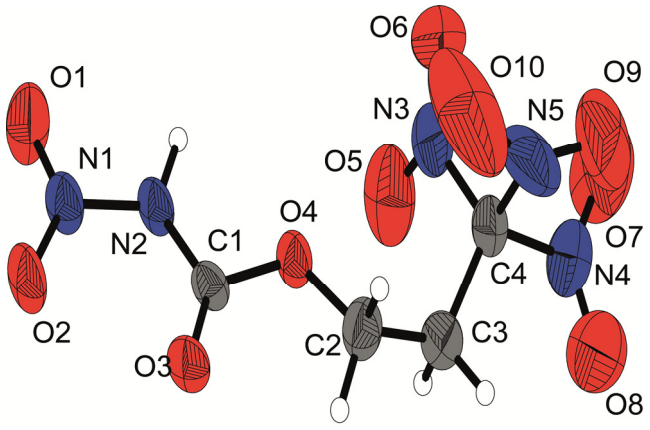

Figure 4.6 Molecular structure of 3,3,3-trinitropropyl nitrocarbamate (**8**). Selected bond lengths [Å] and angles [°]: O4–C1 1.329(5), O4–C2 1.430(6), O3–C1 1.182(4), C1–N2 1.367(5), N2–N1 1.367(6), C2–C3 1.491(8), C3–C4 1.501(8); C2–O4–C1 115.8(3), N2–C1–O4 107.0(4), N1–N2–C1 124.0(4), O1–N1–N2–C1 176.4(4), O2–N1–N2–H1 –176(3), H1–N2–C1–O3 172(3), N2–C1–O4–C2 177.3(3).

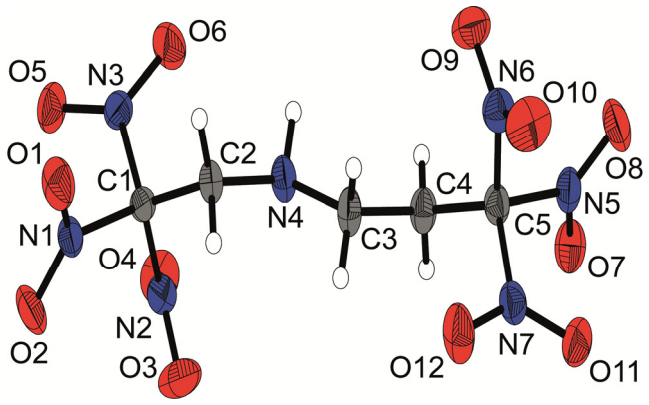

Figure 4.7 Molecular structure of 3,3,3-trinitro-*N*-(2,2,2-trinitroethyl) propan-1-amine (**9**). Selected bond lengths [Å] and angles [°]: N4–C2 1.467(3), N4–C3 1.451(3), N4–H3 0.92(2), C1–C2 1.513(3), C3–C4 1.515(3), C4–C5 1.503(3); C2–C1–N1 112.0(2), C2–C1–N2 110.5(2), C2–C1–N3 114.5(2), C4–C5–N5 111.7(2), C4–C5–N6 113.3(2), C4–C5–N7 114.5(2), C3–N4–H3 109(2), H3–N4–C2 111(2), C3–N4–C2 111.6(2).

which is achieved by delocalization of the nitrogen lone pair on N2. Compared with the carbamate structure of **7**, the carbonyl group (C1–O3) shows a slight shortening as a result of the electron-withdrawing nitro group.

The Mannich condensation product **9** crystallizes in the monoclinic space group $P2_1/c$ with two formula units per unit cell. The asymmetric unit consists of one and a half molecules, which is only possible through a disorder in the half molecule (Figure 4.7). This interesting disorder shows a statistical occupation of nitrogen and oxygen atoms (1:1) at the same position (Appendix A4, Figure A4.2). This disorder occurs as a result of an inversion center that is located on the *b* axis of the cell.[3a] The average of the N–O and C–NO_2 bond lengths of the trinitromethyl units in the ethyl and propyl moiety are all in the same range, which is about 1.21 Å for N–O and 1.52 Å for C–NO_2. Also, both trinitromethyl groups independently show propeller-like orientation of the nitro groups. Additionally, the carbon–carbon bonds are virtually identical, falling within the range 1.50–1.52 Å. The geometry around the nitrogen atom of the secondary amine is nearly tetrahedral with angles of 108.7, 111.6, and 111.6°.

The nitramine **10** crystallizes in the monoclinic space group *Pc* with glide planes as the only symmetry operation. In the unit cell there are two identical formula units (Figure 4.8). The geometric environment of the nitramine shows a more planar structure around the nitrogen atom N4, which is demonstrated by the quite high angle values of 115.6, 116.5, and 122.0°. This is achieved by the delocalization of the electron lone pair of the N4 nitrogen atom and is affected by the strong electronwithdrawing effect of the nitro group. Otherwise, the distances, angles, and the propeller-like structure are very identical to **9**. One very striking parameter for this structure is the high density of 1.902 g cm^{-3} at 173 K. This is even

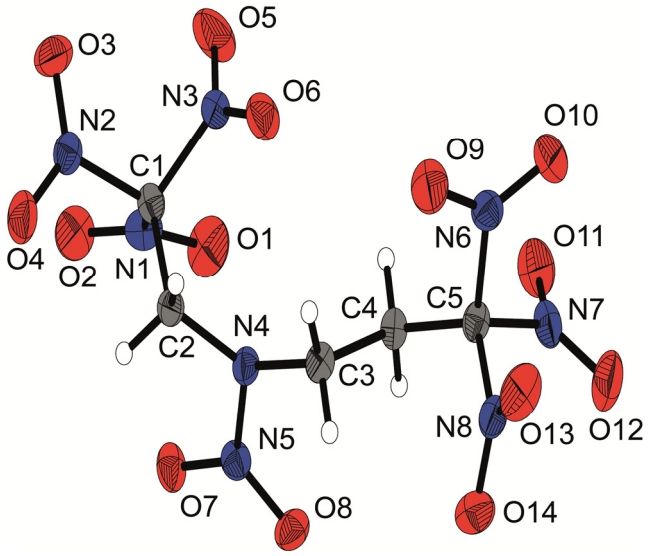

Figure 4.8 Molecular structure of *N*-(2,2,2-trinitroethyl)-*N*-(3,3,3-trinitropropyl) nitramine (**10**). Selected bond lengths [Å] and angles [°]: O8–N5 1.219(3), O7–N5 1.234(2), N5–N4 1.370(3), N4–C2 1.447(3), N4–C3 1.469(3), C1–C2 1.527(3), C3–C4 1.540(3), C5–C4 1.509(3); C2–N4–N5 115.6(2), N5–N4–C3 116.5(2), C2–N4–C3 122.0(2), C2–N4–N5–O8 −159.3(2), O7–N5–N4–C3 175.8(2), C5–C4–C3–N4 −179.6(2), N2–C1–C2–N4 176.8(2).

more remarkable because of the impossibility of forming classical hydrogen bonds. However, for each hydrogen atom, a so-called non-classical hydrogen bond of the type C–H···O is found, the majority of which are classified as quite strong.[22]

4.3.5 Thermal and Energetic Properties

Compounds **4**–**10** are possible energetic materials and, therefore, potential HEDOs. All molecules are stable when exposed to air and or moisture. Table 4.2 summarizes the physical and thermal properties. Melting points and thermal stabilities were investigated by differential scanning calorimetry (DSC) with a heating rate of 5 °C per minute. Quite high and satisfying melting and decomposition points were observed. For example, the oxalamide **5** shows the highest decomposition point at 181 °C. A clear trend in which the 3,3,3-rinitropropyl group shows higher thermal stability than the 2,2,2-trinitroethyl group, as anticipated, could not be confirmed. However, in the case of the nitramine **10**, the exchange of one ethyl for a propyl group leads to a tremendous difference and gives a 57 °C higher decomposition point than the corresponding ethyl derivative, bis(2,2,2-trinitroethyl) nitramine.[23] A comparison with the corresponding 2,2,2-trinitroethyl derivatives and common explosives is illustrated in Table 4.2.

For the manipulation of energetic materials, the sensitivity towards impact, friction, and electrostatic discharge is especially important. The sensitiveness towards impact (IS) of a compound is tested by the action of a dropping weight on a sample. The friction sensitivity

(FS) is determined by rubbing a small amount between a porcelain plate and a pin with different contact pressures.[24] Some compounds can be classified as sensitive toward friction (≥360 N insensitive, 360–80 N sensitive, 80–10 N very sensitive, ≤10 N extremely sensitive), and some are sensitive to impact (≥40 J insensitive, 40–35 J less sensitive, 35–4 J sensitive, ≤3 J very sensitive).[1b, 25] The compounds **9** and **10** take a special position owing to their high sensitiveness to impact and are in the range of the well-known explosive Hexogen (RDX). The relative electrostatic discharge (ESD) sensitivity of an explosive is tested with an apparatus, whereby variable capacitive resistances and loading voltages generate different spark energies. The electric discharge was determined which is needed to initiate a decomposition or an explosion. The lowest value for an initialization was found for the nitramine **10**, with an energy of 0.15 J, which is in the range of secondary explosives such as pentareythritol tetranitrate (PETN) and RDX.[24]

The main performance criteria of energetic materials are the heat of explosion, Q_v, the detonation velocity, V_{Det}, and the detonation pressure, P_{CJ}. All these detonation and combustion parameters are summarized in Table 4.3 (for further values, see Appendix A4). The performance data were calculated by the computer code EXPLO5 (V.6.02)[26] and based on the calculated energy of formation using CBS-4M ab initio calculations. The nitramine **10** has the highest energy of formation $\Delta_f U°$, with a value of −79.7 kJ kg^{-1}, which indicates a high energy content in the molecule. This and the high density are reflected by the very high detonation velocity, V_{Det}, of 9119 m s^{-1} compared with RDX (8838 ms^{-1}). The other compounds also show quite high detonation velocities, V_{Det}, in the range 7732–8713 m s^{-1} and these values are in the range of well-known explosives such as PETN (8403 m s^{-1}) and trinitrotoluene (TNT; 7241 m s^{-1}).

Another very important value, especially for high-energy dense oxidizers, is the specific impulse, I_s. Oxidizers are the main component in composite propellants and are the compounds that release the excess of included oxygen when ignited. This oxygen is used for the oxidation of further added fuel to generate a lot of heat and gases for the propulsion. As an effective fuel, aluminum is often used, which has a very high heat of combustion and thereby produces a very hot burning temperature.[8] Other advantages of aluminum are its low price, the low atomic weight, and its non-hazardous combustion product (Al_2O_3). The so-generated high burning temperature is important because the specific impulse, I_s, is proportional to the square root of the temperature.[1b] A further important factor is the molecular weight of the gaseous products at the nozzle exit of the rocket chamber, which is inversely proportional to the square root of the specific impulse.[1b] This means that for high performance, a high burning temperature and a low weight of the gaseous products, such as CO, CO_2, H_2O, or H_2, is required. For the following discussion, it is important that the payload

of the rocket can be doubled if the specific impulse is increased by 20 s. The specific impulses, I_s, of the compounds **3**–**10** were calculated as neat samples, with aluminum (15%), and with a binder/aluminum system (15% aluminum, 6% polybutadiene acrylic acid, 6% polybutadiene acrylonitrile, and 2% bisphenol A ether). These impulses were compared with the calculated impulse of ammonium perchlorate (AP) in an analogous composition. The specific impulses, I_s, for the neat compounds show altogether much higher values than AP, which is predictable as the compounds have their own fuel in form of the carbon backbone. The neat compounds **9** and **10** show impulse values of 272 s and 264 s, which are already higher than the optimized composite of AP (261 s). A further advantage of the neat compounds are the burning residues, which are harmless and entirely gaseous products, and make the RADAR detection of such propulsion systems quite complicated.[1a] The addition of aluminum (15%) as fuel increases the values for all compounds; the carbamate **7** shows the lowest value at 256 s and the amine **9** has the highest specific impulse with 274 s. The optimized standard mixture for AP is composed of 71% oxidizer, 15% aluminium, and 14% binder. In such a system, all impulses decrease, an effect that is caused by the increase of the carbon content. Only the nitramine **10** can outperform AP with a value of 267 s in such a binder mixture. Therefore, smaller amounts of binder are more suitable for this type of CHNO oxidizers. For example, with only half the amount of binder, the value of the specific impulse of **10** can be enhanced to 275 s.

Table 4.2 Comparison of physical and chemical properties of materials containing the 3,3,3-trinitropropyl and 2,2,2-trinitroethyl groups with common explosives AP, TNT, and RDX.

	4		**5**		**6**		**7**		**8**		**9**		**10**		**AP**	**TNT**	**RDX**
	propyl	**ethyl**	**propyl**	**ethyl**	**propyl**	**ethyl**	**propyl**	**ethyl**	**propyl**	**ethyl**	**propyl**	**ethyl**	**propyl**	**ethyl**			
T_m [°C] (onset)[a]	-	185	-	n.a.	121	115	78	91	68	109	65	114	141	94	-	81	204
T_{dec} [°C] (onset)[b]	160	187	181	n.a.	170	186	152	169	134	153	96	114	153	96	240	248	228
IS [J][c]	20	3	10	n.a.	> 40	10	> 40	40	> 30	10	7	5	7	2	20	15	7
FS [N][d]	120	160	160	n.a.	> 360	> 360	> 360	64	> 288	96	120	120	160	64	360	360	120
ESD [N][e]	0.40	n.a.	0.50	n.a.	0.40	n.a.	0.30	n.a.	0.20	n.a.	0.20	n.a.	0.15	n.a.	0.50	0.45	0.20
N [%][f]	27.1	29.0	25.3	27.1	18.9	20.2	23.5	25.0	24.7	26.0	27.5	28.6	27.9	28.9	11.9	18.5	37.8
O [%][g]	50.2	53.9	50.7	54.1	57.6	61.5	53.8	57.1	56.5	59.5	53.8	56.0	55.7	57.7	54.5	42.3	43.2
N + O [%][h]	77.3	82.9	76.0	81.2	76.5	81.7	77.3	82.1	81.2	85.5	81.3	84.6	83.6	86.6	66.4	60.8	81.0
Ω_{CO} [%][i]	+3.9	+20.7	+3.6	+19.3	+14.4	+30.8	+6.7	+21.4	+19.8	+32.7	+15.7	+25.7	+23.9	+33.0	+34.0	−24.7	0
Ω_{CO2} [%][j]	−20.2	+0.0	−20.3	−3.9	−14.4	+7.7	−20.2	0	−2.8	+14.9	−6.7	+7.0	+4.0	+16.5	+34.0	−74.0	−21.6

[a] Onset melting T_m and [b] onset decomposition point T_{dec} from DSC measurement carried out at a heating rate of 5 °C min^{-1}. [c] Impact sensitivity. [d] Friction sensitivity. [e] Sensitivity towards electrostatic discharge. [f] Nitrogen content. [g] Oxygen content. [h] Sum of nitrogen and oxygen content. [i] Oxygen balance assuming the formation of CO and [j] CO_2, respectively..

Table 4.3 Calculated heats of formation, predicted detonation and combustion parameters (using the EXPLO5 V6.02 code) for **4**–**10** compared with AP.

	4	**5**	**6**	**7**	**8**	**9**	**10**	**AP**
formula	$C_7H_{10}N_8O_{13}$	$C_8H_{10}N_8O_{14}$	$C_8H_8N_6O_{16}$	$C_4H_6N_4O_8$	$C_4H_5N_5O_{10}$	$C_5H_7N_7O_{12}$	$C_5H_6N_8O_{14}$	NH_4ClO_4
density RT[a]	1.75	1.71	1.67	1.73	1.70	1.78	1.89	1.95
$\Delta_f H_m°$ [kJ mol^{-1}][b]	−359.1	−522.3	−789.4	−503.5	−401.7	−86.4	−66.8	−295.8
$\Delta_f U°$ [kJ kg^{-1}][c]	−774.1	−1091.5	−1693.5	−2021.0	−1331.3	−151.7	−79.7	−2623.2
Q_v [kJ kg^{-1}][d]	−5385	−5095	−5126	−4662	−5809	−6565	−6377	−1422
T_{ex} [K][e]	3692	3605	3808	3328	4175	4445	4420	1735
V_0 [L kg^{-1}][f]	739	732	724	724	755	738	756	885
P_{CJ} [kbar][g]	294	268	256	265	269	330	367	158
V_{Det} [m s^{-1}][h]	8227	7937	7732	7896	8134	8713	9119	6368
I_s [s][i]	254	245	250	237	256	272	264	157
I_s [s] (15% Al)[j]	267	263	259	256	261	274	269	235
I_s [s] (15% Al, 14% binder)[k]	251	245	246	240	253	261	267	261

[a] RT densities are recalculated from X-ray densities. [b] Enthalpy and [c] energy of formation calculated by the CBS-4M method using Gaussian 09. [d] Heat of explosion. [e] Explosion temperature. [f] Volume of gaseous products. [g] Detonation pressure and [h] detonation velocity calculated by using the EXPLO5 (Version 6.02) program package.[26] [i] Specific impulse of the neat compound using the EXPLO5 (Version 6.02) program package at 70.0 bar chamber pressure.[26] [j] Specific impulse for compositions with 85% oxidizer/compound and 15% aluminum. [k] Specific impulse for compositions with 71% oxidizer/compound, 15% aluminum, and 14% binder (6% polybutadiene acrylic acid, 6% polybutadiene acrylonitrile, and 2% bisphenol A ether).

4.4 Conclusion

A variety of compounds with energetic properties based on the 3,3,3-trinitropropyl group were synthesized and thoroughly characterized, including X-ray diffraction. The thermal stabilities were measured by different scanning calorimetry (DSC). In general, the expected higher decomposition points compared with the 2,2,2-trinitroethyl group could not be confirmed; however, some higher stabilities were detected. Additionally, this is confirmed by the lower sensitivities of the 3,3,3-trinitropropyl compounds discussed here.

With respect to application as high-energy dense oxidizers in composite solid rocket propellants, several energetic performance data were calculated. The best compound, with excellent detonation parameters, is the nitramine **10**, which has a very high detonation velocity (9119 m s^{-1}) and a strong detonation pressure; both values significantly exceed those of TNT, RDX, and PETN (for details, see Appendix A4). Thus, **10** seems to serve as a good oxidizer candidate for composite rocket propellants. The specific impulse, I_s, reaches 269 s within a mixture of 15% aluminum as fuel, which is a result of the quite high energy of formation and the positive oxygen balance (Ω_{CO} = +23.9). However, the synthesis of such 3,3,3-trinitropropyl-containing materials is more elaborate compared with compounds containing 2,2,2-trinitroethyl groups.

4.5 Experimental Section

General Information

All chemicals were used as supplied. Raman spectra were recorded in a glass tube with a Bruker MultiRAM FT-Raman spectrometer with Nd:YAG laser with excitation up to 1000 mW at 1064 nm in the range 400–4000 cm^{-1}. Infrared spectra were measured with a PerkinElmer Spectrum BX-FTIR spectrometer equipped with a Smiths DuraSamplIR II ATR device. All spectra were recorded at ambient temperature. NMR spectra were recorded with a JEOL Eclipse 400 instrument and chemical shifts were determined with respect to external standards, Me_4Si (^1H, 399.8 MHz; ^{13}C, 100.5 MHz) and $MeNO_2$ (^{15}N, 40.6 MHz; ^{14}N, 28.8 MHz). Mass spectrometric data were obtained with a JEOL MStation JMS 700 spectrometer (DCI+, DEI+). Analysis of C/H/N were performed with an Elemental VarioEL Analyzer. Melting and decomposition points were measured with a PerkinElmer Pyris6 DSC and an OZM Research DTA 552-Ex with a heating rate of 5 °C min^{-1} in a temperature range 15–400 °C and checked by a Büchi Melting Point B-540 apparatus (not corrected). The sensitivity data were performed by using a BAM drophammerand a BAM friction tester.[2, 25]

X-ray Crystallography

Crystals suitable for X-ray crystallography were selected by means of a polarization microscope and mounted on the tip of a glass fiber. The measurements were investigated with an Oxford XCalibur3 (**4**, **5**, **6**, **7**, **9**, and **10**) or a Bruker-Nonius KappaCCD diffractometer (**8**). The diffractometers are equipped with a generator (voltage 50 kV, current 40 mA) and a KappaCCD detector operating with Mo_{Ka} radiation (λ=0.7107 Å). The solution of the structure was performed by direct methods (SIR97)[27] and refined by fullmatrix least-squares on F_2 (SHELXL)[28] implemented in the WINGX software package[29] and finally checked with the PLATON software.[30] All non-hydrogen atoms were refined anisotropically. The hydrogen atom positions were located on a difference Fourier map. ORTEP plots are shown with thermal ellipsoids at the 50% probability level. CCDC-1062382 (**4**), 1062383 (**5**), 1062384 (**6**), 1062385 (**7**), 1062386 (**8**), 1062387 (**9**), and 1062388 (**10**) contain the supplementary crystallographic data for this paper. These data can be obtained free of charge from The Cambridge Crystallographic Data Centre via www.ccdc.cam.ac.uk/data_request/cif.

Quantum Chemical Calculations

All ab initio calculations were carried out by using the program package Gaussian 09 (Rev. A.02)[31] and visualized by GaussView 5.08.[32] Structural optimizations and frequency analyses were performed with Becke's B3 three parameter hybrid functional using the LYP correlation functional (B3LYP). For C, H, N, and O, a correlation-consistent polarized double-zeta basis set cc-pVDZ was used. The structures were optimized with symmetry constraints and the energy was corrected with the zero point vibrational energy.[33] The enthalpies (H) and free energies (G) were calculated by using the complete basis set (CBS) method in order to obtain accurate values. The CBS models used the known asymptotic convergence of pair natural orbital expressions to extrapolate from calculations using a finite basis set to the estimated complete basis set limit. CBS-4M starts with a HF/3-21G(d) geometry optimization, which is the initial guess for the following SCF calculation as a base energy and a final MP2/6-31+G calculation with a CBS extrapolation to correct the energy in second order. The used CBS-4M method additionally implements a MP4(SDQ)/6-31+(d,p) calculation to approximate higher order contributions and also includes some additional empirical corrections.[34] The enthalpies of the gas-phase species were estimated according to the atomization energy method.[35]

Syntheses

CAUTION! All prepared compounds are energetic materials with sensitivity toward heat, impact, and friction. Although no hazards occurred during preparation and manipulation, additional proper protective precautions (face shield, leather coat, earthened equipment and shoes, Kevlar® gloves and ear plugs) should be used when undertaking work with these compounds.

1,1,1-Trinitropropan-3-isocyanate (**1**)

Prepared according to references [5, 12].

^{1}H NMR ($CDCl_3$): δ = 3.90 (m, 2H, CH_2), 3.32 (m, 2H, CH_2) ppm; ^{13}C NMR ($CDCl_3$): δ = 127.4 ($C(NO_2)_3$), 123.6 (NCO), 37.4 (CH$_2$), 35.0 (CH$_2$) ppm; ^{14}N NMR ($CDCl_3$): δ = −31 (C(NO_2)$_3$), −360 (NCO) ppm; elemental analysis calcd (%) for $C_4H_4N_4O_7$ (220.10): C 21.83, H 1.83, N 25.46; found: C 21.31, H 1.80, N 26.07; IR (ATR): ν = 3380 (w), 2956 (w), 2897 (w), 2269 (m, ν(NCO)), 2155 (w), 1721 (m), 1584 (s, $\nu_{as}(NO_2)$), 1423 (m), 1364 (m), 1297 (s, $\nu_s(NO_2)$), 1227 (m), 1195 (m), 1148 (m), 1092 (w), 1065 (w), 980 (w), 897 (w), 854 (m), 811 (m), 798 (s), 754 (m), 667 (w) cm^{-1}; Raman (1000 mW): ν = 2953 (70), 2156 (13), 2147 (13), 1718 (11), 1610 (24, $\nu_{as}(NO_2)$), 1451 (18), 1421 (22), 1363 (37), 1304 (30, $\nu_s(NO_2)$), 1100 (10), 1051 (13), 914 (20), 887 (12), 856 (100), 811 (10), 535 (10), 502 (16), 460 (10), 375 (68), 305 (17), 279 (22), 254 (20) cm^{-1}.

3,3,3-Trinitropropan-1-amine hydrochloride (**2**)

Prepared according to references [6b, 12].

^{1}H NMR (CD_3CN): δ = 7.92 (br, NH_3), 3.69 (m, 2H, CH_2), 3.42 (m, 2H, CH_2) ppm; ^{13}C NMR (CD_3CN): δ = 125.7 ($C(NO_2)_3$), 34.6 (CH$_2$), 30.8 (CH$_2$) ppm; ^{14}N NMR (CD_3CN): δ = −31 (C(NO_2)$_3$), −349 (NH$_3$) ppm; elemental analysis calcd (%) for $C_3H_9N_4O_7$ (230.56): C 15.63, H 3.06, N 24.30; found: C 15.94, H 3.06, N 24.30; IR (ATR): ν = 3132 (m), 3101 (m), 3035 (m), 2977 (m), 2890 (m), 2833 (m), 2783 (w), 2705 (w), 2655 (w), 2567 (w), 2500 (w), 1597 (s, $\nu_{as}(NO_2)$), 1499 (w), 1478 (w), 1458 (m), 1425 (w), 1303 (m, $\nu_s(NO_2)$), 999 (w), 973 (w), 954 (w), 895 (w), 790 (w) cm^{-1}; Raman (300 mW): ν = 3038 (9), 2993 (18), 2965 (34), 2937 (37), 2850 (6), 2806 (8), 1606 (45, $\nu_{as}(NO_2)$), 1471 (10), 1434 (12), 1370 (52), 1346 (17), 1312 (26, $\nu_s(NO_2)$), 1301 (23, $\nu_s(NO_2)$), 1162 (12), 1147 (14), 1022 (11), 989 (15), 924 (12), 911 (17), 858 (100), 802 (8), 739 (6), 656 (6), 643 (6), 557 (9), 408 (66), 383 (64), 343 (47), 289 (20), 221 (7) cm^{-1}; IS: 20 J (grain size 100–250 mm); FS: 360 N (grain size 100–250

mm); ESD: >0.5 J (grain size 100–250 mm); ESD: >0.4 J (grain size 100–250 mm); DSC (5 °C min^{-1}, onset): 161 °C (m.p.), 178 °C (dec.).

3,3,3-Trinitropropanol (**3**)

3,3,3-Trinitropropan-1-amine hydrochloride (**2**) (1.0 g, 4.3 mmol) was dissolved in water (10 mL) and a solution of $NaNO_2$ (0.60 g, 8.7 mmol) in water (10 mL) was slowly added at 0 °C. The yellow solution was stirred at 0 °C for 1 h and at 60 °C for 1.5 h. The reaction mixture was extracted with dichloromethane (3 × 25 mL), washed with brine (25 mL), and dried over $MgSO_4$. After removing the solvent in vacuo, 3,3,3-trinitropropanol (**3**) was obtained as a slightly yellow oil (0.65 g, 78%).

^{1}H NMR ($CDCl_3$): δ = 4.12 (m, 2H, CH_2), 3.33 (m, 2H, CH_2), 1.99 (s, 1H, OH) ppm; ^{13}C NMR ($CDCl_3$): δ = 128.1 ($C(NO_2)_3$), 56.5 ($C$$H_2$OH), 36.6 ($C$$H_2$) ppm; ^{14}N NMR ($CDCl_3$): δ = −30 (NO_2) ppm; elemental analysis calcd (%) for $C_3H_5N_3O_7$ (195.09): C 18.47, H 2.58, N 21.54; found: C 18.92, H 2.59, N 21.49; IR (ATR): ν = 3599 (w), 3385 (br, w, ν(OH)), 2947 (w), 2904 (w), 1581 (s, $\nu_{as}(NO_2)$), 1473 (w), 1420 (w), 1368 (m), 1296 (s, $\nu_s(NO_2)$), 1223 (w), 1140 (w), 1071 (m), 1035 (m), 984 (w), 924 (w), 854 (m), 842 (m), 811 (m), 798 (s), 771 (m) cm^{-1}; Raman (300 mW): ν = 2992 (60), 2984 (60), 2949 (100), 2913 (41), 1608 (19, $\nu_{as}(NO_2)$), 1478 (7), 1458 (9), 1425 (15), 1368 (35), 1350 (23), 1306 (25, $\nu_s(NO_2)$), 1082 (8), 926 (7), 857 (57), 472 (6), 375 (23), 336 (6) cm^{-1}; IS: >40 J; FS: >360 N; DSC (5 °C min^{-1}, onset): 141 °C (boil. with dec.).

Bis(3,3,3-trinitropropyl) urea (**4**)

3,3,3-Trinitropropyl-1-isocyanate (**1**) (2.20 g, 10 mmol) was dissolved in a mixture of acetone/water (3:1; 12 mL) and heated at reflux for 3 h. After evaporating the solvent in vacuo, a yellow solid was obtained, which was recrystallized from chloroform. Bis(3,3,3-trinitropropyl) urea (**4**) was obtained as a pure colorless solid (1.82 g, 88%).

^{1}H NMR ($CDCl_3$): δ = 4.58 (br, 2H, NH), 3.64 (m, 4H, CH_2), 3.35 (m, 4H, CH_2) ppm; ^{13}C NMR ($(CD_3)_2CO$): δ = 158.5 (CO), 130.8 ($C(NO_0)_3$), 35.9 ($C$$H_2$), 35.0 ($C$$H_2$) ppm; ^{14}N NMR ($CDCl_3$): δ = −30 (NO_2) ppm; elemental analysis calcd (%) for $C_7H_{10}N_8O_{13}$ (414.20): C 20.30, H 2.43, N 27.05; found: C 20.32, H 2.36, N 26.80; IR (ATR): ν = 3345 (w), 2945 (w), 2881 (w), 1642 (m, ν(CO)), 1587 (s, $\nu_{as}(NO_2)$), 1566 (s), 1460 (w), 1442 (w), 1425 (w), 1392 (w), 1365 (w), 1298 (m, $\nu_s(NO_2)$), 1262 (m), 1246 (m), 1144 (m), 1101 (w), 1037 (w), 943 (w), 892 (w), 856 (m), 826 (w), 796 (s), 770 (w) cm^{-1}; Raman (1000 mW): ν = 2979 (35), 2944 (53), 1644 (12, ν(CO)), 1593 (28, $\nu_{as}(NO_2)$), 1443 (19), 1427 (24), 1388 (25), 1367 (50), 1309 (33,

$\nu_s(NO_2)$), 1147 (16), 1119 (15), 1045 (30), 977 (10), 924 (14), 896 (14), 859 (100), 800 (10), 769 (9), 635 (14), 597 (11), 518 (19), 406 (53), 376 (51), 278 (34) cm^{-1}; IS: 20 J (grain size 100–250 mm); FS: 120 N (grain size 100–250 mm); ESD: >0.4 J (grain size 100–250 mm); DSC (5 °C min^{-1}, onset): 160 °C (dec.).

Bis(3,3,3-trinitropropyl) oxalamide (**5**)

3,3,3-Trinitropropan-1-amine hydrochloride (**2**) (1.00 g, 4.3 mmol) was dissolved in water (15 mL). The solution was overlayed with diethyl ether (30 mL) and cooled to 0 °C. Sodium hydrogen carbonate (0.40 g, 4.8 mmol) was added in small portions and the mixture was stirred for 30 min at 0 °C. The organic layer was separated and the aqueous solution was extracted with diethyl ether (2 × 25 mL). The combined organic phase was dried over $MgSO_4$ and cooled to 0 °C. Oxalyl chloride (0.20 g, 1.7 mmol) was slowly added to the organic phase. After 20 min, the precipitated solid was filtered off, washed with cooled diethyl ether and dried. Bis(3,3,3-trinitropropyl) oxalamide (**5**) was obtained as a pure colorless solid (0.61 g, 75%).

^{1}H NMR ($(CD_3)_2CO$): δ = 8.56 (br, 2H, N*H*), 3.83 (m, 4H, CH_2), 3.69 (m, 4H, CH_2) ppm; ^{13}C NMR ($(CD_3)_2CO$): δ = 160.8 (*C*(O)O), 130.4 (*C*$(NO_2)_3$), 35.0 (*C*H_2), 33.8 (*C*H_2) ppm; ^{14}N NMR ($(CD_3)_2CO$): δ = −29 (NO_2) ppm; elemental analysis calcd (%) for $C_8H_{10}N_8O_{14}$ (442.21): C 21.73, H 2.28, N 25.34; found: C 21.63, H 2.29, N 25.26; IR (ATR): ν = 3273 (w), 3066 (w), 2949 (w), 2892 (w), 1687 (w), 1659 (m, ν(CO)), 1621 (m), 1583 (s, $\nu_{as}(NO_2)$), 1521 (s), 1444 (w), 1423 (w), 1376 (w), 1325 (w), 1297 (m, $\nu_s(NO_2)$), 1258 (m), 1227 (m), 1147 (w), 1112 (w), 1053 (w), 1029 (w), 939 (w), 857 (w), 825 (m), 798 (m), 781 (m), 751 (w), 725 (w) cm^{-1}; Raman (300 mW): ν = 3298 (7), 3282 (8), 3025 (10), 2985 (24), 2950 (67), 1694 (41, n(CO)), 1607 (22, $\nu_{as}(NO_2)$), 1561 (18), 1447 (18), 1430 (19), 1367 (39), 1336 (22), 1299 (40, $\nu_s(NO_2)$), 1244 (17), 1117 (10), 1050 (22), 947 (16), 885 (18), 859 (100), 801 (12), 750 (7), 648 (8), 584 (12), 515 (9), 452 (11), 422 (28), 397 (37), 382 (54), 309 (9), 275 (35), 229 (14) cm^{-1}; IS: 10 J (grain size 100–250 mm); FS: 160 N (grain size 100–250 mm); ESD: >0.5 J (grain size 100–250 mm); DSC (5 °C min^{-1}, onset): 181 °C (dec.).

Bis(3,3,3-trinitropropyl) oxalate (**6**)

3,3,3-Trinitropropanol (**3**) (0.50 g, 2.6 mmol) was added slowly at 0 °C to a solution of oxalyl chloride (0.16 g, 1.3 mmol) in THF (10 mL). The reaction mixture was stirred for 1 h at 25 °C and heated at reflux for further 16 h. The reaction mixture was cooled and the solvent

was removed in vacuo. The crude solid product was recrystallized from acetone, yielding pure bis(3,3,3-trinitropropyl) oxalate (**6**) (0.50 g, 87%) as a colorless solid.

^{1}H NMR ($(CD_3)_2CO$): δ = 4.83 (m, 2H, CH_2), 4.02 (m, 2H, CH_2) ppm; ^{13}C NMR ($(CD_3)_2CO$): δ = 156.3 (C(O)O), 129.8 ($C(NO_2)_3$), 60.6 (CH_2O), 33.2 (CH_2) ppm; ^{14}N NMR ($(CD_3)_2CO$): δ = −30 (NO_2) ppm; elemental analysis calcd (%) for $C_8H_8N_6O_{16}$ (444.18): C 21.63, H 1.82, N 18.92; found: C 22.01, H 1.91, N 18.62; IR (ATR): ν = 2998 (w), 2960 (w), 1764 (m, n(CO)), 1753 (m), 1600 (s, $\nu_{as}(NO_2)$), 1580 (s), 1463 (w), 1412 (w), 1387 (w), 1373 (w), 1296 (m, $\nu_s(NO_2)$), 1261 (w), 1244 (w), 1193 (s), 1143 (w), 1105 (w), 1043 (m), 922 (w), 854 (w), 832 (w), 801 (m), 792 (m), 765 (m), 660 (w) cm^{-1}; Raman (300 mW): ν = 3029 (16), 2998 (46), 2982 (58), 2959 (77), 2905 (11), 1769 (51, n(CO)), 1615 (25, $\nu_{as}(NO_2)$), 1597 (22), 1462 (17), 1415 (21), 1377 (32), 1352 (15), 1292 (29, $\nu_s(NO_2)$), 1246 (14), 1107 (12), 1053 (23), 938 (22), 923 (24), 855 (100), 821 (10), 801 (8), 767 (7), 632 (8), 510 (11), 466 (15), 416 (41), 391 (64), 368 (58), 323 (8), 258 (18), 230 (15) cm^{-1}; IS: >40 J (grain size <100 mm); FS: >360 N (grain size <100 mm); ESD: >0.4 J (grain size <100 mm); DSC (5 °C min^{-1}, onset): 121 °C (melt.), 170 °C (dec.).

3,3,3-Trinitropropyl carbamate (**7**)

3,3,3-Trinitropropanol (**3**) (1.20 g, 6.1 mmol) was dissolved in dry acetonitrile (20 mL) and cooled to 0 °C. Chlorosulfonyl isocyanate (CSI, 0.95 g, 6.7 mmol) was added slowly. The ice bath was removed and stirring at room temperature was continued for 1 h. The reaction mixture was again cooled with an ice bath and water (10 mL) was added with caution. The reaction mixture was stirred further 10 min at room temperature to complete hydrolysis. The organic solvent was removed in vacuo and the formed precipitate was filtered. The light yellow precipitate was recrystallized from a mixture of ethanol and water (7:1) and colorless 3,3,3-trinitropropyl carbamate (**7**) was obtained (1.06 g, 82%).

^{1}H NMR ($(CD_3)_2CO$): δ = 6.07 (br, NH_2), 4.51 (m, 2H, CH_2O), 3.78 (m, 2H, CH_2) ppm; ^{13}C NMR ($(CD_3)_2CO$): δ = 156.5 (CO), 130.1 ($C(NO_2)_3$), 58.0 (CH_2O), 34.3 (CH_2) ppm; ^{14}N NMR ($(CD_3)_2CO$): δ = −29 (NO_2), −311 (NH_2) ppm; elemental analysis calcd (%) for $C_4H_6N_4O_8$ (238.11): C 20.18, H 2.54, N 23.53; found: C 20.10, H 2.63, N 23.22; IR (ATR): ν = 3393 (w), 3334 (w), 3275 (w), 3197 (w), 2985 (w), 1751 (w), 1704 (m, ν(CO)), 1608 (m), 1583 (s, $\nu_{as}(NO_2)$), 1469 (w), 1410 (m), 1371 (w), 1353 (m), 1332 (m), 1298 (m, $\nu_s(NO_2)$), 1132 (m), 1103 (m), 1081 (s), 976 (m), 934 (w), 893 (w), 854 (w), 819 (m), 800 (m), 780 (m), 758 (w), 673 (w) cm^{-1}; Raman (500 mW): ν = 3264 (5), 3196 (6), 3021 (15), 2993 (39), 2949 (60), 1699 (15, ν(CO)), 1617 (36, $\nu_{as}(NO_2)$), 1589 (24), 1471 (13), 1414 (20), 1373 (47), 1339

(19), 1299 (25, νs(NO_2)), 1282 (24), 1141 (20), 1104 (11), 1018 (11), 978 (23), 936 (25), 895 (24), 855 (100), 820 (12), 802 (11), 758 (11), 670 (10), 654 (10), 633 (12), 542 (19), 508 (21), 475 (23), 416 (55), 396 (68), 373 (83), 291 (17) cm^{-1}; IS: >40 J (grain size 500–1000 mm); FS: >360N (grain size 500–1000 mm); ESD: >0.3 J (grain size 500–1000 mm); DSC (5 °C min^{-1}, onset): 78 °C (melt.; 82 °C Lit.[15]), 152 °C (dec.).

3,3,3-Trinitropropyl nitrocarbamate (**8**)

Nitric acid (100%, 2 mL) was dropped into concentrated sulfuric acid (2 mL) at 0 °C. Into this nitration mixture, chilled in an ice bath, **7** (0.48 g, 2.0 mmol) was added in small portions. The suspension was stirred for 10 min at 0 °C and one hour at ambient temperature. The nitration mixture was poured onto ice-water (200 mL), extracted with ethyl acetate (3 × 50 mL), and the combined organic phases were dried over magnesium sulfate. The solvent was removed under reduced pressure and the crude solid product was recrystallized from carbon tetrachloride to obtain colorless 3,3,3-trinitropropyl nitrocarbamate (**8**, 0.37 g, 65%).

^{1}H NMR ($(CD_3)_2CO$): δ =13.6 (br, N*H*), 4.80 (m, 2H, CH_2O), 3.98 (m, 2H, CH_2) ppm; ^{13}C NMR ($(CD_3)_2CO$): δ = 148.7 (*C*O), 129.9 (br, *C*(NO_2)$_3$), 60.3 (*C*H_2O), 33.6 (*C*H_2) ppm; ^{14}N NMR ($(CD_3)_2CO$): δ = −29 (*N*O_2), −46 (*N*O_2) ppm; elemental analysis calcd (%) for $C_4H_5N_5O_{10}$ (283.11): C 16.97, H 1.78, N 24.74; found: C 16.89, H 1.87, N 24.33; IR (ATR): ν=3134 (w), 3037 (w), 2895 (w), 1758 (m, ν(CO)), 1590 (s, ν_{as}(NO_2)), 1458 (m), 1410 (w), 1390 (w), 1367 (w), 1334 (m), 1291 (m, ν_s(NO_2)), 1255 (m), 1175 (s), 1099 (m), 1046 (m), 1001 (m), 921 (m), 851 (m), 798 (s), 749 (m), 736 (m) cm^{-1}; Raman (500 mW): ν = 3149 (6), 2994 (35), 2958 (55), 1760 (41, ν(CO)), 1617 (32, ν_{as}(NO_2)), 1455 (24), 1413 (24), 1370 (43), 1330 (49), 1307 (30, ν_s(NO_2)), 1290 (31, ν_s(NO_2)), 1255 (11), 1182 (12), 1152 (6), 1103 (13), 1049 (35), 996 (50), 935 (25), 855 (100), 802 (10), 765 (8), 738 (11), 659 (8), 633 (8), 529 (17), 484 (20), 459 (30), 425 (33), 383 (62), 307 (17), 250 (23), 206 (32) cm^{-1}; IS: 30 J (grain size <100 mm); FS: 288 N (grain size <100 mm); ESD: >0.2 J (grain size <100 mm); DSC (5 °C min^{-1}, onset): 68 °C (melt.), 134 °C (dec.).

3,3,3-Trinitro-N-(2,2,2-trinitroethyl)propan-1-amine (**9**)[5, 6]

2,2,2-Trinitroethanol (0.41 g, 2.2 mmol) was dissolved in water (20 mL) and added to a solution of **2** (0.50 g, 2.2 mmol) in water (5 mL). A solution of sodium hydroxide (1 mL, 2M) was added and the reaction mixture was stirred at 25 °C for 1 h. The precipitated solid was filtered off, washed with small portions of cold water, dried, and stored in a desiccator.

3,3,3-Trinitro-*N*-(2,2,2-trinitroethyl)propan-1-amine (**9**) was obtained as a yellow solid (0.49 g, 63%).

^{1}H NMR ($CDCl_3$): δ = 4.15 (m, 2H, CH_2), 3.24 (m, 2H, CH_2), 3.15 (m, 2H, CH_2), 2.16 (m, 1H, NH) ppm; ^{13}C NMR ($CDCl_3$): δ = 128.0 ($C(NO_2)_3$), 126.9 ($C(NO_2)_3$), 52.6, 44.5, 34.9 ppm; ^{14}N NMR ($CDCl_3$): δ = −31 (NO_2), −32 (NO_2) ppm; elemental analysis calcd (%) for $C_5H_7N_7O_{12}$ (357.15): C 16.82, H 1.98, N 27.45; found: C 16.68, H 2.12, N 27.08; IR (ATR): ν = 3366 (w), 2945 (w), 2880 (w), 1581 (s, $\nu_{as}(NO_2)$), 1479 (w), 1416 (w), 1367 (w), 1302 (s, $\nu_s(NO_2)$), 1236 (w), 1185 (w), 1132 (m), 1039 (w), 901 (w), 878 (w), 856 (w), 829 (w), 800 (s), 766 (m), 655 (w) cm^{-1}; Raman (700 mW): ν = 2983 (17), 2952 (31), 2881 (12), 1604 (21, $\nu_{as}(NO_2)$), 1474 (11), 1420 (9), 1373 (29), 1348 (16), 1309 (27, $\nu_s(NO_2)$), 1151 (10), 1001 (6), 933 (6), 859 (87), 800 (5), 646 (10), 543 (13), 405 (47), 376 (62), 313 (9), 273 (5), 244 (7) cm^{-1}; IS: 7 J (grain size 100–250 mm); FS: 120 N (grain size 100–250 mm); ESD: >0.4 J (grain size 100–250 mm); DSC (5 °C min^{-1}, onset): 44 °C (phase trans.), 65 °C (melt.), 96 °C (dec.).

N-(2,2,2-Trinitroethyl)-N-(3,3,3-trinitropropyl) nitramine (**10**)

The synthesis was performed according to the literature procedure[5] with minor changes. Acetic anhydride (1.4 mL, 14.8 mmol) was added to nitric acid (100%, 1.4 mL, 33.6 mmol) at 0 °C. Amine **9** (240 mg, 0.7 mmol) was added and the mixture was allowed to warm to 30 °C until **9** was completely dissolved (1.5 h). After 15 h at 25 °C, the reaction mixture was poured onto ice-water (25 mL). The precipitated solid was filtered, washed with water, and dried. *N*-(2,2,2-Trinitroethyl)-*N*-(3,3,3-trinitropropyl) nitramine (**10**) was obtained as a colorless solid (204 mg, 75%).

^{1}H NMR (CD_3CN): δ = 5.59 (s, 2H, CH_2), 4.27 (m, 2H, CH_2), 3.65 (m, 2H, CH_2) ppm; ^{13}C NMR (CD_3CN): δ = 129.4 ($C(NO_2)_3$), 124.2 ($C(NO_2)_3$), 55.2, 49.5, 31.6 ppm; ^{15}N NMR (CD_3CN): δ = −31.0 (t, ^{3}J = 2.8 Hz, C(NO_2)$_3$), −32.9 (m, NNO_2), −34.5 (t, ^{3}J = 1.9 Hz, C(NO_2)$_3$), −213.7 (m, NNO_2) ppm; elemental analysis calcd (%) for $C_5H_6N_8O_{14}$ (402.15): C 14.93, H 1.50, N 27.86; found: C 15.02, H 1.55, N 27.58; IR (ATR): ν = 3020 (w), 1599 (s, $\nu_{as}(NO_2)$), 1555 (s, $\nu_{as}(NO_2)$), 1454 (w), 1412 (w), 1395 (w), 1342 (w), 1285 (s, $\nu_s(NO_2)$), 1268 (s, $\nu_s(NO_2)$), 1208 (w), 1138 (w), 1062 (w), 1007 (w), 876 (w), 858 (m), 799 (s), 780 (m), 763 (m), 662 (w) cm^{-1}; Raman (300 mW): ν = 3046 (11), 3020 (15), 3000 (19), 2977 (36), 2958 (41), 1613 (35, $\nu_{as}(NO_2)$), 1456 (9), 1429 (7), 1413 (10), 1396 (15), 1386 (18), 1367 (20), 1345 (40), 1294 (23, $\nu_s(NO_2)$), 1270 (25, $\nu_s(NO_2)$), 1063 (9), 1049 (12), 989 (7), 919 (12), 877 (26), 858 (100), 640 (10), 599 (7), 549 (9), 452 (8), 428 (16), 408 (41), 391 (37), 375 (34), 364 (40), 294 (25), 235 (11) cm^{-1}; IS: 7 J (grain size 100–250 mm); FS: 160 N (grain size

100–250 mm); ESD: >0.4 J (grain size 100–250 mm); DSC (5 °C min^{-1}, onset): 141 °C (melt.), 153 °C (dec.).

4.6 References

[1] a) Q. Zhang, J. Zhang, D. A. Parrish, J. M. Shreeve, *Chem. Eur. J.* **2013**, *19*, 11000–11006; b) T. M. Klapötke, *Chemistry of High-Energy Materials*, 2nd ed., de Gruyter, Berlin (Germany), **2012**.

[2] a) T. M. Klapötke, B. Krumm, S. F. Rest, M. Sućeska, *Z. Anorg. Allg. Chem.* **2014**, *640*, 84–92; b) A. Baumann, A. Erbacher, C. Evangelisti, T. M. Klapötke, B. Krumm, S. F. Rest, M. Reynders, V. Sproll, *Chem. Eur. J.* **2013**, *19*, 15627–15638.

[3] a) T. M. Klapötke, B. Krumm, R. Moll, S. F. Rest, W. Schnick, M. Seibald, J. *Fluorine Chem.* **2013**, *156*, 253–261; b) A. S. Ermakov, P. V. Bulatov, D. B. Vinogradov, V. A. Tartakovskii, *Russ. J. Org. Chem.* **2004**, *40*, 1062–1063; c) Q. J. Axthammer, T. M. Klapötke, B. Krumm, R. Moll, S. F. Rest, *Z. Anorg. Allg. Chem.* **2014**, *640*, 76–83.

[4] a) H. Feuer, T. Kucera, J. *Org. Chem.* **1960**, *25*, 2069–2070; b) W. H. Gilligan, S. L. Stafford, *Synthesis* **1979**, 600–602.

[5] M. B. Frankel, *Tetrahedron* **1963**, *19*, 213–217.

[6] a) M. B. Frankel, K. Klager, *J. Chem. Eng. Data* **1962**, *7*, 412–413; b) M. H. Gold, M. B. Frankel, G. B. Linden, K. Klager, *J. Org. Chem.* **1962**, *27*, 334–336.

[7] NASA Space Shuttle News Reference, ntrs.nasa.gov/archive/nasa/casi.ntrs.nasa.gov/19810022734_1981022734.pdf (March 15, 2015).

[8] J. Akhavan, *The Chemistry of Explosives*, 2nd ed., The Royal Society of Chemistry, Cambridge (UK), **2004**.

[9] A. M. Mebel, M. C. Lin, K. Morokuma, C. F. Melius, *J. Phys. Chem.* **1995**, *99*, 6842–6848.

[10] C. Hogue, *Chem. Eng. News* **2011**, *89*, 6.

[11] a) J. Dumont, The Effects of Ammonium Perchlorate on Reproduction and Development of Amphibians, SERDP Project ER-1236, **2008**; b) E. D. McLanahan, M. E. Andersen, J. Campbell, J. W. Fisher, *Toxicol. Sci.* **2009**, *117*, 731–738.

[12] Q. J. Axthammer, C. Evangelisti, T. M. Klapötke, R. Meyer, *New Trends Res. Energ. Mater. Proc. Semin. 17th*, **2014,** *2*, 549–562.

[13] W. M. Koppes, M. E. Sitzmann, H. G. Adolph, *J. Chem. Eng. Data* **1986**, *31*, 119–123.

[14] M. B. Frankel (Aerojet-General Corporation), US 3000945, **1961**.

[15] M. E. Sitzmann, R. D. Gilardi, *J. Fluorine Chem.* **1993**, *63*, 203–215.

[16] a) R. Graf, *Angew. Chem. Int. Ed. Engl.* **1968**, *7*, 172–182; *Angew. Chem.* **1968**, *80*, 179–189; b) J. K. Rasmussen, A. Hassner, *Chem. Rev.* **1976**, *76*, 389–408; c) Q. J.

Axthammer, B. Krumm, T. M. Klapötke, *Eur. J. Org. Chem.* **2015**, 723–729; d) Q. J. Axthammer, B. Krumm, T. M. Klapötke, *J. Org. Chem.* **2015**, *80*, 6329–6335.

[17] a) S. V. Lieberman, E. C. Wagner, *J. Org. Chem.* **1949**, *14*, 1001–1012; b) H. Feuer, G. B. Bachman, C. R. Koller, W. A. Swarts, *Tetrahedron* **1963**, *19*, 165–176.

[18] M. Hesse, H. Meier, B. Zeeh, *Spektroskopische Methoden in der Organischen Chemie*, 7th ed., Thieme, Stuttgart (Germany), **2005**.

[19] Y. Oyumi, T. B. Brill, A. L. Rheingold, *J. Phys. Chem.* **1985**, *89*, 4824–4828

[20] T. M. Klapötke, B. Krumm, R. Moll, S. F. Rest, Y. V. Vishnevskiy, C. Reuter, H.-G. Stammler, N. W. Mitzel, *Chem. Eur. J.* **2014**, *20*, 12962–12973.

[21] C. Romers, *Acta Crystallogr.* **1953**, *6*, 429.

[22] T. Steiner, Angew. *Chem. Int. Ed.* **2002**, *41*, 48–76.

[23] D. A. Nesterenko, V. A. Garanin, A. I. Kazakov, A. G. Korepin, L. B. Romanova, *Russ. J. Phys. Chem. B* **2014**, *8*, 701–711.

[24] R. Meyer, J. Köhler, A. Homburg, *Explosives*, Wiley-VCH, Weinheim (Germany), **2007**.

[25] Commission communication in the framework of the implementation of the Council Directive 93/15/EEC of 5 April 1993 on the harmonisation of the provisions relating to the placing on the market and supervision of explosives for civil uses, Vol. 221, **2006**.

[26] M. Sućeska, *EXPLO5V.6.02*, Zagreb (Croatia), **2013**.

[27] A. Altomare, M. C. Burla, M. Camalli, G. L. Cascarano, C. Giacovazzo, A. Guagliardi, A. G. G. Moliterni, G. Polidori, R. Spagna, *J. Appl. Crystallogr.* **1999**, *32*, 115–119.

[28] a) G. M. Sheldrick, SHELX-97, Programs for Crystal Structure Determination, **1997**; b) G. M. Sheldrick, *Acta Crystallogr.* **2008**, *64A*, 112–122.

[29] L. Farrugia, *J. Appl. Crystallogr.* **1999**, *32*, 837–838.

[30] A. Spek, *Acta Crystallogr.* **2009**, *65D*, 148–155.

[31] Gaussian 09, Rev. A.02, M. J. Frisch, G. W. Trucks, H. B. Schlegel, G. E. Scuseria, M. A. Robb, J. R. Cheeseman, V. B. G. Scalmani, B. Mennucci, G. A. Petersson, H. Nakatsuji, M. Caricato, X. Li, H. P. Hratchian, A. F. Izmaylov, J. Bloino, G. Zheng, J. L. Sonnenberg, M. Hada, M. Ehara, K. Toyota, R. Fukuda, J. Hasegawa, M. Ishida, T. Nakajima, Y. Honda, O. Kitao, H. Nakai, T. Vreven, J. A. Montgomery Jr. , J. E. Peralta, F. Ogliaro, M. Bearpark, J. J. Heyd, E. Brothers, K. N. Kudin, V. N. Staroverov, R. Kobayashi, J. Normand, K. Raghavachari, A. Rendell, J. C. Burant, S. S. Iyengar, J. Tomasi, M. Cossi, N. Rega, J. M. Millam, M. Klene, J. E. Knox, J. B. Cross, V. Bakken, C. Adamo, J. Jaramillo, R. Gomperts, R. E. Stratmann, O. Yazyev, A. J. Austin, R. Cammi, C. Pomelli, J. W. Ochterski, R. L. Martin, K. Morokuma, V. G. Zakrzewski, G. A. Voth, P. Salvador, J. J.

Dannenberg, S. Dapprich, A. D. Daniels, Ö. Farkas, J. B. Foresman, J. V. Ortiz, J. Cioslowski, D. J. Fox, Gaussian, Inc., Wallingford CT, **2009**.

[32] R. D. Dennington, T. A. Keith, J. M. Millam, *GaussView*, Ver. 5.08 ed., SemiChem, Inc., Wallingford CT, **2009**.

[33] J. A. Montgomery, M. J. Frisch, J. W. Ochterski, G. A. Petersson, J. Chem. Phys. **2000**, *112*, 6532–6542.

[34] J. W. Ochterski, G. A. Petersson, J. A. Montgomery, *J. Chem. Phys.* **1996**, *104*, 2598–2619.

[35] E. F. C. Byrd, B. M. Rice, *J. Phys. Chem. A* **2005**, *109*, 1005–1013.

[36] M. Sućeska, *Propellants Explos. Pyrotech.* **1991**, *16*, 197–202.

OXALYL CHLORIDE AND HYDRAZIDE BASED ENERGETIC POLYNITRO DERIVATIVES

Thomas M. Klapötke, Burkhard Krumm, Regina Scharf

as published in

European Journal of Inorganic Chemistry **2016**, 3086–3093.

Dedicated to our friend and colleague Professor Konstantin Karaghiosoff on the occasion of his 60th birthday

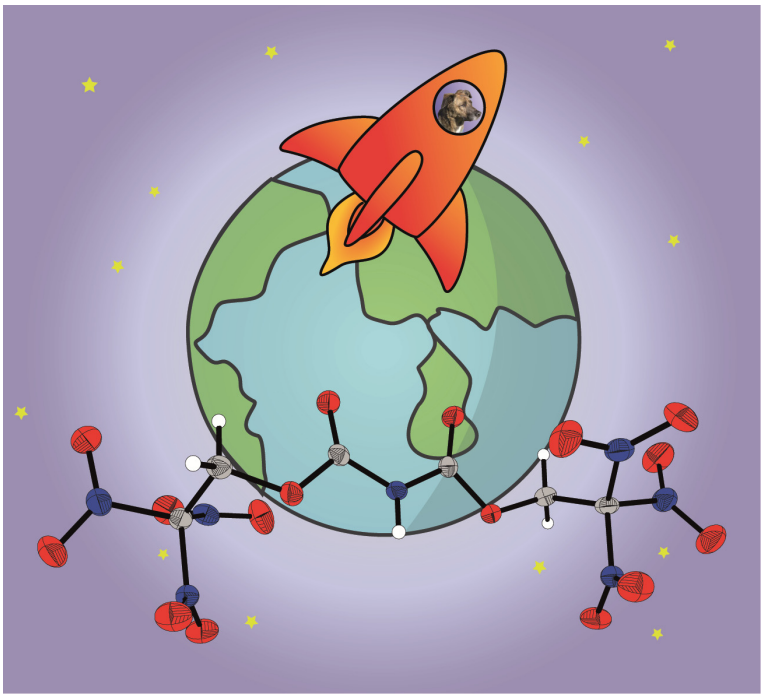

5.1 Abstract

Several new compounds as potential high-energy dense oxidizers (HEDOs) were synthesized from the nitro alcohols 2,2,2-trinitroethanol and 3,3,3-trinitropropanol with oxalyl chloride and hydrazide. The materials were characterized thoroughly by spectroscopic methods, and some of their crystal structures were determined through X-ray diffraction. The energetic properties, thermal stabilities, and sensitivities of the oxalates, carbonyl azides, and imidodicarboxylate were determined. Furthermore, the enthalpies of all compounds were calculated, and their energetic performances were explored with the EXPLO5 code.

5.2 Introduction

The applications of ammonium perchlorate (AP) are manifold. Owing to its easy and cheap synthesis from sodium chloride, its high thermal stability, and its inherent energy, it is used in air-bag inflators, safety and hazard flares, and fireworks. However, the main application of AP is still as oxidizer in solid rocket propellants.[1] During the decomposition of AP, in which the ammonium ion acts as a reducing agent and the perchlorate ion acts as an oxidizing agent, gaseous products such as nitrogen, oxygen, and hydrogen chloride are mainly formed.[2] The excess oxygen is further reduced through reaction with aluminum, which is added in composite propellants as a fuel and provides a very high heat of combustion and, therefore, a high burning temperature.[3] Nevertheless, AP also has several disadvantages. As the diameter of the perchlorate ion is similar to the diameter of the iodide ion, it acts as a competitive inhibitor in the thyroid gland and leads to growth and development disturbances, especially in vertebrates.[1a,4] Moreover, slow cook-off tests showed that AP decomposes to form acidic side-products, which in turn react with the binder, causing cracks and cavities in the composite.[1a] For this reason, halogen-free alternative oxidizers are needed.

As potential replacements for AP, high-energy dense oxidizers (HEDOs) have been discussed recently. Such compounds consist entirely of C, H, N, and O, preferably with a high oxygen content. 2,2,2-Trinitroethanol (TNE) is a suitable starting material with an oxygen balance (Ω_{CO}) of 30.9% and is easily synthesized from trinitromethane and formaldehyde through a Henry reaction.[5] Another eligible starting material for the synthesis of HEDOs is 3,3,3-trinitropropanol, which is synthesized in several steps from acrylamide and

trinitromethane.[6] Although the oxygen balance of 3,3,3-trinitropropanol (Ω_{CO} = 12.3%) is, not surprisingly, lower than that of 2,2,2-trinitroethanol, this polynitroalcohol exhibits several benefits concerning its stability towards bases and nucleophiles.

We have synthesized a large number of compounds with these two moieties during our recent studies, but little is known about the chemistry of TNE with oxalyl chloride.[7] This contribution gives a detailed account about this topic and related compounds.

5.3 Results and Discussion

5.3.1 Synthesis

The commercially available reactive oxalyl chloride represents the central precursor for this study (Scheme 5.1). The reaction of oxalyl chloride with TNE furnishes different products depending on the stoichiometry. With 2 equiv. of TNE, bis(2,2,2-trinitroethyl) oxalate (**1**) was obtained as a colorless solid, whereas the moisture-sensitive 2,2,2-trinitroethyl chloro(oxo)acetate (**2**) was obtained as a colorless liquid with 1 equiv. of TNE. These two compounds were previously briefly mentioned and only insufficiently characterized.[7,8] The further reaction of **2** with 3,3,3-trinitropropanol afforded the asymmetric ester 2,2,2-trinitroethyl (3,3,3-trinitropropyl) oxalate (**3**). With sodium azide, **2** was converted into the corresponding carbonyl azide, 2,2,2-trinitroethyl azido(oxo)acetate (**4**), which is a very sensitive material, as expected. The corresponding isocyanate of **4** was generated in situ

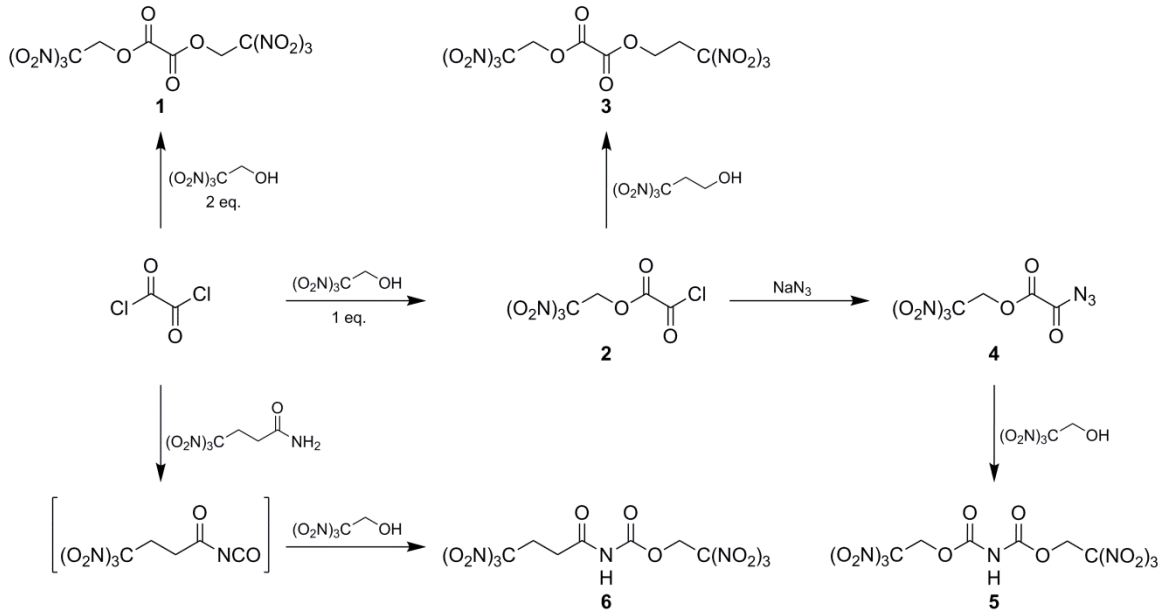

Scheme 5.1 Syntheses of polynitro compounds **1**–**6**.

through a Curtius rearrangement, and further treatment with TNE resulted in the formation and isolation of the diester bis(2,2,2-trinitroethyl) imidodicarboxylate (**5**).

A further convenient method for the preparation of acyl isocyanate is the reaction of amides with oxalyl chloride.[9] A readily available oxygen-rich amide for the synthesis of such an acyl isocyanate is 4,4,4-trinitrobutanamide, which is synthesized by a simple Michael addition of trinitromethane and acrylamide.[6b] The reaction with oxalyl chloride yielded the corresponding carbonyl isocyanate with hydrogen chloride elimination.The immediate reaction of this carbonyl isocyanate with TNE produced 2,2,2-trinitroethyl *N*-(4,4,4-trinitrobutanoyl)carbamate (**6**) as a colorless solid in high purity.

Another interesting precursor and cheap starting material for further chemistry in this context is the dihydrazide of oxalic acid. This derivative is readily available from oxalic diester and hydrazine hydrate.[10] The reaction with nitrous acid generates oxalyl diazide,[11] which was not isolated owing to its high sensitivity. Further treatment with 1 equiv. of TNE formed 2,2,2-trinitroethylcarbamate carbonyl azide (**7**) through a Curtius rearrangement, which still exhibits a high sensitivity (Scheme 5.2).

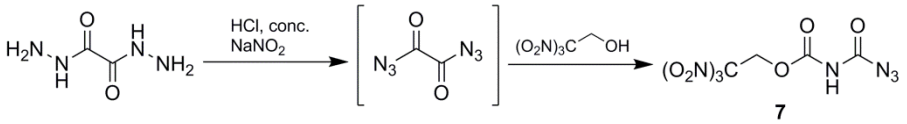

Scheme 5.2 Synthesis of **7** via oxalyl diazide.

5.3.2 NMR Spectroscopy

All compounds presented herein were characterized by ^{1}H, ^{13}C, and ^{14}N NMR spectroscopy in $CDCl_3$ (for **2**, **4**, and **7**) or [D_6]acetone (for **1**, **3**, **5**, and **6**). In the ^{1}H NMR spectra of all compounds, the CH_2 resonances of the trinitroethyl moiety appear as singlets within the narrow range δ = 6.12 to 5.47 ppm. In the spectra of the asymmetric oxalate **3** and the carbamate **6**, two further signals are observed for the protons of the propyl moieties at δ = 4.88 and 4.03 (**3**) and 3.77 and 3.29 ppm (**6**) with typical AA′XX′ spin-system patterns.[12] The NH resonances are observed as broadened signals at δ = 10.7 (**5**), 10.4 (**6**), and 7.9 ppm (**7**).

In the ^{13}C NMR spectra, the resonances for the carbonyl moiety appear within the range δ = 170.3 to 149.1 ppm. The carbon atoms of the trinitromethyl moiety are observed as broadened signals in the narrow range δ = 125.1 to 121.9 ppm. Only the trinitromethyl carbon resonances of the propyl units are shifted slightly to lower fields [δ = 129.6 (**3**) and 131.6 ppm (**6**)].

The ^{14}N NMR resonances of the trinitroethyl moiety appear as relatively sharp signals within the range δ = –33 to –37 ppm. For oxalate **3** and carbamate **6**, two additional signals

are identified for the trinitropropyl and trinitrobutanoyl moieties at δ = –29 ppm. The N_β atoms of the azide compounds **4** and **7** are assigned at δ = –148 (**4**) and –147 ppm (**7**). For the azido(oxo)acetate **4**, resonances for N_γ (δ = –130 ppm) and N_α (δ = –315 ppm) are also observed, whereas those for **7** were too broad to be observed.

5.3.3 Vibrational Spectroscopy

The IR and Raman spectra for **1** and **3**–**7** show characteristic vibrations for the carbonyl and nitro moieties, as summarized in Table 5.1. The carbonyl stretching vibrations ν(C=O) are within the range ν = 1814 to 1770 cm^{-1} in the IR spectra and between ν = 1818 and 1719 cm^{-1} in the Raman spectra.[12] The asymmetric stretching vibrations of the nitro groups $\nu_{as}(NO_2)$ of the trinitromethyl moieties are assigned between ν = 1623 and 1581 cm^{-1}, whereas the symmetric stretching vibrations $\nu_s(NO_2)$ appear at ν = 1312 to 1268 cm^{-1}.[13] In the IR spectra, characteristic bands are also observed for the cumulated double bonds of the azide groups of **4** and **7** at ν = 2178 (**4**) and 2163 cm^{-1} (**7**).[12] For **5**, **6**, and **7**, strong bands attributed to the amide units are observed in the range ν = 1532 to 1507 cm^{-1}.

Table 5.1 Selected IR and Raman bands for **1**–**7**.[a]

	1		**3**		**4**	
	IR	**Raman**	**IR**	**Raman**	**IR**	**Raman**
ν(CO)	1772 (m)	1795 (57)	1770 (s)	1796 (28) 1772 (13)	1770 (m) 1715 (m)	1771 (65) 1719 (78)
$\nu_{as}(NO_2)$	1590 (s)	1623 (23) 1614 (21) 1605 (25) 1595 (19)	1581 (s)	1619 (28)	1612 (m) 1592 (s)	1615 (38) 1602 (27)
$\nu_s(NO_2)$	1295 (m)	1305 (32) 1268 (13)	1295 (s) 1281 (s)	1310 (35)	1304 (m) 1277 (m)	1306 (41) 1280 (32)

	5		**6**		**7**	
	IR	**Raman**	**IR**	**IR**	**Raman**	**IR**
ν(CO)	1814 (m)	1818 (18)	1788 (m)	1814 (m)	1818 (18)	1788 (m)
$\nu_{as}(NO_2)$	1609 (m)	1619 (24) 1610 (47) 1590 (17)	1585 (s)	1609 (m)	1619 (24) 1610 (47) 1590 (17)	1585 (s)
$\nu_s(NO_2)$	1304 (m) 1279 (m)	1312 (33) 1294 (23) 1283 (26)	1299 (m)	1304 (m) 1279 (m)	1312 (33) 1294 (23) 1283 (26)	1299 (m)

[a] Wavenumbers in cm^{-1}. IR intensities: s = strong, m = medium, w = weak; Raman intensities in parentheses.

5.3.4 Single-Crystal X-ray Diffraction

Single crystals suitable for X-ray diffraction measurements were obtained for **1**, **4**, and **5** by recrystallization from chloroform (**1** and **4**) or methanol (**5**). Selected structural data as well as the parameters and refinements of the measurement are compiled in Appendix A5.

The oxalate **1** crystallizes in the monoclinic space group $P2_1/c$ with four molecules in the unit cell. However, the asymmetric unit consists of only two half molecules. The molecular structure of **1**, as depicted in Figure 5.1, is completed by an inversion center in the center of the C1–C1′ bond. As is common for oxalate structures, the C1–O2 bond is between an ordinary C–O single and double bond with an bond length of 1.343(2) Å.[14] The oxalate unit as well as both CH_2 groups are arranged in a perfectly planar manner. Only the trinitromethyl moiety is slightly twisted out of plane with a torsion angle of 156.7° (C1–O2–C2–C3). The structure is stabilized through a N···O intramolecular attraction between N3 and O2 with an interatomic distance shorter than the sum of the van der Waals radii (2.73 Å). For steric reasons, the nitro groups in the trinitromethyl unit arrange around the carbon atom in a propeller-like orientation. In this fashion, intramolecular interactions are formed between the partially positively charged nitrogen atoms and the partially negatively charged oxygen atoms, which stabilize the geometry.

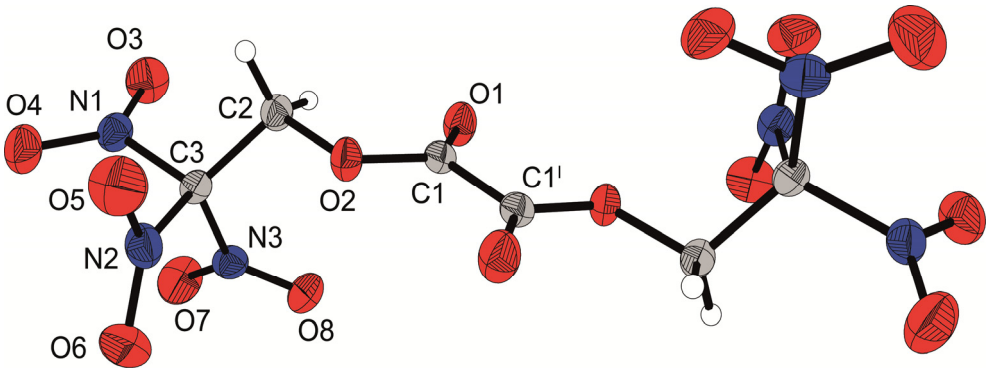

Figure 5.1 X-ray molecular structure of **1**.

Similarly to oxalate **1**, the azido(oxo)acetate **4** crystallizes in the monoclinic space group $P2_1/c$ with one molecule in the asymmetric unit (Figure 5.2). Typical for such a covalent azide structure is the shortened C1–N1 bond followed by shortened distances between the nitrogen atoms of the azide moiety, which are in the range of a N–N double bond (N1–N2 1.27 Å) and a N–N triple bond (N2–N3 1.11 Å).[15] Also common for carbonyl azides is the slight bending of the azide moiety, which has a N1–N2–N3 angle of 173.5°.

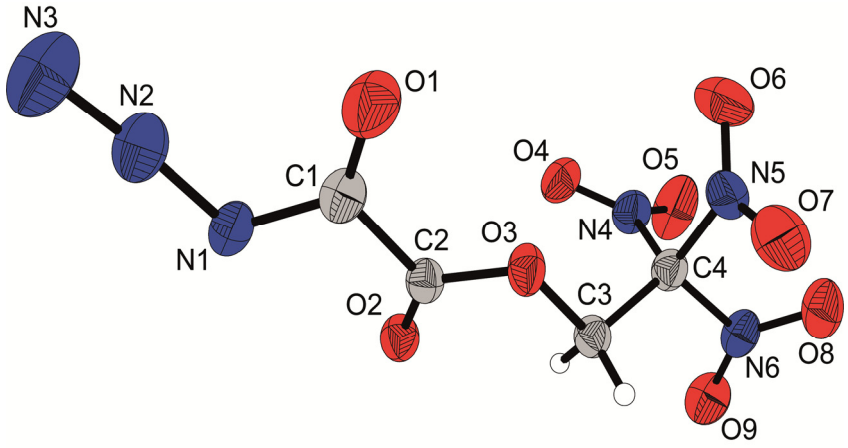

Figure 5.2 X-ray molecular structure of **4**.

The imidodicarboxylate **5** crystallizes in the orthorhombic space group *Fdd*2 with eight molecules in the unit cell and a high calculated density of 1.915 g cm^{-3} at –100 °C. The asymmetric unit consists of half a molecule, which is completed by a twofold rotation axis through N1 along the *c* axis (Figure 5.3). The moieties surrounding the N1 atom are orientated in a trigonal planar arrangement, which is also depicted by the angles of 118.3 (C1–N1–H1) and 123.3° (C1–N1–C1′). This geometry is achieved through a delocalization of the electron lone pair caused by the electron-withdrawing effect of the carbonyl and trinitromethyl moieties and can also be seen in the shortened C1–N1 bond length of only 1.37 Å, which is in the range between a C–N single and double bond.

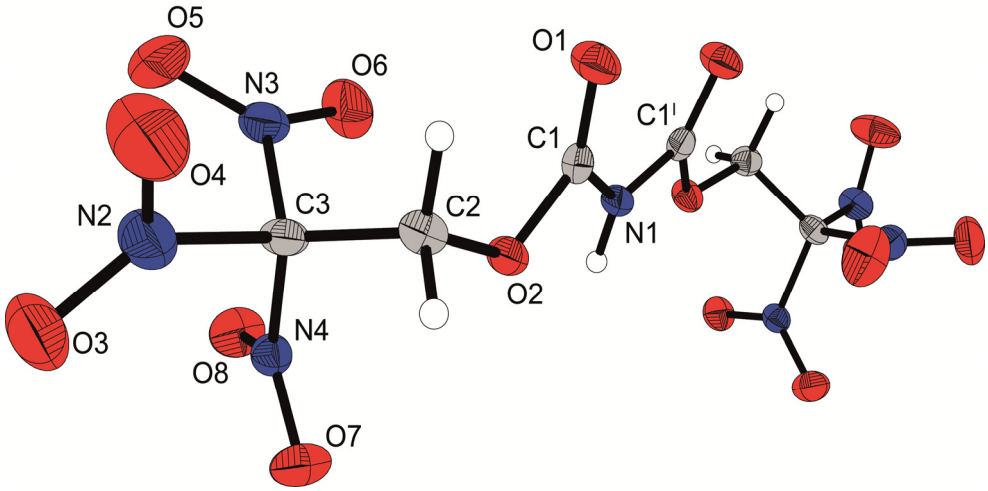

Figure 5.3 X-ray molecular structure of **5**.

5.3.5 Thermal and Energetic Properties

All compounds, except the chloro(oxo)acetate **2**, are stable to air and moisture. The thermal stabilities of **1** and **3**–**7** were tested by differential scanning calorimetry (DSC) with a heating rate of 5 °C min^{-1} and are listed in Table 5.2. Compounds **1**, **5**, and **6** exhibit satisfying decomposition temperatures with values between 183 and 186 °C. As expected, the thermal stability of the asymmetric oxalate **3**, especially the melting point of 63 °C, is lower than that of the symmetric analogues **1** (T_m = 115 °C, T_{dec} = 186 °C) and bis(3,3,3-trinitropropyl) oxalate (T_m = 120 °C, T_{dec} = 170 °C).[6a] Both azide compounds **4** and **7** show low decomposition temperatures of 50 and 127 °C, respectively. For the azido(oxo)acetate **4**, two exothermic signals are observed; the first signal is assigned to the exothermic rearrangement of the carbonyl azide to the corresponding intermediate isocyanate $(NO_2)_3CCH_2OC(O)NCO$, followed by hydrolysis to the corresponding 2,2,2-trinitroethyl carbamate, which decomposes at 167 °C.[16]

For classification of their sensitivities, the impact (IS), friction (FS), and electrostatic discharge sensitivities (ESD) of all compounds were tested.[17] The IS measurements were performed with a BAM fall hammer according to STANAG 4489.[18] For the FS measurements, a BAM friction tester was used according to STANAG 4487.[19] The azide **4** exhibits extreme sensitivity to impact and friction and should, therefore, be handled with caution. Furthermore, the imidodicarboxylate **5**, the carbamate **6**, and the azide **7** with values of 3 (**5** and **7**) and 4 J (**6**) are very sensitive or sensitive to impact and also sensitive to friction with values of 120 (**7**), 288 (**6**), and 324 N (**5**). However, the oxalate **1** has an impact sensitivity of 10 J and a friction sensitivity of 360 N and is even less sensitive than the well-known explosive hexogen (RDX),[20] whereas the unsymmetrical oxalate **3** is insensitive to impact and friction.

For energetic materials, the heat of explosion (Q_v) as well as the detonation pressure (P_{CJ}) and detonation velocity (V_{det}) are important parameters. These values were calculated with the EXPLO5 V6.02 code on the basis of previously computed enthalpies and free energies of formation and are listed in Table 5.3 (further values are summarized in the Appendix A5). Owing to its high room-temperature density of 1.92 g cm^{-3}, the imidodicarboxylate **5** achieves the highest detonation velocity of all compounds presented here with a value of 8675 m s^{-1} and outperforms the common explosive pentaerythritol tetranitrate (PETN, V_{det} = 8404 m s^{-1}). All other compounds show satisfying detonation velocities with values in the range of 7213–8275 m s^{-1}.

Table 5.2 Physical and chemical properties of **1**, **3**–**7**, and AP.

	1	**3**	**4**	**5**
Formula	$C_6H_4N_6O_{16}$	$C_7H_6N_6O_{16}$	$C_4H_2N_6O_9$	$C_6H_5N_7O_{16}$
MW [g mol^{-1}]	416.12	430.15	278.09	431.14
T_m [°C] (onset)[a]	115	63	38	–
T_{dec} [°C] (onset)[b]	186	168	50	183
IS [J][c]	10	40	<1	3
FS [N][d]	>360	>360	<5	324
ESD [J][e]	0.7	0.7	0.015	0.16
N [%][f]	20.2	19.5	30.2	22.7
O [%][g]	61.5	59.5	51.8	59.4
N + O [%][h]	81.7	79.0	82.0	82.1
Ω_{CO} [%][i]	+30.8	+22.3	+23.0	+27.8
Ω_{CO2} [%][j]	+7.7	−3.7	0	+5.6

	6	**7**	**AP**
Formula	$C_7H_7N_7O_{15}$	$C_4H_3N_7O_9$	NH_4ClO_4
MW [g mol^{-1}]	429.17	293.11	117.49
T_m [°C] (onset)[a]	–	–	–
T_{dec} [°C] (onset)[b]	183	127	240
IS [J][c]	4	3	20
FS [N][d]	288	120	>360
ESD [J][e]	0.1	0.015	0.5
N [%][f]	22.9	33.5	11.9
O [%][g]	55.9	49.1	54.5
N + O [%][h]	78.8	82.6	66.4
Ω_{CO} [%][i]	+16.8	+19.1	+34.0
Ω_{CO2} [%][j]	−9.3	−2.7	+34.0

[a] Melting temperature determined by DSC. [b] Decomposition temperature determined by DSC. [c] Impact sensitivity. [d] Friction sensitivity. [e] Sensitivity towards electrostatic discharge. [f] Nitrogen content. [g] Oxygen content. [h] Sum of nitrogen and oxygen content. [i] Oxygen balance assuming the formation of CO at combustion. [j] Oxygen balance assuming the formation of CO_2 at combustion.

Table 5.3 Calculated heat of formation and predicted detonation and combustion parameters (EXPLO5 V6.02 code)[21] of **1**, **3**–**7**, and AP.

	1	**3**	**4**	**5**
Formula	$C_6H_4N_6O_{16}$	$C_7H_6N_6O_{16}$	$C_4H_2N_6O_9$	$C_6H_5N_7O_{16}$
Density RT[a]	1.84	1.73	1.75	1.92
$\Delta_f H_m°$ [kJ mol^{-1}][b]	–688.0	–705.2	–170.5	–775.2
$\Delta_f U°$ [kJ kg^{-1}][c]	–1575.9	–1558.7	–537.3	–1717.5
Q_v [kJ kg^{-1}][d]	–5177	–5839	–5701	–5062
T_{ex} [K] [e]	3943	4262	4394	3936
V_0 [L kg^{-1}] [f]	705	711	707	724
P_{CJ} [kbar][g]	286	270	280	237
V_{det} [m s^{-1}][h]	8275	8071	8223	8675
I_s [s][i]	240	252	250	240
I_s [s] (15% Al) [j]	250	257	257	250
I_s [s] (15% Al, 14% binder)[k]	256	251	247	252

	6	**7**	**AP**
Formula	$C_7H_7N_7O_{15}$	$C_4H_3N_7O_9$	NH_4ClO_4
Density RT[a]	1.63	1.50	1.95
$\Delta_f H_m°$ [kJ mol^{-1}][b]	–645.7	–271.4	–295.8
$\Delta_f U°$ [kJ kg^{-1}][c]	–1420.7	–845.7	–2623.2
Q_v [kJ kg^{-1}][d]	–5371	–5199	–1422
T_{ex} [K] [e]	4028	4219	1735
V_0 [L kg^{-1}] [f]	741	745	885
P_{CJ} [kbar][g]	241	189	158
V_{det} [m s^{-1}][h]	7703	7213	6368
I_s [s][i]	252	247	157
I_s [s] (15% Al) [j]	259	255	235
I_s [s] (15% Al, 14% binder)[k]	248	243	261

[a] The r.t. densities were recalculated from the X-ray densities or determined experimentally by pycnometer measurements. [b] Enthalpy calculated by the CBS-4 M method with Gaussian 09. [c] Energy of formation calculated by the CBS-4 M method with Gaussian 09. [d] Heat of explosion. [e] Explosion temperature. [f] Volume of gaseous products. [g] Detonation pressure. [h] Detonation velocity; Q_v, T_{ex}, V_0, P_{CJ}, and V_{det} were calculated with the EXPLO5 V6.02 code.[21] [i] Specific impulse for the neat compound [EXPLO5 V6.02 code; 70.0 bar chamber pressure, isobaric combustion conditions (1 bar), equilibrium expansion].[21] [j] Specific impulse for compositions with 85% oxidizer/compound and 15% aluminum [70.0 bar chamber pressure, isobaric combustion conditions (1 bar), equilibrium expansion]. [k] Specific impulse for compositions with 71% oxidizer/compound, 15% aluminum and 14% binder [6% polybutadiene acrylic acid, 6% polybutadiene acrylonitrile and 2% bisphenol A ether; 70.0 bar chamber pressure, isobaric combustion conditions (1 bar), equilibrium expansion].

The specific impulse I_s is the most relevant parameter for the utilization of these compounds as composite propellants. It is important to know that the payload of a rocket can be approximately doubled if the specific impulse is increased by 20 s.[1a] As the specific impulse is proportional to the square root of the ratio of the temperature of the combustion chamber T_c and the average molecular mass of the combustion products, a high burning temperature is crucial. Therefore, aluminum is added. In addition to its low price, the benefits of aluminum are its high heat of combustion and nonhazardous combustion product Al_2O_3, which is formed when aluminum is oxidized by the excess oxygen provided by the oxidizer. For composite propellants, **1** and **3**–**7** were calculated as neat samples, with aluminum (15%), and in a binder/aluminum system (15% aluminum, 6% polybutadiene acrylic acid, 6% polybutadiene acrylonitrile, and 2% bisphenol A). Since the carbon backbones of the synthesized compounds can also be oxidized in composite propellants and, therefore, act as fuel, the highest value of 259 s was obtained by the carbamate **6** in a mixture with 15% aluminum. These specific impulses are considerably higher than that of a comparable mixture of ammonium perchlorate and aluminum (I_s = 235 s). Even the specific impulses of the other compounds with values of 250–255 s exceed that of ammonium perchlorate in such a composite. When 14% binder was added to the composite propellants, the specific impulses were slightly lower than that for a similar mixture with ammonium perchlorate (I_s = 261 s) but are still in a satisfying range. Compounds **3** and **5** exhibit specific impulses of 251 and 252 s, respectively. However, the highest value was obtained for the oxalate **1**, which has an specific impulses of 256 s.

5.4 Conclusions

Several new compounds were synthesized from 2,2,2-trinitroethanol and oxalyl chloride and characterized comprehensively, including by multinuclear NMR and vibrational spectroscopy. The thermal stabilities of the compounds were determined by DSC measurements, and all compounds except the azides showed satisfying decomposition temperatures above 150 °C. Since these compounds are classified as potential high-energy dense oxidizers, their physical and energetic properties were determined. Most compounds (**1**, **5**, **6**, and **7**) are rather sensitive to external stimuli such as impact and friction. Special care should be taken when working with the azide **4**, which is extremely sensitive to both impact and friction. The asymmetric oxalate **3** is completely insensitive and additionally achieves a promising specific impulse of 257 s in a composite propellant consisting of 85% oxidizer and 15% aluminum, which is higher than that of a comparable mixture of ammonium perchlorate and aluminum. The calculated specific impulse in an

oxidizer/fuel/binder system decreases slightly. As a consequence of their high oxygen contents and high enthalpies of formation, the best results were obtained for the oxalate **1** and the carbamate **6** (I_s = 256 s); these specific impulses are lower than the calculated value for ammonium perchlorate (I_s = 262 s) but still in the range for promising oxidizers.

5.5 Experimental Section

General Information

All chemicals were used as supplied; oxalyl chloride was obtained from Aldrich. The Raman spectra of samples in a glass tube were recorded in the range ν = 400–4000 cm^{-1} with a Bruker MultiRAM FT-Raman spectrometer with Nd:YAG laser excitation (1000 mW at 1064 nm). The IR spectra were recorded with a Perkin–Elmer Spectrum BX-FTIR spectrometer equipped with a Smiths DuraSamplIR II attenuated total reflectance (ATR) device. All spectra were recorded at ambient temperature. The NMR spectra were recorded with a JEOL Eclipse 400 instrument, and the chemical shifts were determined with respect to the external standards Me_4Si (^1H, 399.8 MHz; ^{13}C, 100.5 MHz) and $MeNO_2$ (^{14}N, 28.8 MHz). The MS data were obtained with a JEOL MStation JMS 700 spectrometer [desorption chemical ionization (DCI+), desorption electron ionization (DEI+)]. The C/H/N analyses were performed with an Elemental VarioEL analyzer. The melting and decomposition points were measured with Perkin–Elmer Pyris6 DSC and OZM Research DTA 552-Ex instruments at a heating rate of 5 °C min^{-1} in a temperature range of 15 to 400 °C and checked with a Buchi Melting Point B-540 apparatus. The sensitivity data were determined with a BAM drophammer and a BAM friction tester.[18,19]

X-ray Crystallography

Crystals suitable for X-ray crystallography were selected with a polarization microscope and mounted on the tip of a glass fiber. All measurements were performed with an Oxford XCalibur3 diffractometer (**1**, **4**, and **5**). The diffractometer was equipped with a generator (voltage 50 kV, current 40 mA) and a KappaCCD detector and operated with Mo-K_α radiation (λ = 0.7107 Å). The structures were solved by direct methods (SIR97),[22] refined by full-matrix least-squares techniques on F^2 (SHELXL)[23] with the WINGX software package,[24] and finally checked with the PLATON software.[25] All non-hydrogen atoms were refined anisotropically. The hydrogen atom positions were located in a difference Fourier map. ORTEP plots are shown with thermal ellipsoids at the 50% probability level.

CCDC 1469963 (for **1**), 1469964 (for **4**), and 1469965 (for **5**) contain the supplementary crystallographic data (excluding structure factors) for this paper. These data can be obtained free of charge from The Cambridge Crystallographic Data Centre.

Quantum Chemical Calculations

All ab initio calculations were performed with the program package Gaussian 09 (rev. A.02)[26] and visualized by GaussView 5.08.[27] The structure optimizations and frequency analyses were performed with the Becke B3 threeparameter hybrid functional with the Lee–Yang–Parr (LYP) correlation functional (B3LYP). For C, H, N, and O, the correlation-consistent polarized double-zeta basis set cc-pVDZ was used. The structures were optimized with symmetry constraints, and the energies were corrected with the zero-point vibrational energy.[28] The enthalpies (*H*) and free energies (*G*) were calculated by the complete basis set (CBS) method to obtain accurate values. The CBS models used the known asymptotic convergence of pair natural orbital expressions to extrapolate the estimated complete basis set limit from calculations with a finite basis set. CBS-4M starts with a HF/3-21G(d) geometry optimization, which is the initial guess for the following selfconsistent field (SCF) calculation as a base energy and a final MP2/ 6-31+G calculation with a CBS extrapolation to correct the secondorder energy. The used CBS-4M method additionally implements a MP4(SDQ)/6-31+(d,p) calculation to approximate higher-order contributions and also includes some additional empirical corrections.[29] The enthalpies of the gas-phase species were estimated according to the atomization-energy method.[30]

Calculation of Energetic Performance

All calculations of the detonation parameters were performed with the EXPLO5 V6.02 program package.[21,31] The detonation parameters were calculated at the Chapman‐Jouguet (CJ) point with the aid of the steady-state detonation model and a modified Becker‐Kistiakowski‐Wilson equation of state to model the system. The CJ point was found from the Hugoniot curve of the system by its first derivative. The specific impulses were also calculated with the EXPLO5 V6.02 program for an assumed isobaric combustion of a composition of 70% oxidizer, 16% aluminum as fuel, 6% polybutadiene acrylic acid, 6% polybutadiene acrylonitrile as binder, and 2% bisphenol A ether as an epoxy curing agent. A chamber pressure of 70.0 bar and an ambient pressure of 1.0 bar with frozen expansion conditions were assumed for the calculations.

Syntheses

CAUTION! All prepared compounds are energetic materials with sensitivity toward heat, impact, and friction. No hazards occurred during the preparation and manipulation.

However, additional proper protective precautions (face shield, leather coat, earthed equipment and shoes, Kevlar® gloves, and ear plugs) should be used when undertaking work with these compounds.

Bis(2,2,2-trinitroethyl) Oxalate (**1**)[7]

Oxalyl chloride (1.0 g, 7.9 mmol) and 2,2,2-trinitroethanol (5.7 g, 31.5 mmol) were dissolved in 1,2-dichloroethane (10 mL), and $AlCl_3$ (0.1 g, 8.7 mmol) was added. The solution was heated under reflux for 5 h. After the reaction mixture cooled, a colorless solid precipitated. The solid was collected by filtration and washed with cold water. Recrystallization from chloroform yielded **1** as colorless crystals (27%).

^{1}H NMR ([D_6]acetone): δ = 6.12 (s, 4 H, CH_2) ppm. ^{13}C NMR ([D_6]acetone): δ = 153.8 [C(O)O], 124.6 [$C(NO_2)_3$], 63.4 (CH$_2$) ppm. ^{14}N NMR ([D_6]acetone): δ = –35 [C(NO_2)$_3$] ppm. $C_6H_4N_6O_{16}$ (416.12): calcd. C 17.32, H 0.97, N 20.20; found C 17.42, H 1.08, N 20.13. IR (ATR): ν = 3018 (w), 2968 (w), 2895 (w), 1790 (w), 1772 (m), 1612 (m), 1590 (s), 1435 (w), 1394 (w), 1351 (w), 1295 (m), 1282 (m), 1268 (w), 1173 (s), 1158 (s), 1095 (w), 1028 (w), 968 (w), 884 (w), 855 (w), 824 (w), 806 (w), 791 (m), 776 (m), 765 (w), 714 (w), 661 (w) cm^{-1}. Raman (300 mW): ν = 3018 (19), 2977 (40), 2969 (39), 1795 (57), 1623 (23), 1614 (21), 1605 (25), 1595 (19), 1439 (13), 1397 (16), 1358 (35), 1305 (32), 1268 (13), 1168 (9), 1107 (7), 1094 (8), 1056 (20), 1008 (10), 911 (27), 857 (100), 802 (15), 777 (7), 641 (8), 546 (9), 441 (13), 409 (59), 378 (58), 327 (12), 306 (6), 274 (16), 249 (10), 236 (18) cm^{-1}. IS: 10 J (grain size < 100 µm). FS: >360 N (grain size <100 µm). ESD: 0.7 J (grain size <100 µm). DSC (5 °C min^{-1}, onset): 115 (m.p.), 186 °C (dec.).

2,2,2-Trinitroethyl Chloro(oxo)acetate (**2**)[7]

2,2,2-Trinitroethanol (4.1 g, 22.6 mmol) was dissolved in diethyl ether (6 mL), and oxalyl chloride (11.8 g, 93.2 mmol) was added. The solution was heated under reflux at 50 °C for 12 h. The solvent was removed in vacuo, and **2** was obtained as a colorless liquid (62%) and used without further purification.

^{1}H NMR ($CDCl_3$): δ = 5.59 (s, 2 H, CH_2) ppm. ^{13}C NMR ($CDCl_3$): δ = 158.5 [C(O)O], 153.1 [C(O)Cl], 121.9 [C(NO2)$_3$], 63.0 (CH$_2$) ppm. ^{14}N NMR ($CDCl_3$): δ = –37 [C(NO_2)$_3$] ppm. IR (ATR): ν = 3019 (w), 2970 (w), 2894 (w), 1782 (s), 1591 (s), 1437 (w), 1386 (w), 1349 (w), 1292 (m), 1222 (s), 1168 (w), 1153 (w), 1094 (w), 1048 (m), 1011 (m), 946 (w), 916 (m), 876 (m), 855 (m), 824 (w), 793 (s), 777 (m), 715 (m), 640 (w) cm^{-1}.

2,2,2-Trinitroethyl (3,3,3-Trinitropropyl) Oxalate (**3**)

To a solution of **2** (1.0 g, 3.7 mmol) in chloroform (10 mL), 3,3,3-trinitropropanol[6a] (0.7 g, 3.7 mmol) was added, and the reaction mixture was heated under reflux for 12 h. The removal of the solvent with a rotary evaporator yielded a yellow oil, which was completely solidified by ultrasonic treatment in water. Compound **3** (69%) was obtained as a colorless solid.

^{1}H NMR ([D$_6$]acetone): δ = 6.09 (s, 2 H, CH_2), 4.88 (m, 2 H, CH_2), 4.03 (m, 2 H, CH_2) ppm. ^{13}C NMR ([D$_6$]acetone): δ = 155.4 [C(O)O], 154.9 [C(O)O], 129.6 [C^{Pr}(NO$_2$)$_3$], 124.7 [C^{Et}(NO$_2$)$_3$], 63.1 (CH$_2$), 61.1 (CH$_2$), 33.2 (CH$_2$) ppm. ^{14}N NMR ([D$_6$]acetone): δ = –29 [C(NO$_2$)$_3$], –34 [C(NO$_2$)$_3$] ppm. C$_7$H$_6$N$_6$O$_{16}$ (430.15): calcd. C 19.55, H 1.41, N 19.54; found C 19.93, H 1.66, N 19.26. IR (ATR): ν = 3019 (w), 2897 (w), 1793 (w), 1770 (s), 1581 (s), 1464 (m), 1441 (w), 1414 (m), 1388 (w), 1372 (w), 1295 (s), 1280 (s), 1173 (s), 1099 (m), 1039 (m), 1011 (m), 922 (w), 874 (m), 854 (m), 831 (m), 791 (s), 763 (m), 720 (m) cm^{-1}. Raman (300 mW): ν = 1796 (28), 1772 (13), 1619 (28), 1464 (10), 1441 (12), 1416 (13), 1390 (20), 1373 (20), 1358 (29), 1309 (35), 11251 (5), 1102 (7), 1055 (19), 935 (13), 923 (14), 908 (20), 878 (6), 857 (100), 814 (6), 802 (6), 793 (5), 641 (8), 543 (11), 467 (9), 439 (20), 413 (44), 394 (45), 373 (85), 307 (16), 274 (11), 260 (14), 225 (13) cm^{-1}. IS: 40 J (grain size <100 µm). FS: >360 N (grain size < 100 µm). ESD: 0.7 J (grain size < 100 µm). DSC (5 °C min^{-1}, onset): 63 (m.p.), 168 °C (dec.).

2,2,2-Trinitroethyl Azido(oxo)acetate (**4**)

A solution of **2** (500 mg, 1.8 mmol) in chloroform (10 mL) was added at 0 °C to sodium azide (276 mg, 4.2 mmol) dissolved in water (10 mL). The emulsion was stirred at 0 °C for 15 min. The organic layer was separated, and the aqueous solution was extracted with ice-cold chloroform (2 × 20 mL). The combined organic phase was washed with ice-cold water (20 mL), an ice-cold solution of 5% sodium bisulfate (20 mL), ice-cold water (20 mL), and brine (20 mL) and dried with magnesium sulfate. The volume of the solvent was reduced to 5 mL with a rotary evaporator at 10 °C, and *n*-hexane (5 mL) was added. The solution was stored at –30 °C for 24 h, and **4** was obtained as colorless crystals (48%).

^{1}H NMR (CDCl$_3$): δ = 5.53 (s, 4 H, CH_2) ppm. ^{13}C NMR (CDCl$_3$): δ = 161.7 [C(O)O], 154.7 [C(O)N$_3$], 122.2 [C(NO$_2$)$_3$], 62.3 (CH$_2$) ppm. ^{14}N NMR (CDCl$_3$): δ = –36 [C(NO$_2$)$_3$], –130 (N_γ), –148 (N_β), –315 (N_α) ppm. C$_4$H$_2$N$_6$O$_9$ (278.09): calcd. C 17.28, H 0.72, N 30.22; found C 17.46, H 0.88, N 30.08. IR (ATR): ν = 3018 (w), 2973 (w), 2897 (w), 2327 (w), 2230 (w), 2178 (w), 1770 (m), 1715 (s), 1612 (m), 1592 (s), 1443 (w), 1391 (w), 1354 (w), 1304 (m), 1277 (m), 1173 (s), 1106 (w), 1061 (m), 1023 (w), 966 (w), 907 (w), 879 (w), 856 (w), 817 (w), 794

(s), 774 (m), 722 (w) cm^{-1}. Raman (300 mW): ν = 3019 (24), 2974 (62), 2181 (25), 2149 (7), 1771 (65), 1719 (78), 1615 (38), 1602 (27), 1444 (12), 1392 (24), 1356 (35), 1306 (41), 1280 (32), 1165 (12), 1106 (7), 1062 (25), 1026 (11), 969 (7), 909 (48), 857 (100), 817 (7), 801 (16), 776 (7), 651 (13), 544 (16), 427 (24), 404 (25), 404 (62), 373 (78), 338 (8), 287 (21), 271 (27), 218 (28) cm^{-1}. IS: <1 J (grain size < 100 µm). FS: <5 N (grain size < 100 µm). ESD: 0.015 J (grain size < 100 µm). DSC (5 °C min^{-1}, onset): 38 (m.p.), 50 °C (dec.).

Bis(2,2,2-trinitroethyl) Imidodicarboxylate (**5**)

To a solution of sodium azide (276 mg, 4.2 mmol) in water (10 mL) at 0 °C was added a solution of **2** (500 mg, 1.8 mmol) in chloroform (10 mL). The reaction mixture was stirred at 0 °C for 15 min. The organic layer was separated, and the aqueous solution was extracted with ice-cold chloroform (2 × 20 mL). The combined organic phase was washed with brine (20 mL) and dried with magnesium sulfate. 2,2,2-Trinitroethanol (330 mg, 1.8 mmol) was added to the solution, and the reaction mixture was heated under reflux for 12 h under a nitrogen atmosphere. The reaction mixture was cooled, the solvent was removed in vacuo, and water (5 mL) was added. A colorless solid precipitated and was collected by filtration, washed with water, and dried in vacuo. Compound **5** was obtained as a colorless solid in 64% yield.

^{1}H NMR ([D_6]acetone): δ = 10.69 (s, 1 H, N*H*), 5.93 (s, 4 H, CH_2) ppm. ^{13}C NMR ([D_6]acetone): δ = 149.1 [C(O)O], 125.0 [$C(NO_2)_3$], 62.6 (CH$_2$) ppm. ^{14}N NMR ([D_6]acetone): δ = –33 [C(NO_2)$_3$] ppm. $C_6H_5N_7O_{16}$ (431.14): calcd. C 16.72, H 1.17, N 22.74; found C 16.88, H 1.22, N 22.55. IR (ATR): ν = 3382 (w), 3009 (w), 2965 (w), 2891 (w), 2164 (w), 1814 (m), 1743 (w), 1609 (m), 1586 (s), 1507 (m), 1443 (w), 1400 (w), 1349 (w), 1304 (m), 1279 (m), 1249 (w), 1173 (m), 1143 (m), 1117 (m), 1089 (m), 928 (w), 882 (w), 856 (w), 799 (m), 781 (m), 770 (m), 736 (w), 658 (w) cm^{-1}. Raman (300 mW): ν = 3384 (4), 3010 (33), 2966 (75), 2869 (4), 1818 (18), 1747 (5), 1619 (24), 1610 (47), 1589 (17), 1441 (11), 1390 (22), 1356 (51), 1312 (33), 1294 (23), 1283 (26), 1146 (6), 1112 (11), 1067 (17), 1010 (24), 995 (21), 890 (13), 859 (100), 807 (5), 786 (12), 748 (6), 649 (10), 615 (4), 536 (18), 464 (10), 414 (68), 401 (62), 375 (66), 362 (38), 281 (16), 267 (13), 243 (10), 232 (12) cm^{-1}. IS: 3 J (grain size < 100 µm). FS: 324 N (grain size < 100 µm). ESD: 0.16 J (grain size < 100 µm). DSC (5 °C min^{-1}, onset): 183 °C (dec.).

2,2,2-Trinitroethyl (4,4,4-Trinitrobutanoyl) Carbamate (**6**)

4,4,4-Trinitrobutanamide[6b] (500 mg, 2.3 mmol) was suspended in 1,2-dichloroethane (10 mL). Oxalyl chloride (317 mg, 2.5 mmol) was added, and gas evolution started

immediately. The reaction mixture was heated under reflux for 2 h. 2,2,2-Trinitroethanol (407 mg, 2.3 mmol) was added, and the clear solution was heated under reflux for further 5 h. The mixture was cooled to room temperature, and a colorless solid precipitated. The solid was collected by filtration, washed with 1,2-dichloroethane, and dried. Compound **6** was obtained as a colorless solid in 68% yield.

^{1}H NMR ([D$_6$]acetone): δ = 10.38 (N*H*), 5.91 (s, 2 H, CH_2O), 3.77 (m, 2 H, CH_2), 3.29 (m, 2 H, CH_2) ppm. ^{13}C NMR ([D$_6$]acetone): δ = 170.3 (*C*O), 150.4 (*C*O), 131.6 [C^{Bu}(NO$_2$)$_3$], 125.1 [C^{Et}(NO$_2$)$_3$], 62.4 (*C*H$_2$O), 31.5 (*C*H$_2$), 29.2 (*C*H$_2$) ppm. ^{14}N NMR ([D$_6$]acetone): δ = –29 (*N*O$_2$), –33 (*N*O$_2$) ppm. $C_7H_7N_7O_{15}$ (429.17): calcd. C 19.59, H 1.64, N 22.85; found C 19.68, H 1.66, N 22.76. IR (ATR): ν = 3292 (w), 3224 (w), 3012 (w), 1788 (m), 1718 (w), 1585 (s), 1522 (s), 1444 (w), 1425 (w), 1363 (w), 1299 (m), 1268 (w), 1216 (m), 1174 (m), 1108 (w), 1083 (m), 1065 (m), 1020 (w), 921 (w), 880 (w), 857 (w), 801 (m), 785 (m), 701 (m) cm^{-1}. Raman (500 mW): ν = 3015 (21), 3001 (21), 2953 (52), 1798 (20), 1716 (16), 1608 (31), 1447 (15), 1417 (22), 1386 (21), 1363 (28), 1354 (30), 1305 (37), 1110 (13), 1068 (32), 991 (32), 859 (100), 542 (12), 433 (21), 402 (49), 376 (53), 262 (15) cm^{-1}. IS: 4 J (grain size < 100 µm). FS: 288 N (grain size < 100 µm). ESD: 0.1 J (grain size < 100 µm). DTA (onset): 183 °C (dec.).

2,2,2-Trinitroethyl Carbamate Carbonyl Azide (**7**)

Oxalyl dihydrazide[10] (300 mg, 2.5 mmol) was suspended in conc. HCl (5 mL), and the suspension was overlayed with chloroform (50 mL). A solution of $NaNO_2$ (420 mg, 6.1 mmol) in water (6 mL) was added slowly at 0 °C. The reaction mixture was stirred for 15 min at 0 °C. The organic layer was separated, washed with ice water (2 × 20 mL) and brine (20 mL), and dried with magnesium sulfate. 2,2,2- Trinitroethanol (360 mg, 2.0 mmol) was added, and the solution was heated to 35 °C for 15 h. After the removal of the solvent in vacuo, the obtained yellow oil was washed with water to yield a colorless solid. Recrystallization from chloroform yielded **7** (61%) as colorless crystals.

^{1}H NMR ($CDCl_3$): δ = 7.93 (s, 1H, N*H*), 5.47 (s, 2H, CH_2) ppm. ^{13}C NMR ($CDCl_3$): δ = 153.3 [*C*(O)N$_3$], 147.7 [*C*(O)O], 122.6 [*C*(NO$_2$)$_3$], 62.0 (*C*H$_2$) ppm. ^{14}N NMR ($CDCl_3$): δ = –35 [C(*N*O$_2$)$_3$], –147 (N_β) ppm. $C_4H_3N_7O_9$ (293.11): calcd. C 16.39, H 1.03, N 33.45; found C 16.58, H 1.11, N 33.37. IR (ATR): ν = 3262 (w), 3223 (w), 3049 (w), 2962 (w), 2892 (w), 2163 (m), 1814 (w), 1780 (m), 1708 (w), 1593 (s), 1532 (s), 1442 (w), 1353 (w), 1298 (m), 1285 (m), 1167 (s), 1115 (m), 1102 (m), 1079 (s), 1026 (m), 930 (m), 880 (w), 855 (w), 816 (m), 796 (w), 780 (m), 763 (m), 729 (w), 700 (w), 662 (w) cm^{-1}. Raman (1000 mW): ν = 3238 (8), 3225 (8), 3009 (19), 2963 (34), 2169(37), 1814 (8), 1781 (77), 1713 (9), 1616 (24), 1600 (18), 1532 (8),1446 (18), 1386 (25), 1354 (38), 1303 (29), 1266 (10), 1218 (9), 1178(10),

1085 (18), 1031 (36), 1002 (52), 882 (10), 857 (100), 783 (10), 546 (13), 519 (33), 485 (8), 461 (10), 415 (42), 374 (64), 269 (30), 223 (21) cm^{-1}. IS: 3 J (grain size <100 µm). FS: 120 N (grain size < 100 µm). ESD: 0.015 J (grain size < 100 µm). DSC (5 °C min^{-1}, onset): 127 °C (b.p., dec.).

5.6 References

[1] a) T. M. Klapötke, *Chemistry of High-Energy Materials*, 3rd ed., de Gruyter, Berlin, **2015**; b) C. W. Trumpolt, M. Crain, G. D. Cullison, S. J. P. Flanagan, L. Siegel, S. Lathrop, *Remediation* **2005**, *16*, 65–89; c) Interstate Technology & Regulatory Council Perchlorate Team, *Perchlorate: Overview of Issues, Status, and Remedial Options*, Interstate Technology & Regulatory Council, Washington, D. C., **2005**.

[2] A. E. Simchen, *J. Appl. Chem.* **1963**, *13*, 369–374.

[3] J. Akhavan, *The Chemistry of Explosives*, 2nd ed., The Royal Society of Chemistry, Cambridge, UK, **2004**.

[4] J. Wolff, *Pharmacol. Rev.* **1998**, *50*, 89–105.

[5] a) M. A. Epishina, I. V. Ovchinnikov, A. S. Kulikov, N. N. Makhova, V. A. Tartakovsky, *Mendeleev Commun.* **2011**, *21*, 21–23; b) R. Schenck, Nitroglycerin Aktiebolaget Gyttorp, SE135832, **1952**.

[6] a) Q. J. Axthammer, B. Krumm, T. M. Klapötke, R. Scharf, *Chem. Eur. J.* **2015**, *21*, 16229–16239; b) Q. J. Axthammer, C. Evangelisti, T. M. Klapötke, R. Meyer, *New Trends Res. Energ. Mater. Proc. Semin. 17th* **2014**, *2*, 549–562; c) W. M. Koppes, M. E. Sitzmann, H. G. Adolph, *J. Chem. Eng. Data* **1986**, *31*, 119–123.

[7] A. S. Ermakov, P. V. Bulatov, D. B. Vinogradov, V. A. Tartakovskii, *Russ. J. Org. Chem.* **2004**, *40*, 1062–1063.

[8] F. J. Zerilli, R. M. Doherty, J. M. Short, R. R. McGuire, M. J. Kamlet, *Combust. Flame* **1988**, *74*, 295–310.

[9] a) A. J. Speziale, L. R. Smith, J. E. Fedder, *J. Org. Chem.* **1965**, *30*, 4306– 4307; b) A. J. Speziale, L. R. Smith, J. E. Fedder, *J. Org. Chem.* **1965**, *30*, 4303–4305; c) A. J. Speziale, L. R. Smith, *J. Org. Chem.* **1963**, *28*, 1805– 1811; d) A. J. Speziale, L. R. Smith, *J. Org. Chem.* **1962**, *27*, 4361–4365.

[10] T. Curtius, G. Schofer, N. Schwan, *J. Prakt. Chem.* **1895**, *51*, 180–196.

[11] H. Roesky, O. Glemser, *Chem. Ber.* **1964**, *97*, 1710–1712.

[12] M. Hesse, H. Meier, B. Zeeh, *Spektroskopische Methoden in der Organischen Chemie*, 7th ed., Thieme, Stuttgart, Germany, **2005**.

[13] G. Socrates, *Infrared and Raman Characteristic Group Frequencies: Tables and Charts*, 3rd ed., John Wiley & Sons, Chichester, UK, **2004**.

[14] a) S. Joseph, R. Sathishkumar, S. Mahapatra, G. R. Desiraju, *Acta Crystallogr.,* **2011**, *67B*, 525–534; b) C. O. Della Vedova, R. Boese, H. Willner, H. Oberhammer, *J. Phys. Chem. A* **2004**, *108*, 861–865; c) C. George, P. M. Lahti, D. A. Modarelli, A. Inceli, *Acta Crystallogr.* **1994**, *50C*, 1308; d) M. W. Dougill, G. A. Jeffrey, *Acta Crystallogr.* **1953**, *6*, 831–837.

[15] a) A. Wolter-Steingrube, B. E. C. Bugenhagen, C. Herrmann, J. Heck, *Eur. J. Inorg. Chem.* **2014**, 4115–4122; b) A. Baumann, A. Erbacher, C. Evangelisti, T. M. Klapötke, B. Krumm, S. F. Rest, M. Reynders, V. Sproll, *Chem. Eur. J.* **2013**, *19*, 15627–15638; c) G. C. Hsu, L. M. Singer, D. B. Cordes, M. Findlater, *Acta Crystallogr.* **2013**, *69E*, 1298; d) J. Lapic, A. Pezerovic, M. Cetina, S. Djakovic, V. Rapic, *J. Mol. Struct.* **2011**, *990*, 209–216; e) G. Laus, V. Kahlenberg, K. Wurst, S. Nerdinger, H. Schottenberger, *Z. Naturforsch. B* **2011**, *66*, 479–486; f) D. Siebler, C. Forster, T. Gasi, K. Heinze, *Organometallics* **2011**, *30*, 313–327; g) L. Parkanyi, G. Besenyei, *J. Mol. Struct.* **2004**, *691*, 97–106; h) F. M. Menger, J. Bian, V. A. Azov, *Angew. Chem. Int. Ed.* **2002**, *41*, 2581–2584; *Angew. Chem.* **2002**, *114*, 2693; i) Y. Jiao, E. Valente, S. T. Garner, X. Wang, H. Yu, *Tetrahedron Lett.* **2002**, *43*, 5879–5881.

[16] Q. J. Axthammer, T. M. Klapötke, B. Krumm, R. Moll, S. F. Rest, *Z. Anorg. Allg. Chem.* **2014**, *640*, 76–83. [17] Test methods according to: *Recommendations on the Transport of Dangerous Goods, Manual of Tests and Criteria,* 4th ed., United Nations, New York, Geneva, **2003**; impact, insensitive: >40 J, less sensitive: ≥35 J, sensitive: ≥4 J, very sensitive: ≤3 J; friction, insensitive: >360 N, less sensitive: 360 N, sensitive: <360 to >80 N, very sensitiveL ≤80 N, extremely sensitive: ≤10 N.

[18] NATO, Standardization Agreement 4489 (STANAG 4489), Explosives, Impact Sensitivity Tests, **1999**.

[19] NATO, Standardization Agreement 4487 (STANAG 4487), Explosives, Friction Sensitivity Tests, **2002**.

[20] R. Meyer, J. Kohler, A. Homburg, *Explosives*, Wiley-VCH, Weinheim, Germany, **2007**.

[21] M. Sućeska, *EXPLO5*, version 6.02, Zagreb, Croatia, **2013**.

[22] A. Altomare, M. C. Burla, M. Camalli, G. L. Cascarano, C. Giacovazzo, A. Guagliardi, A. G. G. Moliterni, G. Polidori, R. Spagna, *J. Appl. Crystallogr.* **1999**, *32*, 115–119.

[23] a) G. M. Sheldrick, *Acta Crystallogr.* **2008**, *64A*, 112–122; b) G. M. Sheldrick, *SHELX-97*, *Programs for Crystal Structure Determination*, **1997**.

[24] L. Farrugia, *J. Appl. Crystallogr.* **1999**, *32*, 837–838.

[25] A. Spek, *Acta Crystallogr.* **2009**, *65D*, 148–155.

[26] M. J. Frisch, G. W. Trucks, H. B. Schlegel, G. E. Scuseria, M. A. Robb, J. R. Cheeseman, G. Scalmani, V. Barone, B. Mennucci, G. A. Petersson, H. Nakatsuji, M. Caricato, X. Li, H. P. Hratchian, A. F. Izmaylov, J. Bloino, G. Zheng, J. L. Sonnenberg, M. Hada, M. Ehara, K. Toyota, R. Fukuda, J. Hasegawa, M. Ishida, T. Nakajima, Y. Honda, O. Kitao, H. Nakai, T. Vreven, J. A. Montgomery Jr., J. E. Peralta, F. Ogliaro, M. Bearpark, J. J. Heyd, E. Brothers, K. N. Kudin, V. N. Staroverov, R. Kobayashi, J. Normand, K. Raghavachari, A. Rendell, J. C. Burant, S. S. Iyengar, J. Tomasi, M. Cossi, N. Rega, J. M. Millam, M. Klene, J. E. Knox, J. B. Cross, V. Bakken, C. Adamo, J. Jaramillo, R. Gomperts, R. E. Stratmann, O. Yazyev, A. J. Austin, R. Cammi, C. Pomelli, J. W. Ochterski, R. L. Martin, K. Morokuma, V. G. Zakrzewski, G. A. Voth, P. Salvador, J. J. Dannenberg, S. Dapprich, A. D. Daniels, O. Farkas, J. B. Foresman, J. V. Ortiz, J. Cioslowski, D. J. Fox, *Gaussian 09*, rev. A.02, Gaussian, Inc., Wallingford CT, **2009**.

[27] R. D. Dennington II, T. A. Keith, J. M. Millam, *GaussView*, version 5.08 ed., Semichem, Inc., Wallingford CT, **2009**.

[28] J. A. Montgomery, M. J. Frisch, J. W. Ochterski, G. A. Petersson, *J. Chem. Phys.* **2000**, *112*, 6532–6542.

[29] J. W. Ochterski, G. A. Petersson, J. A. Montgomery, *J. Chem. Phys.* **1996**, *104*, 2598–2619.

[30] E. F. C. Byrd, B. M. Rice, *J. Phys. Chem. A* **2005**, *110*, 1005–1013.

[31] M. Sućeska, *Propellants Explos. Pyrotech.* **1991**, *16*, 197–202.

From Amino Acids to High-Energy Dense Oxidizers: Polynitro Materials Derived from β-Alanine and L-Aspartic Acid

Thomas M. Klapötke, Burkhard Krumm, and Regina Scharf

as published in

Zeitschrift für anorganische und allgemeine Chemie **2016**, *642*, 887–895.

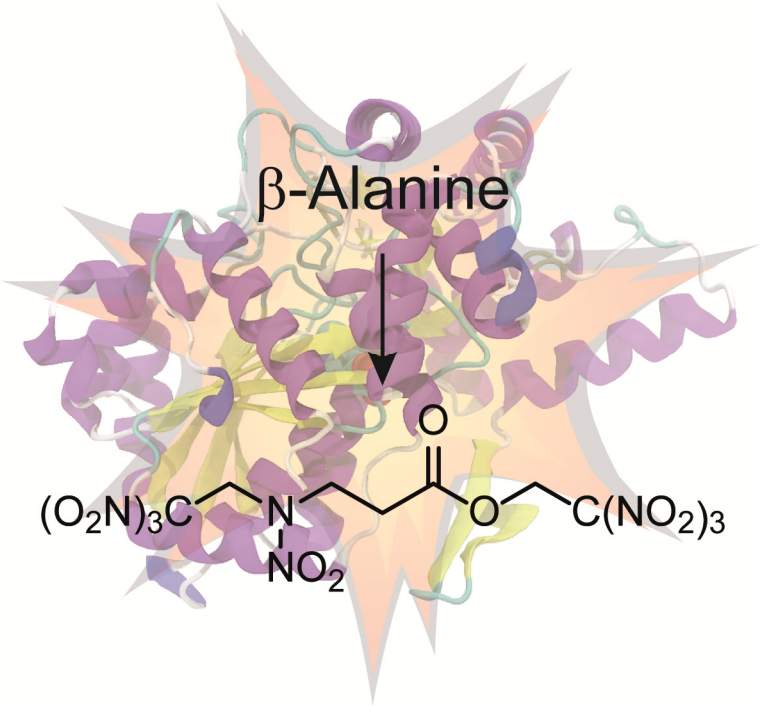

6.1 Abstract

New oxygen-rich compounds starting from the amino acids β-alanine and L-aspartic acid were synthesized and comprehensively analyzed including multinuclear NMR spectroscopy and vibrational spectroscopy. Thermal stabilities were measured and the behavior towards external stimuli like friction or impact were determined. Detonation and combustion parameters were predicted by using the EXPLO5 V6.02 code and were compared with common explosives. In addition, crystal structures were obtained for two compounds.

6.2 Introduction

Amino acids are one of the most important building blocks of life. In general an amino acid consists of an amine, a carboxylic acid, and an additional functional group.[1] Next to the 21 proteinogenic amino acids found in eukaryotes there are more than 400 naturally occurring non-proteinogenic amino acids with biological function like β- and γ-amino acids.[2] In this classification β-alanine forms one of the most simple representatives of such non-proteinogenic amino acids. β-Alanine is formed via decarboxylation of L-aspartic acid and is a constitutional isomer of the proteinogenic amino acid L-alanine, in which the amino function is connected to the β position starting the consecutive numbering from the carboxyl group. Despite the fact that it is a non-proteinogenic amino acid, it is a component of several natural peptides like pantothenic acid (vitamin B5), which in turn is a component of the important coenzym A.[3]

Due to their natural occurrence, their low toxicity, and their reactive functionalities, amino acids, particularly glycine, have been investigated as high-energy dense oxidizers (HEDOs) for replacing ammonium perchlorate (AP) in the area of solid rocket boosters.[4] In recent years much effort has been carried out in order to find an alternative in view of the fact that AP shows several drawbacks. The toxic decomposition products of AP such as hydrogen chloride cause environmental problems and are in addition easily visible and detectable leading to tactical disadvantages.[5] Furthermore slow cook-off tests showed slow decomposition of formulations containing AP forming acidic side-products. These acidic side-products in turn react with the binder-system leading to cracks and cavities and negatively affect the performance of such composite propellants.[5a] However the major disadvantage of AP still is the toxicity of the perchlorate anion towards vertebrates. Since

the diameter of the perchlorate ion is similar to the diameter of the iodide ion, it acts as a competitive inhibitor of the thyroid gland system.[5a,6]

The main requirements for an alternative oxidizer replacing AP are a high density and thermal stability as well as a positive oxygen balance (Ω_{CO}) and a performance comparable to AP.[7]

In this contribution new possible replacements containing the amino acids β-alanine and L-aspartic acid were synthesized and characterized on the basis of Mannich-type reactions of amino acids and 2,2,2-trinitroethanol (TNE). In 1963, a three step synthesis of 3-[nitro(2,2,2-trinitroethyl)amino]propanoic acid (**1**) starting from β-alanine was first described.[8] Further reaction with TNE yields compounds with high oxygen contents. L-Aspartic acid was chosen due to its numerous functional sites, which would allow an introduction of oxygen-rich groups and therefore, could eventually lead to promising oxidizers.

6.3 Results and Discussion

6.3.1 Synthesis

The syntheses of several new polynitro compounds starting from the readily available β-alanine ethyl ester hydrochloride is shown in Scheme 6.1. In the first step β-alanine ethyl ester hydrochloride was reacted with formaldehyde and trinitromethane in a Mannich reaction yielding ethyl 3-[(2,2,2-trinitroethyl)amino]propanoate as a slightly yellow oil, which was used in the following step without further purification. In the second step the amine function was nitrated in a 1:1 mixture of acetic anhydride and nitric acid. Ethyl 3-[nitro(2,2,2-trinitroethyl)amino]propanoate was obtained as a colorless liquid. The protecting group of the carboxylic acid was removed in the third step by refluxing in hydrochloric acid and acetic acid (2:1) leaving the propanoic acid **1** as a colorless solid in high purity. The carboxylic chloride 3-[nitro(2,2,2-.trinitroethyl)amino]propanoyl chloride (**2**) was synthesized by the reaction of **1** with thionyl chloride.[8] The following reaction of **2** with 2,2,2-trinitroethanol afforded 2,2,2-trinitroethyl 3-[nitro(2,2,2-trinitroethyl)amino]propanoate (**3**) as a colorless solid, whereas the sensitive 3-[nitro(2,2,2-trinitroethyl)amino]propanoyl azide (**4**) was obtained by the reaction of **2** and sodium azide. During this reaction it is important to keep the temperature always below 10 °C in order to avoid side product formation. Thermal induced decomposition of the carbonyl azide **4** to the corresponding isocyanate via the Curtius rearrangement and direct

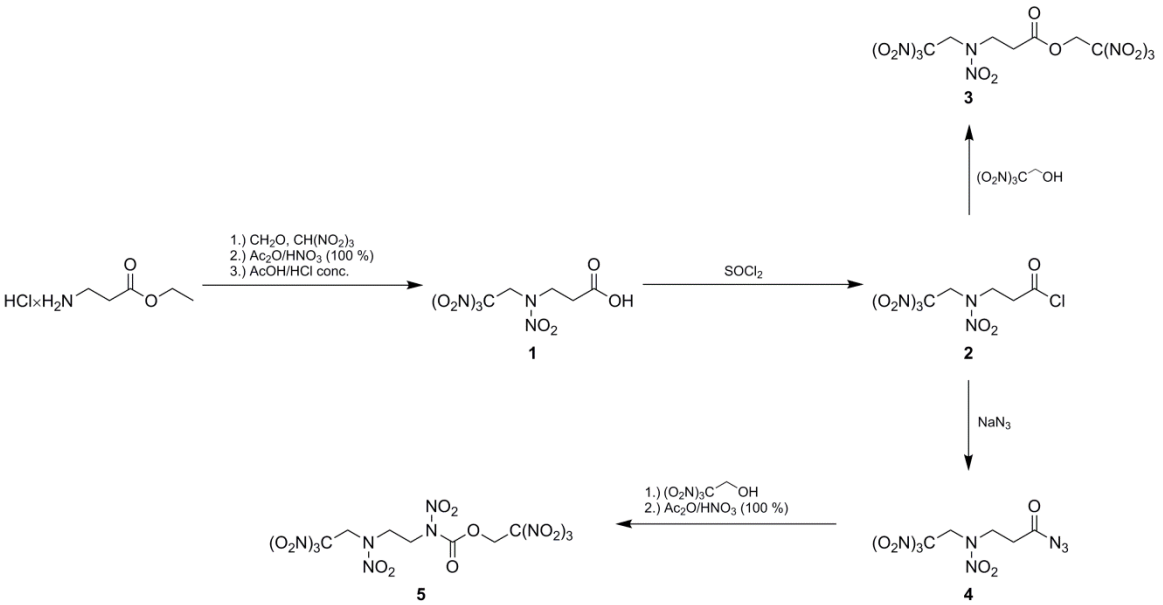

Scheme 6.1 Synthesis overview of polynitro compounds **1**–**5** containing the β-alanine moiety.

reaction with 2,2,2-trinitroethanol yielded 2,2,2-trinitroethyl [2-(nitro(2,2,2-trinitroethyl)amino)ethyl]carbamate as a pale yellow oil. Subsequently, this oil was nitrated in a 1:1 mixture of acetic anhydride and nitric acid to obtain 2,2,2-trinitroethyl nitro[2-(nitro(2,2,2-trinitroethyl)amino)ethyl]carbamate (**5**) as a colorless pure solid.

As shown in Scheme 6.2, the 2,2,2-trinitroethyl *N*-nitro-*N*-(2,2,2-trinitroethyl)-L-aspartic acid (**6**) was synthesized similar to the acid **1** starting from diethyl-L-aspartate hydrochloride.[8] Further chlorination was successful with phosphorus(V) chloride (no reaction with $SOCl_2$) to give *N*-nitro-*N*-(2,2,2-trinitroethyl)-L-aspartoyl dichloride (**7**) as a colorless crystalline solid. The subsequent reaction of **7** with 2,2,2-trinitroethanol afforded (*S*)-2-[nitro(2,2,2-trinitroethyl)amino]-4-oxo-4-(2,2,2-trinitroethoxy)butanoic acid (**8**) in

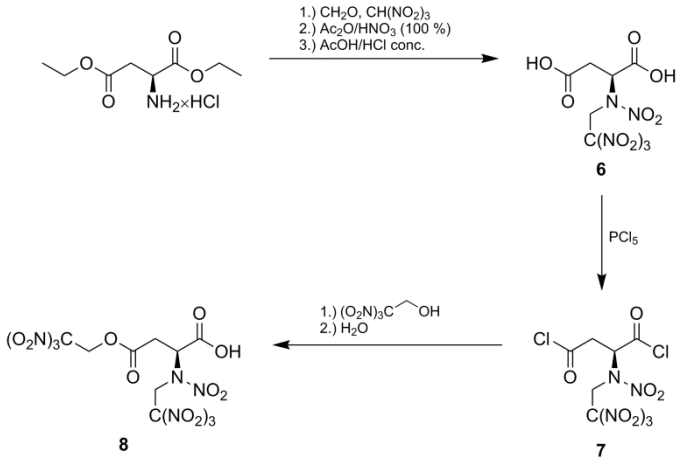

Scheme 6.2 Synthesis of 2-[nitro(2,2,2-trinitroethyl)amino]-4-oxo-4-(2,2,2-trinitroethoxy)-butanoic acid (**8**) starting from diethyl-L-aspartate hydrochloride.

high yield and high purity. Although reaction conditions were varied and different Lewis acids were used, 2,2,2-trinitroethanol reacted only with one carbonyl chloride moiety. The second carbonyl chloride was hydrolyzed during the aqueous work up.

6.3.2 Mulitnuclear NMR Spectroscopy

All herein described compounds were investigated by ^{1}H, $^{13}C\{^{1}H\}$ and ^{14}N NMR spectroscopy. The spectra were either recorded in $CDCl_3$ (**2**, **4**, and **7**) or [D_6]acetone (**1**, **3**, **5**, **6**, and **8**). In the ^{1}H NMR spectra of the molecules containing the β-alanine moiety (**1**–**5**) the resonances of the trinitroethyl groups connected to the nitramine are found as singlets in the narrow range of 6.00–5.56 ppm. For the ester **3** as well as the carbamate **5**, further singlets are observed at δ = 5.86 ppm (**3**) and 6.15 ppm (**5**) for the second trinitroethyl moiety. The chemical shifts of the protons of the β-alanine moiety are in the wide range of 4.65–2.90 ppm. Owing to an A_2B_2-spin system the signals are split into triplets with J_{AB} coupling constants between 5.6 Hz and 6.4 Hz (Figure 6.1, top).

For those molecules containing the aspartate moiety (**6**–**8**) the protons of the trinitroethyl unit are in the range of 6.15–5.45 ppm. Because of an AB spin system the signals are split into doublets with J_{AB} coupling constants of 17.2 Hz (**6**, **7**, and **8**) and 14.0 Hz (**8**). The resonances of the C*H* protons in the aspartate unit are observed between 5.41–5.04 ppm, while the protons of the neighboring CH_2 group are in the range of 4.12–

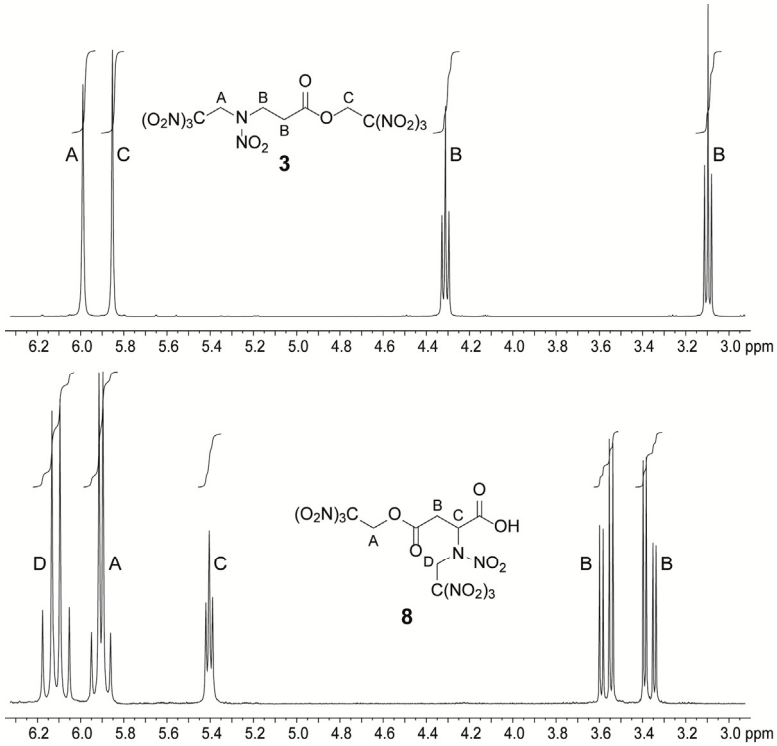

Figure 6.1 ^{1}H NMR spectra of **3** (top) and **8** (botton) in [D_6]acetone.

3.37 ppm. For the aspartate unit a higher order ABX-type spin system is observed, due to the strong coupling in the AB part (Figure 6.1, bottom). Therefore, in first approximation the resonances are split into doublets of doublets with estimated coupling constants of 18.6 Hz (J_{AB}), 5.9 Hz (J_{AX}) and 6.1 Hz (J_{BX}).

In the ^{13}C NMR spectra the resonances for the carbonyl moiety of compounds **1**–**4** are observed between 179.2–170.1 ppm whereas the carbonyl signal of the nitrocarbamate is shifted to higher field at δ = 149.3 ppm. For compounds **6**–**8** two signals for the carbonyl moieties appear between 172.4 and 167.9 ppm. The resonances of the carbon atoms of the trinitromethyl moiety are found as broadened signals in the range of 125.4–121.9 ppm.

In order to verify the structure of compound **8**, 2D-NMR spectra (^{1}H,^{1}H-COSY, ^{1}H,^{13}C-HMQC and ^{1}H,^{13}C-HMBC) as well as a proton coupled ^{13}C NMR spectrum were recorded. While the 2D spectra allowed a clear assignment of the observed ^{1}H and ^{13}C signals, the position of the trinitroethyl group could be derived only from the ^{1}H coupled ^{13}C spectrum evaluating the splitting pattern constants of the two carbonyl carbon atoms (Figure 6.2). The signal shifted to higher field at δ = 168.1 ppm is split into a doublet of doublets of doublets. The larger coupling constant of 8.4 Hz correlates to the two-bond coupling of the carbon atom to the single proton of the neighboring C*H* group. The couplings of 3.4 Hz and 4.0 Hz are three-bond couplings of the carbon to the more distant CH_2 group. The signal of the second carbonyl unit (δ = 169.5 ppm) is split into a triplet of doublets of triplets. Assuming that the trinitroethyl moiety is bound to this carbonyl group this splitting pattern would be expected. The larger triplet with a coupling constant of 7.9 Hz corresponds to a ^{2}J coupling to the adjacent CH_2 group. The doublet (4.6 Hz) as well as the smaller triplet

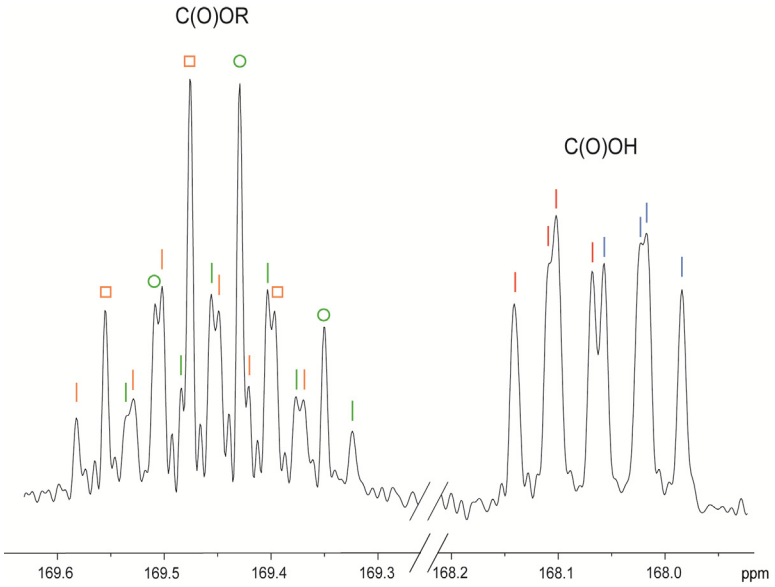

Figure 6.2 Excerpt of the ^{1}H coupled ^{13}C NMR spectrum of **8** showing the carbonyl resonances ([D$_6$]acetone).

(2.7 Hz) can be assigned to the coupling to the C*H* and CH_2 moieties, respectively. The smaller ^3J coupling constant of only 2.7 Hz can be explained by the coupling across the oxygen. This is also in agreement with coupling constants found in the literature.[9]

6.3.3 Vibrational Spectroscopy

In addition to NMR spectroscopy all compounds were analyzed also by IR and Raman spectroscopy. For the carbonyl moieties strong to medium bands are observed in the range of 1789–1701 cm^{-1} in the IR and Raman spectra due to the C=O stretching vibration ν(C=O).[10] The nitro groups show bands for the asymmetric stretching vibration $\nu_{as}(NO_2)$ in the region of 1620–1579 cm^{-1} and for the symmetric stretching vibration $\nu_s(NO_2)$ at 1306–1253 cm^{-1}. For the carbonyl azide **4** further bands are found between 2174 and 2138 cm^{-1}, which are assigned to the asymmetric stretching vibration of the azide moiety.[10]

6.3.4 Single Crystal Structure Analysis

Single crystals suitable for X-ray measurements were obtained for compounds **2** and **4** by crystallization from *n*-hexane and chloroform/*n*-hexane, respectively. Structural data, parameters and refinements of the measurements are summarized in Appendix A6 for both compounds.

The carbonyl chloride **2** crystallizes in the monoclinic space group *Pc* with four molecules in the unit cell and two molecules as asymmetric unit. The molecular structure of **2** as it is depicted in Figure 3.1, is stabilized by strong intra- (C3–H3···O6 2.694 Å, C4–H5···O1 2.411 Å) and intermolecular hydrogen bonds (C3–H4···O1 2.376 Å, C4–H6···O12 2.385 Å), as well as intramolecular attractions with atom distances shorter than the sum of the van der Waals radii (N2···O4 2.943 Å, N3···O3 2.918 Å).[11] Due to the electron withdrawing nitro group, the N1–N2 atom distance is with a value of 1.361 Å slightly shortened compared to a

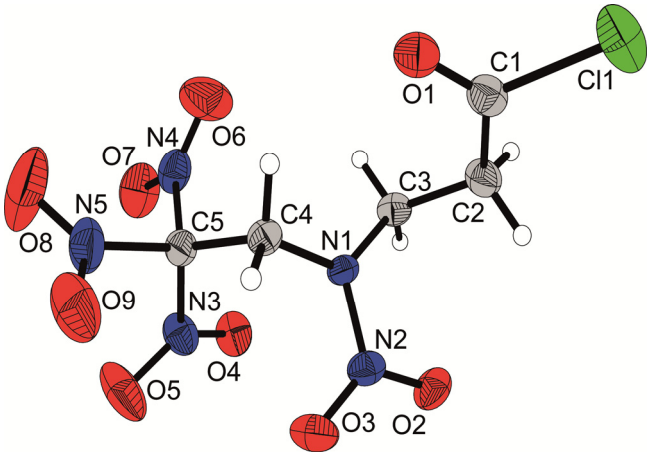

Figure 6.3 X-ray molecular structure of **2**.

common N–N single bond. Furthermore the moieties surrounding N1 are organized in a trigonal planar arrangement with angles of 125.38° (C3–N1–C4), 118.30° (C3–N1–N2), and 116.19° (C4–N1–N2), which is also an effect of the delocalization of the electron pair at the nitrogen N1.

The trinitromethyl moieties of half of the molecules in the unit cell are disordered. The distribution of the electron density is shown by the different color intensities in Figure 6.4. The oxygen atoms O13, O14 and O15 are fully occupied while the other oxygen positions as well as the nitrogen positions are only occupied to 75% and 25%, respectively. Nevertheless, both geometries form the propeller-like orientation as it is often observed for the trinitromethyl unit.

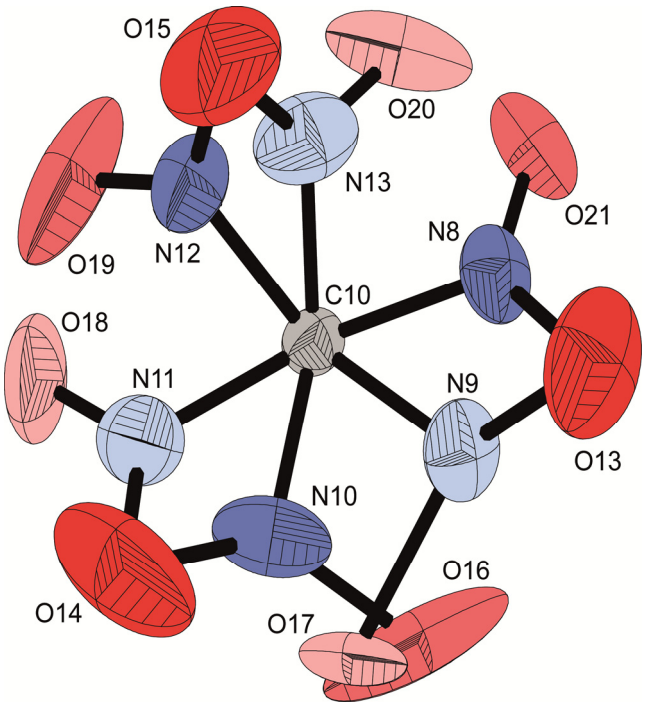

Figure 6.4 Disorder of the trinitromethyl moiety in the molecular structure of **2**. The distribution of the electron density is shown by the intensities of the different colors.

The carbonyl azide **4** crystallizes in the monoclinic space group $P2_1/n$ with one molecule in the asymmetric unit. In this structure the mostly favored propeller-like arrangement of the trinitromethyl unit is not observed. Instead two nitro groups are rather parallel oriented. This orientation is stabilized both by intramolecular attractions between the nitrogen N6 and the oxygen O7 (N6···O7 2.703 Å) and the nitrogen N8 and the oxygen O5 (N8···O5 2.610 Å), respectively, and intramolecular hydrogen bonds (C3–H3···O6 2.342 Å, C4–H6···O1 2.381 Å). As common for covalent carbonyl azides, the azide moiety is slightly bent with an angle of 172.93° while the atom distances between the nitrogen atoms are between a typical double (N2–N3 1.267 Å) and triple bond (N1–N2 1.106 Å)[4,12] (Figure 6.5).

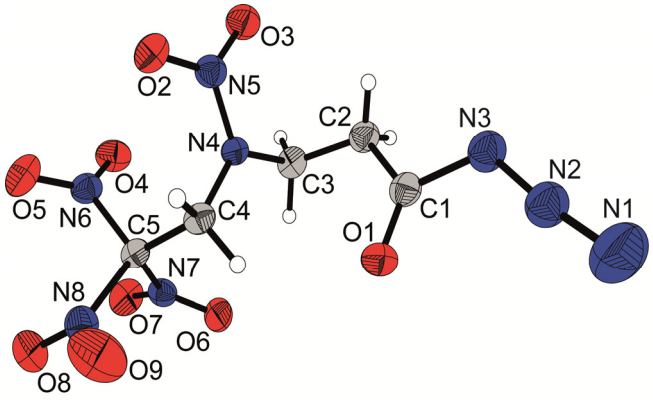

Figure 6.5 X-ray molecular structure of **4**.

6.3.5 Thermal Stabilities and Energetic Properties

The thermal and energetic properties were determined for all compounds except the acid chlorides **2** and **7**. Differential scanning calorimetry measurements (DSC) with a heating rate of 5 K min^{-1} showed satisfying decomposition temperatures with values higher than 150 °C for most of the compounds (Table 6.1). Only the carbonyl azide **4** exhibits an exothermic signal at 65 °C which is attributed to the Curtius rearrangement to the corresponding isocyanate. As compiled also in Table 6.1, the synthesized compounds generally possess nitrogen and oxygen contents of almost +80% (**1**, **4**, **6**, and **8**) or even higher (**3** and **5**) and the oxygen balance assuming the formation of CO (Ω_{CO}) is positive for all compounds. The carbamate **5** even has a Ω_{CO} value of +21.5%.

For all compounds the sensitivities towards impact (IS) and friction (FS) were tested according to STANAG 4489[13] and STANAG 4487[14] using a BAM fall hammer and BAM friction tester, respectively.[15] Most compounds are sensitive towards both impact and friction. Only the carboxylic acids **1** and **6** are insensitive. However, with impact sensitivities of 9 J (**3**) and 10 J (**5**) and friction sensitivities of 192 N (**3**) and 216 N (**5**) both compounds are less sensitive than Hexogen (RDX = 1,3,5-trinitroperhydro-1,3,5-triazine) and therefore achieve the requirements for HEDOs.[7] As expected, special care should be taken when working with the carbonyl azide **4** (IS = 2 J, 256 FS = 80 N).

Since most of the compounds are classified as energetic materials, detonation and combustion parameters were predicted for compounds **1**, **3**–**6**, and **8** by using the EXPLO5 V6.02 code.[16] These values, together with the previously computed enthalpies and free energies (CBS-4M ab initio calculations), are summarized in Table 6.2. For the use as secondary explosive the detonation velocity and pressure as well as the thermal stability are crucial factors. Due to its high room temperature density of 1.89 g cm^{-3} the best performance is predicted for the nitrocarbamate **5** with a detonation velocity of 9083 m s^{-1}

Table 6.1 Physical and chemical properties of **1**, **3–6**, **8** and ammonium perchlorate (AP).

	1	**3**	**4**	**5**
formula	$C_5H_7N_5O_{10}$	$C_7H_8N_8O_{16}$	$C_5H_6N_8O_9$	$C_7H_8N_{10}O_{18}$
MW [g mol^{-1}]	297.15	460.18	322.15	520.19
T_m [°C] (onset) [a]	-	72	-	103
T_{dec} [°C] (onset) [b]	146	164	65	157
IS [J] [c]	15	9	2	10
FS [N] [d]	>360	192	80	216
ESD [J] [e]	0.20	0.30	0.02	0.15
N [%] [f]	23.6	24.4	34.8	26.9
O [%] [g]	53.8	55.6	44.7	55.4
N+*O* [%] [h]	77.4	80.0	79.5	82.3
Ω_{CO} [%] [i]	+8.1	+17.4	+5.0	+21.5
Ω_{CO2} [%] [j]	−18.8	−7.0	−19.9	0

	6	**8**	**AP**
formula	$C_6H_7N_5O_{12}$	$C_8H_8N_8O_{18}$	NH_4ClO_4
MW [g mol^{-1}]	341.15	504.19	117.49
T_m [°C] (onset) [a]	-	-	-
T_{dec} [°C] (onset) [b]	160	159	240
IS [J] [c]	40	3	20
FS [N] [d]	>360	216	> 360
ESD [J] [e]	0.10	0.15	0.5
N [%] [f]	20.5	22.22	11.9
O [%] [g]	56.3	57.1	54.5
N+*O* [%] [h]	76.8	79.3	66.4
Ω_{CO} [%] [i]	+11.7	+19.0	+34.0
Ω_{CO2} [%] [j]	−16.4	−6.3	+34.0

[a] Melting temperature determined by DSC measurement carried ou at a heating rate of 5 K min^{-1}. [b] Decomposition temperature determined by DSC measurement (heating rate 5 K min^{-1}). [c] Impact sensitivity. [d] Friction sensitivity. [e] Sensitivity toward electrostatic discharge. [f] Nitrogen content. [g] Oxygen content. [h] Sum of nitrogen and oxygen content. [i] Oxygen balance assuming the formation of CO at the combustion. [j] Oxygen balance assuming the formation of CO_2 at the combustion.

Table 6.2 Calculated heat of formation and predicted detonation and combustion parameters (by using the EXPLO5 V6.02 code)[16] of **1**, **3–6**, **8** and ammonium perchlorate (AP).

	1	**3**	**4**	**5**	**6**	**8**	**AP**
formula	$C_5H_7N_5O_{10}$	$C_7H_8N_8O_{16}$	$C_5H_6N_8O_9$	$C_7H_8N_{10}O_{18}$	$C_6H_7N_5O_{12}$	$C_8H_8N_8O_{18}$	NH_4ClO_4
density RT [a]	1.72	1.73	1.70	1.89	1.66	1.65	1.95
$\Delta_f H_m°$ [kJ mol^{-1}] [b]	−463.1	−398.4	98.3	−292.8	−824.5	−777.5	−295.8
$\Delta_f U°$ [kJ kg^{-1}] [c]	−1466.9	−779.5	393.5	−477.1.4	−2329.5	−1458.5	−2623.2
Q_v [kJ kg^{-1}] [d]	−5108	−6110	−5700	−6328	−4502	−5601	−1422
T_{ex} [K] [e]	3610	4315	4059	4355	3399	4152	1735
V_0 [L kg^{-1}] [f]	738	740	761	746	734	735	885
p_{CJ} [kbar] [g]	277	292	291	365	234	247	158
V_{det} [m s^{-1}] [h]	7987	8300	8285	9083	7515	7801	6368
I_s [s] [i]	247	252	259	250	233	248	155
I_s [s] (15% Al) [j]	258	260	268	259	248	253	232
I_s [s] (20% Al) [k]	260	262	262	261	251	255	240
I_s [s] (12% Al, 14% binder) [l]	237	249	236	257	229	242	254
I_s [s] (20% Al, 14% binder) [m]	233	241	236	243	227	236	258

[a] RT densities are recalculated from X-ray densities or experimentally determined by pycnometer measurements. [b] Enthalpy calculated by the CBS-4M method using Gaussian 09. [c] Energy of formation calculated by the CBS-4M method using Gaussian 09. [d] Heat of detonation. [e] Detonation temperature. [f] Volume of gaseous products. [g] Detonation pressure calculated by using the EXPLO5 V6.02 code.[16] [h] Detonation velocity calculated by using the EXPLO5 V6.02 code.[16] [i] Specific impulse for the neat compound using the EXPLO5 V6.02 code (70.0 bar chamber pressure, isobaric combustion conditions (1 bar), equilibrium to throat and frozen to exit).[16] [j] Specific impulse for compositions with 85% oxidizer and 15% aluminum. [k] Specific impulse for compositions with 80% oxidizer and 20% aluminum. [l] Specific impulse for compositions with 74% oxidizer, 12% aluminum and 14% binder (6% polybutadiene acrylic acid, 6% polybutadiene acrylonitrile and 2% bisphenol A ether). [m] Specific impulse for compositions with 66% oxidizer, 20% aluminum and 14% binder (6% polybutadiene acrylic acid, 6% polybutadiene acrylonitrile and 2% bisphenol A ether).

and a detonation pressure of 365 kbar, which is in the range of RDX. However, the thermal stability of **5** (T_{dec} = 157 °C) is slightly below the requirements for secondary explosives.

Due to the high oxygen content most of the compounds may also be employed as oxidizer in composite propellants. To achieve a high specific impulse (I_s) aluminum is added as a high performing fuel. Aluminum is oxidized by the excess oxygen provided by the oxidizer to the non-hazardous combustion product Al_2O_3. This reaction forms a high heat of combustion which is essential, since the specific impulse is proportional to the square root of the ratio of the combustion temperature T_c and the average molecular mass of the gaseous combustion products.[5a] To predict the highest specific impulses each compound was calculated as neat sample, with different amounts of aluminum and in binder/aluminum systems. In Table 6.2 the specific impulses for several composite propellants are listed (further values are summarized in the Appendix A6). The best specific impulses with values higher than 260 s were obtained for composite propellants existing of 85% oxidizer and 15% aluminum (I_s = 268 s (**4**)) and 80% oxidizer and 20% fuel (I_s = 261 s (**5**), *I*s = 262 s (**3**), *I*s = 260 s (**1**)), respectively. However, most of the specific impulses decrease when the binder is added. The only compound with a specific impulse comparable to AP is the carbamate **5** with a value of 257 s in a composite of 74% oxidizer, 12% aluminium, and 14% binder.

6.4 Conclusion

New oxygen rich compounds starting from the readily available amino acids β-alanine and L-aspartic acid were synthesized and characterized including multinuclear NMR and vibrational spectroscopy. Furthermore physical and chemical properties were determined. DSC measurements showed satisfying decomposition temperatures around 150 °C for all compounds except the carbonyl azide **4**. As expected, compound **4** exhibits an exothermic signal at 65 °C, probably due to the Curtius rearrangement to the corresponding isocyanate. The impact and friction sensitivities indicate that most compounds are sensitive materials. Extreme care should be taken when working with the very sensitive carbonyl azide **4**. Furthermore detonation and combustion parameters were determined. Compound **5** possesses a high detonation velocity (V_{det} = 9083 m s^{-1}) and detonation pressure (P_{CJ} = 365 kbar), which is comparable to RDX. The specific impulses show satisfying values for oxidizer/fuel systems of higher than 260 s (**1**, **3**, **4**, and **5**). When predicting the specific impulse for oxidizer/fuel/binder systems the values for most compounds decrease significantly. Only the carbamate **5** shows in such a composite propellant a specific impulse comparable to AP (I_s = 257 s).

6.5 Experimental Section

General Information

All chemicals were used as supplied. Raman spectra were recorded in a glass tube with a Bruker MultiRAM FTRaman spectrometer with Nd:YAG laser excitation up to 1000 mW at 1064 nm in the range between 400 and 4000 cm^{-1}. Infrared spectra were measured with a Perkin-Elmer Spectrum BX-FT-IR spectrometer equipped with a Smiths DuraSamplIR II ATR device. All spectra were recorded at ambient temperature. NMR spectra were recorded with a JEOL Eclipse 400 instrument and chemical shifts were determined with respect to external standards Me_4Si (^1H, 399.8 MHz; ^{13}C, 100.5 MHz) and $MeNO_2$ (^{14}N, 28.8 MHz). Mass spectrometric data were obtained with a JEOL MStation JMS 700 spectrometer (DCI+, DEI+). Analysis of C/H/N were performed with an Elemental VarioEL Analyzer. Melting and decomposition points were measured with a Perkin-Elmer Pyris6 DSC and an OZM Research DTA 552-Ex with a heating rate of 5 K min^{-1} in a temperature range of 15 to 400 °C and checked by a Büchi Melting Point B-540 apparatus (not corrected). The sensitivity data were performed using a BAM drophammer and a BAM friction tester.[13–14]

X-ray Crystallography

Crystals suitable for X-ray crystallography were selected by means of a polarization microscope, mounted on the tip of a glass fiber. All measurements were investigated with an Oxford XCalibur3 (**2**, and **4**). The diffractometer is equipped with a generator (voltage 50 kV, current 40 mA) and a KappaCCD detector operating with Mo-*K*α radiation (λ = 0.7107 Å). The solution of the structure was performed by direct methods (SIR97)[17] and refined by full-matrix least-squares on *F*2 (SHELXL)[18] implemented in the WINGX software package[19] and finally checked with the PLATON software[20]. All non-hydrogen atoms were refined anisotropically. The hydrogen atom positions were located in a difference Fourier map. ORTEP plots are shown with thermal ellipsoids at the 50% probability level.

Crystallographic data (excluding structure factors) for the structures in this paper have been deposited with the Cambridge Crystallographic Data Centre, CCDC, 12 Union Road, Cambridge CB21EZ, UK. Copies of the data can be obtained free of charge on quoting the depository numbers CCDC-1484172 (**2**) and CCDC-1484173 (**4**) (Fax: +44-1223-336-033; E-Mail: deposit@ccdc.cam.ac.uk, http://www.ccdc.cam.ac.uk).

Quantum Chemical Calculations

All ab initio calculations were carried out using the program package Gaussian 09 (Rev. A.02)[21] and visualized by GaussView 5.08.[22] Structure optimizations and frequency analyses were performed with Becke's B3 three parameter hybrid functional using the LYP

correlation functional (B3LYP). For C, H, N and O a correlation consistent polarized double-zeta basis set ccpVDZ was used. The structures were optimized with symmetry constraints and the energy is corrected with the zero point vibrational energy.[23] The enthalpies (*H*) and free energies (*G*) were calculated using the complete basis set (CBS) method in order to obtain accurate values. The CBS models used the known asymptotic convergence of pair natural orbital expressions to extrapolate from calculations using a finite basis set to the estimated complete basis set limit. CBS-4M starts with a HF/3-21G(d) geometry optimization, which is the initial guess for the following SCF calculation as a base energy and a final MP2/6-31+G calculation with a CBS extrapolation to correct the energy in second order. The used CBS-4M method additionally implements a MP4(SDQ)/6-31+(d,p) calculation to approximate higher order contributions and also includes some additional empirical corrections.[24] The enthalpies of the gas-phase species were estimated according to the atomization energy method.[25]

Calculation of Energetic Performance

All calculations affecting the detonation parameters were carried out using the program package EXPLO5 V6.02.[16,26] The detonation parameters were calculated at the CJ point with the aid of the steady-state detonation model using a modified Becker-Kistiakowski-Wilson equation of state for modeling the system. The CJ point is found from the Hugoniot curve of the system by its first derivative. The specific impulses were also calculated with the EXPLO5 V6.02 program, assuming an isobaric combustion of a composition of 70% oxidizer, 16% aluminum as fuel, 6% polybutadiene acrylic acid, 6% polybutadiene acrylonitrile as binder and 2% bisphenol A ether as epoxy curing agent. A chamber pressure of 70.0 bar and an ambient pressure of 1.0 bar with frozen expansion conditions were assumed for the calculations.

Synthesis

CAUTION! All prepared compounds are energetic materials with sensitivity towards heat, impact, and friction. No hazards occurred during the preparation and manipulation. However, additional proper protective precautions (face shield, leather coat, earthed equipment and shoes, Kevlar® gloves, and ear plugs) should be used when undertaking work with these compounds.

3-[Nitro(2,2,2-trinitroethyl)amino]propanoic Acid (**1**)

β-Alanine ethyl ester hydrochloride[27] (6.0 g, 39.1 mmol), trinitromethane (6 g, 39.7 mmol), and an aqueous solution of formaldehyde (3.4 mL, 45.7 mmol, 37%) were added to 20 mL water and the mixture was cooled to 0 °C. Sodium hydroxide (1.6 g, 40.0 mmol) dissolved in

10 mL water was added to the pre-cooled solution with immediate separation of a yellow oil. The reaction mixture was stirred at 0 °C for 2 h. 20 mL chloroform was added and the organic phase was separated. The aqueous solution was again extracted with chloroform (2 × 20 mL), the combined organic phases were dried with magnesium sulfate and the solvent was removed in vacuo. The residual oil was dissolved in 15 mL acetic anhydride and cooled to 0 °C. Nitric acid (15 mL, 100%) was added slowly and the solution was stirred at 0 °C for 2 h before quenching on crushed ice. The reaction mixture was extracted with chloroform (2 × 50 mL), the combined organic phases were dried with magnesium sulfate and the solvent was removed in vacuo. The remaining colorless liquid was dissolved in acetic acid (15 mL) and concentrated hydrochloric acid (30 mL) and refluxed for 15 h. The solvent was removed on the rotary evaporator leaving a precipitate which was washed with toluene twice. 3-[Nitro(2,2,2-trinitroethyl) amino]propanoic acid (**1**) was obtained as a colorless solid (22%).

^{1}H NMR ([D$_6$]acetone): δ = 11.10 (s, 1H, O*H*), 6.00 (s, 2H, C*H*$_2$C(NO$_2$)$_3$) ppm; A$_2$B$_2$ spectrum: δ_A = 4.21, δ_B = 2.88 ppm, J_{AB} = 6.2 Hz, C(O)C*H*$_2$C*H*$_2$N. ^{13}C{^{1}H} NMR ([D$_6$]acetone): δ = 173.4 (*C*(O)), 125.4 (*C*(NO$_2$)$_3$), 55.8 (*C*H$_2$), 50.8 (*C*H$_2$) 31.7 (*C*H$_2$) ppm. ^{14}N NMR ([D$_6$]acetone): δ = –31 (N(*N*O$_2$)$_3$), –32 (C(*N*O$_2$)$_3$) ppm. C$_5$H$_7$N$_5$O$_{10}$ (297.15): calcd. C 20.21, H 2.37, N 23.57%; found C 20.57, H 2.41, N 23.59%. IR (ATR): ν = 3022 (w), 2361 (w), 1708 (m), 1602 (s), 1588 (s), 1549 (s), 1454 (m), 1437 (w), 1405 (m), 1358 (w), 1338 (w), 1293 (m), 1274 (s), 1253 (s), 1229 (m), 1122 (w), 1043 (w), 1008 (w), 962 (w), 943 (m), 865 (m), 854 (m), 827 (m), 802 (m), 762 (m), 685 (w) cm^{-1}. Raman (300 mW): ν = 3023 (31), 2983 (71), 2939 (77), 1645 (7), 1611 (42), 1589 (19), 1549 (18), 1453 (15), 1413 (30), 1380 (31), 1363 (23), 1343 (81), 1294 (30), 1276 (29), 1232 (9), 1208 (9), 1122 (5), 1098 (8), 1045 (22), 1007 (11), 971 (36), 945 (22), 869 (44), 855 (100), 829 (41), 805 (12), 768 (5), 664 (7), 635 (12), 617 (17), 577 (5), 540 (19), 523 (8), 425 (31), 407 (41), 391 (48), 370 (81), 286 (33), 268 (6), 247 (17), 234 (14) cm^{-1}. DSC (5 K min^{-1}, onset): 146 °C (mp. with dec.). IS: 15 J (grain size <100 µm). FS: 360 N (grain size <100 µm). ESD: 0.20 J (grain size <100 µm).

3-[Nitro(2,2,2-trinitroethyl)amino]propanoyl Chloride (**2**)

The propanoic acid **1** (500 mg, 1.7 mmol) was dissolved in thionyl chloride (10 mL) and refluxed for 5 h. After cooling to ambient temperature *n*-hexane (75 mL) was added and the reaction mixture was stored at −30 °C overnight. A colorless solid precipitated, which was filtered off yielding 3-[nitro(2,2,2-trinitroethyl)amino]propanoyl chloride (**2**) (90%).

^{1}H NMR (CDCl$_3$): δ = 5.65 (s, 2H, C*H*$_2$C(NO$_2$)$_3$) ppm; A$_2$B$_2$ spectrum: δ_A = 4.04, δ_B = 3.46 ppm, J_{AB} = 5.6 Hz, C(O)C*H*$_2$C*H*$_2$N. ^{13}C{^{1}H} NMR (CDCl$_3$): δ = 174.0 (*C*(O)), 122.3 (*C*(NO$_2$)$_3$), 53.7

(CH_2), 48.3 (CH_2) 44.3 (CH_2) ppm. ^{14}N NMR ($CDCl_3$): δ = −34 ($C(NO_2)_3$/$N(NO_2)$) ppm. $C_5H_6N_5O_9Cl$ (315.58): calcd. C 19.03, H 1.92, N 22.19%; found C 19.32, H 2.14, N 22.00%. IR (ATR): ν = 3018 (w), 2973 (w), 1775 (m), 1611 (m), 1585 (s), 1562 (s), 1448 (m), 1408 (w), 1393 (m), 1364 (w), 1341 (w), 1291 (s), 1277 (s), 1228 (m), 1208 (w), 1125 (m), 1039 (m), 1006 (m), 982 (m), 914 (m), 864 (m), 853 (m), 825 (m), 801 (s), 760 (m), 709 (s), 675 (w) cm^{-1}. Raman (300 mW): ν = 3020 (32), 2980 (67), 2936 (60), 1783 (15), 1612 (29), 1453 (18), 1381 (34), 1365 (30), 1343 (59), 1293 (34), 1283 (31), 1100 (13), 1041 (27), 984 (25), 868 (28), 855 (100), 828 (26), 803 (9), 764 (9), 715 (19), 677 (12), 606 (17), 541 (15), 502 (19), 469 (40), 418 (33), 394 (44), 371 (67), 322 (12), 268 (27), 217 (13) cm^{-1}.

2,2,2-Trinitroethyl 3-[nitro(2,2,2-trinitroethyl)amino]propanoate (**3**)

The propanoyl chloride **2** (480 mg, 1.5 mmol) was dissolved in chloroform (10 mL). 2,2,2-Trinitroethanol (344 mg, 1.9 mmol) and dry aluminum(III) chloride (226 mg, 1.7 mmol) were added and the reaction mixture was refluxed for 3 h. Any solid was filtered off and the filtrate was washed with 10 mL 2 M hydrochloric acid and water (2 × 10 mL). The organic solvent was removed in vacuo yielding 2,2,2-trinitroethyl 3-[nitro(2,2,2-trinitroethyl)amino]propanoate (**3**) as a colorless solid (64%).

^{1}H NMR ([D$_6$]acetone): δ = 5.99 (s, 2H, $CH_2C(NO_2)_3$), 5.86 (s, 2H, $CH_2(NO_2)_3$) ppm; A_2B_2 spectrum: δ_A = 4.32, δ_B = 3.10 ppm, J_{AB} = 6.4 Hz, $C(O)CH_2CH_2N$. ^{13}C{^{1}H} NMR ([D$_6$]acetone): δ = 170.1 ($C(O)$), 125.1 ($C(NO_2)_3$), 61.9 (CH_2), 55.5 (CH_2), 50.2 (CH_2), 31.7 (CH_2) ppm. ^{14}N NMR ([D$_6$]acetone): δ = −32 ($N(NO_2)_3$), −33 ($C(NO_2)$), −33 ($C(NO_2)_3$) ppm. $C_7H_8N_8O_{16}$ (460.18): calcd. C 18.27, H 1.75, N 24.35%; found C 18.40, H 1.86, N 24.17%. IR (ATR): ν = 3021 (w), 3007 (w), 2967 (w), 2894 (w), 1770 (m), 1600 (s), 1583 (s), 1546 (s), 1466 (w), 1451 (m), 1419 (w), 1395 (m), 1344 (w), 1303 (s), 1292 (s), 1275 (s), 1148 (s), 1115 (m), 1067 (w), 1030 (w), 1006 (w), 917 (w), 869 (m), 854 (m), 802 (m), 782 (s), 764 (m), 736 (w), 718 (w), 652 (w) cm^{-1}. Raman (300 mW): ν = 3022 (15), 2969 (39), 2949 (19), 2933 (22), 1772 (11), 1616 (20), 1551 (5), 1440 (7), 1425 (15), 1388 (16), 1350 (32), 1327 (11), 1305 (25), 1295 (21), 1276 (31), 1197 (5), 1068 (12), 1005 (10), 919 (11), 883 (9), 856 (100), 805 (4), 786 (6), 717 (5), 606 (9), 548 (13), 488 (6), 431 (33), 386 (60), 366 (40), 302 (12), 279 (12), 245 (14) cm^{-1}. DSC (5 K min^{-1}, onset): 72 °C (mp.), 164 °C (dec.). IS: 9 J (grain size <100 μm). FS: 192 N (grain size <100 μm). ESD: 0.30 J (grain size <100 μm).

3-(Nitro-(2,2,2-trinitroethyl)amino)propanoyl Azide (**4**)

To a solution of sodium azide (156 mg, 1.4 mmol) in 10 mL water was added slowly at 0 °C the propanoyl chloride **2** (380 mg, 1.2 mmol) dissolved in chloroform (10 mL). The reaction

mixture was stirred at 0 °C for 1 h. The organic layer was separated and the aqueous layer was extracted with chloroform (2 × 20 mL). The combined organic phase was washed each with 20 mL ice-cold water, ice-cold solution of 5% sodium bisulfate, ice-cold water, and brine and was dried with magnesium sulfate. The solvent was concentrated to 5 mL on the rotary evaporator (water bath temperature 10 °C) and 10 mL *n*-hexane was added. Colorless crystals of 3-[nitro-(2,2,2-trinitroethyl)amino]propanoyl azide (**4**) precipitated at –30 °C overnight (55%).

^{1}H NMR ($CDCl_3$): δ = 5.74 (s, 2H, $CH_2C(NO_2)_3$) ppm; A_2B_2 spectrum: δ_A = 4.04, δ_B= 2.90 ppm, J_{AB} = 5.6 Hz, $C(O)CH_2CH_2N$. ^{13}C{^{1}H} NMR ($CDCl_3$): δ = 179.2 ($C(O)$), 122.7 ($C(NO_2)_3$), 53.9 (CH_2), 48.2 (CH_2), 34.2 (CH_2) ppm. ^{14}N NMR ($CDCl_3$): δ = –35 ($C(NO_2)_3$), –35 ($N(NO_2)$), –137 (N_β), –147 (N_γ) ppm. $C_5H_6N_8O_9$ (322.15): calcd. C 18.64, H 1.88, N 34.78%; found C 18.93, H 1.85, N 34.69%. IR (ATR): ν = 3023 (w), 2978 (w), 2271 (w), 2174 (w), 2140 (w), 1701 (m), 1621 (m), 1603 (s), 1576 (s), 1538 (s), 1444 (m), 1396 (m), 1377 (m), 1330 (m), 1299 (m), 1280 (s), 1222 (m), 1189 (s), 1152 (m), 1087 (m), 1024 (m), 1006 (m), 962 (w), 933 (w), 876 (m), 864 (m), 853 (m), 824 (m), 804 (m), 775 (m), 763 (m), 721 (w), 697 (m), 624 (w), 575 (m) cm^{-1}. Raman (300 mW): ν = 3034 (26), 3025 (30), 2978 (93), 2935 (78), 2171 (13), 2138 (20), 1709 (41), 1620 (28), 1611 (41), 1579 (11), 1446 (24), 1401 (31), 1379 (21), 1366 (25), 1337 (49), 1320 (21), 1306 (23), 1278 (41), 1224 (10), 1204 (11), 1191 (9), 1131 (10), 1092 (13), 1027 (12), 997 (16), 965 (48), 935 (18), 879 (10), 866 (37), 855 (100), 826 (25), 723 (13), 699 (15), 661 (13), 612 (18), 547 (18), 531 (11), 514 (26), 477 (9), 442 (43), 385 (76), 361 (65), 280 (38), 242 (43), 230 (30), 212 (10) cm^{-1}. DSC (5 K min^{-1}, onset): 65 °C (mp. with dec.). IS: 2 J (grain size <100 µm). FS: 80 N (grain size <100 µm). ESD: 20 mJ (grain size <100 µm).

2,2,2-Trinitroethyl nitro[2-(2,2,2-trinitroethyl)amino)ethyl]carbamate (**5**)

To the propanoyl azide **4** (500 mg, 1.5 mmol) dissolved in 10 mL chloroform was added 2,2,2-trinitroethanol (390 mg, 2.2 mmol) and a catalytic amount of aluminum(III) chloride and the reaction mixture was refluxed for 5 h. After cooling to ambient temperature the organic phase was washed with hydrochloric acid (10 mL, 2 M) and water (2 × 10 mL), dried with magnesium sulfate and the organic solvent was removed in vacuo. The residual yellow oil was dissolved in acetic anhydride (8 mL) and cooled to 0 °C. Nitric acid (8 mL, 100%) was added slowly and the reaction mixture was stirred at 20 °C for 2 h before quenching on crushed ice. A colorless solid precipitated, which was filtered off, washed with water and dried in the desiccator. 2,2,2-Trinitroethyl nitro[2-(nitro-(2,2,2,-trinitroethyl)amino)ethyl]carbamate (**5**) was obtained in 26% yield.

^{1}H NMR ([D$_6$]acetone): δ = 6.15 (s, 2H, CH_2C(NO$_2$)$_3$), 5.97 (s, 2H, CH_2C(NO$_2$)$_3$); A$_2$B$_2$ spectrum: δ_A = 4.65, δ_B = 4.40 ppm, J_{AB} = 5.6 Hz, C(O)CH_2CH_2N. ^{13}C{^{1}H} NMR ([D$_6$]acetone): δ = 149.3 (*C*(O)), 124.6 (*C*(NO$_2$)$_3$), 64.4 (*C*H$_2$), 56.0 (*C*H$_2$), 53.0 (*C*H$_2$), 47.8 (*C*H$_2$) ppm. ^{14}N NMR ([D$_6$]acetone): δ = –30 (N(*N*O$_2$)), –33 (C(*N*O$_2$)), –34 (C(*N*O$_2$)$_3$) ppm. C$_7$H$_8$N$_{10}$O$_{18}$ (520.19): calcd. C 16.16, H 1.55, N 26.93%; found C 16.37, H 1.74, N 26.79%. IR (ATR): ν = 3009 (w), 2885 (w), 2362 (w), 1778 (m), 1609 (s), 1593 (s), 1560 (m), 1449 (w), 1435 (w), 1391 (w), 1356 (w), 1298 (s), 1268 (s), 1237 (s), 1198 (w), 1162 (m), 1155 (m), 1136 (w), 1100 (w), 1063 (w), 1041 (w), 1009 (w), 978 (w), 934 (w), 885 (w), 868 (m), 855 (w), 830 (w), 805 (m), 786 (m), 778 (m), 766 (w), 726 (m) cm^{-1}. Raman (300 mW): ν = 3010 (31), 2970 (52), 1777 (15), 1606 (29), 1565 (15), 1438 (19), 1391 (25), 1345 (52), 1300 (49), 1269 (38), 1238 (17), 885 (17), 856 (100), 462 (16), 372 (54), 308 (30) cm^{-1}. DSC (5 K min^{-1}, onset): 103 °C (mp.), 157 °C (dec.). IS: 10 J (grain size <100 µm). FS: 216 N (grain size <100 µm). ESD: 0.15 J (grain size <100 µm).

N-Nitro-*N*-(2,2,2-trinitroethyl)-L-aspartic Acid (**6**)

Diethyl-L-aspartate hydrochloride[28] (17.3 g, 76.6 mmol), trinitromethane (11.5 g, 76.3 mmol) and an aqueous solution of formaldehyde (6.7 mL, 76.3 mmol, 37%) were added in 10 mL water and cooled to 0 °C. Sodium hydroxide (3.1 g, 76.3 mmol) dissolved in 20 mL water was slowly added to the pre-cooled solution and a yellow oil immediately separated. The reaction mixture was stirred for 1 h. Diethyl ether (20 mL) was added and the organic phase was separated. The aqueous solution was again extracted with diethyl ether (2 × 20 mL), the combined organic phases were dried with magnesium sulfate and the solvent was removed in vacuo. The residual oil was dissolved in 30 mL acetic anhydride and cooled to 0 °C. Nitric acid (15 mL, 100%) was added at 0–10 °C and the solution was stirred at 0 °C for 1 h before quenching on crushed ice. The reaction mixture was extracted with chloroform (2 × 50 mL), the combined organic phases were dried with magnesium sulfate, and the solvent was removed in vacuo. The remaining colorless solid was dissolved in acetic acid (170 mL) and concentrated hydrochloric acid (380 mL) and refluxed for 15 h. The solvent was removed on the rotary evaporator leaving a precipitate which was washed with toluene twice. *N*-Nitro-*N*-(2,2,2-trinitroethyl)-L-aspartic acid (**6**) was obtained as colorless solid in 88% yield.

^{1}H NMR ([D$_6$]acetone): δ = 10.2 (br., 1H, O*H*) ppm; AB spectrum: δ_A = 6.10 ppm, δ_B = 6.07 ppm, J_{AB} = 17.2 Hz, CH_2C(NO$_2$)$_3$; ABX spectrum: δ_A = 3.38, δ_B = 3.18, C(O)CH_2, δ_X = 5.36 ppm, NC*H*, J_{AB} = 18.2, J_{AX} = 5.2, J_{BX} = 7.0 Hz. ^{13}C{^{1}H} NMR ([D$_6$]acetone): δ = 172.3 (*C*O), 168.6 (*C*O), 125.3 (*C*(NO$_2$)$_3$), 63.6 (*C*N), 55.7 (*C*H$_2$), 34.5 (*C*H$_2$) ppm. ^{14}N NMR ([D$_6$]acetone): δ = –32

(C(NO_2)$_3$/N(NO_2)) ppm. $C_6H_7N_5O_{12}$ (341.15): calcd. C 21.12, H 2.07, N 20.53%; found C 21.28, H 2.33, N 20.23%. IR (ATR): ν = 3029 (w), 2978 (w), 2962 (w), 2613 (w), 2533 (w), 1721 (s), 1666 (w), 1620 (m), 1608 (m), 1600 (m), 1576 (m), 1564 (m), 1554 (m), 1420 (m), 1403 (m), 1364 (w), 1342 (w), 1290 (s), 1227 (w), 1215 (m), 1197 (w), 1120 (w), 1080 (w), 1025 (w), 952 (w), 927 (w), 905 (w), 871 (m), 855 (w), 837 (w), 805 (w), 786 (w), 764 (w), 752 (w), 711 (w), 694 (w), 678 (w) cm^{-1}. Raman (300 mW): ν = 3029 (40), 3001 (49), 2979 (67), 2954 (84), 1733 (16), 1675 (21), 1661 (26), 1620 (37), 1601 (25), 1577 (18), 1556 (15), 1454 (18), 1425 (20), 1406 (27), 1382 (25), 1365 (35), 1341 (50), 1289 (48), 1128 (18), 953 (70), 871 (25), 856 (100), 839 (25), 752 (15), 694 (19), 549 (21), 427 (48), 387 (79), 376 (49), 360 (53), 295 (30) cm^{-1}. DSC (5 K min^{-1}, onset): 160 °C (dec.). IS: 40 J (grain size <100 µm). FS: 360 N (grain size <100 µm). ESD: 0.10 J (grain size <100 µm).

N-Nitro-*N*-(2,2,2-trinitroethyl)-l-aspartoyl Dichloride (**7**)

The aspartic acid **6** (500 mg, 1.5 mmol) and phosphorus(V) chloride (763 mg, 3.7 mmol) were mixed under inert atmosphere and stirred at 40 °C for 2.5 h. After no further gas evolution was observed chloroform (10 mL) was added and insoluble residues were removed using Schlenk technique. After removing chloroform and phosphoryl chloride in vacuo a colorless solid was obtained, which was recrystallized from a mixture of chloroform and *n*-pentane yielding colorless crystals of *N*-nitro-*N*-(2,2,2-trinitroethyl)-L-aspartoyl dichloride (**7**) in 72% yield.

^{1}H NMR ($CDCl_3$): δ = AB spectrum: δ_A = 5.83 ppm, δ_B = 5.45 ppm, J_{AB}= 17.2 Hz, CH_2C(NO_2)$_3$; ABX spectrum: δ_A = 4.12 ppm, δ_B = 3.56 ppm, C(O)CH_2, δ_X = 5.04 ppm, NCH, J_{AB} = 19.6, J_{AX} = 5.6, $^3J_{BX}$ = 5.8 Hz. ^{13}C{^{1}H} NMR ($CDCl_3$): δ = 172.4 (C(O)Cl), 167.9 (C(O)Cl), 121.9 (C(NO_2)$_3$), 69.5 (CN), 55.1 (CH$_2$), 46.5 (CH$_2$) ppm. ^{14}N NMR ($CDCl_3$): δ = –35 (C(NO_2)$_3$), –38 (N(NO_2)) ppm. $C_6H_5N_5O_{10}Cl_2$ (378.03): calcd. C 19.06, H 1.33, N 18.53%; found C 19.12, H 1.51, N 18.23%. IR (ATR): ν = 3019 (w), 2953 (w), 1771 (s), 1652 (w), 1606 (s), 1597 (s), 1559 (s), 1419 (m), 1357 (w), 1348 (w), 1275 (s), 1213 (m), 1199 (m), 1110 (m), 1078 (w), 1062 (w), 1029 (s), 1007 (m), 970 (w), 938 (w), 925 (w), 863 (m), 855 (m), 821 (w), 802 (w), 775 (w), 759 (w), 720 (m), 709 (w), 677 (s) cm^{-1}. Raman (300 mW): ν̃ = 3019 (46), 2977 (75), 2954 (33), 2939 (94), 1789 (35), 1777 (34), 1612 (48), 1599 (35), 1564 (12), 1422 (18), 1387 (28), 1360 (40), 1342 (77), 1302 (46), 1278 (90), 1215 (8), 1202 (8), 1134 (9), 1113 (8), 1065 (11), 986 (12), 971 (11), 939 (21), 864 (46), 856 (100), 843 (86), 711 (10), 680 (12), 627 (14), 545 (22), 534 (45), 476 (98), 462 (28), 424 (48), 401 (48), 386 (42), 376 (78), 341 (42), 281 (40), 258 (16), 241 (27), 213 (10) cm^{-1}.

(*S*)-2-[Nitro(2,2,2-trinitroethyl)amino]-4-oxo-4-(2,2,2-trinitroethoxy)butanoic Acid (**8**)

To aspartoyl dichloride **7** (450 mg, 1.2 mmol) dissolved in chloroform (10 mL) was added 2,2,2-trinitroethanol (540 mg, 3.0 mmol) and a catalytic amount of aluminum(III) chloride, and the reaction mixture was refluxed for 5 h. After cooling to ambient temperature the solvent was removed in vacuo and water was added to the residual oil. A colorless solid precipitated which was filtered off, washed with water and dried. (*S*)-2-[nitro(2,2,2-trinitroethyl) amino]-4-oxo-4-(2,2,2-trinitroethoxy)butanoic acid (**8**) was obtained in 79% yield.

^{1}H NMR ([D$_6$]acetone): δ = AB spectrum: δ_A = 6.15, δ_B = 6.09 ppm, J_{AB} = 17.2 Hz, NCH_2; AB spectrum: δ_A = 5.94, δ_B = 5.90 ppm, J_{AB} = 14.0 Hz, OCH_2; ABX spectrum: δ_A = 3.57, δ_B = 3.37, C(O)CH_2, δ_X = 5.41 ppm, CH, J_{AB} = 18.0, J_{AX} = 6.8, $^{3}J_{BX}$ = 5.6 Hz. ^{13}C NMR ([D$_6$]acetone): δ = 169.5 (C(O)OCH$_2$, tdt, $^{0}J_{CH}$ = 7.9, $^{3}J_{CH}$ = 4.6, $^{3}J_{CH}$ = 2.7 Hz, 168.1 (C(O)OH, dt, $^{2}J_{CH}$ = 8.4, $^{3}J_{CH}$ = 3.4, $^{3}J_{CH}$ = 4.0 Hz), 125.1 (C(NO$_2$)$_3$, m), 63.3 (CH, dm, $^{1}J_{CH}$ = 138.3 Hz), 62.0 (OCH$_2$, t, $^{1}J_{CH}$ = 160.0 Hz), 55.7 (NCH$_2$, td, $^{1}J_{CH}$= 151.7, $^{3}J_{CH}$ = 2.7 Hz), 34.5 (CH$_2$, ddd, $^{1}J_{CH}$ = 132.7, $^{2}J_{CH}$ = 132.7 Hz). ^{14}N NMR ([D$_6$]acetone): δ = –30 (N(NO$_2$)), –33 (C(NO$_2$)$_3$) ppm. $C_8H_8N_8O_{18}$ (504.19): calcd. C 19.06, H 1.60, N 22.22%; found C 19.10, H 1.74, N 22.15%. IR (ATR): ν = 3013 (w), 2876 (w), 2360 (w), 2341 (w), 1775 (w), 1743 (m), 1731 (w), 1629 (w), 1608 (s), 1592 (s), 1563 (s), 1442 (w), 1423 (w), 1391 (w), 1344 (w), 1292 (s), 1281 (s), 1261 (s), 1116 (w), 1094 (w), 1052 (w), 1023 (w), 973 (w), 887 (m), 862 (m), 854 (m), 808 (m), 800 (m), 778 (m), 764 (m), 720 (w), 668 (w) cm^{-1}. Raman (300 mW): ν = 3014 (26), 3000 (21), 2971 (51), 2943 (30), 2897 (8), 2875 (9), 2702 (8), 1775 (11), 1616 (27), 1566 (8), 1445 (15), 1422 (10), 1391 (25), 1377 (14), 1353 (38), 1298 (35), 1281 (47), 1053 (14), 929 (31), 889 (11), 857 (100), 780 (9), 551 (8), 462 (7), 422 (29), 388 (54), 375 (50), 289 (9), 266 (9) cm^{-1}. DSC (5 K min^{-1}, onset): 159 °C (dec.). IS: 3 J (grain size <100 µm). FS: 216 N (grain size <100 µm). ESD: 0.15 J (grain size <100 µm).

6.6 References

[1] J. M. Berg, J. L. Tymoczko, L. Stryer, *Biochemistry* 7th ed., W. H. Freeman, Basingstoke, UK, **2011**.

[2] P. Nuhn, *Naturstoffchemie: Mikrobielle, pflanzliche und tierische Naturstoffe*, 2nd ed., Hirzel, Stuttgart, Germany, **1990**.

[3] K. Munk, *Biochemie Zellbiologie*, Georg Thieme Verlag, Stuttgart, Germany, **2008**.

[4] A. Baumann, A. Erbacher, C. Evangelisti, T. M. Klapötke, B. Krumm, S. F. Rest, M. Reynders, V. Sproll, *Chem. Eur. J.* **2013**, *19*, 15627–15638.

[5] a) T. M. Klapötke, *Chemistry of High-Energy Materials*, 3rd ed., De Gruyter, Berlin, Germany, **2015**; b) J. P. Agrawal, *High Energy Materials Propellants, Explosives and Pyrotechnics*, 1st ed., Wiley-VCH, Weinheim, Germany, **2010**; c) I. Hargittai, T. Vidóczy, *Combustion Efficiency and Air Quality*, 1st ed., Springer, New York, USA, **1995**.

[6] J. Wolff, *Pharmacol. Rev.* **1998**, *50*, 89–105.

[7] Office of Naval Research Home Page. http://www.onr.navy.mil (accessed March 24, 2016).

[8] H. Feuer, G. B. Bachman, C. R. Koller, W. A. Swarts, *Tetrahedron* **1963**, *19*, 165–176.

[9] H.-O. Kalinowski, S. Berger, S. Braun, *13C-NMR-Spektroskopie*, Georg Thieme Verlag, Stuttgart, Germany, **1984**.

[10] G. Socrates, *Infrared and Raman Characteristic Group Frequencies: Tables and Charts*, 3rd ed., John Wiley & Sons, Chichester, UK, **2004**.

[11] G. A. Jeffrey, *An Introduction to Hydrogen Bonding*, Oxford University Press, New York, US, **1997**.

[12] a) A. Wolter-Steingrube, B. E. C. Bugenhagen, C. Herrmann, J. Heck, *Eur. J. Inorg. Chem.* **2014**, *2014*, 4115–4122; b) G. C. Hsu, L. M. Singer, D. B. Cordes, M. Findlater, *Acta Crystallogr.* **2013**, *69E*, 1298; c) J. Lapic, A. Pezerovic, M. Cetina, S. Djakovic, V. Rapic, *J. Mol. Struct.* **2011**, *990*, 209–216; d) G. Laus, V. Kahlenberg, K. Wurst, S. Nerdinger, H. Schottenberger, *Z. Naturforsch. B* **2011**, *66*, 479–486; e) D. Siebler, C. Forster, T. Gasi, K. Heinze, *Organometallics* **2011**, *30*, 313–327; f) L. Parkanyi, G. Besenyei, *J. Mol. Struct.* **2004**, *691*, 97–106; g) F. M. Menger, J. Bian, V. A. Azov, *Angew. Chem. Int. Ed.* **2002**, *41*, 2581–2584; h) Y. Jiao, E. Valente, S. T. Garner, X. Wang, H. Yu, *Tetrahedron Lett.* **2002**, *43*, 5879–5881.

[13] NATO, Standardization Agreement 4489 (STANAG 4489), Explosives, Impact Sensitivity Tests, **1999**.

[14] NATO, Standardization Agreement 4487 (STANAG 4487), Explosives, Friction Sensitivity Tests, **2002**.

[15] Test methods according to the "UN Manual of Test and Criteria, Recommendations on the Transport of Dangerous Goods", United Nations Publication, New York, Geneva, 4th revised ed., **2003**, Impact: Insensitive > 40 J, less sensitive ≥ 35 J, sensitive ≥ 4 J, very sensitive ≤ 3 J; Friction: Insensitive > 360 N, less sensitive = 360 N, sensitive < 360 N > 80 N, very sensitive ≤ 80 N, extremely sensitive ≤ 10 N.

[16] M. Suc´eska, *EXPLO5 V6.02*, Zagreb, Croatia, **2013**.

[17] A. Altomare, M. C. Burla, M. Camalli, G. L. Cascarano, C. Giacovazzo, A. Guagliardi, A. G. G. Moliterni, G. Polidori, R. Spagna, *J. Appl. Crystallogr.* **1999**, *32*, 115–119.

[18] a) G. M. Sheldrick, *Acta Crystallogr., Sect. A* **2008**, *64*, 112–122; b) G. M. Sheldrick, *SHELX-97*, Programs for Crystal Structure Determination, **1997**.

[19] L. Farrugia, *J. Appl. Crystallogr.* **1999**, *32*, 837–838.

[20] A. Spek, *Acta Crystallogr., Sect. D* **2009**, *65*, 148–155.

[21] M. J. Frisch, G. W. Trucks, H. B. Schlegel, G. E. Scuseria, M. A. Robb, J. R. Cheeseman, V. B. G. Scalmani, B. Mennucci, G. A. Petersson, H. Nakatsuji, M. Caricato, X. Li, H. P. Hratchian, A. F. Izmaylov, J. Bloino, G. Zheng, J. L. Sonnenberg, M. Hada, M. Ehara, K. Toyota, R. Fukuda, J. Hasegawa, M. Ishida, T. Nakajima, Y. Honda, O. Kitao, H. Nakai, T. Vreven, J. J. A. Montgomery, J. E. Peralta, F. Ogliaro, M. Bearpark, J. J. Heyd, E. Brothers, K. N. Kudin, V. N. Staroverov, R. Kobayashi, J. Normand, K. Raghavachari, A. Rendell, J. C. Burant, S. S. Iyengar, J. Tomasi, M. Cossi, N. Rega, J. M. Millam, M. Klene, J. E. Knox, J. B. Cross, V. Bakken, C. Adamo, J. Jaramillo, R. Gomperts, R. E. Stratmann, O. Yazyev, A. J. Austin, R. Cammi, C. Pomelli, J. W. Ochterski, R. L. Martin, K. Morokuma, V. G. Zakrzewski, G. A. Voth, P. Salvador, J. J. Dannenberg, S. Dapprich, A. D. Daniels, Ö. Farkas, J. B. Foresman, J. V. Ortiz, J. Cioslowski, D. J. Fox, *Gaussian 09*, Rev. A.02 ed., Gaussian, Inc., Wallingford CT, **2009**.

[22] R. D. Dennington II, T. A. Keith, J. M. Millam, *GaussView*, Ver. 5.08 ed., Semichem, Inc., Wallingford CT, **2009**.

[23] J. A. Montgomery, M. J. Frisch, J. W. Ochterski, G. A. Petersson, *J. Chem. Phys.* **2000**, *112*, 6532–6542.

[24] J. W. Ochterski, G. A. Petersson, J. A. Montgomery, *J. Chem. Phys.* **1996**, *104*, 2598–2619.

[25] E. F. C. Byrd, B. M. Rice, *J. Phys. Chem. B* **2005**, *110*, 1005–1013.

[26] M. Sućeska, *Propellants Explos. Pyrotech.* **1991**, *16*, 197–202.

[27] V. Liao, T. Liu, R. Codd, *Bioorg. Med. Chem. Lett.* **2012**, *22*, 6200–6204.

[28] D.-R. Hou, J. H. Reibenspies, K. Burgess, *J. Org. Chem.* **2001**, *66*, 206–215.

N-NITROSARCOSINE: AN ECONOMIC PRECURSOR FOR THE SYNTHESIS OF NEW ENERGETIC MATERIALS

Thomas M. Klapötke, Burkhard Krumm, and Regina Scharf

as published in

Chemistry – An Asian Journal **2016**, *11*, 3134–3144.

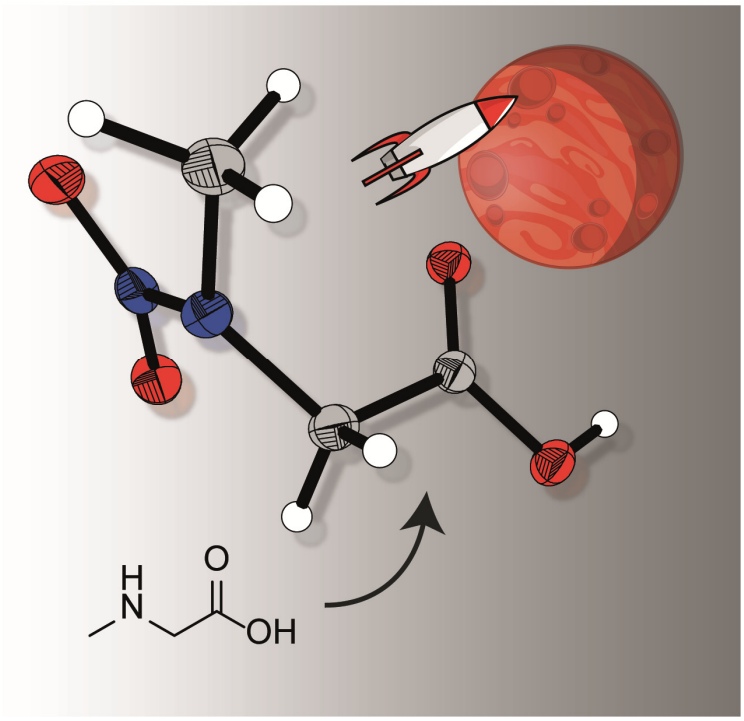

7.1 Abstract

New energetic compounds have been synthesized starting from the readily available *N*-(cyanomethyl)-*N*-methylamine. From this, *N*-nitrosarcosine was prepared in few steps, which serves as a starting material for the synthesis of oxygen-rich compounds. The compounds were thoroughly characterized including multinuclear NMR and vibrational spectroscopy and also molecular structures by single X-ray diffraction were obtained. Their energetic properties were determined including the sensitivities towards impact and friction, their heat of formations were calculated and the detonation and combustion parameters were predicted using EXPLO5 V6.02.

7.2 Introduction

2-(Methylamino)acetic acid, also known as sarcosine, is a naturally occurring non-proteinogenic amino acid derived from glycine. It is found in muscles and other body tissue and was first isolated by Justus von Liebig in 1847 from creatine.[1] The first synthesis of sarcosine was done by Jacob Volhard in 1862.[2] The applications of sarcosine are manifold. Although it is not used for biosynthesis of proteins, it is a building block in the synthesis of several antibiotics. Furthermore it is used as biomarker for prostate cancer screening,[3] for manufacturing biodegradable surfactants or toothpaste[4] and in synthesis of azo compounds for colorants[5].

Several energetic materials have been synthesized containing the similar building block, for example 2-nitro-2-azapropyl chloride (NAP-Cl).[6] However, to the best of our knowledge, no studies are reported employing the low priced and easy to synthesize starting material sarcosine or its nitrated form[7] in the formation of energetic materials. In the recent past our own studies have involved some amino acids such as glycine, alanine and aspartic acid as starting materials for potential energetic materials.[8]

Especially in the field of high-energy dense oxidizers (HEDOs) there is necessity for replacing the currently used oxidizer ammonium perchlorate (AP). Although AP has some advantages such as easy synthesis, high oxygen content, density and specific impulse, it has also been shown that AP has several drawbacks. During its combustion large amounts of hydrogen chloride fumes are formed causing environmentally problems like acid rain.[9] Moreover the exhausted toxic hydrogen chloride gases are easily visible in atmosphere revealing the launch position of the missile and leading to tactical disadvantages.[9a,10] There

are also health risks caused by the perchlorate anion leading to growth disturbances and thyroid diseases in vertebrates.[11] However, the main problem is the incompatibility of AP with the binder system in solid rocket compositions at temperatures sufficiently high to initiate the decomposition of AP. Slow cook-off tests show the formation of acidic side-products which are leading to cracks and cavities in the composite and which in turn negatively affect the performance of rocket propellants.[9a]

For a potential replacement of AP, several requirements have to be fulfilled. The most important criteria are as easy as possible synthesis, high density and a specific impulse comparable to ammonium perchlorate.[12] The compounds currently investigated as halogen-free alternatives for AP are ammonium nitrate (AN) and ammonium dinitramide (ADN). However, neither one reaches the properties of AP; the application of AN is limited due to its hygroscopicity, its numerous phase transitions, and its low burning rate, whereas ADN is also hygroscopic, starts to decompose at 92 °C, and shows incompatibility reactions with the isocyanated-based curing agents in HTPB binder systems.[13]

In this contribution *N*-(cyanomethyl)-*N*-methylnitramine is employed as the starting material for the synthesis of new halogen-free HEDOs. *N*-(Cyanomethyl)-*N*-methylnitramine is readily available starting from sodium cyanide, formaldehyde and methylamine hydrochloride.[14] In order to achieve a high oxygen content, this moiety was linked to trinitroethanol (TNE) by various ways, which itself has an oxygen balance of +30.9% (Ω_{CO}).

7.3 Results and Discussion

7.3.1 Synthesis

The starting material *N*-(cyanomethyl)-*N*-methylamine[14] was first nitrated using a mixture of acetic anhydride and nitric acid to obtain *N*-(cyanomethyl)-*N*-methylnitramine (**1**), which was either reacted with hydrogen chloride gas and methanol to obtain *N*-methyl-*N*-nitroglycine methyl ester (**2**) as colorless liquid, or was converted with concentrated hydrochloric acid to yield *N*-methyl-*N*-nitroglycine (*N*-nitrosarcosine, **3**) as a colorless solid

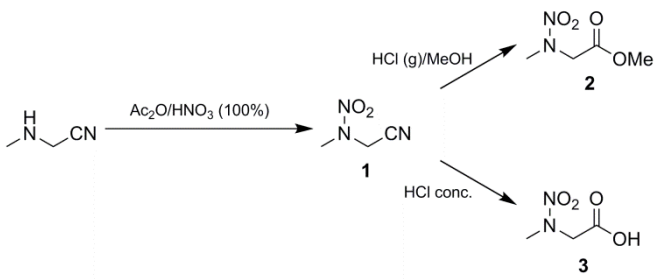

Scheme 7.1 Synthesis of *N*-nitrosarcosine derivatives **1**–**3**.

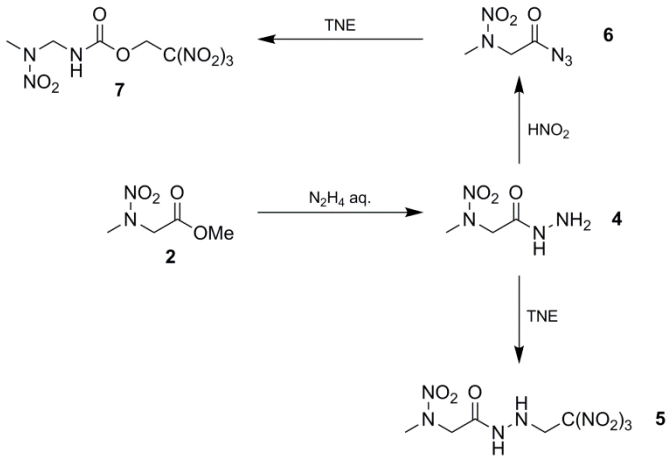

Scheme 7.2 *N*-Nitrosarcosine based energetic materials **4**–**7**.

(Scheme 7.1).[7] Compound **3** was also prepared by nitrosation of sarcosine and further oxidation of the nitroso derivative with trifluoroperoxoacetic acid.[15] However, in the above mentioned synthesis route **3** is obtained in a fast and convenient manner in high quantity.

The reaction of the ester **2** with an aqueous solution of hydrazine afforded *N*-methyl-*N*-nitroglycinoyl hydrazide (**4**),[7] which can be converted with TNE into *N*-methyl-*N*-(2-oxo-2-(2,2,2-trinitroethyl)hydrazinyl)ethyl)nitramine (**5**) by a simple Mannich reaction. The very sensitive *N*-methyl-*N*-nitroglycinoyl azide (**6**) was obtained by reacting **4** with in situ generated nitrous acid (Scheme 7.2). The carbonyl azide **6** can be reacted with TNE to give 2,2,2-trinitroethyl ((methylnitramino)methyl)carbamate (**7**). This carbamate **7** has previously been synthesized by reacting 2-nitro-2-azapropyl chloride (NAP-Cl) and silver cyanate.[6c] However, here a quite simple and convenient alternative route is given by generating the corresponding isocyanate from **6**, and subsequent reaction with TNE to result in 81% yield of **7**.

Chlorination of *N*-nitrosarcosine (**3**) with oxalyl chloride gave the corresponding reactive acyl chloride *N*-methyl-*N*-nitroglycinoyl chloride (**8**), with DMF added as catalyst. The reaction of **8** with hydrazine in chloroform resulted in the formation of the symmetrical bis(*N*-methyl-*N*-nitroglycinoyl) hydrazide (**9**). With TNE the acyl chloride **8** was converted into the 2,2,2-trinitroethyl *N*-methyl-*N*-nitroglycinate (**10**), whereas addition of aqueous ammonia furnished 2-(methylnitramino)acetamide (**11**). The amide **11** was either reacted with oxalyl chloride and TNE to obtain 2,2,2-trinitroethyl (*N*-methyl-*N*-nitroglycyl)carbamate (**12**) or with the mild nitration agent nitronium tetrafluoroborate to yield 2-(methylnitramino)-*N*-nitroacetamide (**13**) (Scheme 7.3).

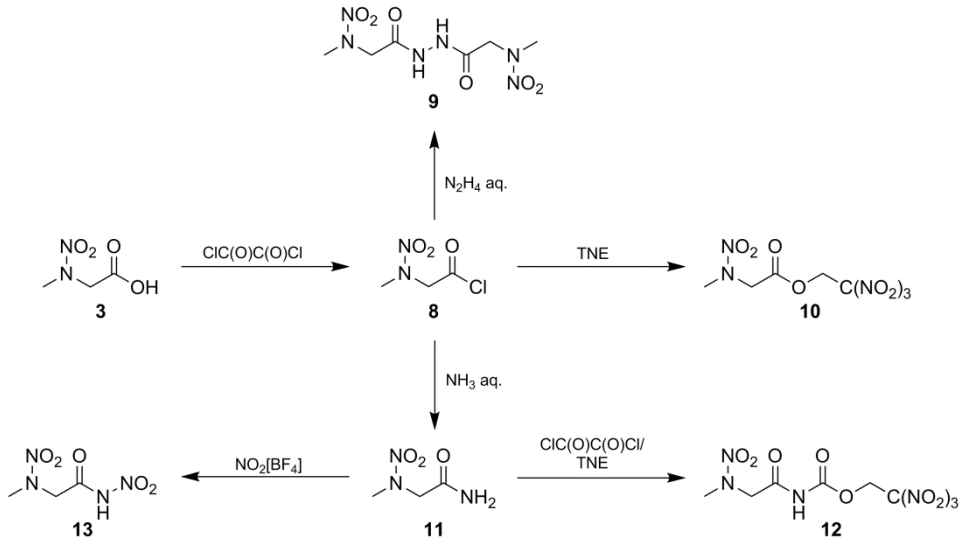

Scheme 7.3 *N*-Nitrosarcosine based energetic materials **8**–**13**.

7.3.2 NMR Spectroscopy

All compounds were thoroughly examined by multinuclear NMR spectroscopy. The spectra were recorded in $CDCl_3$ (**1**, **2**, **6**, and **8**), [D_6]acetone (**3**, **7**, **10**, **11**, **12**, and **13**), [D_4]methanol (**4**), [D_3]acetonitrile (**5**), or [D_6]DMSO (**9**). The resonances of the methyl groups in the ^{1}H NMR spectra are found at approximately δ = 3.45 ppm, those of the methylene groups downfield at to δ = 5.17–4.33 ppm. The methylene moieties are generally observed as singlets, except for **7** which is split into a doublet with a coupling constant of 6.4 Hz due to the neighboring carbamate hydrogen. For compounds **7**, **10**, and **12** singlets are observed for the protons of the trinitroethyl units in the small range δ = 5.96–5.82 ppm. The resonance of the trinitroethyl moiety of compound **5** is split into a doublet due to the hydrazine hydrogen with 6.0 Hz and is slightly shifted upfield to δ = 4.55 ppm.

In the ^{13}C NMR spectra the resonances of the carbon atoms of the carbonyl groups are observed in the typical range δ = 173.8–150.7 ppm. The resonances of the methyl groups are detected at approximately δ = 40 ppm, while those of the methylene groups next to the nitramine are observed between δ = 61.6–40.9 ppm. Owing to the electron withdrawing effect of the oxygen next to the methylene carbon atoms of the trinitroethyl units the resonances are shifted downfield to δ = 62 ppm. The carbon atoms of the trinitromethyl moieties are detected as usually as broadened signals at δ = 125 ppm.

The nitro groups are generally observed in the ^{14}N NMR spectra as relatively sharp signals at δ = −27−−33 ppm. Only the nitro group of the nitramine moiety of compound **13** is located at −45 ppm. The resonance of the nitrile nitrogen atom of compound **1** is found at −126 ppm. The resonances of the azide group of compound **6** are observed at δ = −136 (N_γ) and −147 ppm (N_β), while that of N_α is too broad to be observed.

7.3.3 Vibrational Spectroscopy

Furthermore all compounds were characterized by IR and Raman spectroscopy. For compounds **4**, **5**, **7**, **9**, **11**, **12**, and **13** weak to medium peaks assigned to the NH/NH_2 stretching vibrations are observed in the range of 3387–3195 cm^{-1}. The asymmetric stretching vibration of the azide moiety of compound **6** is detected in the characteristic region at 2146 cm^{-1}. The carbonyl stretching vibration is found at 1799–1605 cm^{-1} in the IR and 1803–1603 cm^{-1} in the Raman spectra. The asymmetric NO_2 stretching vibrations of the nitramine moieties are found as medium to strong signals in the range of 1522–1497 cm^{-1} in the IR spectra. Additional strong signals are observed for the nitro groups of the trinitromethyl moiety of compounds **5**, **7**, **10**, and **11**, which are shifted to higher frequencies (1601–1588 cm^{-1} in the IR).[16] However only weak signals are found in this region in the Raman spectra. The symmetric NO_2 stretching vibrations appear as strong signals in the range of 1308–1260 cm^{-1} in the IR and Raman spectra.[16] In the Raman spectra for all discussed nitro compounds a very strong peak is observed in the region of 890–840 cm^{-1}. However, an unambiguous assignment is not possible, although differing opinions exist in literature.[16b,17]

7.3.4 Single Crystal X-ray Diffraction

Crystals suitable for X-ray measurements were obtained for compounds **1**, **3**, **4**, **6**, **8**, **9**, and **11**–**13** by recrystallization from methanol (**1**), concentrated hydrochloric acid (**3**), ethanol (**4**), chloroform (**6** and **8**), water (**9**), ethyl acetate (**11**), 1,2-dichloroethane (**12**), and dichloromethane (**13**). For all compounds structural data as well as refinement parameters of the measurements are compiled in Table 7.1.

Compounds **1** and **3** crystallize in the monoclinic space group $P2_1/c$ each with four molecules in the unit cell and one molecule as asymmetric unit. As depicted in Figure 7.1 the nitrile group of compound **1** has a linear geometry with an angle of 178.51°. The atom distance between C1 and N1 is with 1.139 Å in the range of an ordinary C–N triple bond. The moieties surrounding the tertiary amine N2 are arranged in a trigonal planar geometry with angles of 118.10° (C2–N2–N3), 118.03° (C3–N2–N3), and 123.66° (C2–N2–C3). The trigonal planar arrangement is achieved through the delocalization of the electron lone pair on the nitrogen N2 by the electron withdrawing nitro group. This effect influences also the atom distance of N2 and N3 which is with 1.343 Å between a N–N single and double bond. With torsion angles of 0.58° (C2–N2–N3–O1) and 6.12° (C3–N2–N3–O2) the nitro group is nearly perfectly oriented in the trigonal planar plane.

Table 7.1 Crystallographic data and structure refinements of **1**, **3**, **4**, **6**, **8**, **9**, **11**, **12**, and **13**.

	1	**3**	**4**	**6**	**8**
formula	$C_3H_5N_3O_2$	$C_3H_6N_2O_4$	$C_3H_8N_4O_3$	$C_3H_5N_5O_3$	$C_3H_5N_2O_3Cl$
formula weight [g mol^{-1}]	115.09	134.10	148.12	159.11	153.54
temperature [K]	123	123	173	173	123
crystal system	monoclinic	monoclinic	monoclinic	monoclinic	monoclinic
space group (No.)	$P2_1/c$ (14)	$P2_1/c$ (14)	$P2_1/c$ (14)	$P2_1/c$ (14)	$P2_1/n$ (14)
a [Å]	6.0991(7)	5.8782(3)	10.8689(12)	11.4947(8)	9.3803(6)
b [Å]	16.8867(14)	9.1488(5)	6.0536(5)	5.5082(3)	5.0836(3)
c [Å]	5.5884(7)	10.2741(5)	9.7660(8)	10.8210(7)	13.0278(7)
α [°]	90	90	90	90	90
β [°]	117.146(15)	93.968(4)	100.440(9)	105.170(7)	97.423(6)
γ [°]	90	90	90	90	90
V [Å^3]	512.17(11)	551.20(5)	631.93(10)	661.26(8)	616.03(6)
Z	4	4	4	4	4
$\rho_{calc.}$ [g cm^{-3}]	1.493	1.616	1.557	1.598	1.645
μ [mm^{-1}]	0.126	0.151	0.136	0.141	0.553
F(000)	240	280	312	328	312
crystal habit	colorless needle	colorless plate	colorless block	colorless plate	colorless block
crystal size [mm]	0.38x0.05x0.05	0.28x0.23x0.05	0.15x0.14x0.10	0.19x0.12x0.14	0.40x0.40x0.40
θ range [°]	4.71–31.49	4.55–32.14	4.59–27.59	4.72–27.98	4.72–31.88
index ranges	$-7 \le h \le 6$	$-7 \le h \le 6$	$-13 \le h \le 13$	$-14 \le h \le 14$	$-11 \le h \le 11$
	$-20 \le k \le 21$	$-11 \le k \le 11$	$-7 \le k \le 6$	$-6 \le k \le 6$	$-6 \le k \le 5$
	$-6 \le l \le 6$	$-12 \le l \le 12$	$-12 \le l \le 12$	$-7 \le l \le 13$	$-16 \le l \le 16$
reflections measured	3726	4028	3982	4040	4529
reflections independent	1039	1129	1297	1287	1262
reflections unique	905	997	967	1028	1123
R_{int}	0.0239	0.0208	0.0337	0.0311	0.0203
R_1, wR_2 (2σ data)	0.0306, 0.0356	0.0284, 0.0334	0.0385, 0.0585	0.0392, 0.0521	0.0246, 0.0285
R_1, wR_2 (all data)	0.0767, 0.0799	0.0726, 0.0758	0.0909, 0.1044	0.0911, 0.1005	0.0621, 0.0637
data/restraints/parameters	1039/0/93	1129/0/106	1297/0/123	1287/0/103	1262/0/102
GOOF on F^2	1.056	1.067	1.072	1.052	1.082
residual el. density [e Å^{-3}]	–0.247/0.138	–0.184/0.249	–0.230/0.221	–0.280/0.216	–0.229/0.269
CCDC	1490177	1490184	1490178	1490179	1490183

	9	**11**	**12**	**13**
formula	$C_6H_{12}N_6O_6$	$C_3H_7N_3O_3$	$C_6H_8N_6O_{11}$	$C_3H_6N_4O_5$
formula weight [g mol−1]	264.20	133.12	340.16	178.10
temperature [K]	123	123	123	100
crystal system	triclinic	monoclinic	monoclinic	orthorhombic
space group (No.)	*P*−1 (2)	*P*21/*n* (14)	*P*21/*c* (14)	*Fdd*2 (43)
a [Å]	6.3435(4)	4.8748(5)	12.6522(12)	18.0701
b [Å]	8.6488(8)	11.0812(11)	9.2288(5)	31.2233(17)
c [Å]	10.5766(9)	11.1178(12)	11.6546(8)	4.8664(3)
α [°]	99.172(7)	90	90	90
β [°]	91.181(6)	96.203(9)	108.379(9)	90
γ [°]	105.107(7)	90	90	90
V [Å3]	551.88(8)	597.05(11)	1291.43(18)	2745.7(3)
Z	2	4	4	16
ρcalc. [g cm^{-3}]	1.590	1.481	1.750	1.724
μ [mm^{-1}]	0.141	0.131	0.170	0.163
F(000)	276	280	696	1472
crystal habit	colorless plate	colorless needle	colorless block	colorless rod
crystal size [mm]	0.25x0.10x0.02	0.40x0.18x0.18	0.35x0.30x0.10	0.25x0.20x0.15
θ range [°]	4.96–31.08	4.77–31.01	4.51–27.76	3.45–26.33
index ranges	−7 ≤ h ≤ 7	−5 ≤ h ≤ 6	−15 ≤ h ≤ 14	−22 ≤ h ≤ 22
	−10 ≤ k ≤ 10	−11 ≤ k ≤ 13	−10 ≤ k ≤ 11	−38 ≤ k ≤ 35
	−13 ≤ l ≤ 12	−13 ≤ l ≤ 13	−14 ≤ l ≤ 13	−5 ≤ l ≤ 6
reflections measured	4196	4373	8926	7830
reflections independent	2233	1201	2642	1367
reflections unique	1725	987	1964	1317
Rint	0.0286	0.0288	0.0421	0.0415
R1, wR2 (2σ data)	0.0385, 0.0562	0.0347, 0.0452	0.0403, 0.0623	0.0569, 0.0598
R1, wR2 (all data)	0.0894, 0.0996	0.0860, 0.0939	0.0890, 0.1021	0.1137, 0.1160
data/restraints/parameters	2233/0/211	1201/0/110	2642/0/240	1367/1/123
GOOF on F2	1.020	1.075	1.048	1.105
residual el. density [e Å^{-3}]	−0.222/0.258	−0.254/0.163	−0.253/0.261	−0.567/0.627
CCDC	1490180	1490181	1490182	1490185

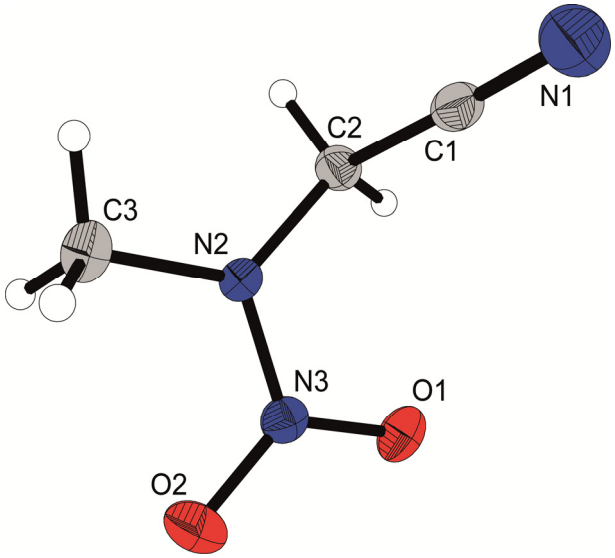

Figure 7.1 Molecular structure of **1**. Selected bond lengths [Å] and angles [°]: C1–C2 1.478(2), C1–N1 1.139(2), C2–N2 1.448(1), C3–N2 1.446(2), N2–N3 1.343(2), N3–O1 1.236(2), N3–O2 1.229(1), C2–C1–N1 178.5(1), C2–N2–C3 123.7(1), C2–N2–N3 118.1(1), C3–N2–N3 118.0(1), C2–N2–N3–O2 –178.9(1).

Figure 7.2 shows two molecules of the carboxylic acid **3**. The dimeric structure is stabilized by hydrogen bonds between the carboxylic moieties which form an almost planar eight-membered ring with a donor acceptor angle of 175.94° (O1–H1···O2) and a donor acceptor distance of 2.659 Å (O1–H1···O2).[18]

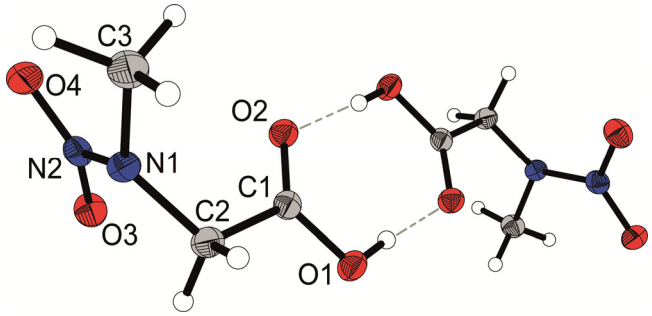

Figure 7.2 Molecular structure of **3**. Selected bond lengths [Å] and angles [°]:C1–C2 1.513(2), C1–O1 1.314(2), C1–O2 1.217(1), C2–N1 1.447(2), C3–N1 1.462(2), N1–N2 1.359(1), N2–O3 1.239(1), N2–O4 1.227(1), O1–H1 0.89(2), O1–C1–O2 125.4(1), C1–O1–H21 107(1), C3–N1–N2 116.19(9), O1–C1–C2–N1 –178.7(1).

Compounds **4**, **6**, and **8**, pictured in Figure 7.3, also crystallize in the monoclinic space groups $P2_1/c$ (**4** and **6**) or $P2_1/n$ (**8**) with four molecules in the unit cell and one molecule as asymmetric unit. Their calculated densities are with values of 1.557 g cm^{-3} (**4**) and 1.598 g cm^{-3} (**6**) rather low. Only for the carbonyl chloride **8** the density increases slightly to 1.645 g cm^{-3}. The structures are quite similar to the nitrile **1** with a trigonal planar arrangement around the tertiary nitrogen and the nitro group oriented in the plane. The

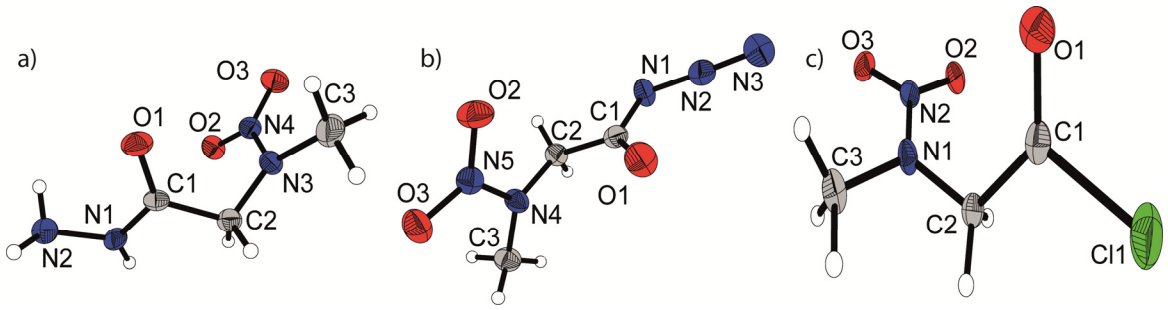

Figure 7.3 Molecular structure of **4** (a), **6** (b), and **8** (c). Selected bond lengths [Å] and angles [°] of a: C1–C2 1.518(3), C1–N1 1.319(2), C1–O1 1.233(2), C2–N3 1.445(2), C3–N3 1.457(2), N1–N2 1.409(2), N3–N4 1.343(2), N4–O2 1.236(2), N4–O3 1.232(2), C1–N1–N2 123.5(1), C2–C1–N1–N2 178.2(2). Selected bond lengths [Å] and angles [°] of b: O1–C1 1.195(2), O2–N5 1.240(2), O3–N5 1.229(2), N1–N2 1.262(2), N1–C1 1.416(3), N2–N3 1.110(3), N4–N5 1.341(2), N4–C2 1.443(3), N4–C3 1.450(2), C1–C2 1.507(3), N1–N2–N3 175.4(2), O1–C1–N1 124.6(2), O1–C1–C2 126.0(2), N1–C1–C2 109.4(1), N1–C1–C2–N4 –176.8(1). Selected bond lengths [Å] and angles [°] of c: Cl1–C1 1.779(1), O3–N2 1.233(1), O1–C1 1.178(1), O2–N2 1.236(1), N1–N2 1.341(1), N1–C3 1.454(2), N1–C2 1.437(2), C2–C1 1.508(2), Cl1–C1–O1 121.37(9), N1–C2–C1–Cl1 174.81(9).

azide group of the carbonyl azide **6** shows an angle of 175.42° (N1–N2–N3) which is common for covalent azides.[8a,19] The distances between the nitrogen atoms are 1.262 Å (N1–N2) and 1.110 Å (N2–N3) and therefore are in the range of typical N–N double and triple bonds, respectively.

The molecular structure of the hydrazide **9**, which crystallizes in the triclinic space group *P*–1 with two molecules in the unit cell and two half molecules in the asymmetric unit, is shown in Figure 7.4. The molecule is completed by an inversion center in the center of the N1–N1' bond. The hydrazine unit as well as C1, C2 and N2 are arranged nearly planar with a staggered conformation. Only the nitramine and methyl moieties are twisted out of plane. The two molecules within the unit cell are twisted to each other with an angle of approximately 30° and form strong intermolecular hydrogen bonds between the hydrazine

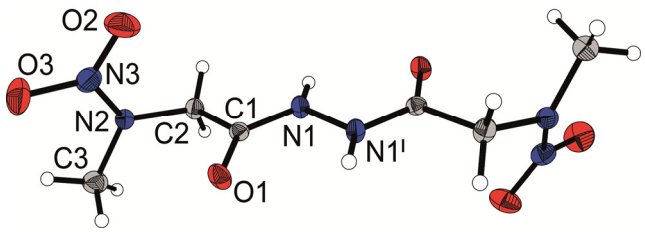

Figure 7.4 Molecular structure of **9**. Selected bond lengths [Å] and angles [°]: C1–C2 1.524(3), C1–N1 1.325(2), C1–O1 1.232(2), C2–N2 1.444(2), C3–N2 1.459(2), N1–N1 1.392(2), N2–N3 1.358(2), N3–O2 1.236(2), N3–O3 1.232(2), C1–C2 1.524(3), C1–N1 1.325(2), C1–O1 1.232(2), C2–N2 1.444(2), C3–N2 1.459(2), N2–N3 1.358(2), N3–O2 1.236(2), N3–O3 1.232(2), N1–C1–C2–N2 –162.6(1), C2–C1–N1–N1 –173.2(1), C1–N1–N1–C1 180.0(1).

and carboxyl units with donor acceptor distances of 2.777 Å (N1–H1···O4) and 2.838 Å (N4–H7···O1).[18]

The amide **11** and carbamate **12** crystallize in the monoclinic space groups $P2_1/n$ (**11**) and $P2_1/c$ (**12**) with four molecules in the unit cell and one molecule as asymmetric unit. The molecular structure of **11** is shown in Figure 7.5. Although intermolecular hydrogen bonds are observed for this structure between the hydrogens of the amine and the oxygens of the carbonyl and nitro moieties, respectively, (N1–H1···O1 2.898 Å, N1–H2···O2 3.067 Å, N1–H2···O3 3.382 Å) the calculated density is with 1.481 g cm^{-3} the lowest density found for any compound discussed herein.

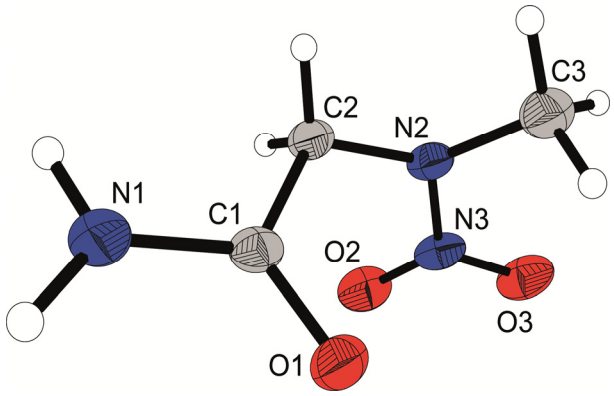

Figure 7.5 Molecular structure of **11**. Selected bond lengths [Å] and angles [°]: C1–C2 1.526(2), C1–N1 1.323(2), C1–O1 1.234(2), C2–N2 1.449(2), C2–H3 0.95(2), C3–N2 1.457(2), C3–H5 0.97(2), N2–N3 1.351(2), N3–O2 1.236(2), N3–O3 1.235(2), N1–C1–C2–N2 176.2(1), C2–N2–N3–O2 16.2(2).

Figure 7.6 depicts the molecular structure of the carbamate **12**. Next to the planar arrangement around the tertiary amine N1, which is discussed earlier in this text, the carbonyl moieties surrounding the secondary amine N3 are also arranged perfectly planar. The geometry is confirmed by shortened C–N bonds with distances of 1.369 Å (N3–C3) and 1.372 Å (N3–C4), respectively, due to the electron withdrawing carbonyl moieties. For the hydrogen atom of the amine unit at N3 a hydrogen bridge to the carbonyl oxygen O3 of a second molecule is found with a donor acceptor distance of 2.886 Å and an angle of 160.85°.[18] The second molecule is rotated by 180° in such manner that an eight-membered ring is formed between the amine N3–H6 and the carbonyl C3–O3 units. The typical propeller-like geometry of the three nitro groups surrounding the carbon C6 is found for the trinitromethyl moiety. The structure is stabilized by non-bonding intramolecular attractions shorter than the sum of the van der Waals radii between the partially positively charged nitrogen atoms and partially negatively charged oxygen atoms (N4···O10 2.545 Å, N5···O7 2.572 Å, and N6···O9 2.597 Å).

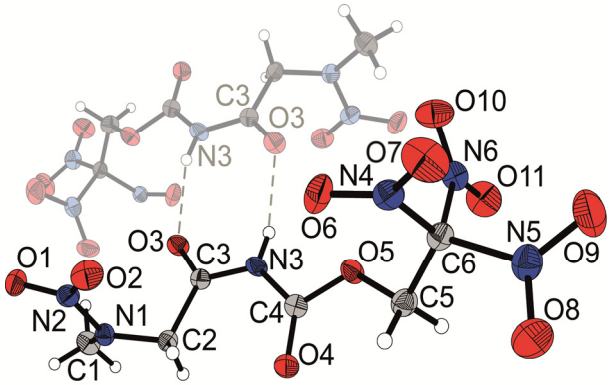

Figure 7.6 Molecular structure of **12**. Selected bond lengths [Å] and angles [°]: C1–N1 1.453(3), C2–C3 1.519(3), C2–N1 1.447(2), C3–N3 1.369(2), C3–O3 1.219(2), C4–N3 1.372(2), C4–O4 1.197(2), C4–O5 1.365(2), C5–C6 1.515(3), C5–O5 1.424(2), C6–N4 1.515(3), C6–N5 1.514(2), C6–N6 1.526(2), N1–N2 1.343(3), N2–O1 1.244(2), N2–O2 1.228(2), N4–O6 1.219(2), N4–O7 1.209(2), N5–O8 1.215(3), N5–O9 1.215(2), N6–O10 1.211(3), N6–O11 1.211(3), N3–H3 0.84(3), N1–C2–C3–N3 162.3(2), C2–C3–N3–C4 3.1(3), N3–C4–O5–C5 166.0(2).

The nitroacetamide **13** crystallizes in the orthorhombic space group *Fdd*2 with 16 molecules in the unit cell and a calculated density of 1.724 g cm^{-3} at −173 °C. The asymmetric unit of **13** is depicted in Figure 7.7. The crystal structure was refined as a 2-component inversion twin having an increased undissolved electron density around the nitramine moiety. This resulted in flattening of the N4 nitro group ellipsoids. Similar to the hydrazide **9**, the molecule adopts a planar staggered conformation including the nitro group of the nitramine moiety. Only the methyl and nitro groups connected to the amine are twisted out of plane.

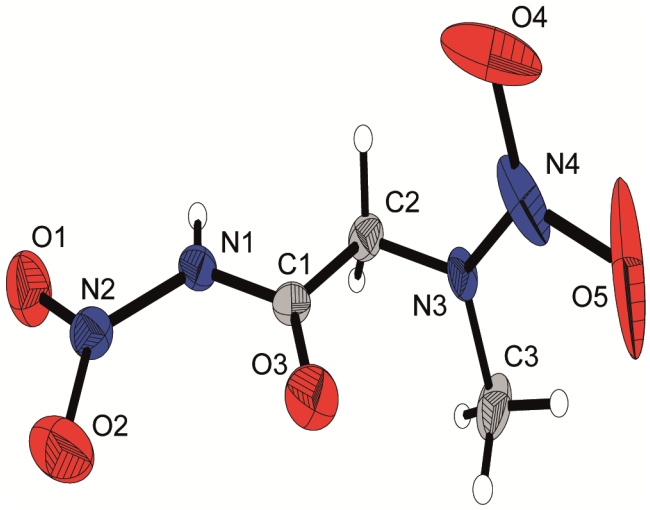

Figure 7.7 Molecular structure of **13**. Selected bond lengths [Å] and angles [°]: O1–N2 1.215(5), O2–N2 1.213(5), O3–C1 1.197(5), O4–N4 1.218(7), O5–N4 1.239(7), N1–N2 1.394(5), N1–C1 1.381(5), N3–N4 1.343(6), N3–C2 1.452(6), N3–C3 1.451(7), C1–C2 1.520(7), N2–N1–C1 125.2(4), N1–C1–C2 111.8(4), N2–N1–C1–C2 172.3(4), N1–C1–C2–N3 −179.3(4).

7.3.5 Thermal and Energetic Properties

For the compounds with energetic potential, physical and energetic properties were determined and the data are summarized in Table 7.2. Thermal stabilities were tested by differential scanning calorimetry (DSC) with a heating rate of 5 °C min^{-1}. The lowest decomposition temperature with a value of 56 °C was found for the carbonyl azide **6**, which is common for this class of compounds due to a Curtius rearrangement of the carbonyl azide to the corresponding isocyanate. The hydrazide compounds **4** and **5** also showed low decomposition temperatures of 116 (**4**) and 108 °C (**5**). However, the hydrazide **9** has the highest decomposition temperature of all herein discussed compounds. For all other compounds, except the nitroacetamide **13** (T_{dec} = 113 °C), satisfying decomposition temperatures between 150–190 °C were determined.

Impact (IS) and friction (FS) sensitivities were determined using a BAM fall hammer and BAM friction tester according to STANAG4489[20] and STANAG 4487.[21, 22] As expected, the most sensitive material is the carbonyl azide **6** with an IS of 4 J and FS of 54 N. Therefore, this compound should only be handled with care. Those compounds containing the trinitroethyl group (**5**, **10**, and **12**) as well as the hydrazide **9** show impact sensitivities of 9–25 J and also have to be classified as sensitive materials. However, the FS decrease for most compounds and only the hydrazines **4**, **5**, and **9** show, with values of 288 (4) and 240 N (**5** and **9**), low sensitivities against friction.

For the use as energetic materials, the nitrogen and oxygen contents are important parameters. Most compounds exceed a nitrogen and oxygen content of 65%. Especially the compounds containing a trinitroethyl moiety (**5**, **10**, and **12**) as well as the nitramine **13** show values in the range of 76.4–78.2%. However, when calculating the oxygen balance assuming the formation of CO and CO_2, a lack of oxygen is found. Only for the ester **10** and the carbamate **12**, a positive oxygen balance for the formation of CO is achieved.

Detonation and combustion parameters were predicted using the EXPLO5 V6.02 code for compounds **1**, **3**–**6**, and **9**–**13**.[23] For calculations, heat of formations previously determined by CBS-4M ab initio calculations were used, and the data are compiled in Table 7.3. High heats of formation as well as high room temperature densities are crucial parameters to achieve satisfying detonation velocities and pressures. Best results were obtained for hydrazide **5** with a detonation velocity of 8304 ms^{-1} which is in the range of PETN.[24] However, both detonation pressure and thermal stability are below the requirements for secondary explosives.

Table 7.2 Physical and chemical properties of **1**, **3**–**6**, and **9**–**13**.

	1	**3**	**4**	**5**	**6**
formula	$C_3H_5N_3O_2$	$C_3H_6N_2O_4$	$C_3H_8N_4O_3$	$C_5H_9N_7O_9$	$C_3H_5N_5O_3$
MW [g mol^{-1}]	115.09	134.09	148.12	311.17	159.11
T_m [°C] (onset)[a]	-	92	-	-	-
T_{dec} [°C] (onset)[b]	193	153	116	108	56
IS [J][c]	> 40	> 40	> 40	9	4
FS [N][d]	> 360	> 360	288	240	54
ESD [J][e]	1.50	1.50	1.50	0.30	0.15
N [%][f]	36.5	20.9	37.8	31.5	44.0
O [%][g]	27.8	47.7	32.4	46.3	30.2
N + *O* [%][h]	64.3	48.6	70.2	77.8	74.2
Ω_{CO} [%][i]	−48.7	−23.9	−43.2	−2.6	−25.1
Ω_{CO2} [%][j]	−90.4	−59.7	−75.6	−28.3	−55.3

	9	**10**	**11**	**12**	**13**
formula	$C_6H_{12}N_6O_6$	$C_5H_7N_5O_{10}$	$C_3H_7N_3O_3$	$C_6H_8N_6O_{11}$	$C_3H_6N_4O_5$
MW [g mol^{-1}]	264.20	297.14	133.11	340.16	178.10
T_m [°C] (onset)[a]	-	108	116	-	-
T_{dec} [°C] (onset)[b]	201	178	186	150	113
IS [J][c]	25	20	> 40	10	> 40
FS [N][d]	240	> 360	> 360	> 360	> 360
ESD [J][e]	0.35	0.30	0.70	0.60	0.60
N [%][f]	31.8	23.6	31.6	24.7	31.5
O [%][g]	36.3	53.8	36.1	51.7	44.9
N + *O* [%][h]	68.1	77.4	67.7	76.4	76.4
Ω_{CO} [%][i]	−36.3	8.1	−42.1	4.7	−9.0
Ω_{CO2} [%][j]	−72.7	−18.8	−78.1	−23.5	−35.9

[a] Melting and [b] decomposition temperature determined by DSC measurement carried out at a heating rate of 5 °C min^{-1}. [c] Impact sensitivity and [d] friction sensitivity. [e] Sensitivity towards electrostatic discharge. [f] Nitrogen content. [g] Oxygen content. [h] Sum of nitrogen and oxygen content. [i] Oxygen balance assuming the formation of CO and the formation of [j] CO_2 at the combustion.

Table 7.3 Calculated heat of formation and predicted detonation and combustion parameters using the EXPLO5 V6.02 code[16] of **1**, **3–6**, and **9–13**.

	1	**3**	**4**	**5**	**6**
formula	$C_3H_5N_3O_2$	$C_3H_6N_2O_4$	$C_3H_8N_4O_3$	$C_5H_9N_7O_9$	$C_3H_5N_5O_3$
density RT [a]	1.46	1.58	1.53	1.72	1.57
$\Delta_f H_m°$ /kJ mol^{-1} [b]	73.6	−449.3	−151.8	−137.6	109.4
$\Delta_f U°$ /kJ kg^{-1} [c]	747.4	−3240.1	−899.3	−342.6	788.9
Q_v /kJ kg^{-1} [d]	−4911	−3461	−4111	−5494	−4952
T_{ex} /K [e]	3092	2455	2604	3660	3366
V_0 /L kg^{-1} [f]	846	824	912	780	817
P_{CJ} /kbar [g]	171	168	194	293	213
V_{det} /m s^{-1} [h]	7151	6961	7669	8304	7670
I_s /s [i]	215	185	202	254	221
I_s /s (15% Al) [j]	245	225	245	272	248
I_s /s (15% Al, 14% binder)[k]	237	216	234	252	239

	9	**10**	**11**	**12**	**13**
formula	$C_6H_{12}N_6O_6$	$C_5H_7N_5O_{10}$	$C_3H_7N_3O_3$	$C_6H_8N_6O_{11}$	$C_3H_6N_4O_5$
density RT [a]	1.55	1.48	1.44	1.71	1.67
$\Delta_f H_m°$ /kJ mol^{-1} [b]	−317.0	−401.4	−267.8	−590.0	−168.7
$\Delta_f U°$ /kJ kg^{-1} [c]	−1087.3	−1259.0	−1890.7	−1643.5	−842.6
Q_v /kJ kg^{-1} [d]	−4257	−5075	−3569	−4744	−5040
T_{ex} /K [e]	2794	3810	2422	3408	3358
V_0 /L kg^{-1} [f]	841	808	884	738	815
P_{CJ} /kbar [g]	181	205	142	258	256
V_{det} /m s^{-1} [h]	7276	7286	6729	7835	8033
I_s /s [i]	200	253	190	237	237
I_s /s (15% Al) [j]	243	271	233	257	265
I_s /s (15% Al, 14% binder)[k]	232	249	222	242	247

[a] RT densities are recalculated from X-ray densities or experimentally determined by pycnometer measurements. [b] Enthalpy and [c] energy of formation calculated by the CBS-4M method using Gaussian 09. [d] Heat of explosion, [e] explosion temperature, [f] volume of gaseous products, [g] detonation pressure and [h] detonation velocity calculated by using the EXPLO5 V6.02 code.[21] [i] Specific impulse for the neat compound using the EXPLO5 V6.02 code (70.0 bar chamber pressure, isobaric combustion conditions (1 bar), equilibrium expansion).[21] [j] Specific impulse for compositions with 85% oxidizer/compound and 15% aluminum (70.0 bar chamber pressure, isobaric combustion conditions (1 bar), equilibrium expansion). [k] Specific impulse for compositions with 71% oxidizer/compound, 15% aluminum and 14% binder (6% polybutadiene acrylic acid, 6% polybutadiene acrylonitrile and 2% bisphenol A ether) (70.0 bar chamber pressure, isobaric combustion conditions (1 bar), equilibrium expansion).

For application as oxidizer in solid rocket composites, a positive oxygen balance is required. However, when calculating the specific impulses (I_s) for the neat compounds, values of 254 s and 253 s were achieved for hydrazide **5** and the ester **10**, although the oxygen balances are only slightly positive or even negative. Since the specific impulse is proportional to the square root of the ratio of the combustion temperature T_c and the average molecular mass of the gaseous combustion products, it is increased when adding aluminum as high-performing fuel.[9a] High specific impulses were obtained in mixtures containing 15% aluminum for compounds **5** (272 s) and **10** (271 s). However, when calculating as composite propellant in a mixture with 71% oxidizer, 15% aluminum and 14% binder (6% polybutadiene acrylic acid, 6% polybutadiene acrylonitrile and 2% bisphenol A ether), the specific impulses decrease. Only the hydrazide **5** achieves a satisfying specific impulse of 252 s (AP 261 s).

7.4 Conclusion

Several nitro-containing materials were synthesized starting from the readily available *N*-(cyanomethyl)-*N*-methylnitramine **1**. All compounds were thoroughly characterized including by NMR and vibrational spectroscopy, some with crystal structures, and their energetic and physical properties were determined. DSC measurements showed quite low decomposition temperatures for the hydrazide compounds *N*-methyl-*N*-nitroglycinoyl hydrazide **4** and *N*-methyl-*N*-(2-oxo-2-(2,2,2-trinitroethyl)hydrazinyl)ethyl)nitramine **5**, as well as for *N*-methyl-*N*-nitroglycinoyl azide **6**, and 2-(methylnitramino)-*N*-nitroacetamide **13**, whereas the highest decomposition temperature of all herein measured compounds is found for the bis(*N*-methyl-*N*-nitroglycinoyl)hydrazide **9** (T_{dec} = 201 °C). Special care should be taken when working with the azide **6**, since both impact and friction show high sensitivities.

For the use as energetic materials, detonation and combustion parameters were predicted. Best detonation velocity was achieved for hydrazide **5** with a value of 8304 m s^{-1}, which is in the range of PETN.[24] However, the detonation pressure and decomposition temperature are too low for the use as secondary explosive. The trinitroethyl-containing compounds **5** as well as **10** show high specific impulses for the neat compounds which increases when aluminum is added as fuel although the oxygen balance assuming the formation of CO is around zero (**10**) or even below (**5**). Even when calculating as composite propellant in a mixture containing 71% oxidizer, 15% aluminum and 14% binder, a specific impulses of 252 s (**10**) was reached, which is comparable to AP (261 s). This study showed the development of materials with good specific impulses, but future work has also to

include the search for similar materials having higher decomposition temperatures and densities.

7.5 Experimental Section

General Information

All chemicals were used as supplied (Sigma–Aldrich, Fluka, Acros Organics), if not stated otherwise. RAMAN spectra were recorded in a glass tube with a Bruker MultiRAM FT-RAMAN spectrometer with Nd:YAG laser excitation up to 1000 mW at 1064 nm in the range between 400 and 4000 cm^{-1}. Infrared spectra were measured with a PerkinElmer Spectrum BX-FTIR spectrometer equipped with a Smiths DuraSamplIR II ATR device. All spectra were recorded at ambient temperature. NMR spectra were recorded with a JEOL Eclipse 400 instrument and chemical shifts were determined with respect to external standards Me_4Si (^1H, 399.8 MHz; ^{13}C, 100.5 MHz) and $MeNO_2$ (^{14}N, 28.8 MHz). Mass spectrometric data were obtained with a JEOL MStation JMS 700 spectrometer (DCI+, DEI+). Analysis of C/H/N was performed with an Elemental VarioEL Analyzer. Melting and decomposition points were measured with a PerkinElmer Pyris6 DSC and an OZM Research DTA 552-Ex with a heating rate of 5 °C min^{-1} in a temperature range of 15 to 400 °C and checked by a Büchi Melting Point B-540 apparatus (not corrected). The sensitivity data were performed using a BAM drophammer and a BAM friction tester.[20,21]

X-ray Crystallography

Crystals suitable for X-ray crystallography were selected by means of a polarization microscope and mounted on the tip of a glass fiber. Measurements were investigated on Oxford XCalibur3 (**1**, **3**, **4**, **6**, **8**, **9**, **11**, and **12**) or on Bruker TXS D8 Venture (**13**). The solution of the structure was performed by direct methods (SIR97)[25] and refined by full-matrix least-squares on F^2 (SHELXL)[26] implemented in the WINGX software package[27] and finally checked with the PLATON software.[28] All non-hydrogen atoms were refined anisotropically. The hydrogen atom positions were located in a difference Fourier map. ORTEP plots are shown with thermal ellipsoids at the 50% probability level.

CCDC 1490177 (**1**), 1490184 (**3**), 1490178 (**4**), 1490179 (**6**), 1490183 (**8**), 1490180 (**9**), 1490181 (**11**), 1490182 (**12**), and 1490185 (**13**) contain the supplementary crystallographic data for this paper. These data can be obtained free of charge from The Cambridge Crystallographic Data Centre.

Quantum Chemical Calculations

All ab initio calculations were carried out using the program package Gaussian 09 (Rev. A.02)[29] and visualized by GaussView 5.08.[30] Structure optimizations and frequency analyses were performed with Becke's B3 three parameter hybrid functional using the LYP correlation functional (B3LYP). For C, H, N and O a correlation consistent polarized double-zeta basis set cc-pVDZ was used. The structures were optimized with symmetry constraints and the energy is corrected with the zero point vibrational energy.[31] The enthalpies (*H*) and free energies (*G*) were calculated using the complete basis set (CBS) method in order to obtain accurate values. The CBS models used the known asymptotic convergence of pair natural orbital expressions to extrapolate from calculations using a finite basis set to the estimated complete basis set limit. CBS-4M starts with a HF/3-21G(d) geometry optimization, which is the initial guess for the following SCF calculation as a base energy and a final MP2/6–31+G calculation with a CBS extrapolation to correct the energy in second order. The used CBS-4M method additionally implements a MP4(SDQ)/6-31+(d,p) calculation to approximate higher order contributions and also includes some additional empirical corrections.[32] The enthalpies of the gas-phase species were estimated according to the atomization energy method.[33]

Calculation of Energetic Performance

All calculations of the detonation parameters were performed with the EXPLO5 V6.02 program package.[23,34] The detonation parameters were calculated at the Chapman‐Jouguet (CJ) point with the aid of the steady-state detonation model and a modified Becker‐Kistiakowski‐Wilson equation of state to model the system. The CJ point was found from the Hugoniot curve of the system by its first derivative. The specific impulses were also calculated with the EXPLO5 V6.02 program for an assumed isobaric combustion of a composition of 70% oxidizer, 16% aluminum as fuel, 6% polybutadiene acrylic acid, 6% polybutadiene acrylonitrile as binder, and 2% bisphenol A ether as an epoxy curing agent. A chamber pressure of 70.0 bar and an ambient pressure of 1.0 bar with frozen expansion conditions were assumed for the calculations.

Syntheses

CAUTION! All prepared compounds are energetic materials with sensitivity toward heat, impact, and friction. No hazards occurred during the preparation and manipulation. However, additional proper protective precautions (face shield, leather coat, earthed equipment and shoes, Kevlar® gloves, and ear plugs) should be used when undertaking work with these compounds.

N-(Cyanomethyl)-*N*-methylnitramine (**1**)

Prepared according to the literature.[7]

^{1}H NMR ($CDCl_3$) δ = 4.65 (s, 2H, CH_2), 3.47 (s, 3H, CH_3) ppm. ^{13}C NMR ($CDCl_3$) δ = 112.7 (*C*N), 40.5 (*C*H_2), 39.2 (*C*H_3) ppm. ^{14}N NMR ($CDCl_3$) δ = −30 (NO_2), −126 (CN) ppm. Elemental analysis $C_3H_5N_3O_2$ (115.09): calcd. C 31.31, H 4.38, N 36.51%; found C 31.52, H 4.51, N 36.53%. IR (ATR): ν = 3007 (w), 2962 (w), 1515 (s), 1469 (m), 1444 (s), 1401 (m), 1361 (m), 1327 (m), 1275 (s), 1154 (m), 1120 (w), 1035 (m), 932 (m), 904 (m), 847 (w), 762 (m), 682 (m) cm^{-1}. Raman (500 mW): ν = 3032 (9), 3007 (19), 2964 (52), 2878 (5), 2858 (5), 2842 (4), 2266 (10), 2251 (22), 1523 (5), 1475 (5), 1445 (11), 1403 (12), 1359 (9), 1327 (5), 1278 (24), 1156 (8), 1039 (11), 933 (22), 908 (5), 848 (100), 683 (7), 617 (20), 497 (10), 421 (10), 361 (4), 332 (10), 260 (5) cm^{-1}. IS: >40 J (grain size 100–500 µm). FS: >360 N (grain size 100–500 µm). ESD: 1.50 J (grain size 100–500 µm). DSC (5 °C min^{-1}, onset): 193 °C (dec.).

N-Methyl-*N*-nitroglycine methyl ester (**2**)

Prepared according to the literature.[7]

^{1}H NMR ($CDCl_3$) δ = 4.44 (s, 2H, CH_2), 3.75 (s, 3H, OCH_3), 3.45 (s, 3H, NCH_3) ppm. ^{13}C NMR ($CDCl_3$) δ = 167.1 (*C*O), 53.4 (*C*H_2), 52.7 (*C*H_3), 39.9 (*C*H_3) ppm. ^{14}N NMR ($CDCl_3$) δ = −28 (NO_2) ppm. Elemental analysis $C_4H_8N_2O_4$ (148.12): calcd. C 32.44, H 5.44, N 18.91%; found C 32.33, H 5.35, N 19.26%. IR (ATR): ν = 3006 (w), 2959 (w), 2360 (w), 1745 (s), 1521 (s), 1437 (m), 1404 (m), 1365 (m), 1292 (s), 1211(s), 1184 (s), 1114 (w), 1031 (m), 1009 (m), 986 (m), 951 (m), 892 (w), 859 (w), 839 (w), 767 (m), 717 (m), 651 (w), 622 (m), 562 (m) cm^{-1}. Raman (500 mW): ν = 3006 (29), 2961 (100), 2854 (18), 1749 (10), 1537 (5), 1446 (15), 1406 (11), 1369 (5), 1292 (16), 1184 (4), 1149 (8), 1037 (6), 988 (8), 954 (13), 893 (55), 860 (42), 840 (21), 721 (3), 652 (6), 623 (13), 566 (6), 423 (12), 248 (3) cm^{-1}. DSC (5 °C min^{-1}, onset): 231 °C (dec.).

N-Methyl-*N*-nitroglycine, (*N*-Nitrosarcosine) (**3**)

Prepared according to the literature.[7]

^{1}H NMR ([D_6]acetone) δ = 4.61 (s, 2H, CH_2), 3.50 (s, 3H, CH_3) ppm. ^{13}C NMR ([D_6]acetone) δ = 168.6 (*C*O), 53.8 (*C*H_2), 40.1 (*C*H_3) ppm. ^{14}N NMR ([D_6]acetone) δ = −27 (NO_2) ppm. Elemental analysis $C_3H_6N_2O_4$ (134.09): calcd. C 26.87, H 4.51, N 20.89%; found C 26.87, H 4.48, N 20.82%. IR (ATR): ν = 3001 (w), 2957 (w), 2868 (w), 2571 (w), 2361 (w), 1711 (s), 1559 (w), 1521 (s), 1473 (w), 1447 (m), 1426 (m), 1400 (m), 1322 (m), 1288 (s), 1240 (s),

1148 (w), 1118 (m), 1036 (m), 952 (m), 915 (m), 891 (m), 865 (w), 768 (m), 716 (m) cm^{-1}. Raman (1000 mW): ν = 3037 (14), 3012 (17), 3002 (21), 2970 (48), 2891 (5), 1660 (4), 1521 (7), 1470 (9), 1453 (9), 1438 (10), 1403 (24), 1354 (10), 1324 (5), 1302 (9), 1279 (32), 1151 (15), 1117 (4), 1035 (13), 952 (13), 891 (15), 867 (100), 772 (3), 711 (5), 632 (10), 617 (16), 554 (8), 442 (7), 422 (10), 330 (5) cm^{-1}. IS: >40 J (grain size <100 µm). FS: >360 N (grain size <100 µm). ESD: 1.50 J (grain size <100 µm). DSC (5 °C min^{-1}, onset): 92 °C (mp.), 153 °C (dec.).

N-Methyl-*N*-nitroglycinoyl hydrazide (**4**)

Prepared according to the literature.[7]

^{1}H NMR ([D_4]methanol) δ = 4.82 (br s, 3H, N*H*NH_2), 4.42 (s, 2H, CH_2), 3.48 (s, 3H, CH_3) ppm. ^{13}C NMR ([D_4]methanol) δ = 168.4 (*C*O), 54.4 (*C*H_2), 40.8 (*C*H_3) ppm. ^{14}N NMR ([D_4]methanol) δ = −27 (*N*O_2) ppm. Elemental analysis $C_3H_8N_4O_3$ (148.12): calcd. C 24.33, H 5.44, N 37.83%; found C 24.28, H 5.14, N 38.06%. IR (ATR): ν = 3326 (m), 3036 (w), 2998 (w), 2960 (w), 2360 (w), 2340 (w), 1649 (m), 1497 (m), 1467 (s), 1437 (s), 1406 (m), 1379 (m), 1328 (s), 1268 (s), 1151 (m), 1126 (w), 1102 (m), 1027 (m), 979 (s), 946 (s), 900 (m), 852 (m), 767 (s), 746 (m), 716 (m) cm^{-1}. Raman (1000 mW): ν = 3343 (8), 3324 (7), 3285 (10), 3213 (6), 3035 (13), 2999 (27), 2961 (42), 2875 (6), 1655 (16), 1611 (5), 1537 (6), 1445 (20), 1410 (18), 1382 (9), 1328 (15), 1288 (38), 1273 (35), 1151 (22), 1135 (13), 1033 (28), 982 (11), 950 (24), 909 (21), 857 (100), 751 (7), 657 (10), 622 (19), 572 (5), 547 (5), 435 (23), 378 (19), 321 (5), 228 (5) cm^{-1}. IS: >40 J (grain size <100 µm). FS: 288 N (grain size <100 µm). ESD: 1.50 J (grain size <100 µm). DSC (5 °C min^{-1}, onset): 116 °C (dec.).

N-Methyl-*N*-(2-oxo-2-(2,2,2-trinitroethyl)hydrazinyl)ethyl)nitramine (**5**)

To a solution of *N*-methyl-*N*-nitroglycinoyl hydrazide (**4**) (500 mg, 3.4 mmol) in 10 mL water was added 2,2,2-trinitroethanol (610 mg, 3.4 mmol) and the solution was stirred at ambient temperature for 2 h. A viscose oil separated which was completely solidified by ultrasound treatment. The solid was filtered off, washed with water and dried in the desiccator. A light yellow solid of *N*-methyl-*N*-(2-oxo-2-(2,2,2-trinitroethyl)hydrazinyl)-ethyl)nitramine (**5**) was obtained in 63% yield.

^{1}H NMR ([D_3]acetonitrile) δ = 8.40 (s, 1H, N*H*), 5.26 (dt, 1H, N*H*, $^{3}J_{NHNH}$ = 4.6 Hz, $^{3}J_{NHCH2}$ = 6.0 Hz), 4.55 (d, 2H, OCH_2, $^{3}J_{NHCH2}$ = 6.0 Hz), 4.33 (s, 2H, NCH_2), 3.42 (s, 3H, CH_3) ppm. ^{13}C NMR ([D_3] acetonitrile) δ = 168.0 (*C*O), 128.6 (C(NO_2)$_3$), 55.7 (*C*H_2), 54.3 (*C*H_2), 40.9 (*C*H_3) ppm. ^{14}N NMR ([D_3]acetonitrile) δ = −27 (N*N*O_2/C(*N*O_2)$_3$) ppm. Elemental analysis

$C_5H_9N_7O_9$ (311.17): calcd. C 19.30, H 2.92, N 31.51%; found C 19.54, H 3.02, N 31.42%. IR (ATR): ν = 3390 (w), 3307 (w), 1686 (m), 1601 (s), 1588 (s), 1504 (m), 1482 (m), 1454 (m), 1401 (w), 1376 (w), 1326 (m), 1302 (s), 1241 (m), 1159 (w), 1140 (w), 1110 (w), 1046 (w), 1006 (w), 968 (w), 944 (w), 877 (w), 855 (w), 814 (w), 775 (m), 763 (m), 742 (w), 697 (w), 677 (w), 664 (m), 628 (m), 595 (w), 544 (w), 482 (m), 465 (m) cm^{-1}. IS: 9 J (grain size <100 µm). FS: 240 N (grain size <100 µm). ESD: 0.30 J (grain size <100 µm). DSC (5 °C min^{-1}, onset): 108 °C (dec.).

N-Methyl-*N*-nitroglycinoyl azide (**6**)[7]

N-Methyl-*N*-nitroglycinoyl hydrazide (**4**) (1.0 g, 6.8 mmol) dissolved in 5 ml water was overlayed with 10 ml chloroform and hydrochloric acid (3.4 mL, 2 M, 6.8 mmol) was added at 0 °C. Sodium nitrit (0.5 g, 7.0 mmol) dissolved in 2 mL water was added dropwise while keeping the temperature at 0 °C. The reaction mixture was stirred for 15 min. The organic layer was separated and the aqueous solution was extracted with ice-cold chloroform (3×10 mL). The combined organic extracts were washed with ice-cold water (2×10 mL), ice-cold brine (10 mL) and were dried over magnesium sulfate. The solvent was concentrated on the rotary evaporator to 5 mL (water bath temperature 10 °C) and the solution was stored at −30 °C over night yielding colorless crystals of *N*-methyl-*N*-nitroglycinoyl azide (**6**) in 54% yield.

^{1}H NMR ($CDCl_3$) δ = 4.48 (s, 2H, CH_2), 3.48 (s, 3H, CH_3) ppm. ^{13}C NMR ($CDCl_3$) δ = 173.9 (*C*O), 55.2 (*C*H_2), 40.1 (*C*H_3) ppm. ^{14}N NMR ($CDCl_3$) δ = −29 (NO_2), −136 (N_γ), −147 (N_β) ppm. Elemental analysis $C_3H_5N_5O_3$ (159.11): calcd. C 22.65, H 3.17, N 44.02%; found C 22.76, H 3.27, N 43.76%. IR (ATR): ν = 2974 (w), 2943 (w), 2319 (w), 2257 (w), 2146 (s), 1718 (s), 1684 (w), 1656 (w), 1510 (s), 1481 (m), 1451 (m), 1397 (m), 1355 (m), 1295 (s), 1274 (s), 1173 (s), 1147 (s), 1102 (s), 1086 (s), 1017 (s), 945 (s), 908 (m), 864 (m), 763 (m), 747 (m), 662 (m) cm^{-1}. Raman (1000 mW): ν = 2975 (50), 2946 (79), 2892 (17), 2155 (30), 1737 (11), 1717 (66), 1545 (7), 1529 (8), 1454 (13), 1410 (22), 1361 (18), 1317 (13), 1304 (13), 1271 (32), 1176 (12), 1159 (8), 1093 (5), 1025 (14), 947 (16), 910 (69), 866 (100), 752 (21), 667 (14), 622 (30), 580 (5), 522 (8), 506 (32), 420 (18), 377 (18), 308 (10), 293 (8) cm^{-1}. IS: 4 J (grain size 100–500 µm). FS: 54 N (grain size 100–500 µm). ESD: 0.15 J (grain size 100–500 µm). DSC (5 °C min^{-1}, onset): 56 °C (dec.).

2,2,2-Trinitroethyl ((methylnitramino)methyl)carbamate (**7**)

To a solution of *N*-methyl-*N*-nitroglycinoyl azide (**6**)[7] (670 mg, 4.2 mmol) in chloroform (10 mL) was added 2,2,2-trinitroethanol (815 mg, 4.5 mmol) and a catalytical amount of dry

aluminum(III) chloride. The solution was refluxed for 18 h. The solvent was removed on the rotary evaporator and the residual solid was washed with water. 2,2,2-Trinitroethyl ((methylnitramino)methyl)carbamate (**7**) was obtained as a colorless solid in 81% yield.

^{1}H NMR ([D$_6$]acetone) δ = 8.16 (s, 1H, N*H*), 5.82 (s, 2H, OC*H*$_2$), 5.17 (d, 2H, ^{3}J = 6.4 Hz, C*H*$_2$), 3.44 (s, 3H, NC*H*$_3$) ppm. ^{13}C NMR ([D$_6$]acetone) δ = 155.1 (*C*O), 125.4 (*C*(NO$_2$)$_3$), 62.3 (O*C*H$_2$) 58.8 (*C*H$_2$), 39.0 (*C*H$_3$) ppm. ^{14}N NMR ([D$_6$]acetone) δ = −28 (*N*O$_2$), −32 (C(*N*O$_2$)$_3$) ppm. Elemental analysis $C_5H_8N_6O_{10}$ (312.15): calcd. C 19.24, H 2.58, N 26.92%; found C 19.28, H 2.71, N 26.64%. IR (ATR): ν = 3320 (m), 3036 (w), 2986 (w), 1754 (w), 1731 (m), 1598 (s), 1581 (m), 1542 (m), 1510 (m), 1468 (m), 1452 (m), 1419 (m), 1342 (m), 1299 (s), 1261 (m), 1222 (s), 1135 (m), 1040 (m), 1027 (m), 1001 (m), 902 (w), 867 (m), 853 (m), 842 (w), 802 (m), 787 (m), 769 (m), 725 (w), 689 (m), 670 (m) cm^{-1}. Raman (1000 mW): ν = 3321 (6), 3035 (26), 3001 (46), 2986 (42), 2954 (25), 2891 (6), 1731 (14), 1616 (18), 1543 (5), 1471 (5), 1454 (11), 1428 (24), 1421 (30), 1394 (9), 1384 (10), 1351 (29), 1307 (43), 1223 (13), 1144 (6), 1116 (6), 1102 (7), 1046 (14), 1029 (14), 1004 (23), 904 (8), 870 (12), 856 (100), 844 (87), 806 (5), 778 (5), 726 (5), 673 (8), 648 (7), 608 (14), 541 (13), 459 (12), 430 (20), 394 (20), 367 (41), 292 (15), 217 (6) cm^{-1}. DSC (5 °C min^{-1}, onset): 134 °C (melt), 172 °C (dec.).

N-Methyl-*N*-nitroglycinoyl chloride (**8**)

To *N*-methyl-*N*-nitroglycine (**3**)[7] (500 mg, 3.7 mmol) suspended in 10 mL dichloromethane was added oxalyl chloride (470 mg, 3.7 mmol) and one drop of dimethylformamide as catalyst. Gas evolution was observed immediately. The reaction mixture was stirred 1 h at ambient temperature and was refluxed additional 2 h until gas evolution ceased. The solvent was removed on the rotary evaporator (water bath temperature 10 °C) yielding *N*-methyl-*N*-nitrogycinoyl chloride (**8**) as a colorless solid (97%).

^{1}H NMR (CDCl$_3$) δ = 4.84 (s, 2H, C*H*$_2$), 3.49 (s, 3H, C*H*$_3$) ppm. ^{13}C NMR (CDCl$_3$) δ = 168.7 (*C*O), 61.6 (*C*H$_2$), 39.7 (*C*H$_3$) ppm. ^{14}N NMR (CDCl$_3$) δ = −30 (*N*O$_2$) ppm. IR (ATR): ν = 2995 (w), 2952 (w), 1790 (s), 1522 (s), 1466 (m), 1444 (m), 1388 (m), 1344 (m), 1277 (s), 1143 (w), 1116 (w), 1053 (w), 1019 (m), 951 (s), 928 (m), 859 (w), 763 (s), 689 (w), 635 (w) cm^{-1}. Raman (1000 mW): ν = 2990 (29), 2956 (67), 2886 (10), 1796 (22), 1532 (7), 1445 (12), 1389 (10), 1348 (19), 1278 (30), 1115 (9), 1046 (10), 929 (18), 861 (100), 772 (26), 704 (5), 648 (7), 620 (18), 613 (18), 522 (4), 452 (69), 416 (16), 371 (8), 303 (11), 253 (19) cm^{-1}.

Bis(*N*-methyl-*N*-nitroglycinoyl) hydrazide (**9**)

To a solution of *N*-methyl-*N*-nitrogycinoyl chloride (**8**) (560 mg, 3.7 mmol) in 10 mL chloroform was added dropwise anhydrous hydrazine (60 mg, 1.9 mmol) dissolved in 10 mL chloroform at 0 °C. A colorless solid precipitated immediately. The reaction mixture was stirred 1 h at 0 °C and was refluxed for additional 1 h. The solid was filtered off, washed with chloroform and recrystallized from water. Bis(*N*-methyl-*N*-nitroglycinoyl) hydrazide (**9**) was obtained as colorless crystals in 86% yield.

^{1}H NMR (DMSO) δ = 10.38 (s, 2H, N*H*), 4.52 (s, 4H, CH_2), 3.42 (s, 6H, CH_3) ppm. ^{13}C NMR (DMSO) δ = 164.8 (*C*O), 53.1 (*C*H$_2$), 40.3 (*C*H$_3$) ppm. ^{14}N NMR (DMSO) δ = −27 (NO$_2$) ppm. Elemental analysis $C_6H_{12}N_6O_6$ (264.20): calcd. C 27.28, H 4.58, N 31.81%; found C 27.28, H 4.52, N 32.11%. IR (ATR): ν = 3195 (m), 3064 (w), 2967 (w), 1605 (m), 1497 (s), 1460 (m), 1440 (s), 1405 (m), 1327 (m), 1290 (s), 1229 (s), 1147 (m), 1103 (m), 1024 (m), 949 (m), 918 (m), 863 (w), 765 (m), 716 (w), 655 (m), 620 (s), 549 (m), 473 (m) cm^{-1}. Raman (1000 mW): ν = 3033 (6), 3004 (20), 2964 (43), 2871 (5), 1696 (17), 1603 (45), 1528 (4), 1446 (10), 1409 (15), 1376 (13), 1271 (60), 1260 (50), 1156 (10), 1049 (36), 1020 (5), 949 (29), 858 (100), 773 (6), 644 (8), 619 (12), 538 (6), 420 (16), 375 (5), 259 (12), 241 (9) cm^{-1}. IS: 25 J (grain size <100 µm). FS: 240 N (grain size <100 µm). ESD: 0.35 J (grain size <100 µm). DSC (5 °C min^{-1}, onset): 201 °C (dec.).

2,2,2-Trinitroethyl *N*-methyl-*N*-nitroglycinate (**10**)

To *N*-methyl-*N*-nitrogycinoyl chloride (**8**) (560 mg, 3.7 mmol) dissolved in 10 mL chloroform were added 2,2,2-trinitroethanol (815 mg, 4.5 mmol) and dry aluminum(III) chloride (490 mg, 3.7 mmol). The reaction mixture was refluxed for 3 h until gas evolution ceased. The organic solution was washed with 2 M hydrochloric acid (10 mL) and water (10 mL) and was dried over magnesium sulfate. The solvent was removed on the rotary evaporator and 2,2,2-trinitroethyl *N*-methyl-*N*-nitroglycinate (**10**) was obtained as a colorless solid in 56% yield.

^{1}H NMR ([D$_6$]acetone) δ = 5.96 (s, 2H, OCH_2), 4.85 (s, 2H, NCH_2), 3.51 (s, 3H, CH_3) ppm. ^{13}C NMR ([D$_6$]acetone) δ = 166.1 (*C*O), 125.1 (*C*(NO$_2$)$_3$), 62.2 (O*C*H$_2$), 53.8 (N*C*H$_2$), 40.1 (*C*H$_3$) ppm. ^{14}N NMR ([D$_6$]acetone) δ = −28 (NO$_2$), −33 (C(NO$_2$)$_3$) ppm. Elemental analysis $C_5H_7N_5O_{10}$ (297.14): calcd. C 20.21, H 2.37, N 23.57%; found C 20.23, H 2.47, N 23.43%. IR (ATR): ν = 3029 (w), 3004 (w), 2982 (w), 2955 (w), 2360 (w), 1783 (m), 1591 (s), 1516 (s), 1468 (w), 1441 (m), 1399 (m), 1369 (w), 1349 (w), 1286 (s), 1169 (s), 1105 (w), 1052 (m), 1028 (w), 1000 (w), 946 (w), 911 (w), 865 (w), 856 (w), 804 (m), 784 (m), 765 (m), 732 (w), 709 (m), 652 (w) cm^{-1}. Raman (1000 mW): ν = 3031 (31), 3005 (46), 2984 (52), 2961

(82), 2882 (9), 2859 (17), 1788 (23), 1612 (15), 1604 (23), 1524 (7), 1443 (22), 1410 (10), 1400 (19), 1371 (29), 1352 (31), 1291 (37), 1152 (13), 1107 (10), 1051 (9), 1032 (14), 1002 (8), 949 (11), 913 (28), 869 (100), 858 (60), 808 (7), 788 (7), 652 (7), 623 (26), 560 (13), 536 (10), 465 (7), 422 (40), 392 (29), 375 (54), 346 (12), 312 (7), 271 (19), 234 (16), 224 (13) cm^{-1}. IS: 20 J (grain size <100 µm). FS: >360 N (grain size <100 µm). ESD: 0.30 J (grain size <100 µm). DSC (5 °C min^{-1}, onset): 108 °C (mp.), 178 °C (dec.).

2-(Methylnitramino)acetamide (**11**)

N-Methyl-*N*-nitrogycinoyl chloride (**8**) (560 mg, 3.7 mmol) dissolved in 2 mL tetrahydrofuran was added to an aqueous ammonia solution (10 mL) at 0 °C. The reaction mixture was stirred 10 min. at 0 °C and extracted with ethyl acetate (3×50 mL). The combined organic extracts were washed with brine (20 mL) and dried over magnesium sulfate. The solvent was removed on the rotary evaporator to obtain 2-(methylnitramino)acetamide (**11**) as pure colorless solid in 63% yield.

^{1}H NMR ([D_6]acetone) δ = 7.09 (s, 1H, NH_2), 6.59 (s, 1H, NH_2), 4.49 (s, 2H, CH_2), 3.47 (s, 3H, CH_3) ppm. ^{13}C NMR ([D_6]acetone) δ = 168.5 (*C*O), 55.1 (*C*H_2), 40.5 (*C*H_3) ppm. ^{14}N NMR ([D_6]acetone) δ = −26 (NO_2) ppm. Elemental analysis $C_3H_7N_3O_3$ (133.11): calcd. C 27.07, H 5.30, N 31.57%; found C 27.25, H 5.20, N 31.14%. IR (ATR): ν = 3387 (m), 3176 (w), 2996 (w), 2961 (w), 2361 (w), 1693 (s), 1623 (w), 1506 (s), 1458 (m), 1443 (m), 1413 (m), 1398 (m), 1327 (m), 1291 (s), 1270 (s), 1142 (w), 1109 (m), 1034 (m), 955 (m), 841 (m), 797 (w), 761 (s), 713 (m) cm^{-1}. Raman (1000 mW): ν = 3161 (12), 3034 (27), 2999 (50), 2963 (91), 2912 (14), 1683 (10), 1612 (10), 1532 (7), 1468 (11), 1442 (22), 1422 (15), 1404 (26), 1325 (20), 1314 (18), 1301 (23), 1271 (36), 1144 (30), 1112 (24), 1036 (45), 956 (43), 871 (72), 842 (100), 766 (8), 713 (10), 625 (15), 602 (22), 538 (17), 419 (34), 342 (12), 324 (24), 236 (7) cm^{-1}. IS: 40 J (grain size <100 µm). FS: 360 N (grain size <100 µm). ESD: 0.70 J (grain size <100 µm). DSC (5 °C min^{-1}, onset): 116 °C (mp.), 186 °C (dec.).

2,2,2-Trinitroethyl (*N*-methyl-*N*-nitroglycyl)carbamate (**12**)

To a suspension of 2-(methylnitramino)acetamide (**11**) (500 mg, 3.8 mmol) in 10 mL 1,2-dichloroethane oxalyl chloride (508 mg, 4.0 mmol) was added. The reaction mixture was refluxed for 1 h until gas evolution ceased. 2,2,2-Trinitroethanol (688 mg, 3.8 mmol) was added and the solution was refluxed additional 5 h. After cooling to room temperature a colorless solid precipitated which was filtered off, washed with 1,2-dichloroethane and dried. 2,2,2-Trinitroethyl (*N*-methyl-*N*-nitroglycyl)carbamate (**12**) was obtained as a colorless solid in 63% yield.

^{1}H NMR ([D$_6$]acetone) δ = 10.55 (s, 1H, NH_2), 5.94 (s, 2H, OCH_2), 5.00 (s, 2H, NCH_2), 3.49 (s, 3H, CH_3) ppm. ^{13}C NMR ([D$_6$]acetone) δ = 168.1 (CO), 150.7 (CO), 125.1 (C(NO$_2$)$_3$), 62.6 (OCH$_2$), 56.7 (NCH$_2$), 40.2 (CH$_3$) ppm. ^{14}N NMR ([D$_6$]acetone) δ = −27 (NNO$_2$), −34 (C(NO$_2$)$_3$) ppm. Elemental analysis $C_6H_8N_6O_{11}$ (340.16): calcd. C 21.19, H 2.37, N 24.71%; found C 21.36, H 2.48, N 24.42%. IR (ATR): ν = 3252 (w), 3183 (w), 3003 (w), 2969 (w), 1799 (m), 1785 (m), 1705 (m), 1599 (s), 1510 (m), 1498 (m), 1444 (m), 1396 (m), 1301 (s), 1252 (m), 1193 (m), 1111 (m), 1080 (m), 1034 (m), 953 (w), 885 (w), 856 (w), 842 (w), 804 (m), 785 (m), 770 (m), 754 (m), 731 (m), 654 (w), 622 (w), 601 (m), 536 (m) cm^{-1}. Raman (1000 mW): ν = 3024 (19), 3004 (24), 2975 (61), 2962 (66), 2859 (17), 1803 (17), 1785 (47), 1708 (18), 1607 (31), 1593 (13), 1523 (7), 1444 (23), 1382 (20), 1351 (32), 1307 (38), 1269 (15), 1192 (5), 1153 (18), 1115 (7), 1034 (24), 955 (15), 886 (20), 870 (69), 859 (100), 844 (17), 807 (12), 787 (9), 645 (6), 624 (21), 600 (9), 540 (17), 430 (18), 412 (44), 376 (62), 314 (19), 274 (17) cm^{-1}. IS: 10 J (grain size <100 µm). FS: >360 N (grain size <100 µm). ESD: 0.60 J (grain size <100 µm). DSC (5 °C min^{-1}, onset): 150 °C (dec.).

2-(Methylnitramino)-*N*-nitroacetamide (**13**)

To a suspension of 2-(methylnitramino)acetamide (**11**) (200 mg, 1.5 mmol) in 5 mL ethyl acetate was added at −10 °C nitronium tetrafluoroborate (230 mg, 1.7 mmol). The reaction mixture was stirred at −10 to 5 °C for 2 h before pouring on 10 mL ice-water. The organic layer was separated and the aqueous phase was extracted with ethyl acetate (1×20 mL). The combined organic extracts were washed with brine (20 mL), dried over magnesium sulfate and the solvent was removed on the rotary evaporator. 2-(Methylnitramino)-*N*-nitroacetamide (**13**) was obtained as pure colorless solid in 82% yield.

^{1}H NMR ([D$_6$]acetone) δ = 13.62 (s, br, 1H, NH), 5.00 (s, 2H, CH_2), 3.51 (s, 3H, CH_3) ppm. ^{13}C NMR ([D$_6$]acetone) δ = 164.7 (CO), 56.0 (NCH$_2$), 40.3 (CH$_3$) ppm. ^{14}N NMR ([D$_6$]acetone) δ = −27 (NNO$_2$), −45 (NHNO$_2$) ppm. Elemental analysis $C_3H_6N_4O_5$ (178.10): calcd. C 20.23, H 3.40, N 31.46%; found C 20.48, H 3.43, N 31.16%. IR (ATR): ν = 3281 (w), 3218 (w), 3011 (w), 2976 (w), 1749 (m), 1613 (m), 1505 (m), 1451 (m), 1401 (m), 1287 (s), 1107 (s), 1032 (m), 974 (m), 960 (m), 943 (m), 863 (w), 759 (m), 730 (m), 613 (m), 505 (m) cm^{-1}. Raman (1000 mW): ν = 3012 (34), 2975 (63), 2955 (39), 2885 (9), 1751 (30), 1622 (13), 1529 (7), 1454 (20), 1436 (24), 1404 (41), 1358 (18), 1308 (54), 1277 (40), 1155 (21), 1114 (5), 1038 (23), 979 (47), 963 (25), 943 (53), 865 (100), 767 (30), 732 (9), 630 (15), 618 (31), 450 (38), 420 (22), 386 (6), 339 (7), 300 (18) cm^{-1}. IS: J (grain size <100 µm). FS: >360 N (grain size <100 µm). ESD: 0.60 J (grain size <100 µm). DSC (5 °C min^{-1}, onset): 113 °C (dec. with melt.).

7.6 References

[1] J. Liebig, *Justus Liebigs Ann. Chem.* **1847**, *62*, 257–369.

[2] J. Volhard, *Justus Liebigs Ann. Chem.* **1862**, *123*, 261–265.

[3] A. Sreekumar, L. M. Poisson, T. M. Rajendiran, A. P. Khan, Q. Cao, J. Yu, B. Laxman, R. Mehra, R. J. Lonigro, Y. Li, M. K. Nyati, A. Ahsan, S. Kalyana-Sundaram, B. Han, X. Cao, J. Byun, G. S. Omenn, D. Ghosh, S. Pennathur, D. C. Alexander, A. Berger, J. R. Shuster, J. T. Wei, S. Varambally, C. Beecher, A. M. Chinnaiyan, *Nature* **2009**, *457*, 910–914.

[4] D. F. H. Wallach, R. Mathur, G. J. M. Redziniak, J. F. Tranchant, *J. Soc. Cosmet. Chem.* **1992**, *43*, 113–118.

[5] H. Zollinger, *Chemie der Azofarbstoffe*, 1st ed., Springer Basel AG, Basel (CH), **1958**.

[6] a) T. M. Klapötke, C. Pflüger, M. W. Reintinger, *Eur. J. Inorg. Chem.* **2016**, *2016*, 138–147; b) M. A. Kettner, T. M. Klapötke, *Chem. - Eur. J.* **2015**, *21*, 3755–3765; c) B. Aas, M. A. Kettner, T. M. Klapötke, M. Suceska, C. Zoller, *Eur. J. Inorg. Chem.* **2013**, *2013*, 6028–6036; d) O. P. Shitov, V. L. Korolev, V. A. Tartakovsky, *Russ. Chem. Bull.* **2009**, *58*, 2347–2355; e) N. Fischer, T. M. Klapötke, D. Piercey, S. Scheutzow, J. Stierstorfer, *Z. Anorg. Allg. Chem.* **2010**, *636*, 2357–2363; f) T. M. Klapötke, B. Krumm, M. Scherr, G. Spiess, F. X. Steemann, *Z. Anorg. Allg. Chem.* **2008**, *634*, 1244–1246; g) E. T. Apasov, A. V. Kalinin, S. L. Ioffe, V. A. Tartakovsky, *Izv. Akad. Nauk, Ser. Khim.* **1993**, 1666–1668; h) O. A. Luk'yanov, N. I. Shlykova, V. A. Tartakovsky, *Izv. Akad. Nauk, Ser. Khim.* **1994**, 1775–1778; i) G. A. Gareev, L. P. Kirillova, V. M. Shul'gina, S. R. Buzilova, L. P. Vologdina, L. I. Vereshchagin, *Zh. Org. Khim.* **1988**, *24*, 2221–2226.

[7] M. B. Frankel, *J. Org. Chem.* **1958**, *23*, 1811–1813.

[8] a) A. Baumann, A. Erbacher, C. Evangelisti, T. M. Klapötke, B. Krumm, S. F. Rest, M. Reynders, V. Sproll, *Chem. – Eur. J.* **2013**, *19*, 15627–15638; b) T. M. Klapötke, B. Krumm, R. Scharf, *Z. Anorg. Allg. Chem.* **2016**, *642*, 887–895.

[9] a) T. M. Klapötke, *Chemistry of High-Energy Materials*, 3rd ed., De Gruyter, Berlin (Germany), **2015**; b) J. P. Agrawal, *High Energy Materials Propellants, Explosives and Pyrotechnics*, 1st ed., Wiley-VCH, Weinheim (Germany), **2010**; c) I. Hargittai, T. Vidóczy, *Combustion Efficiency and Air Quality*, 1st ed., Springer, New York (US), **1995**.

[10] A. Davenas, *Solid Rocket Propulsion Technology*, 1st ed., Pergamon Press, Oxford (UK), **1993**.

[11] J. Wolff, *Pharmacol. Rev.* **1998**, *50*, 89–105.

[12] Office of Naval Research Home Page. http://www.onr.navy.mil (accessed March 24, 2016).

[13] a) C. Oommen, S. R. Jain, *J. Haz. Mater.* **1999**, *67*, 253–281; b) S. Löbbecke, H. H. Krause, A. Pfeil, *Propellants, Explos., Pyrotech.* **1997**, *22*, 184–188.

[14] T. P. Holler, F. Ruan, A. Spaltenstein, P. B. Hopkins, *J. Org. Chem.* **1989**, *54*, 4570–4575.

[15] H. T. Nagasawa, W. P. Muldoon, F. N. Shirota, J. Med. Chem. **1977**, *20*, 1588 –1591.

[16] a) M. Hesse, H. Meier, B. Zeeh, *Spektroskopische Methoden in der Organischen Chemie*, 7th rev. ed., Thieme, Stuttgart (Germany), **2005**; b) G. Socrates, *Infrared and Raman Characteristic Group Frequencies: Tables and Charts*, 3rd ed., John Wiley & Sons, Chichester (UK), **2004**.

[16] K. Nakamoto, *Infrared and Raman Spectra of Inorganic and Coordination Compounds*, 4th ed., Wiley-Interscience, New York (US), **1986**.

[18] T. Steiner, *Angew. Chem., Int. Ed.* **2002**, *41*, 48-76.

[19] a) A. Wolter-Steingrube, B. E. C. Bugenhagen, C. Herrmann, J. Heck, *Eur. J. Inorg. Chem.* **2014**, *2014*, 4115–4122; b) G. C. Hsu, L. M. Singer, D. B. Cordes, M. Findlater, *Acta Crystallogr.* **2013**, *69E*, 1298; c) J. Lapic, A. Pezerovic, M. Cetina, S. Djakovic, V. Rapic, *J. Mol. Struct.* **2011**, *990*, 209–216; d) G. Laus, V. Kahlenberg, K. Wurst, S. Nerdinger, H. Schottenberger, *Z. Naturforsch.* **2011**, *66B*, 479–486; e) D. Siebler, C. Forster, T. Gasi, K. Heinze, *Organometallics* **2011**, *30*, 313–327; f) L. Parkanyi, G. Besenyei, *J. Mol. Struct.* **2004**, *691*, 97–106; g) F. M. Menger, J. Bian, V. A. Azov, *Angew. Chem., Int. Ed.* **2002**, *41*, 2581–2584; h) Y. Jiao, E. Valente, S. T. Garner, X. Wang, H. Yu, *Tetrahedron Lett.* **2002**, *43*, 5879–5881.

[20] NATO, Standardization Agreement 4489 (STANAG 4489), Explosives, Impact Sensitivity Tests, **1999**.

[21] NATO, Standardization Agreement 4487 (STANAG 4487), Explosives, Friction Sensitivity Tests, **2002**.

[22] Test methods according to the *UN Manual of Test and Criteria, Recommendations on the Transport of Dangerous Goods*, United Nations Publication, New York, Geneva, 4th revised ed., **2003**, Impact: Insensitive > 40 J, less sensitive ≥ 35 J, sensitive ≥ 4 J, very sensitive ≤ 3 J; Friction: Insensitive > 360 N, less sensitive = 360 N, sensitive < 360 N > 80 N, very sensitive ≤ 80 N, extremely sensitive ≤ 10 N.

[23] M. Sućeska, *EXPLO5 V6.02*, Zagreb (Croatia), **2013**.

[24] R. Meyer, J. Köhler, A. Homburg, *Explosives*, 7th ed., Wiley-VCH, Weinheim (Germany), **2015**.

[25] A. Altomare, M. C. Burla, M. Camalli, G. L. Cascarano, C. Giacovazzo, A. Guagliardi, A. G. G. Moliterni, G. Polidori, R. Spagna, *J. Appl. Crystallogr.* **1999**, *32*, 115–119.

[26] G. M. Sheldrick, *Acta Crystallogr.* **2008**, *64A*, 112–122.

[27] L. Farrugia, *J. Appl. Crystallogr.* **1999**, *32*, 837–838.

[28] A. L. Spek, *Platon*, Utrecht University, Utrecht,The Netherlands, **1999**.

[29] M. J. Frisch, G. W. Trucks, H. B. Schlegel, G. E. Scuseria, M. A. Robb, J. R. Cheeseman, V. B. G. Scalmani, B. Mennucci, G. A. Petersson, H. Nakatsuji, M. Caricato, X. Li, H. P. Hratchian, A. F. Izmaylov, J. Bloino, G. Zheng, J. L. Sonnenberg, M. Hada, M. Ehara, K. Toyota, R. Fukuda, J. Hasegawa, M. Ishida, T. Nakajima, Y. Honda, O. Kitao, H. Nakai, T. Vreven, J. J. A. Montgomery, J. E. Peralta, F. Ogliaro, M. Bearpark, J. J. Heyd, E. Brothers, K. N. Kudin, V. N. Staroverov, R. Kobayashi, J. Normand, K. Raghavachari, A. Rendell, J. C. Burant, S. S. Iyengar, J. Tomasi, M. Cossi, N. Rega, J. M. Millam, M. Klene, J. E. Knox, J. B. Cross, V. Bakken, C. Adamo, J. Jaramillo, R. Gomperts, R. E. Stratmann, O. Yazyev, A. J. Austin, R. Cammi, C. Pomelli, J. W. Ochterski, R. L. Martin, K. Morokuma, V. G. Zakrzewski, G. A. Voth, P. Salvador, J. J. Dannenberg, S. Dapprich, A. D. Daniels, Ö. Farkas, J. B. Foresman, J. V. Ortiz, J. Cioslowski, D. J. Fox, *Gaussian 09*, Rev. A.02 ed., Gaussian, Inc., Wallingford CT (US), **2009**.

[30] R. D. Dennington II, T. A. Keith, J. M. Millam, *GaussView*, Ver. 5.08 ed., Semichem, Inc., Wallingford CT (US), **2009**.

[31] J. A. Montgomery, M. J. Frisch, J. W. Ochterski, G. A. Petersson, *J. Chem. Phys.* **2000**, *112*, 6532–6542.

[32] J. W. Ochterski, G. A. Petersson, J. J. A. Montgomery, *J. Chem. Phys.* **1996**, *104*, 2598–2619.

[33] E. F. C. Byrd, B. M. Rice, *J. Phys. Chem.* **2005**, *110*, 1005–1013.

[34] M. Sućeska, Propellants, Explos., Pyrotech. **1991**, 16, 197–202.

TOXICITY ASSESSMENT OF ENERGETIC MATERIALS BY USING THE LUMINESCENT BACTERIA INHIBITION TEST

unpublished results

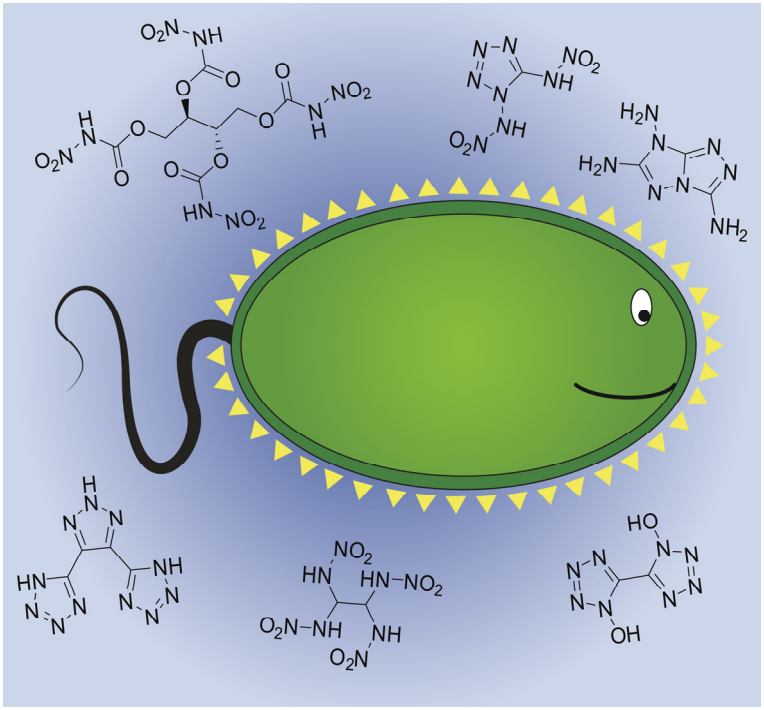

8.1 Abstract

The aquatic toxicities (EC_{50} after 15 min and 30 min) of several neutral as well as ionic energetic materials were determined by the luminescent bacteria inhibition test. The measurements were performed at 15 °C on a LUMIstox 300 made by the HACH LANGE GmbH. Liquid dried luminescent bacteria of the strain *Vibrio fischeri* NRRL-B-11177 were used. In addition to well known energetic materials such as RDX, ammonium azide, ammonium nitrate and ammonium perchlorate numerous new materials were tested and compared with each other.

8.2 Introduction

Strong research efforts are ongoing to find new energetic materials with better energetic properties like higher performance, lower sensitivities and better stabilities during the last decades.[1] However, not only energetic properties are important but also environmentally friendly substances are requested for saver handling since the commonly used explosives hexogene (RDX), 2,4,6-trinitrotoluene (TNT) and octahydro-1,3,5,7-tetranitro-1,3,5,7-tetrazocine (HMX) have shown to be toxic for human and animal organisms.[2] Furthermore, priming mixtures usually contain lead azide (LA) and lead styphnate as the primary explosives. Lead is a highly poisonous metal whether it is inhaled or swallowed affecting the whole body and may even cause death in high concentrations.[3] Studies showed that at shooting ranges and military training grounds the maximum accepted concentration of lead (0.15 mg m^{-3})[4] is often exceeded by far.[5] [33] In addition LA is decomposed by the atmospheric carbon dioxide with liberation of the highly volatile and toxic hydrazoic acid.[6] Therefore, there is need for new environmentally benign primary and secondary explosives without heavy metals.

Several tests have been implemented to determine the toxicity of compounds or ground waters utilizing plants, algea, fishes, rats, mice or water fleas.[7] However most of these tests show disadvantages like huge test volume, long exposure periods, difficulties with the standardizations of the organisms and subsequent low reproducibilities.[8] The Luminescent Bacteria Inhibition Test provides a quick, simple and reproducible possibility to test these new energetic materials towards their environmental acceptability for aquatic organisms. Since the bioluminescent bacterium *Vibrio fischeri* is an excellent representative for aquatic life it is used as indicator for groundwater pollution.[9]

Bioluminescence is a form of chemiluminescence where light is released by a chemical reaction. The complex biochemical mechanism of the bioluminescent marine bacteria *Vibrio fischeri* is shown in Figure 8.1.[10] In the system three enzymatic complexes are involved: the Flavin Reductase (FMN Reductase), the Luciferase and the Fatty Acid Reductase. In the first step flavin mononucleotide (FMN) is reacted to its reduced form ($FMNH_2$) catalyzed by the FMN Reductase. The reduced flavin molecule is able to bind to the Luciferase and in combination with an aliphatic aldehyde and under consumption of oxygen the peroxihemiacetal complex L--FMNH-O-O-CHOH-R is formed. In the following step aliphatic acid is released and a singlet excited hydroxide complex (L--FMNH-OH)* is generated which directly reacts to the hydroxide complex L--FMNHOH in the ground state under liberation of light. The emitted light with a wavelength of 490 nm can be observed and measured by a photomultiplier. [10,11] Since the intensity of the luminescence depends on the cell density this is a convenient method to determine the toxicity of compounds.

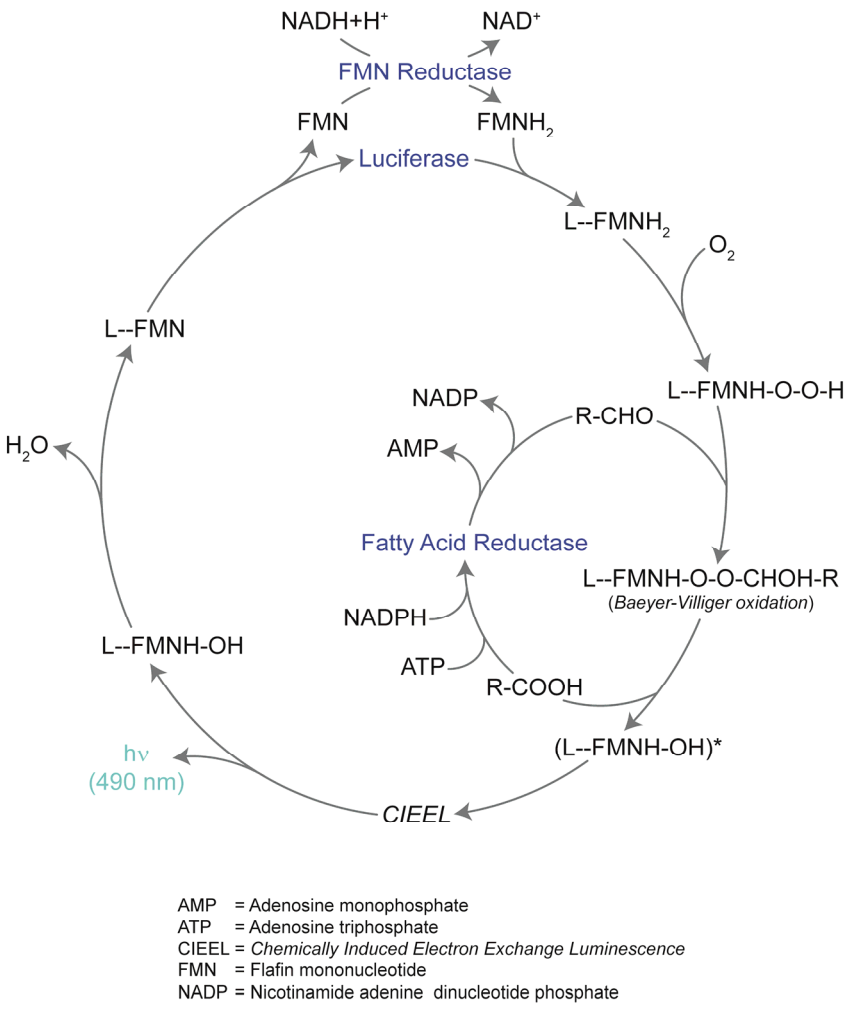

Figure 8.1 Schematic overview of the biochemical light-emitting pathway of the bioluminescent bacteria V*ibrio fischeri* and *Photobacterium*.

When testing the compounds the EC_{50} (effective concentration) value is determined. The EC_{50} value gives the concentration of the sample at which the luminescence of *Vibrio fischeri* is reduced by 50%. This concentration is determined after 15 min and 30 min, respectively, for various energetic materials such as RDX, ammonium azide and several new synthesized neutral and ionic compounds.

8.3 Experimental Section

Measurement

Liquid-dried luminescent bacteria of the strain *V. fischeri* NRRL-B-11177 obtained by HACH LANGE GmbH (Düsseldorf, Germany) were used for the luminescent bacteria inhibition test.

Prior to the measurements a 2% NaCl stock solution was prepared using HPLC-grade water to ensure optimal salt conditions for the bacteria. The tested compounds of known weight are diluted in this stock solution and after complete solvation were adjusted to a final volume. A dilution series was prepared out of this test solution referring to DIN 38412 L34, L341. The dilutions range from 1:2 to 1:32. Due to the low solubility of RDX in water RDX was first dissolved in acetone and then diluted in 2% NaCl stock solution to obtain a 1% (vol%) acetone concentration for each dilution. A 1% acetone concentration in the control of the measurement showed a negligible effect on the bacteria.

The measurements were performed on a *LUMIStox 300* obtained by HACH LANGE GmbH (Düsseldorf, Germany). The samples were incubated at 15°C and the luminescence was tested in the beginning of each experiment and after 15 min and 30 min. Each dilution step was measured twice. To calculate the correction factor of a non-toxic control two bacteria suspensions with 1% NaCl were measured at the beginning of each measurement.

Calculation

The correction factor (*fK*) is calculated with the following formula (1)

$$fK = {}^{I_t}/_{I_0} \tag{1}$$

where I_t is the luminescence of the control at a specific time and I_0 is the luminescence of the control at the beginning. The corrected luminescence I_{ct} is obtained by multiplying I_0 of all concentrations with *fK* (2)

$$I_{ct} = fK * I_0 \tag{2}$$

and the inhibition is calculated as follows:

$$inhibition\ (\%) = {}^{(I_{ct} - I_t) * 100}/_{I_{ct}} \tag{3}$$

For calculating the EC_{50} value of a substance Γ was plotted against the concentration c in a diagram with a logarithmic scale:

$$\Gamma = {inhibition\ (\%)}\Big/{100 - inhibition\ (\%)}. \quad (4)$$

All toxicity data with an inhibition range between 10–90% were used to fit a straight line. The EC_{50} value is identical with the point where the line crosses the X-axis at $\Gamma = 1$.

8.4 Results and Discussion

Table 2.1 summarizes the toxicity data of several neutral and ionic compounds like ammonium, hydroxylammonium, sodium and potassium salts (Figure 8.2). Most of the compiled compounds are useful energetic materials or potential precursors. An important factor when measuring the toxicities of energetic materials is the water solubility of the substances. To increase the water solubility RDX was first dissolved in acetone and then diluted to get a 1% acetone solution. The EC_{50} value of RDX after 15 min incubation (EC_{50} = 0.327 g L^{-1}) fits well with the EC_{50} given in the literature.[12] Nevertheless, it was not possible to obtain a concentration high enough to determine the EC_{50} values of pentaerythritol tetranitrate (PETN), cyclotetramethylene tetranitramine (HMX), 2,4,6,8,10,12-hexanitro-2,4,6,8,10,12-hexanitrohexaazaisowurtzitane (CL-20) and 2,2-dinitroethene-1,1-diamine (FOX-7). For classification of the toxicity the compounds with EC_{50} values lower than 0.10 g L^{-1} are categorized as very toxic while compounds with EC_{50} values between 0.10 g L^{-1} and 1.00 g L^{-1} are rated as toxic and above 1.00 g L^{-1} as less toxic to the marine bacteria *V. fischeri* after 30 min incubation time.[12] Therefore mainly the EC_{50} value after 30 min incubation will be discussed.

The toxicity measurements of commercially available salts like potassium chlorate, bromate and iodate as well as ammonium nitrate and perchlorate showed almost no toxicity of the salts towards the bacteria. The toxicity of these salts is presumably more influenced by the anion whereat the highest toxicity is observed for the azide anion followed by the periodate anion. The perchlorate anion showed no effect on the luminescence of the bacteria. This is astonishing since studies showed a toxicity of the perchlorate anion towards vertebrates.[13] Similar to the perchlorate ion is the effect of the chlorate, bromate and iodate ions on the bacteria. No inhibition of luminescence was observed with concentrations of 2.5 g L^{-1} and an incubation time of 30 min.

The primary explosives dipotassium 1,5-di(nitramino)tetrazolate (**1a**)[14] and dipotassium 1,1'-di(nitramino)-5,5'-bitetrazolate (**2a**)[14] [34] as well as copper(I) 5-nitrotetrazolate (DBX-1)[15] are potential lead free replacements for lead azide. Since DBX-1 is nearly insoluble in water no EC_{50} value could be determined. Therefore the precursor of DBX-1 sodium 5-nitrotetrazolate (**3a**)[15b] was measured. With EC_{50} values higher than 3.9 g L^{-1} all of these compounds are classified as not toxic towards the marine bacteria *V. fischeri*.[12]

Table 8.1 Toxicity data of several neutral and ionic compounds after 15 min and 30 min of incubation.

	EC_{50} (15 min) [g L^{-1}]	EC_{50} (30 min) [g L^{-1}]	Toxicity level[a]		EC_{50} (15 min) [g L^{-1}]	EC_{50} (30 min) [g L^{-1}]	Toxicity level[a]
NaN_3	0.25	0.18	o	**6a**	0.39	0.18	o
$NaIO_4$	0.77	0.65	o	**6b**	1.73	1.03	+
KIO_4	0.89	0.68	o	**7a**	0.32	0.24	o
$KClO_3$	> 2.49	> 2.49	+	**8a**	0.33	0.19	o
$KBrO_3$	> 2.49	> 2.49	+	**9**	0.13	0.07	–
KIO_3	> 2.53	> 2.53	+	**9a**	0.75	0.35	o
NH_4N_3	0.26	0.15	o	**10a**	> 1.04	3.78	+
NH_4NO_3	10.485	6.39	+	**11**	5.01	4.84	+
NH_4ClO_4	14.58	11.13	+	**11a**	3.56	3.36	+
NH_4IO_4	0.58	0.48	o	**12a**	2.97	1.82	+
$NH_4N(NO_2)_2$	7.25	4.50	+	**13**	0.59	0.55	o
RDX	0.33	0.24	o	**14a**	2.88	2.80	+
1a	> 1.63	3.92	+	**15a**	0.09	0.07	–
2a	> 5.93	11.63	+	**16a**	1.19	0.71	o
3a	14.08	4.35	+	**17a**	5.73	5.42	+
4a	1.17	0.58	o	**18**	0.01	0.01	–
5a	1.63	0.33	o	**19a**	> 15.07	> 15.07	+
5b	4.21	3.68	+	**20**	0.87	0.87	o
6	0.60	0.49	o	**21**	0.29	0.22	o

[a] Toxicity level (incubation 30 min): very toxic (–) < 0.10 g L^{-1}; toxic (o) 0.10–1.00 g L^{-1}; less toxic (+) > 1.00 g L^{-1}.[12]

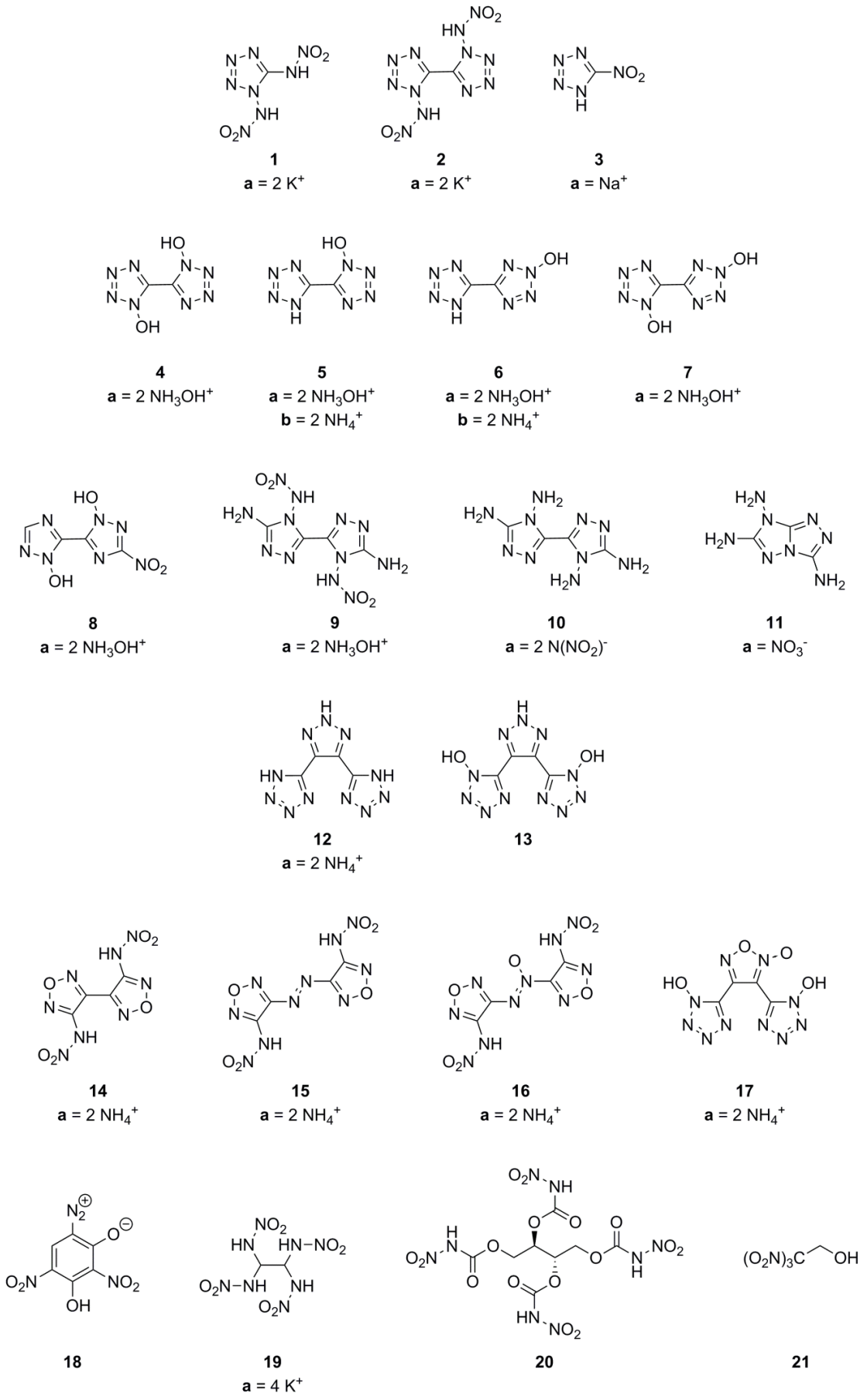

Figure 8.2 Overview of the measured compounds.

The toxicities of different hydroxyl ammonium and ammonium bitetrazolates were determined. Bis(hydroxylammonium) 5,5'-bitetrazole-1,1'-dioxide (**4a**, TKX-50)[16], bis(hydroxylammonium) and bis(ammonium) 5-(1-oxidotetrazolyl)-tetrazolate (**5a** and **5b**)[17], bis(hydroxylammonium) and bis(ammonium) 5-(2-oxidotetrazolyl)-tetrazolate (**6a** and **6b**)[18] and bis(hydroxylammonium) 5,5'-bitetrazole 1,2'- dioxide (**7a**)[19] are potential replacements for the secondary explosive RDX. All of these salts as well as the neutral compound 5-(1*H*-tetrazolyl)-2-hydroxytetrazole monohydrate (**6**)[18] were tested by the luminescent bacteria inhibition test. In Figure 8.3 the inhibition of the luminescent bacteria is plotted against the concentration of these hydroxylammonium and ammonium salts. The ammonium salts **5b** and **6b** showed with EC_{50} values of 3.68 g L^{-1} and 1.03 g L^{-1}, respectively, low toxicities towards the marine bacteria. However, the exchange of the none toxic ammonium cation with the hydroxylammonium cation significantly increases the toxicity of the bitetrazolate salts. With EC_{50} values in the range of 0.18–0.58 g L^{-1} after 30 min incubation the compounds are classified as toxic. Nevertheless for compounds **4a** (EC_{50} (30 min) = 0.58 g L^{-1}) and **5a** (EC_{50} (30 min) = 0.33 g L^{-1}) lower toxicities than for RDX (EC_{50} (30 min) = 0.24 g L^{-1}) were observed. The EC_{50} value for the neutral bitetrazole **6** (EC_{50} (30 min) = 0.33 g L^{-1}) is between the value for the hydroxylammonium salt **6a** and the ammonium salt **6b**.

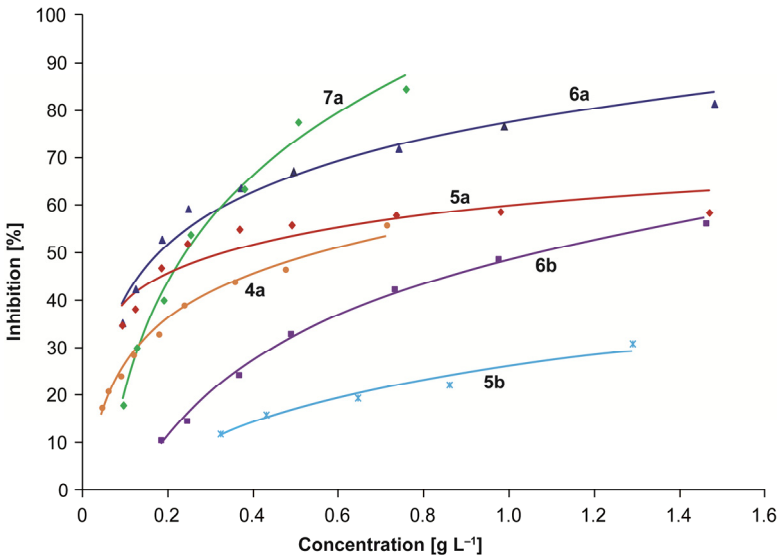

Figure 8.3 Diagram of the inhibition of the hydroxylammonium and ammonium salts of compounds **4**–**7** after 30 min of incubation.

Also the toxicities of the hydroxylammonium salts of 3,3'-dinitro-5,5'-bi-1,2,4-triazole-1,1'-diol (**8a**, MAD-X1)[20] and 5,5'-diamino-4,4'-dinitramino-3,3'-bi-1,2,4-triazole (**9a**)[21] have been investigated (Figure 8.4). Both compounds are toxic to aquatic life with EC_{50} values of 0.24 g L^{-1} (**8a**) and 0.35 g L^{-1} (**9a**). The neutral compound 5,5'-diamino-4,4'-

dinitramino-3,3'-bi-1,2,4-triazole (**9**)[21] is classified as very toxic (EC_{50} (30 min) = 0.07 g L^{-1}).

The thermally stable nitrogen-rich aromatic cations have been investigated, too. Toxicity measurements for 4,4',5,5'-tetramino-3,3'-bi-1,2,4-triazolium dinitramide (**10a**)[22] as well as 3,6,7-triamino-7*H*-[1,2,4]triazolo[4,3-b][1,2,4]triazolium nitrate (**11a**)[23] and its neutral analogue 3,6,7-triamino-7*H*-[1,2,4]triazolo[4,3-b][1,2,4]triazole (**11**)[24] showed EC_{50} values higher than 3.36 g L^{-1} and are therefore low toxic for marine organisms.

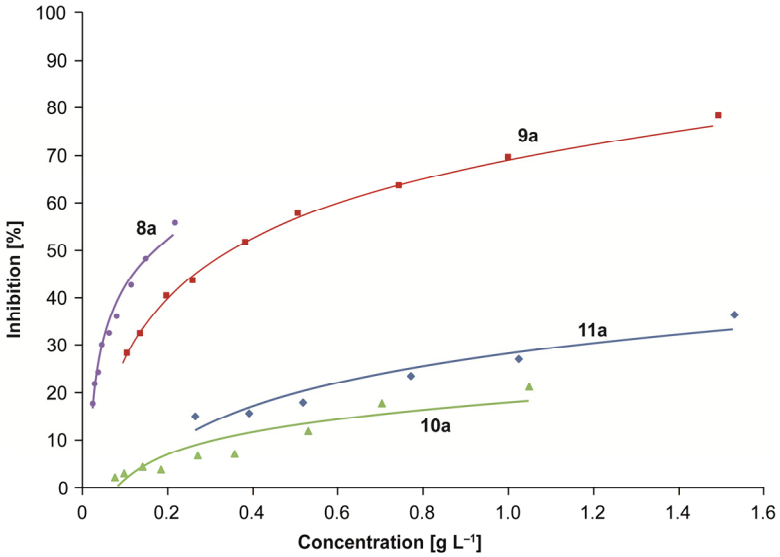

Figure 8.4 Diagram of the inhibition of the 1,2,4-triazoles salts **8**–**11** after 30 min of incubation.

The compounds 4,5-bi-(1*H*-tetrazol-5-yl)-2*H*-1,2,3-triazole (**12**) and 4,5-bi-(1-hydroxytetrazol-5-yl)-2*H*-1,2,3-triazole (**13**) combine the advantages of the triazole and tetrazole heterocycles by forming energetic and thermally stable molecules.[25] For toxicity measurements the ammonium salt of compound **12** as well as the neutral compound **13** were investigated. While bis(ammonium) 4,5-bi-(1*H*-tetrazol-5-yl)-2*H*-1,2,3-triazolate (**12a**) is less toxic to *V. fischeri* (EC_{50} (30 min) = 1.82 g L^{-1}) a decrease of luminescence is observed for compound **13** (EC_{50} (30 min) = 0.55 g L^{-1}). Nevertheless, compound **13** is still less toxic than the secondary explosive RDX.

The energetic nitrofurazans 3,3'-dinitramino-4,4'-bifurazan (**14**), 3,3'-dinitramino-4,4'-azobifurazan (**15**), 3,3'-dinitramino-4,4'-azoxybifurazan (**16**) and bi (1-oxidotetrazolyl)-furazan (**17**) and their salts are also possible RDX replacements.[26] For toxicity assessment the ammonium salts of these compounds (**14a**, **15a**, **16a** and **17a**) were tested (Figure 8.5). The bifurazan salt **14a** and the bi(tetrazolyl)-furazan salt **17a** show both low toxicities while the azo-bridged compounds posses moderate (**16a**) to high toxicities (**15a**) towards aquatic life. Unfortunately, also the thermal stabilities and sensitivities of most of the furazan compounds are worse than of RDX.

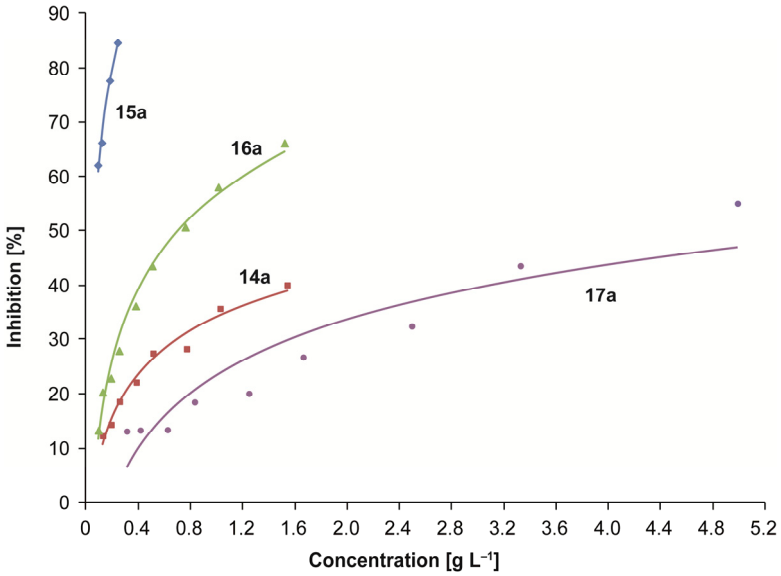

Figure 8.5 Diagram of the inhibition of the furazan salts **14**–**17** after 30 min of incubation.

6-Diazonium-3-hydroxy-2,4-dinitrophenolate (**18**) is a derivative of the commercially used primary explosive 2-diazonium-4,6-dinitrophenolate (DDNP). Chemical and physical studies as well as detonation calculations showed similar or even better properties than DDNP. However toxicity measurements of the benzene derivative **18** revealed a high toxic effect on the marine bacteria (EC_{50} (30 min) = 0.01 g L^{-1}).

1,1,2,2-Tetranitraminoethan (**19**) was first synthesized in 1988 as an intermediate for the synthesis of CL-20.[27] However, compound **19** itself and the salts thereof are already energetic materials with a high oxygen content, high density and high thermal stability. Toxicity measurements of the potassium salt of **19** (**19a**)[28] showed even at high concentrations negligible effects on the luminescence of the bacteria (EC_{50} = > 15.07 g L^{-1}). Therefore compound **19a** is more than 50 times less toxic to the bacteria *V. fischeri* than RDX.

The synthesis of *meso*-erythritol tetranitrocarbamate (**20**) started from corresponding sugar alcohol by an economically benign two-step synthesis.[29] Primary nitrocarbamates form a new class of energetic materials with good detonation performances and lower sensitivities than the commonly used nitrate ester explosive PETN. During the toxicity measurements a moderate inhibition of luminescence was observed for compound **20** (EC_{50} = 0.87 g L^{-1}) which is in comparison to RDX still less toxic.

An important building block for the synthesis of oxygen rich energetic compounds is the 2,2,2-trinitroethanol (**21**). It is formed by a simple HENRY reaction starting from trinitromethane and formaldehyde.[5b,30] In contact with nucleophiles and bases it

decomposes into its starting materials. When measuring the toxicity of the alcohol **21** and its decomposition products by the luminescent bacteria inhibition test an EC_{50} value of 0.22 g L^{-1} was determined. Therefore compound **21** has to be classified as toxic.

8.5 Conclusion

The toxicities of several neutral as well as ionic energetic compounds have been tested using the luminescence bacteria inhibition test. During the measurements of commercially available and energetic salts a minor toxic effect of the ammonium, potassium and sodium cations was found whereas the hydroxylammonium cation showed a considerable toxicity.
For the primary explosives measured (**1a** and **2a**) and the sodium salt **3a**, a precursor for the synthesis of DBX-1, hardly no toxicities towards the marine bacteria were observed. Also most of the secondary explosives revealed good to excellent properties regarding the toxicity to aquatic life. The potassium salt **19a** exhibits with a value higher than 15.07 g L^{-1} the lowest toxicity and is therefore more than 50 times less toxic than RDX (EC_{50} = 0.24 g L^{-1}) followed by several ammonium salts. The highest toxicities were observed for the neutral bitetrazole **9** as well as for the azoxy coupled furazan ammonium salt **15a** and the phenol derivative **18**. For the intensively investigated secondary explosives **4a** (TKX-50) and **8a** (MAD-X1) EC_{50} values similar to RDX were observed.

8.6 References

[1] P. F. Pagoria, G. S. Lee, A. R. Mitchell, R. D. Schmidt, *Thermochim. Acta* **2002**, *384*, 187–204.

[2] a) B. S. Levine, E. M. Furedi, D. E. Gordon, J. M. Burns, P. M. Lish, *Toxicol. Lett.* **1981**, *8*, 241–245; b) J. K. Haseman, J. Huff, G. A. Boorman, *Toxicol. Pathol.* **1984**, *12*, 126–135; c) P. Richter-Torres, A. Dorsey, C. S. Hodes, U.S. Department of Health and Human Services, Agency for Toxic Sbstances and Disease Registry, *Toxicological profile for 2,4,6-trinitrotoluene*, Atlanta, Georgia, **1995**; d) E. L. Etnier, W. R. Hartley, *Regul. Toxicol Pjarmacol.* **1990**, *11*, 118–122; e) Y. P. Robidoux, J. Hawari, G. Bardai, L. Paquet, G. Ampleman, S. Thiboutot, I. G. Sunahara, *Archives of Environmental Contamination and Toxicology*, *43*, 379–388.

[3] H. Abadin, A. Ashizawa, Y.-W. Stevens, F. Llados, G. Diamond, G. Sage, M. Citra, A. Qinones, S. Bosch, S. Swarts, Agency for Toxic Substances and Disease Registry, *Toxicological Profile for Lead*, Atlanta, Georgia, **2007**.

[4] Institut für Arbeitsschutz der Deutschen Gesetzlichen Unfallversicherung. http://www.dguv.de/ifa/index.jsp (accessed April 06, 2016).

[5] a) P. Mühle, *Untersuchung der Bleiaufnahme bei kurzzeitigen Aufenthalten in Schießständen*, Dissertation, Ludwig-Maximilians-Universität München (Munich), **2010**; b) T. M. Klapötke, *Chemistry of High-Energy Materials*, 3rd ed., De Gruyter, Berlin (Germany), **2015**.

[6] R. Meyer, J. Köhler, A. Homburg, *Explosives*, Wiley-VCH, Weinheim, **2007**.

[7] M. Farré, D. Barceló, *TrAC, Trends Anal. Chem.* **2003**, *22*, 299–310.

[8] S. Parvez, C. Venkataraman, S. Mukherji, *Environ. Int.* **2006**, *32*, 265–268.

[9] K. L. Kaiser, *Environ. Health Perspect.* **1998**, *106*, 583–591.

[10] J.-J. Bourgois, F. E. Sluse, F. Baguet, J. Mallefet, *J. Bioenerg. Biomembr.*, *33*, 353–363.

[11] S. Inouye, *FEBS Lett.* **1994**, *347*, 163–168.

[12] C. J. Cao, M. S. Johnson, M. M. Hurley, T. M. Klapötke, *JANNAF J. Propuls. Energet.* **2012**, *5*, 41–51.

[13] a) A. Srinivasan, T. Viraraghavan, *International Journal of Environmental Research and Public Health* **2009**, *6*, 1418–1442; b) J. Wolff, *Pharmacol. Rev.* **1998**, *50*, 89–105.

[14] D. Fischer, T. M. Klapötke, J. Stierstorfer, *Angew. Chem., Int. Ed.* **2015**, *54*, 10299–10302.

[15] a) J. W. Fronabarger, M. D. Williams, W. B. Sanborn, J. G. Bragg, D. A. Parrish, M. Bichay, *Propellants, Explos., Pyrotech.* **2011**, *36*, 541–550; b) T. M. Klapötke, D. G. Piercey, N. Mehta, K. D. Oyler, M. Jorgensen, S. Lenahan, J. S. Salan, J. W. Fronabarger, M. D. Williams, *Z. Anorg. Allg. Chem.* **2013**, *639*, 681–688.

[16] N. Fischer, D. Fischer, T. M. Klapötke, D. G. Piercey, J. Stierstorfer, *J. of Mater. Chem.* **2012**, *22*, 20418–20422.

[17] D. Fischer, T. M. Klapötke, M. Reymann, P. C. Schmid, J. Stierstorfer, M. Sućeska, *Propellants, Explos., Pyrotech.* **2014**, *39*, 550–557.

[18] T. M. Klapötke, M. Q. Kurz, R. Scharf, P. C. Schmid, J. Stierstorfer, M. Suceska, *ChemPlusChem* **2015**, *80*, 97–106.

[19] K. Hafner, T. M. Klapötke, P. C. Schmid, J. Stierstorfer, *Eur. J. Inorg. Chem.* **2015**, *2015*, 2794–2803.

[20] T. M. Klapötke, A. Dippold **2014**, WO2014086599A1.

[21] T. M. Klapötke, M. Leroux, P. C. Schmid, J. Stierstorfer, *Chem. – Asian J.* **2016**, *11*, 844–851.

[22] T. M. Klapötke, P. C. Schmid, S. Schnell, J. Stierstorfer, *J. Mater. Chem.* **2015**, *3A*, 2658–2668.

[23] T. M. Klapötke, P. C. Schmid, S. Schnell, J. Stierstorfer, *Chem. – Eur. J.* **2015**, *21*, 9219–92228.

[24] K. T. Potts, H. R. Burton, J. Bhattacharyya, *J. Org. Chem.* **1966**, *31*, 260–265.

[25] A. A. Dippold, D. Izsak, T. M. Klapötke, C. Pflüger, *Chem. - Eur. J.* **2016**, *22*, 1768–1778.

[26] D. Fischer, T. M. Klapötke, M. Reymann, J. Stierstorfer, *Chem. – Eur. J.* **2014**, *20*, 6401–6411.

[27] a) Y. Zheng, J. Zhou, D. Zhou, M. Zhang, *Binggong Xuebao* **1988**, 59–63; b) D. Wan, *Proc. Int. Pyrotech. Semin.* **1991**, *17th*, 231–234.

[28] Y. Lee, P. Goede, N. Latypov, H. Oestmark, *Int. Annu. Conf. ICT* **2005**, *36th*, 124/121–124/129.

[29] Q. J. Axthammer, T. M. Klapötke, B. Krumm, *Chem. – Asian J.* **2016**, *11*, 568–575.

[30] Q. Zhang, J. Zhang, D. A. Parrish, J. M. Shreeve, *Chem. – Eur. J.* **2013**, *19*, 11000–11006.

III Summary and Conclusion

Currently the most commonly used oxidizer in solid rocket propellants is ammonium perchlorate (AP). However, there are environmental, toxic and tactical reasons for which AP should be replaced. Additionally to this, it was found that AP is incompatible with the binder system and shows low-temperature thermal decomposition. Therefore, research is driven to find an alternative replacing AP for the application in solid rockt propellants. For the utilization as high-energy dense oxidizers (HEDOs) the compounds have to fulfill several requirements like high oxygen content (Ω_{co} > 25%), high thermal stability (T_{dec} >150 °C), moderate sensitivity (IS >4 J, FS > 80 N), and high specific impulses (I_s > 250 s). The specific impulse is an important performance parameter since an increase by 20 s approximately doubles the maximum possible carried payload.

In the course of this thesis, many novel energetic materials based on the insertion of fluorodinitromethyl and trinitromethyl moieties have been synthesized and thoroughly characterized. Most compounds show satisfying thermal stabilities as well as adequate stabilities towards external stimuli. Due to their high oxygen contents most compounds achieve a positive oxygen balance. Therefore, these materials are classified as HEDOs suitable for the use as environmental friendly oxidizer in solid rocket composite propellants.

1 Carbonyl Diisocyanate $CO(NCO)_2$

In the first chapter the solid and gas phase structures of carbonyl diisocyanate $CO(NCO)_2$ (**S1**) were investigated. Compound **S1** is a derivative of the well-known but unstable carbonic acid H_2CO_3. Due to its high reactivity **S1** is a suitable starting material for the synthesis of HEDOs as well as energetic polymers. In this chapter a convenient synthesis was presented starting from trichloroisocyanuric acid (Scheme S1.1) using trichloromethyl chloroformate (diphosgene), which is liquid at room temperature, instead of the gaseous phosgene.

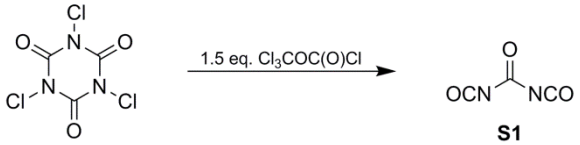

Scheme S1.1 Synthesis of carbonyl diisocyanate (**S1**) by reaction of trichloroisocyanuric acid with diphosgene.

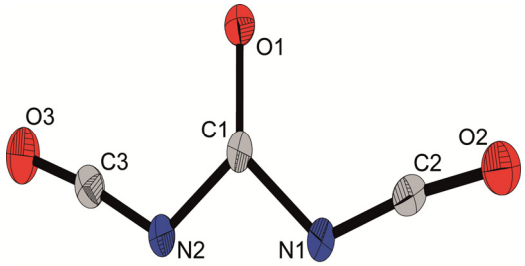

Figure S1.1 Solid phase structure of carbonyl diisocyanate (**S1**).

The molecular structure of **S1** is shown in Figure S1.1. In the solid state solely molecules in the planar *syn–syn* conformation were observed. Additional gas-phase electron diffraction (GED) was used to determine the structure of the free molecule of **S1** in the gas-phaseexperimentally. During the experiments a distribution of the *syn–syn* and *anti–syn* conformers of 2:1 was found, whereat the *syn–syn* conformer is the dominant conformation.

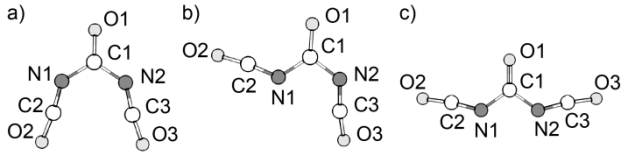

Figure S1.2 Optimized structures of *anti–anti* (a), *syn–anti* (b) and *syn–syn* conformers (c).

2 (2-FLUORO-2,2-DINITROETHYL)-2,2,2-TRINITROETHYLNITRAMINE

(2-Fluoro-2,2-dinitroethyl)-2,2,2-trinitroethylamine (**S3**) was synthesized by a Mannich type reaction of 2-fluoro-2,2-dinitroethylamine (**S2**) and 2,2,2-trinitroethanol. Further nitration of **S3** furnished the corresponding oxygen-rich (2-fluoro-2,2-dinitroethyl)-2,2,2-trinitroethylnitramine (**S4**) in good yields (Scheme S2.1).

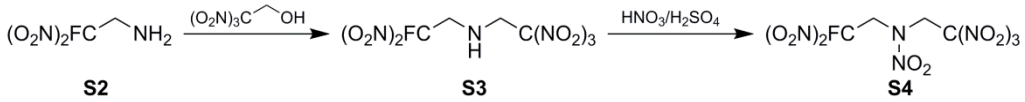

Scheme S2.1 Synthesis of (2-fluoro-2,2-dinitroethyl)-2,2,2-trinitroethylamine (**S3**) and its nitration to **S4**.

All compounds were comprehensively characterized including X-ray molecular structures. Compound **S4** is a promising candidate for replacing AP in solid rocket composite propellants. It has a decomposition temperature of 166 °C, a suitable oxygen balance Ω_{co} of 28.8%, and an improved specific impulse I_s of 266 s compared to the specific

impulse I_s of AP (258 s). The specific impulses were calculated for composite propellants consisting of fuel, oxidizer and additives (EXPLO5 V6.01, equilibrium expansion).

3 MICHAEL ADDITION OF TRINITROMETHANE

The Michael addition of trinitromethane and acrylamide furnished several compounds with a positive oxygene balance in a simple and straightforward synthesis. The most promising molecules of this chapter are the chloride, nitrate, perchlorate, and dinitramide salts of 3,3,3-trinitropropanammonium (**S5a–d**) (Figure S3.1).

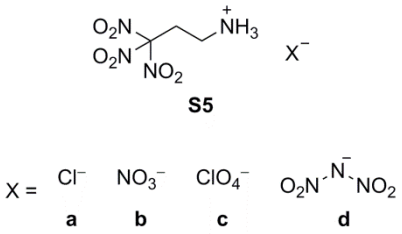

Figure S3.1 Selected synthesized salts of 3,3,3-trinitropropanammonium (**S5a–d**).

Table S3.1 Physical and energetic properties as well as selected detonation and combustion parameters of compounds **S5a–c** compared to AP.

	S5b	**S5c**	**S5d**	**AP**
formula	$C_3H_7N_5O_9$	$C_3H_7N_4O_{10}Cl$	$C_3H_7N_7O_{10}$	NH_4ClO_4
ρ [g cm^{-3}][a]	1.77	1.97	1.84	1.95
T_{dec} [°C][b]	138	164	112	240
Ω_{CO} [%][c]	+15.6	+21.7	+18.6	+34.6
$\Delta H°_f$ [kJ mol^{-1}][d]	−169	−119	32	−296
$-Q_v$ [kJ kg^{-1}][e]	6697	6250	6671	1422
p_{CJ} [kbar][f]	335	390	372	158
V_{det} [m s^{-1}][g]	8913	9096	9282	6368
I_{sp} [s] [h]	274	265	274	157
I_{sp} [s] (15% Al)[i]	278	270	278	235
I_{sp} [s] (15% Al, 14% binder)[j]	270	272	275	261

[a] Density at room temperature. [b] Decomposition temperature. [c] Oxygen balance assuming the formation of CO. [d] Enthalpy of formation. [e] Heat of detonation. [f] Detonation pressure. [g] Detonation velocity. [h] Specific impulse. [i] Specific impulse in compositions containing 15% aluminum. [j] Specific impulse in compositions containing 15% aluminum and 14% binder (6% polybutadiene acrylic acid, 6% polybutadiene acrylonitrile and 2% bisphenol A ether).

Especially the dinitramide salt **S5d** shows extraordinary detonation and combustion parameters. With a detonation velocity of 9282 m s^{-1} and a detonation pressure of 372 kbar it exceeds TNT, PETN, and RDX by far. Also the specific impulse I_s calculated for a mixture consisting of 15% aluminum, 14% binder and 71% oxidizer achieved a remarkable value of 275 s in comparison to a similar mixture of AP [261 s (EXPLO5 V6.02, equilibrium expansion)] as shown in Table S3.1. Also the salts **S5b** and **S5c** show an improved specific impulse I_s of 270 s (**S5b**) and 272 s (**S5c**) compared to AP. However, the thermal stabilities of the nitrate and dinitramide salt **S5d** (138 °C) and **S5d** (112 °C) are rather low while the perchlorate salt **S5c** has to face the same environmental and toxic problems as AP.

4 THE 3,3,3-TRINITROPROPYL UNIT

In Chapter 4 the 3,3,3-trinitropropyl unit was introduced to several different functionalities. In the first step the amine **S5** was reacted with nitric acid to obtain 3,3,3- trinitropropanol (**S6**) in good yields (Scheme S4.1). The amine **S5a** as well as the alcohol **S6** were suitable starting materials for the synthesis of several new oxygen-rich compounds. An excerpt of the most promising synthesized molecules is shown in Figure S4.1.

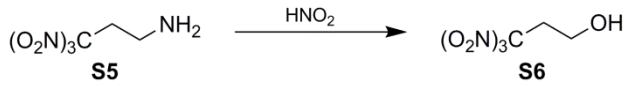

Scheme S4.1 Synthesis of 3,3,3-trinitropropanol (**S6**) from 3,3,3-trinitropropan-amine (**S5**) and nitric acid.

The molecule with the highest oxygen and nitrogen contents is the nitramine **S10** (Figure S4.2) which was synthesized by a simple Mannich type reaction of the amine **S5a** and the alcohol 2,2,2-trinitroethanol followed by a nitration. With a decomposition temperature of

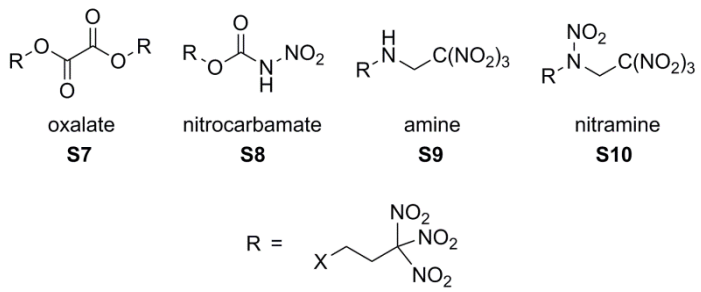

Figure S4.1 Overview of the most promising molecules containing the 3,3,3-trinitropropyl unit.

153 °C, a room temperature density of 1.89 g cm^{-3} and sensitivities to external stimuli lower than PETN it has promising physical properties. The calculated detonation velocity (9119 m s^{-1}) is higher than for the commonly used secondary explosives RDX, PETN, and TNT and the specific impulse in a mixture of oxidizer, fuel, and binder (267 s) exceeds the specific impulse of a similar mixture containing AP as oxidizer [261 s (EXPLO5 V6.02, equilibrium expansion)].

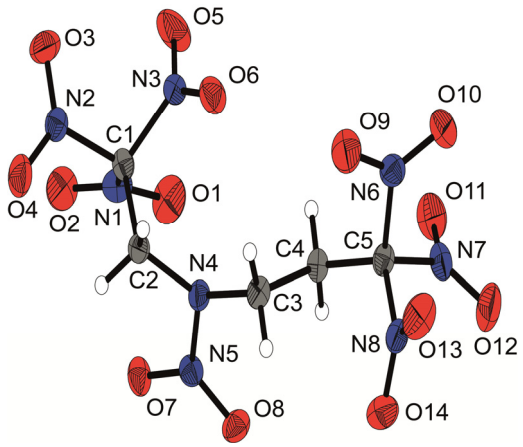

Figure S4.2 X-ray molecular structure of *N*-(2,2,2-trinitroethyl)-*N*-(3,3,3-trinitropropyl) nitramine **S10**.

5 Oxalyl Based Energetic Polynitro Derivatives

In Chapter 5 new compounds with high oxygen contents were synthesized and characterized based on oxalyl chloride. Amongst other interesting molecules bis(2,2,2-trinitroethyl) oxalate (**S11**) and the unsymmetrical 2,2,2-trinitroethyl (3,3,3-trinitropropyl) oxalate (**S12**) were obtained (Figure S5.1).

For a better comparability several physical and energetic properties of the oxalates **S11**, **S12,** and **S7** (Chapter 4) are summarized in Table S5.1. With decreasing carbon content the room temperature densities increase [1.67 g cm^{-3} (**S7**), 1.84 g cm^{-3} (**S11**)]. The highest decomposition temperature was found the oxalate **S11** (186 °C) (Figure S5.2), while the

Figure S5.1 Molecular structures of bis(2,2,2-trinitroethyl) oxalate (**S11**) and 2,2,2-trinitroethyl (3,3,3-trinitropropyl) oxalate (**S12**).

lowest was measured for the unsymmetrical oxalate **S12** (168 °C). With 30.8% the oxalate **S11** possesses the highest oxygen content assuming the formation of CO of all compounds discussed in this thesis. Corresponding to the densities and oxygen balances are the calculated detonation and combustion parameters. While for **S11** a detonation velocity of 8275 m s^{-1} was found, it was decreased by more than 500 m s^{-1} for **S7**. The best specific impulse in mixtures consisting of fuel, oxidizer, and binder was calculated for **S11** with 256 s, followed by **S12** with 251 s (EXPLO5 V6.02, equilibrium expansion). The insertion of two methylene moieties lowers the specific impulse to 246 s (**S7**).

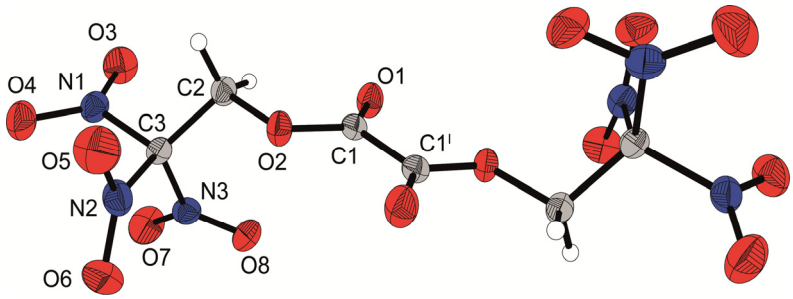

Figure S5.2 X-ray molecular structure of bis(2,2,2-trinitroethyl) oxalate (**S11**).

Table S5.1 Physical and energetic properties as well as selected detonation and combustion parameters of compounds **S11**, **S12**, and **S7** compared to AP.

	S11	**S12**	**S7**	**AP**
formula	$C_6H_4N_6O_{16}$	$C_7H_6N_6O_{16}$	$C_3H_7N_7O_{10}$	NH_4ClO_4
ρ [g cm^{-3}][a]	1.84	1.73	1.67	1.95
T_{dec} [°C][b]	186	168	170	240
Ω_{CO} [%][c]	+30.8	+22.3	+14.4	+34.6
$\Delta H°_f$ [kJ mol^{-1}][d]	−688.0	−705.2	−789.4	−296
$-Q_v$ [kJ kg^{-1}][e]	5177	5839	5126	1422
p_{CJ} [kbar][f]	286	270	256	158
V_{det} [m s^{-1}][g]	8275	8071	7732	6368
I_{sp} [s] [h]	240	252	250	157
I_{sp} [s] (15% Al)[i]	250	257	259	235
I_{sp} [s] (15% Al, 14% binder)[j]	256	251	246	261

[a] Density at room temperature. [b] Decomposition temperature. [c] Oxygen balance assuming the formation of CO. [d] Enthalpy of formation. [e] Heat of detonation. [f] Detonation pressure. [g] Detonation velocity. [h] Specific impulse. [i] Specific impulse in compositions containing 15% aluminum. [j] Specific impulse in compositions containing 15% aluminum and 14% binder.

6 β-ALANINE AND L-ASPARTIC ACID

Not only for life but also for the synthesis of polynitro compounds amino acids are interesting building blocks due to their natural occurrence, their low toxicity, and their reactive functionalities. In Chapter 6 the amino acids β-alanine and L-aspartic acid were used as basis modules for the synthesis of several new energetic compounds. The most interesting compounds with the highest oxygen contents are the ester **S14**, the nitrocarbamate **S15**, and the acid **S16** (Scheme S6.1).

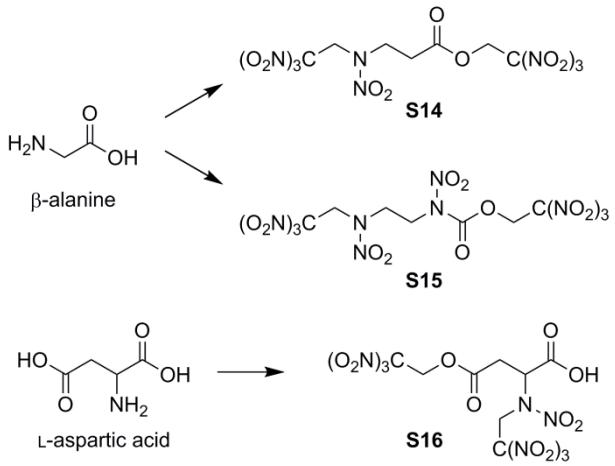

Scheme S6.1 Overview of the oxygen-rich molecules resulting from β-alanine and L-aspartic acid.

Although different reaction conditions were used L-aspartic acid only reacted once with the alcohol 2,2,2-trinitroethanol by forming the ester **S16**. In order to verify the structure of compound **S16** a proton coupled ^{13}C NMR spectrum was recorded. On the basis of splitting patterns and coupling constants the molecular structure of **S16** was determined with the utmost probability. An excerpt of the proton coupled ^{13}C NMR spectrum showing the carbonyl resonances is depicted in Figure S6.1.

All three compounds show satisfying decomposition temperatures, medium sensitivities towards impact and friction, and high nitrogen as well as oxygen contents. Good energetic properties were determined for the nitrocarbamate **S15** with a detonation velocity of 9083 m s^{-1}, a detonation pressure of 365 kbar and a specific impulse in a mixture consisting of fuel, oxidizer and binder of 257 s [AP 258 s (EXPLO5 V6.02, equilibrium to throat and frozen to exit)].

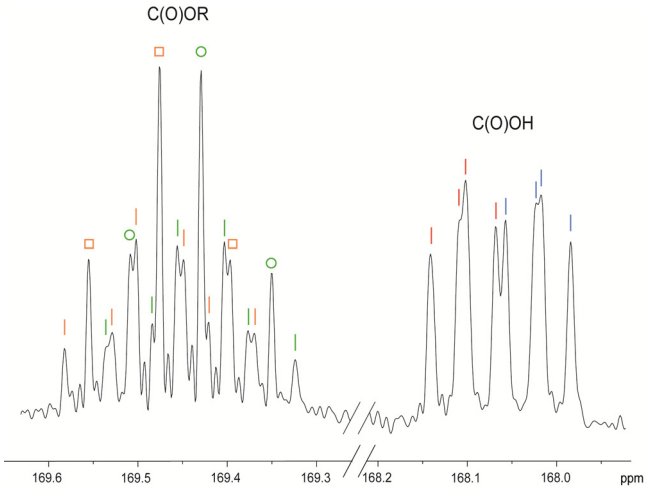

Figure S6.1 Excerpt of the ^{1}H coupled ^{13}C NMR spectrum of **8** showing the carbonyl resonances ([D_6]acetone).

7 *N*-NITROSARCOSINE

N-Methylglycine (sarcosine) is a non-proteinogenic amino acid and a derivative of glycine. Nitration of sarcosine yielded *N*-nitrosarcosine which could be functionalized on the carboxyl group in many different ways. An overview of some of the synthesized polynitro compounds of *N*-nitrosarcosine is given in Scheme S7.1.

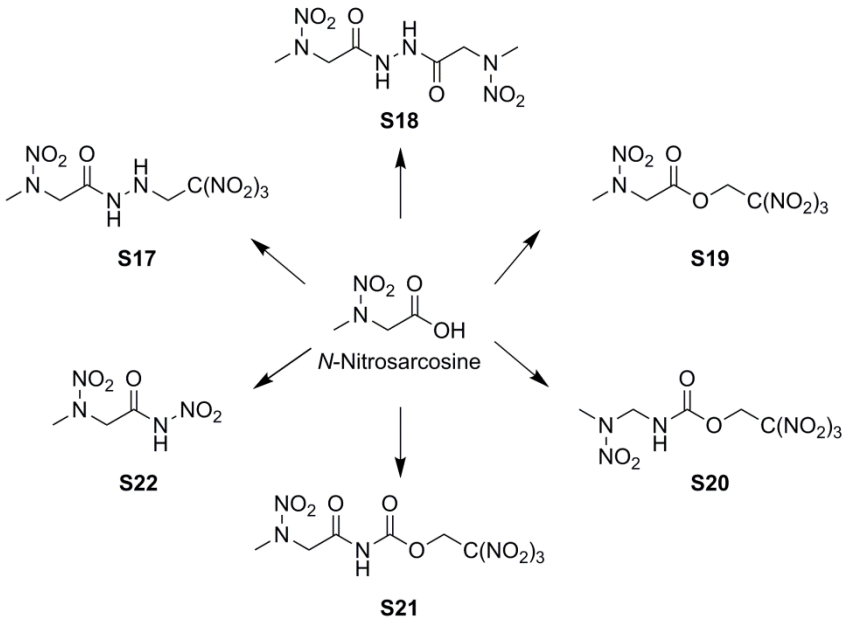

Scheme S7.1 Overview of synthesized polynitro molecules starting from *N*-nitrosarcosine.

The compounds were thoroughly characterized and X-ray molecular structures were obtained. Most compounds show moderate to low sensitivities to impact and friction. For the nitramine **S17** a detonation velocity of 8304 m s^{-1} was calculated which is in the range of PETN. The best specific impulse in mixtures consisting of fuel, oxidizer and additives is found for **S17** (252 s) although no positive oxygen balance was achieved (EXPLO5 V6.02).

8 Toxicity Assessment of Energetic Materials

The aquatic toxicity of various energetic materials is determined by the luminescent bacteria inhibition test. This test uses the bioluminescent bacteria *Vibrio fischeri* (*V. fischeri*) which are an ideal model organism for aquatic life. During the test the decrease of bioluminescence is determined after a certain time in vials with different concentrations of the tested substance and compared to a non-toxic control. From these values a diagram is generated and the effective concentration (EC_{50}) is determined. The EC_{50} value gives the concentrations at which the bioluminescence is inhibited by 50%.

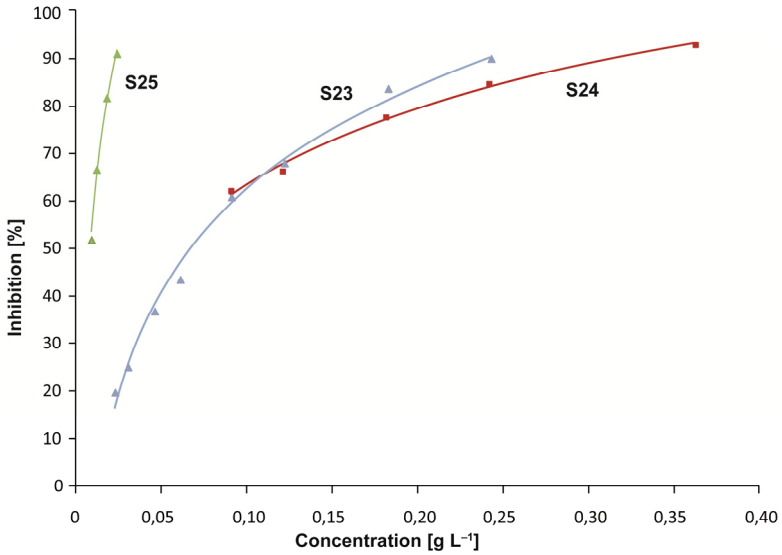

Figure S8.1 Diagram of the inhibition of the very toxic compounds **S23**–**S25** after 30 min of incubation.

For the ammonium, potassium and sodium cations a minor effect on the luminescence of *V. fischeri* is found whereas the hydroxylammonium cation shows a considerable toxicity. Most energetic compounds exhibit a moderate toxicity towards the marine bacteria. For the neutral compound 5,5'-diamino-4,4'-dinitramino-3,3'-bi-1,2,4-triazole (**S23**) (EC_{50} = 0.07 g L^{-1}), the ammonium salt of 3,3'-dinitramino-4,4'-azobifurazan (**S24**) (EC_{50} = 0.07 g L^{-1}) as well as 6-diazonium-3-hydroxy-2,4-dinitrophenolate (**S25**) (EC_{50} =

0.01 g L^{-1}) the highest toxicities are found, while the potassium salt of 1,1,2,2-tetranitraminoethane (**S26**) (EC_{50} > 15.07 g L^{-1}) shows a more than 50 times less toxic effect to the bacteria than RDX (EC_{50} = 0.24 g L^{-1}).

9 General Conclusion

Several interesting new compounds with high oxygen contents have been synthesized and thoroughly characterized. In general these compounds contain a carbamate or nitrocarbamate, nitramine, nitramide or oxalyl moiety. Good thermal stabilities, moderate sensitivities towards impact, friction and electrostatic discharge and promising energetic properties were achieved.

High oxygen contents were attained with the trinitromethyl and fluorodinitromethyl functionalities. For the syntheses the Mannich addition of an organic nitro compound like trinitromethane, an aldehyde and an amine was employed as well as the Michael addition of an nucleophile to an α,β-unsaturated carbonyl compound. In this way trinitroethyl and trinitropropyl units were introduced to various compounds.

Oxalyl chloride as well as different proteinogenic and non-proteinogenic amino acids served as basis molecules for the synthesis of HEDOs. Satisfying decomposition temperatures in combination with specific impulses of more than 250 s were obtained. However, to predict the specific impulses solely from the oxygen content of the compounds is not possible. Also small molecules with a lower oxygen content could reach promising specific impulses.

With regard to future works on HEDOs especially small molecules with high oxygen contents would be of great interest. Amino acids or in the biosynthesis of vertebrates natural occurring molecules are suitable and interesting starting compounds for the synthesis of environmental benign oxygen-rich compounds, since they are easily available, show no toxicity and possess multiple functionalities to introduce oxygen-rich moieties.

IV Appendix

1 Appendix A1

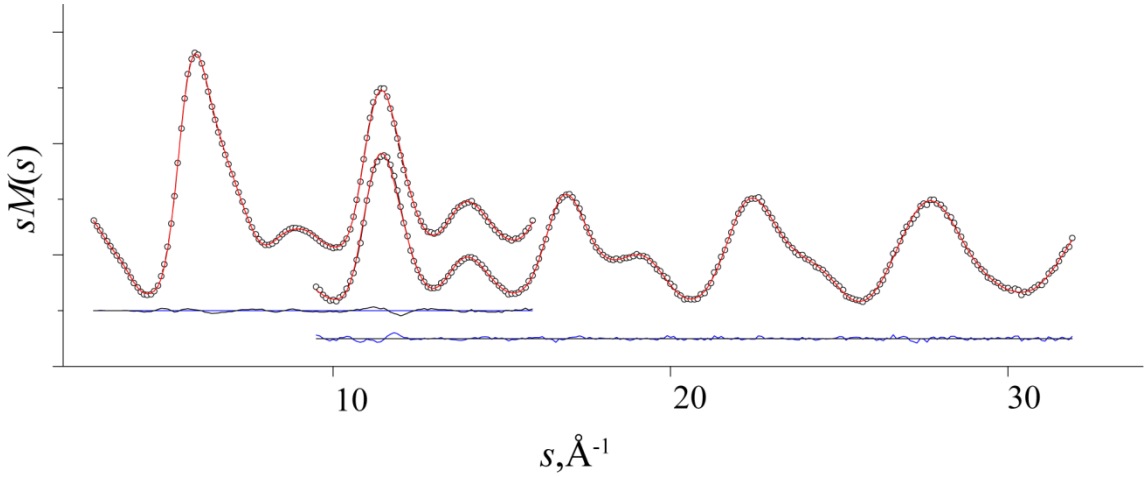

Figure A1.1 Experimental (dots) and model (lines) molecular intensity curves of $C(O)(NCO)_2$ for short and long nozzle-to-plate distances. Difference curves are shown at the bottom.

Table A1.1 Interatomic distances(r_a), mean square vibrational amplitudes (l) and vibrational corrections (corr) to equilibrium geometry in the optimized GED model of *syn-syn* C(O)(NCO)$_2$.[a] Gu indicates grouping of amplitudes for common refinement.

At1	At2	r_a	l	corr	Gu
C6	O8	1.186720	0.068873	-0.036900	101
C7	O9	1.186720	0.068873	-0.036900	101
C1	O3	1.198820	0.017973	-0.003100	101
N4	C6	1.218410	0.041873	-0.005700	101
N5	C7	1.218410	0.041873	-0.005700	101
C1	N5	1.400126	0.027173	-0.008300	101
C1	N4	1.400126	0.027173	-0.008300	101
N4	N5	2.234950	0.060226	-0.011000	102
N5	O3	2.325554	0.056826	-0.008500	102
N4	O3	2.325554	0.056826	-0.008500	102
C1	C7	2.328585	0.077926	-0.007000	102
C1	C6	2.328585	0.077926	-0.007000	102
N4	O8	2.361249	0.044826	-0.004700	102
N5	O9	2.361249	0.044826	-0.004700	102
C7	O3	2.843662	0.118387	-0.020600	103
C6	O3	2.843662	0.118587	-0.020600	103
N5	C6	3.406185	0.063017	-0.004300	104
N4	C7	3.406185	0.063017	-0.004300	104
C1	O8	3.423561	0.122717	-0.003000	104
C1	O9	3.423561	0.122417	-0.003000	104
O3	O8	3.741284	0.210617	-0.019200	104
O3	O9	3.741284	0.210217	-0.019200	104
C6	C7	4.564038	0.113028	-0.021600	105
N5	O8	4.567898	0.109128	-0.017300	105
N4	O9	4.567898	0.109328	-0.017300	105
C7	O8	5.685456	0.134170	-0.004300	106
C6	O9	5.685456	0.134170	-0.004300	106
O8	O9	6.871280	0.160112	-0.057000	107

[a] All values in Å, corrections were calculated using SHRINK program from MP2/cc-pVTZ and cubic force fields. The amplitudes were refined in groups by multiplying on the scale factors (one per group), which were treated as independent parameters.

Table A1.2 Interatomic distances (r_a), mean square vibrational amplitudes (l) and vibrational corrections (corr) to equilibrium geometry in the optimized GED model of *syn-anti* C(O)$(NCO)_2$.[a] Gu indicates grouping of amplitudes for common refinement.

At1	At2	r_a	l	corr	Gu
C6	O8	1.153390	0.014973	-0.004500	101
C7	O9	1.154710	0.014973	-0.004500	101
C1	O3	1.193840	0.017673	-0.003200	101
N5	C7	1.221420	0.044973	-0.006400	101
N4	C6	1.248730	0.112073	-0.036600	101
C1	N5	1.396716	0.027073	-0.008100	101
C1	N4	1.416006	0.028973	-0.007900	101
N5	O3	2.284259	0.055526	-0.008400	102
N4	N5	2.306144	0.061726	-0.010500	102
N4	O3	2.326070	0.057526	-0.008600	102
C1	C6	2.349413	0.074826	-0.010100	102
C1	C7	2.360329	0.079226	-0.007700	102
N5	O9	2.380523	0.077526	-0.018700	102
N4	O8	2.399904	0.199426	-0.041900	102
N4	C7	2.676094	0.040826	-0.004200	102
C6	O3	2.830863	0.055587	-0.005700	103
C1	O8	3.432876	0.116417	-0.007700	104
C7	O3	3.439893	0.150117	-0.024300	104
C1	O9	3.454816	0.124817	-0.004100	104
N5	C6	3.467569	0.063017	-0.004000	104
N4	O9	3.493918	0.067417	-0.004600	104
O8	O3	3.714042	0.098617	-0.016000	104
C6	C7	3.881164	0.168517	-0.004900	104
O9	O3	4.576805	0.227628	-0.024700	105
N5	O8	4.610847	0.082128	-0.004400	105
C6	O9	4.642079	0.196128	-0.013000	105
C7	O8	5.011018	0.270228	-0.002700	105
O8	O9	5.725083	0.361770	-0.020500	106

[a] All values in Å, corrections were calculated using SHRINK program from MP2/cc-pVTZ and cubic force fields. The amplitudes were refined in groups by multiplying on the scale factors (one per group), which were treated as independent parameters.

Table A1.3 Cartesian coordinates (Å) of *syn-syn* $C(O)(NCO)_2$ in the optimized GED model.

N	At	An	Mass	*X*	*Y*	*Z*
1	C	6	12.00000000	-0.000000000000	-0.228094054700	0.000000000000
2	X	-1	0.00000000	-0.000000000000	-0.228094054700	-3.001000000000
3	O	8	15.99491462	-0.000000000000	-1.423814439045	-0.000000000000
4	N	7	14.00307401	1.111974912020	0.608979328273	-0.000000000000
5	N	7	14.00307401	-1.111974912020	0.608979328273	0.000000000000
6	C	6	12.00000000	2.271219123078	0.252862303367	0.000000000000
7	C	6	12.00000000	-2.271219123078	0.252862303367	0.000000000000
8	O	8	15.99491462	3.407140047643	0.074619296799	0.000000000000
9	O	8	15.99491462	-3.407140047643	0.074619296799	0.000000000000

Table A1.4 Cartesian coordinates (Å) of *syn-anti* $C(O)(NCO)_2$ in the optimized GED model.

N	At	An	Mass	*X*	*Y*	*Z*
1	C	6	12.00000000	0.029280686104	-0.855125648982	0.000000000000
2	X	-1	0.00000000	0.029280686104	-0.855125648982	-3.001000000000
3	O	8	15.99491462	0.595695028031	-1.902407520349	-0.000000000000
4	N	7	14.00307401	0.637852218046	0.414678919465	-0.000000000000
5	N	7	14.00307401	-1.353461316465	-0.727534944214	0.000000000000
6	C	6	12.00000000	1.828977881107	0.639355850748	0.000000000000
7	C	6	12.00000000	-2.030707269191	0.281232845661	0.000000000000
8	O	8	15.99491462	2.930683398822	0.965230163137	0.000000000000
9	O	8	15.99491462	-2.770506209129	1.161960645110	-0.000000000000

Table A1.4 Z-matrix used in UNEX program for refinement of syn-syn C(O)(NCO)2. The numbers behind the variables indicate the groups the parameters were refined in.

```
C
X,    1,B9
O,    1,B1, 2,A9
N,    1,B2, 2,A9, 3,A2  1
N,    1,B2, 2,A9, 3,A2  -1
C,    4,B3, 1,A4, 5,D3
C,    5,B3, 1,A4, 4,D3
O,    6,B4, 4,A5, 1,D6
O,    7,B4, 5,A5, 1,D6
Variables:
B1    1.19605    3
B2    1.39139    2
B3    1.21304    3
B4    1.15015    3
A2    127.04166  4
A4    125.97200  6
A5    171.86158  6
D3    180.00
D6    180.00
Constants:
B9    3.001
A9    90.0
```

Table A1.5 Z-matrix used in UNEX program for refinement of syn-anti C(O)(NCO)2 . The numbers behind the variables indicate the groups the parameters were refined in.

```
C
X,    1,B91
O,    1,B11, 2,A91
N,    1,B21, 2,A91, 3,A21  1
N,    1,B22, 2,A91, 3,A22  -1
C,    4,B31, 1,A41, 5,D31
C,    5,B32, 1,A42, 4,D32
O,    6,B41, 4,A51, 1,D61
O,    7,B42, 5,A52, 1,D62
Variables:
B11   1.19097
B21   1.40767    2
B22   1.38818    2
B31   1.21246    3
B32   1.21535    3
B41   1.14922    3
B42   1.15054    3
A21   126.06316  5
A22   123.75464  5
A41   126.46383  7
A42   129.32294  7
A51   174.37938  7
A52   174.02119  7
D31   180.00
D32   0.00
D61   180.00
D62   180.00
Constants:
B91   3.001
A91   90.0
```

Table A1.6 Full listing of structural parameters for *syn-syn* $C(O)(NCO)_2$. r_a, r_g, r_e values are given in Å. Errors correspond to one time standard deviation.

No.	Type	*i*	*j*	*k*	*l*	*a*-Value	*g*-Value	*c*-Value	Error
1	stretch	1	3	0	0	1.19882	1.19909	1.19572	0.00029
2	stretch	1	4	0	0	1.40013	1.40065	1.39183	0.00035
3	stretch	1	5	0	0	1.40013	1.40065	1.39183	0.00035
4	stretch	4	6	0	0	1.21841	1.21985	1.21271	0.00029
5	stretch	5	7	0	0	1.21841	1.21985	1.21271	0.00029
6	stretch	6	8	0	0	1.18672	1.19072	1.14982	0.00029
7	stretch	7	9	0	0	1.18672	1.19072	1.14982	0.00029
8	bend	3	1	4	0			126.97173	0.06562
9	bend	3	1	5	0			126.97173	0.06562
10	bend	4	1	5	0			106.05654	0.13124
11	bend	1	4	6	0			125.95144	0.21560
12	bend	1	5	7	0			125.95144	0.21560
13	bend	4	6	8	0			171.84102	0.21560
14	bend	5	7	9	0			171.84102	0.21560
15	torsion	3	1	4	6			-0.00000	0.00000
16	torsion	3	1	5	7			0.00000	0.00000
17	torsion	6	4	1	5			180.00000	0.00000
18	torsion	4	1	5	7			180.00000	0.00000
19	torsion	1	4	6	8			180.00000	0.00000
20	torsion	1	5	7	9			180.00000	0.00000
21	o.o.p	3	4	1	5			-0.00000	0.00000

Table A1.7 Full listing of structural parameters for *syn-anti* $C(O)(NCO)_2$. r_a, r_g, r_e values are given in Å. Errors correspond to one time standard deviation.

No.	Type	*i*	*j*	*k*	*l*	*a*-Value	*g*-Value	*c*-Value	Error
1	stretch	1	3	0	0	1.19384	1.19410	1.19064	0.00029
2	stretch	1	4	0	0	1.41601	1.41660	1.40811	0.00035
3	stretch	1	5	0	0	1.39672	1.39724	1.38862	0.00035
4	stretch	4	6	0	0	1.24873	1.25879	1.21213	0.00029
5	stretch	5	7	0	0	1.22142	1.22308	1.21502	0.00029
6	stretch	6	8	0	0	1.15339	1.15358	1.14889	0.00029
7	stretch	7	9	0	0	1.15471	1.15490	1.15021	0.00029
8	bend	3	1	4	0			125.98688	0.11115
9	bend	3	1	5	0			123.67836	0.11115
10	bend	4	1	5	0			110.33476	0.22231
11	bend	1	4	6	0			126.28867	0.32853
12	bend	1	5	7	0			129.14778	0.32853
13	bend	4	6	8	0			174.20422	0.32853
14	bend	5	7	9	0			173.84603	0.32853
15	torsion	3	1	4	6			-0.00000	0.00000
16	torsion	3	1	5	7			-180.00000	0.00000
17	torsion	6	4	1	5			180.00000	0.00000
18	torsion	4	1	5	7			0.00000	0.00000
19	torsion	1	4	6	8			180.00000	0.00000
20	torsion	1	5	7	9			180.00000	0.00000
21	o.o.p	3	4	1	5			-0.00000	0.00000

2 APPENDIX A2

Table A2.1 Hydrogen bonds of (2-fluoro-2,2-dinitroethyl)-2,2,2-trinitroethylamine (**2**).

D–H···A			sym. of A	H···A	D–H	D···A	angle, DHA
N10	H2	O10	*x*, *y*, *z*	2.588(3)	0.831(3)	3.327(3)	148.8(1)
C2	H2B	O20	1–*x*, –*y*, 0.5+*z*	2.485(2)	0.991(2)	3.260(3)	134.8(1)
C3	H3A	O12	0.5–*x*, 0.5+*y*, 0.5+*z*	2.480(2)	0.989(2)	3.457(3)	169.2(1)
C3	H3B	O4	*x*, –1+*y*, *z*	2.364(2)	0.990(2)	3.155(3)	136.2(1)
C6	H6A	O6	1–*x*, –*y*, –0.5+*z*	2.578(2)	0.989 (2)	3.483(3)	152.2(1)
C6	H6A	O7	0.5–*x*, 0.5+*y*, –0.5+*z*	2.578(2)	0.989 (2)	3.302(3)	131.9(1)
C7	H7A	O14	*x*, 1+*y*, *z*	2.558(2)	0.990(2)	3.169(3)	127.9(1)
C7	H7B	O6	1–*x*, –*y*, –0.5+*z*	2.414	0.991(2)	3.347(3)	156.9(1)

Table A2.2 Hydrogen bonds of (2-fluoro-2,2-dinitroethyl)-2,2,2-trinitroethylnitramine (**3**).

D–H···A			sym. of A	H···A	D–H	D···A	angle, DHA
C2	H2A	O11	–0.5+*x*, –0.5+*y*, 0.5+*z*	2.543(2)	0.990(2)	3.373(2)	141.2(1)
C3	H3A	O2	0.5–*x*, –0.5+*y*, 0.5+*z*	2.482(1)	0.990(2)	3.179(2)	127.1(1)

Additionally a short dipolar N···O interaction was observed between the nitramine nitrogen N4 with oxygen O4 of a neighbored nitro group. The distance N4···O4 with 2.912(2) Å is shorter than the sum of the van der Waals radii of nitrogen and oxygen (3.07 Å).[1]

3 APPENDIX A3

Table A3.1 Crystallographic data and structure refinements of **1**, **2**, **4**, and **6a**.

	1	**2**	**4**	**6a**
formula	$C_4H_6N_4O_7$	$C_4H_5N_3O_8$	$C_4H_4N_6O_7$	$C_3H_7N_4O_6Cl \times H_2O$
formula weight [g mol^{-1}]	222.11	223.11	248.13	248.58
temperature [K]	100(2)	100(2)	100(2)	100(2)
crystal system	triclinic	monoclinic	triclinic	triclinic
space group (No.)	*P–1*(2)	$P2_1/n$ (14)	*P–1*(2)	*P–1*(2)
a [Å]	6.1081(5)	6.1307(7)	7.4160(5)	6.7434(6)
b [Å]	7.5366(6)	16.7082(6)	7.5385(6)	7.8045(8)
c [Å]	8.8543(7)	8.5025(4)	9.0347(8)	10.0663(10)
α [°]	80.728(7)	90	70.713(8)	90.393(8)
β [°]	87.505(7)	98.296(4)	80.100(7)	98.800(8)
γ [°]	88.355(6)	90	81.601(7)	114.135(9)
V [Å^3]	401.80(6)	861.82(7)	467.47(6)	476.36(8)
Z	2	4	2	2
$\rho_{calc.}$ [g cm^{-3}]	1.836	1.720	1.763	1.733
μ [mm^{-1}]	0.177	0.171	0.168	0.430
F(000)	228	456	252	256
crystal habit	colorless plate	colorless block	colorless block	colorless plate
crystal size [mm]	0.35×0.21×0.05	0.25×0.22×0.18	0.35×0.27×0.25	0.32×0.27×0.08
q range [°]	4.27 – 28.27	4.15 – 26.37	4.20 – 26.36	4.23 – 28.28
index ranges	$-8 \le h \le 8$	$-7 \le h \le 5$	$-9 \le h \le 9$	$-7 \le h \le 8$
	$-10 \le k \le 10$	$-18 \le k \le 20$	$-9 \le k \le 9$	$-10 \le k \le 8$
	$-11 \le l \le 11$	$-8 \le l \le 10$	$-11 \le l \le 11$	$-13 \le l \le 13$
reflections measured	3448	3513	4352	4182
reflections independent	1971	1750	1909	2345
reflections unique	1685	1484	1653	2050
R_{int}	0.019	0.019	0.021	0.021
R_1, wR_2 (2σ data)	0.0308, 0.0735	0.0306, 0.0708	0.0309, 0.0726	0.0287, 0.0641
R_1, wR_2 (all data)	0.0380, 0.0794	0.0384, 0.0764	0.0384, 0.0782	0.0355, 0.0680
data/restraints/parameters	1971/0/154	1750/0/156	1909/0/170	2345/0/172
GOOF on F^2	1.060	1.040	1.040	1.083
residual el. density [e Å^{-3}]	−0.228/0.388	−0.198/0.228	−0.215/0.302	−0.292/0.336
CCDC	1506284	1506285	1506286	1506287

Table A3.2 Crystallographic data and structure refinements of **6b**, **6d**, and **8**.

	6b	**6d**	**8**
formula	$C_3H_7N_4O_6 \cdot NO_3$	$C_3H_7N_4O_6 \cdot N_3O_4$	$C_6H_6N_6O_{14}$
formula weight [g mol^{-1}]	257.14	301.16	386.14
temperature [K]	173(2)	123(2)	173(2)
crystal system	orthorhombic	triclinic	monoclinic
space group (No.)	$P2_12_12_1$ (14)	$P\bar{1}$ (2)	$P2_1/n$ (14)
a [Å]	5.6622(4)	6.7087(5)	5.7264(3)
b [Å]	10.2826(7)	11.2547(7)	21.6530(11)
c [Å]	16.2582(18)	15.2144(9)	11.0910(6)
α [°]	90	75.527(5)	90
β [°]	90	79.280(5)	93.555(4)
γ [°]	90	75.733(6)	90
V [Å^3]	946.59(14)	1068.48(13)	1372.57(12)
Z	4	4	4
$\rho_{calc.}$ [g cm^{-3}]	1.804	1.872	1.869
μ [mm^{-1}]	0.181	0.188	0.188
F(000)	528	616	784
crystal habit	colorless plate	colorless block	colorless plate
crystal size [mm]	0.32×0.28×0.08	0.36×0.13×0.04	0.12×0.11×0.04
q range [°]	4.11 – 31.44	4.19 – 26.00	4.14 – 27.09
index ranges	$-8 \le h \le 7$	$-8 \le h \le 6$	$-3 \le h \le 7$
	$-15 \le k \le 7$	$-13 \le k \le 13$	$-21 \le k \le 27$
	$-11 \le l \le 23$	$-18 \le l \le 18$	$-14 \le l \le 14$
reflections measured	5194	8204	6223
reflections independent	3069	4176	3023
reflections unique	2567	3456	2572
R_{int}	0.029	0.021	0.021
R_1, wR_2 (2σ data)	0.0424, 0.0793	0.0336, 0.0436	0.0301, 0.0652
R_1, wR_2 (all data)	0.0584, 0.0883	0.1020, 0.1144	0.0390, 0.0700
data/restraints/parameters	3069/0/175	4176/0/361	3023/0/259
GOOF on F^2	1.058	0.826	1.025
residual el. density [e Å^{-3}]	−0.229/0.418	−0.288/0.278	−0.240/0.379
CCDC	1506288	1506289	1506290

Table A3.3 Hydrogen bonds of 4,4,4-trinitrobutanamide (**1**).

D–H···A			sym. of A	H···A	D–H	D···A	angle, DHA
C3	H3	O5	1–*x*, 1–*y*, –*z*	2.702	0.96	3.600	155.6
C2	H2	O4	1–*x*, 1–*y*, 1–*z*	2.434	0.95	3.276	145.7
N4	H6	O7	2–*x*, –*y*, 1–*z*	2.073	0.89	2.933	170.9
N4	H5	O6	2–*x*, 1–*y*, –*z*	2.440	0.86	3.314	168.3
C2	H1	O7	2–*x*, 1–*y*, 1–*z*	2.640	0.95	3.531	156.2

Table A3.4 H*y*drogen bonds of 4,4,4-trinitrobutanoic acid (**2**).

D–H···A			sym. of A	H···A	D–H	D···A	angle, DHA
C2	H1	O1	–1+*x*, *y*, *z*	2.628	0.96	3.565	166.3
O8	H8	O7	1–*x*, –*y*, –*z*	1.769	0.86	2.632	176.5
C2	H2	O4	–0.5+*x*, 0.5–*y*, –0.5+*z*	2.547	0.94	3.253	136.1
C2	H2	O2	–0.5+*x*, 0.5–*y*, 0.5+*z*	2.653	0.94	3.389	132.5

Table A3.5 Hydrogen bonds of 4,4,4-trinitrobutanoyl azide (**4**).

D–H···A			sym. of A	H···A	D–H	D···A	angle, DHA
C2	H2	O1	–*x*, 1–*y*, –*z*	2.535	0.96	3.373	144.7
C2	H1	O7	1–*x*, 1–*y*, –*z*	2.386	1.00	3.221	141.3

Table A3.6 Hydrogen bonds of 3,3,3-trinitropropan-1-ammonium chloride (**6a**).

D–H···A			sym. of A	H···A	D–H	D···A	angle, DHA
N4	H6	O7		1.909	0.88	2.779	168.7
N4	H7	Cl1	–*x*+1, –*y*+2, –*z*+1	2.549	0.88	3.254	137.6
N4	H7	O5	*x*+1, *y*+1, *z*	2.574	0.88	3.206	129.3
N4	H8	Cl1		2.273	0.88	3.146	169.6
O7	H9	Cl1	*x*+1, *y*, *z*	2.469	0.82	3.235	155.2
O7	H10	Cl1	–*x*+1, –*y*+1, –*z*+1	2.380	0.82	3.184	169.0

Table A3.7 Hydrogen bonds of 3,3,3-trinitropropan-1-ammonium nitrate (**6b**).

D–H···A			sym. of A	H···A	D–H	D···A	angle, DHA
N4	H5	O9	−*x*+1, *y*−0.5, −*z*+½	1.948	0.91	2.859	173.6
N4	H6	O7		1.957	0.90	2.818	160.0
N4	H6	N5		2.667	0.90	3.391	138.3
N4	H7	O7	−*x*+2, *y*−0.5, −*z*+0.5	2.080	0.92	2.954	158.0
N4	H7	O9	−*x*+2, *y*−0.5, −*z*+0.5	2.361	0.92	3.094	136.5
N4	H7	N5	−*x*+2, *y*−0.5, −*z*+0.5	2.570	0.92	3.465	164.4
C2	H2	O7	−*x*+2, *y*−0.5, −*z*+0.5	2.546	0.91	3.286	138.4

Table A3.8 Hydrogen bonds of 3,3,3-trinitropropan-1-ammonium dinitramide (**6d**).

D–H···A			sym. of A	H···A	D–H	D···A	angle, DHA
C1	H4	O3		2.398	0.990	3.027	120.79
C1	H5	O4		2.828	0.990	3.446	121.23
C2	H7	O4		2.930	0.990	3.608	126.54
C1	H5	O2	−*x*, −*y*, 1−*z*	2.485	0.990	3.439	161.87
N1	H1	O7	−1+*x*, −1+*y*, *z*	2.425	0.892	3.281	161.01
C4	H12	O6		2.935	0.990	3.887	161.55
C2	H7	O10	−1+*x*, *y*, *z*	2.709	0.990	3.673	164.62
C1	H4	O11	*x*, −1+*y*, *z*	2.487	0.990	3.146	123.74
N1	H2	O15	−1+*x*, *y*, *z*	2.056	0.904	2.960	178.00
N1	H2	O16	−1+*x*, *y*, *z*	2.600	0.904	3.221	126.51
C2	H6	O13		2.574	0.990	3.460	148.97
N1	H3	O19		2.000	0.898	2.845	156.46
C2	H6	O19		2.579	0.990	3.460	134.42
N5	H9	O16		2.790	0.893	3.422	128.91
C5	H14	O14		2.641	0.990	3.605	164.55
N5	H10	O14	1+*x*, *y*, *z*	2.256	0.921	2.966	133.51
N5	H10	O16	2−*x*, 1−*y*, −*z*	2.356	0.921	3.089	136.31
C5	H13	O20	*x*, 1+*y*, *z*	2.508	0.990	3.334	140.81
N5	H8	O19	1−*x*, 1−*y*, −*z*	2.147	0.875	2.990	161.70
C4	H11	O17	2−*x*, 1−*y*, −*z*	2.408	0.990	3.335	155.71

Table A3.9 Hydrogen bonds of 2,2,2-trinitroethyl-4,4,4-trinitrobutanoate (**8**).

D–H···A			sym. of A	H···A	D–H	D···A	∠DHA
C2	H3	O6	−1+*x*, *y*, *z*	2.673	0.95	3.556	155.5
C5	H6	O10	−1+*x*, *y*, *z*	2.612	0.94	3.388	140.4
C2	H4	O7	−*x*, 1−*y*, 1−*z*	2.509	0.96	3.391	152.1
C3	H1	O12	−0.5+*x*, 0.5−*y*, 0.5+*z*	2.618	0.95	3.419	142.1

4 APPENDIX A4

Table A4.1 Crystallographic data and structure refinements of **4**, **5**, **6**, and **7**.

	4	**5**	**6**	**7**
formula	$C_7H_{10}N_8O_{13}$	$C_8H_{10}N_8O_{14}$	$C_8H_8N_6O_{16}$	$C_4H_6N_4O_8$
formula weight [g mol^{-1}]	414.20	442.21	444.18	238.11
temperature [K]	173	173	173	173
crystal system	orthorhombic	monoclinic	monoclinic	orthorhombic
space group (No.)	*Pccn* (56)	$P2_1/c$ (14)	$P2_1/c$ (14)	*Pbca* (61)
a [Å]	12.2453(6)	9.8760(6)	10.9196(7)	7.3738(3)
b [Å]	40.795(3)	15.2750(10)	6.7591(4)	9.7135(4)
c [Å]	9.3517(4)	11.2720(9)	11.8923(8)	25.2033(10)
α [°]	90	90	90	90
β [°]	90	93.027(7)	98.330(5)	90
γ [°]	90	90	90	90
V [Å^3]	4671.6(5)	1698.1(2)	868.5(1)	1805.2(1)
Z	12	4	2	8
$\rho_{calc.}$ [g cm^{-3}]	1.767	1.730	1.699	1.752
μ [mm^{-1}]	0.171	0.167	0.169	0.172
F(000)	2544	904	452	976
crystal habit	colorless plate	colorless block	colorless plate	colorless plate
crystal size [mm]	0.18×0.16×0.02	0.32×0.25×0.22	0.24×0.15×0.09	0.38×0.24×0.01
q range [°]	4.43 – 30.23	4.24 – 28.22	4.57 – 32.02	4.83 – 32.17
index ranges	$-7 \le h \le 15$	$-12 \le h \le 12$	$-11 \le h \le 13$	$-7 \le h \le 9$
	$-50 \le k \le 40$	$-17 \le k \le 18$	$-7 \le k \le 8$	$-10 \le k \le 12$
	$-6 \le l \le 11$	$-13 \le l \le 13$	$-10 \le l \le 14$	$-31 \le l \le 31$
reflections measured	13453	6716	3723	13212
reflections independent	4756	3321	1582	1835
reflections unique	3554	2541	1361	1707
R_{int}	0.0632	0.0231	0.0195	0.0183
R_1, wR_2 (2σ data)	0.0938, 0.1201	0.0385, 0.0568	0.0370, 0.0443	0.0284, 0.0308
R_1, wR_2 (all data)	0.1745, 0.1856	0.0777, 0.0869	0.0854, 0.0902	0.0681, 0.0695
data/restraints/parameters	4756/5/494	3321/0/311	1582/0/152	1835/0/169
GOOF on F^2	1.175	1.019	1.060	1.062
residual el. density [e Å^{-3}]	−0.330/0.356	−0.358/0.323	−0.255/0.333	−0.161/0.270
CCDC	1062382	1062383	1062384	1062385

Table A4.2 Crystallographic data and structure refinements of **8**, **9**, and **10**.

	8	**9**	**10**
formula	$C_4H_5N_5O_{10}$	$C_5H_7N_7O_{12}$	$C_5H_6N_8O_{14}$
formula weight [g mol^{-1}]	283.11	357.02	402.15
temperature [K]	295	173	173
crystal system	orthorhombic	monoclinic	monoclinic
space group (No.)	*Pccn* (56)	$P2_1/c$ (14)	*Pc* (7)
a [Å]	10.5771(6)	18.5978(12)	5.9260(3)
b [Å]	23.7040(12)	9.6138(3)	11.3220(4)
c [Å]	8.8283(4)	11.5247(5)	11.9577(6)
α [°]	90	90	90
β [°]	90	106.059(6)	118.944(4)
γ [°]	90	90	90
V [Å^3]	2213.3(2)	1980.2(2)	702.1(1)
Z	8	2	2
$\rho_{calc.}$ [g cm^{-3}]	1.699	1.797	1.902
μ [mm^{-1}]	0.171	0.178	0.192
F(000)	1152	1092	408
crystal habit	colorless block	colorless plate	colorless needle
crystal size [mm]	0.10×0.10×0.09	0.10×0.08×0.02	0.18×0.05×0.02
q range [°]	3.12 – 23.83	4.42 – 27.61	5.27 – 30.01
index ranges	$-12 \le h \le 11$	$-22 \le h \le 22$	$-8 \le h \le 7$
	$-26 \le k \le 26$	$-11 \le k \le 5$	$-15 \le k \le 15$
	$-10 \le l \le 9$	$-13 \le l \le 8$	$-16 \le l \le 15$
reflections measured	29604	6861	6578
reflections independent	1698	3669	3144
reflections unique	1297	2864	2770
R_{int}	0.0282	0.0211	0.0414
R_1, wR_2 (2σ data)	0.0840, 0.1020	0.0424, 0.0611	0.0367, 0.0448
R_1, wR_2 (all data)	0.2392, 0.2577	0.0886, 0.0981	0.0759, 0.0817
data/restraints/parameters	1698/0/176	3669/0/353	3144/2/323
GOOF on F^2	1.083	1.034	1.032
residual el. density [e Å^{-3}]	−0.342/0.409	−0.231/0.348	−0.221/0.270
CCDC	1062386	1062387	1062388

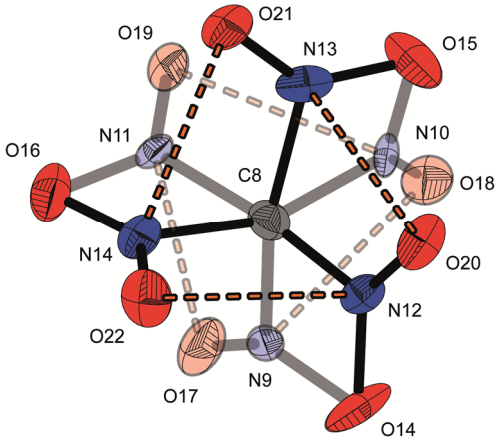

Figure A4.1 Disorder of the trinitromethyl group in the molecular structure of bis(3,3,3-trinitropropyl) urea (**4**). The orange dotted lines indicate the nitrogen oxygen non-bonded intramolecular interactions.

Table A4.3 Hydrogen bonds of bis(3,3,3-trinitropropyl) urea (**4**).

D–H···A			sym. of A	H···A	D–H	D···A	angle, DHA
C2	H2	O8	0.5−*x*, *y*, −0.5+*z*	2.791	0.89	3.682	174.9
C3	H3	O18	*x*, *y*, *z*	2.643	0.95	3.583	166.9
C3	H3	O19	0.5−*x*, *y*, −0.5+*z*	2.728	0.95	3.450	133.7
C3	H3	O20	*x*, *y*, *z*	2.907	0.95	3.823	160.0
C3	H4	O16	*x*, *y*, −1+*z*	2.611	1.03	3.624	169.2
C3	H4	O19	*x*, *y*, −1+*z*	2.556	1.03	3.384	136.6
N4	H5	O19	*x*, *y*, −1+*z*	2.829	0.69	3.323	130.8
N4	H5	O21	*x*, *y*, −1+*z*	2.976	0.69	3.533	139.2
N4	H5	O7	0.5−*x*, *y*, −0.5+*z*	2.349	0.69	2.985	154.0
N5	H6	O7	0.5−*x*, *y*, −0.5+*z*	2.151	0.85	2.946	154.7
C5	H7	O12	−0.5+*x*, −*y*, −0.5−*z*	2.487	1.11	3.463	145.4
C5	H8	O9	−*x*, −*y*, −*z*	2.756	1.05	3.535	131.2
C9	H11	O5	*x*, *y*, *z*	2.555	0.95	3.503	174.6
C9	H12	O1	*x*, *y*, −1+*z*	2.895	0.89	3.697	151.0
C9	H12	O2	*x*, *y*, −1+*z*	2.896	0.89	3.647	143.2
C10	H13	O2	*x*, 0.5−*y*, −0.5+*z*	2.772	1.01	3.586	138.3
C10	H14	O14	*x*, 0.5−*y*, −0.5+*z*	2.743	0.98	3.702	165.8
N15	H15	O23	1.5−*x*, *y*, −0.5+*z*	2.104	0.88	2.947	159.7

Table A4.4 Hydrogen bonds of bis(3,3,3-trinitropropyl) oxalamide (**5**).

D–H···A			sym. of A	H···A	D–H	D···A	angle, DHA
C2	H1	O9	*x*, *y*, *z*	2.836	0.96	3.279	131.0
C2	H1	O5	*x*, 0.5−*y*, −0.5+*z*	2.572	0.96	3.625	140.5
C2	H2	O13	1+*x*, *y*, *z*	2.895	0.93	3.694	135.6
C2	H2	O1	*x*, 0.5−*y*, −0.5+*z*	2.968	0.93	3.715	147.4
C3	H3	O10	2−*x*, 0.5+*y*, 1.5−*z*	2.641	0.97	3.604	172.7
N4	H5	O14	*x*, *y*, *z*	2.061	0.84	2.845	155.5
C6	H6	O1	1+*x*, 0.5−*y*, 0.5+*z*	2.977	0.96	3.859	154.1
C6	H7	O5	*x*, 0.5−*y*, 0.5+*z*	2.945	0.93	3.785	150.2
C7	H8	O3	1+*x*, *y*, *z*	2.860	0.96	3.789	163.4
N8	H10	O7	1+*x*, *y*, *z*	2.054	0.84	2.845	157.8

Table A4.5 Hydrogen bonds of bis(3,3,3-trinitropropyl) oxalate (**6**).

D–H···A			sym. of A	H···A	D–H	D···A	angle, DHA
C2	H2	O7	*x*, 0.5−*y*, 0.5+*z*	2.687	0.96	3.446	136.6
C3	H3	O1	−*x*, 0.5+*y*, 0.5−*z*	2.611	0.95	3.204	121.1
C3	H3	O8	*x*, 0.5−*y*, 0.5+*z*	2.664	0.95	3.458	142.0
C3	H4	O4	*x*, −1+*y*, *z*	2.809	0.94	3.460	127.3
C3	H4	O5	1−*x*, −0.5+*y*, 0.5−*z*	2.847	0.94	3.727	129.5
C3	H4	O6	1−*x*, −0.5+*y*, 0.5−*z*	2.882	0.94	3.554	156.4

Table A4.6 Hydrogen bonds of 3,3,3-trinitropropyl carbamate (**7**).

D–H···A			sym. of A	H···A	D–H	D···A	angle, DHA
N1	H1	O1	1−*x*, −*y*, −*z*	2.074	0.86	2.925	170.4
N1	H2	O1	0.5−*x*, 0.5+*y*, *z*	2.090	0.85	2.938	174.0
C2	H3	O8	0.5−*x*, −0.5+*y*, *z*	2.633	0.95	3.378	135.1
C2	H4	O7	−0.5−*x*, −0.5+*y*, *z*	2.784	0.98	3.457	126.3
C3	H5	O3	−0.5−*x*, −0.5+*y*, *z*	2.614	0.98	3.380	135.4
C3	H6	O5	0.5+*x*, *y*, 0.5−*z*	2.692	0.96	3.555	149.3

Table A4.7 Hydrogen bonds of 3,3,3-trinitropropyl nitrocarbamate (**8**).

D–H···A			sym. of A	H···A	D–H	D···A	angle, DHA
N2	H1	O3	0.5−*x*, *y*, −0.5+*z*	1.922	0.94	2.784	150.7
N2	H1	O2	0.5−*x*, *y*, −0.5+*z*	2.318	0.94	3.034	132.2
C2	H2A	O1	−0.5+*x*, 1−*y*, 0.5−*z*	2.796	0.97*	3.718	159.1
C3	H3A	O2	−0.5+*x*, 1−*y*, 0.5−*z*	2.574	0.97*	3.285	130.3
C3	H3B	O7	−0.5−*x*, *y*, −0.5+*z*	2.875	0.97*	3.622	134.5
C3	H3B	O8	−0.5−*x*, *y*, −0.5+*z*	2.976	0.97*	3.763	139.0

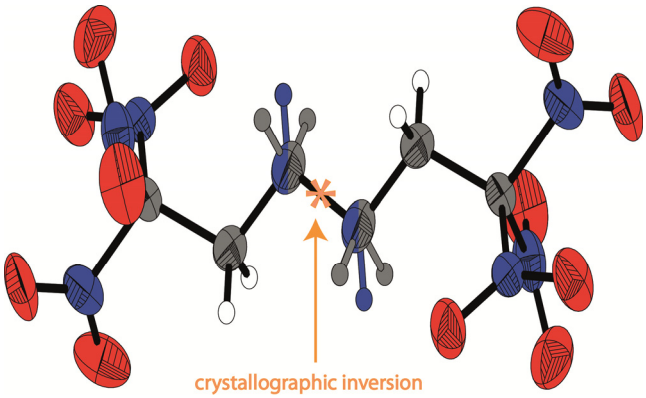

Figure A4.2 X-ray molecular structure of 3,3,3-trinitro-*N*-(2,2,2-trinitroethyl) propan-1-amine (**9**) showing a C/N-disorder.

Table A4.8 Hydrogen bonds of 3,3,3-trinitro-*N*-(2,2,2-trinitroethyl)propan-1-amine (**9**).

D–H···A			sym. of A	H···A	D–H	D···A	angle, DHA
C2	H1	O3	*x*, 1.5−*y*, −0.5+*z*	2.533	0.96	3.389	148.2
N4	H3	O5	1−*x*, −0.5+*y*, 1.5−*z*	2.966	0.92	3.566	166.2
C3	H4	O18	−1+*x*, *y*, *z*	2.768	0.89	3.523	150.3
C3	H5	O7	*x*, 0.5−*y*, −0.5+*z*	2.867	0.88	3.258	133.1
C3	H5	O15	−1+*x*, 1.5−*y*, 0.5+*z*	2.575	0.88	3.370	136.5
C4	H6	O4	1−*x*, 1−*y*, 1−*z*	2.589	0.88	3.574	148.7
C4	H7	O9	*x*, 0.5−*y*, −0.5+*z*	2.817	0.94	3.622	138.0
C8A	H8A	O10	1−*x*, −0.5+*y*, 0.5−*z*	2.496	0.99*	3.622	138.8
C8A	H8A	O14	2−*x*, −0.5+*y*, 0.5−*z*	2.666	0.99*	3.306	135.9
C8A	H9A	O12	−1+*x*, *y*, *z*	2.640	0.99*	3.447	171.3
C7A	H10A	O11	1−*x*, 1−*y*, −*z*	2.850	0.99*	3.810	163.6
C7A	H11A	O14	*x*, 1.5−*y*, −0.5+*z*	2.693	0.99*	3.615	155.1

Table A4.9 Hydrogen bonds of *N*-(2,2,2-trinitroethyl)-*N*-(3,3,3-trinitropropyl) nitramide (**10**).

D–H···A			sym. of A	H···A	D–H	D···A	angle, DHA
C2	H1	O3	*x*, 1.5−*y*, −0.5+*z*	2.533	0.96	3.389	148.2
N4	H3	O5	1−*x*, −0.5+*y*, 1.5−*z*	2.966	0.92	3.566	166.2
C3	H4	O18	−1+*x*, *y*, *z*	2.768	0.89	3.523	150.3
C3	H5	O7	*x*, 0.5−*y*, −0.5+*z*	2.867	0.88	3.258	133.1
C3	H5	O15	−1+*x*, 1.5−*y*, 0.5+*z*	2.575	0.88	3.370	136.5
C4	H6	O4	1−*x*, 1−*y*, 1−*z*	2.589	0.88	3.574	148.7
C4	H7	O9	*x*, 0.5−*y*, −0.5+*z*	2.817	0.94	3.622	138.0
C8A	H8A	O10	1−*x*, −0.5+*y*, 0.5−*z*	2.496	0.99*	3.622	138.8
C8A	H8A	O14	2−*x*, −0.5+*y*, 0.5−*z*	2.666	0.99*	3.306	135.9
C8A	H9A	O12	−1+*x*, *y*, *z*	2.640	0.99*	3.447	171.3
C7A	H10A	O11	1−*x*, 1−*y*, −*z*	2.850	0.99*	3.810	163.6
C7A	H11A	O14	*x*, 1.5−*y*, −0.5+*z*	2.693	0.99*	3.615	155.1

Table A4.10 Further predicted detonation and combustion parameters using EXPLO5 V6.02.

	4	**5**	**6**	**7**	**8**	**9**	**10**	**AP**
density RT	1.75	1.71	1.67	1.73	1.70	1.78	1.89	1.95
formula	$C_7H_{10}N_8O_{13}$	$C_8H_{10}N_8O_{14}$	$C_8H_8N_6O_{16}$	$C_4H_6N_4O_8$	$C_4H_5N_5O_{10}$	$C_5H_7N_7O_{12}$	$C_5H_6N_8O_{14}$	NH_4ClO_4
$\Delta H°_f$ [kJ mol^{-1}]	–359.1	–522.3	–789.4	–503.5	–401.7	–86.4	–66.8	–295.8
$\Delta U°_f$ [kJ kg^{-1}]	–774.1	–1091.5	–1693.5	–2021.0	–1331.3	–151.7	–79.7	–2623.2
Q_v [kJ kg^{-1}]	–5385	–5095	–5126	–4662	–5809	–6565	–6377	–1422
T_{ex} [K]	3692	3605	3808	3328	4175	4445	4420	1735
V_0 [L kg^{-1}]	739	732	724	724	755	738	756	885
P_{CJ} [kbar]	294	268	256	265	269	330	367	158
V_{Det} [m s^{-1}]	8227	7937	7732	7896	8134	8713	9119	6368
I_s [s]	254	245	250	237	256	272	264	157
I_s [s] (5% Al)	259	253	255	246	257	273	266	198
I_s [s] (10% Al)	265	259	257	252	260	274	268	224
I_s [s] (15% Al)	267	263	259	256	261	274	269	235
I_s [s] (20% Al)	268	267	260	262	262	274	269	244
I_s [s] (25% Al)	257	247	258	252	261	271	267	247
I_s [s] (30% Al)	245	240	246	242	254	262	262	247
I_s [s] (5% Al, 14% binder)	227	220	223	213	238	254	261	250
I_s [s] (10% Al, 14% binder)	242	235	237	227	247	261	266	257
I_s [s] (15% Al, 14% binder)	251	245	246	240	253	261	267	261

Table A4.11 Comparison of physical and chemical properties of the 3,3,3-trinitropropyl and 2,2,2-trinitroethyl group with different moieties.

	4		**5**		**6**		**7**		**8**		**9**		**10**	
moiety	**urea**		**oxamide**		**oxalate**		**carbamate**		**nitrocarbamate**		**amine**		**nitramine**	
propyl *vs* ethyl	**propyl**	**ethyl**	**propyl**	**ethyl**	**propyl**	**ethyl**	**propyl**	**ethyl**	**propyl**	**ethyl**	**propyl**	**ethyl**	**propyl**	**ethyl**
T_m [°C (onset)]	-	185	-	n.a.	121	115	78	91	68	109	65	114	141	94
T_{dec} [°C] (onset)	160	187	181	n.a.	170	186	152	169	134	153	96	114	153	96
IS [J]	20	3	10	n.a.	> 40	10	> 40	40	> 30	10	7	5	7	2
FS [N]	120	160	160	n.a.	> 360	> 360	> 360	64	> 288	96	120	120	160	64
N [%]	27.1	29.0	25.3	27.1	18.9	20.2	23.5	25.0	24.7	26.0	27.5	28.6	27.9	28.9
O [%]	50.2	53.9	50.7	54.1	57.6	61.5	53.8	57.1	56.5	59.5	53.8	56.0	55.7	57.7
N+O [%]	77.3	82.9	76.0	81.2	76.5	81.7	77.3	82.1	81.2	85.5	81.3	84.6	83.6	86.6
Ω_{CO} [%]	+3.9	+20.7	+3.6	+19.3	+14.4	+30.8	+6.7	+21.4	+19.8	+32.7	+15.7	+25.7	+23.9	+33.0
Ω_{CO2} [%]	−20.2	+0.0	−20.3	−3.9	−14.4	+7.7	−20.2	0.0	−2.8	+14.9	−6.7	+7.0	+4.0	+16.5
density [g cm^{-3}]	1.75	1.86	1.71	1.80	1.67	1.86	1.73	1.82	1.70	1.72	1.78	1.84	1.89	1.92
$\Delta_f H_m°$ [kJ mol^{-1}]	−359.1	−306.8	−522.3	−446.5	−789.4	−689.1	−503.5	−459.1	−401.7	−366.1	−86.4	−74.8	−66.8	−5.7
$\Delta_f U°$ [kJ kg^{-1}]	−774.1	−707.7	−1091.5	−994.2	−1693.5	−1578.6	−2021.0	−1960.8	−1331.3	−1278.2	−151.7	−131.4	−79.7	+68.3

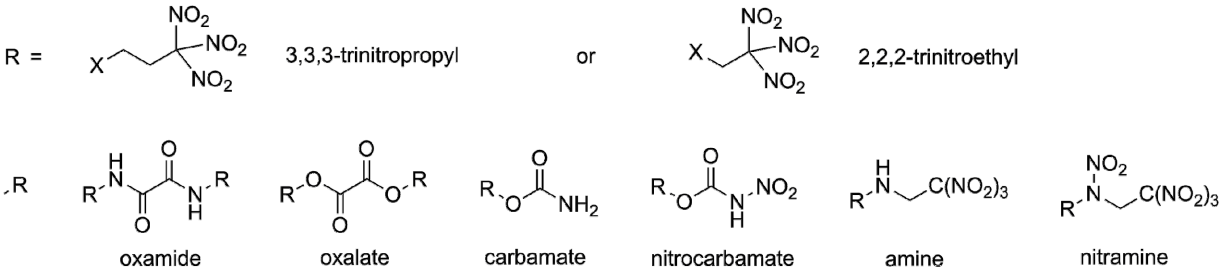

5 APPENDIX A5

Table A5.1 Hydrogen Crystallographic data and structure refinements of **1**, **4**, and **5**.

	1	**4**	**5**
formula	$C_6H_4N_6O_{16}$	$C_4H_3N_7O_9$	$C_6H_5N_7O_{16}$
formula weight [g mol^{-1}]	416.12	293.11	431.14
temperature [K]	173	173	173
crystal system	monoclinic	monoclinic	orthorhombic
space group (No.)	$P2_1/c$ (14)	$P2_1/c$ (14)	F$dd2$ (43)
a [Å]	10.5849(5)	6.3221(3)	16.4396(10)
b [Å]	21.6214(11)	16.7221(8)	14.8283(9)
c [Å]	6.5071(3)	10.0367(5)	12.0446(7)
α [°]	90	90	90
β [°]	98.485(5)	103.147(5)	90
γ [°]	90	90	90
V [Å^3]	1472.92(12)	1033.26(9)	2936.1(3)
Z	4	4	8
$\rho_{calc.}$ [g cm^{-3}]	1.877	1.788	1.951
μ [mm^{-1}]	0.193	0.177	0.199
F(000)	840	560	1744
crystal habit	colorless block	colorless block	colorless block
crystal size [mm]	0.30×0.21×0.17	0.40×0.40×0.15	0.35×0.31×0.22
q range [°]	4.72 – 32.07	4.43 – 30.18	4.62 – 24.63
index ranges	$-15 \le h \le 15$	$-7 \le h \le 7$	$-20 \le h \le 21$
	$-32 \le k \le 30$	$-20 \le k \le 20$	$-19 \le k \le 18$
	$-9 \le l \le 9$	$-12 \le l \le 12$	$-16 \le l \le 16$
reflections measured	11888	15471	9438
reflections independent	3002	2107	1767
reflections unique	2502	1782	1494
R_{int}	0.0234	0.0260	0.0489
R_1, wR_2 (2σ data)	0.0285, 0.0378	0.0325, 0.0407	0.0386, 0.0547
R_1, wR_2 (all data)	0.0686,°0.0637	0.0715, 0.0756	0.0724, 0.0821
data/restraints/parameters	3002/0/269	2107/0/180	1767/1/142
GOOF on F^2	1.021	1.034	1.131
residual el. density [e Å^{-3}]	–0.209/0.306	–0.197/0.220	–0.229/0.062
CCDC	1469963	1469964	1469965

Table A5.2 Hydrogen bonds of bis(2,2,2-trinitroethyl) oxalate (**1**).

D–H···A			sym. of A	H···A	D–H	D···A	angle, DHA
C2	H1	O15	*x*, −1+*y*, −1+*z*	2.997	0.975	3.894	153.44
C2	H1	O16	*x*, −1+*y*, −1+*z*	2.751	0.975	3.582	143.46
C2	H2	O9	1−*x*, 1−*y*, 2−*z*	2.470	0.961	3.320	147.37
C5	H3	O5	1−*x*, 1−*y*, 1−*z*	2.533	0.958	3.341	141.92
C5	H3	O6	1−*x*, 1−*y*, 1−*z*	2.794	0.958	3.692	156.26
C5	H4	O12	*x*, *y*, −1+*z*	2.536	0.939	3.231	131.04
C5	H4	O13	*x*, 1.5−*y*, 0.5+*z*	2.845	0.939	3.714	154.25

Table A5.3 Hydrogen bonds of 2,2,2-trinitroethyl azido(oxo)acetate (**4**).

D–H···A			sym. of A	H···A	D–H	D···A	angle, DHA
C3	H2	O1	−1+*x*, *y*, *z*	2.611	0.94	3.405	142.19
C3	H1	O2	*x*, 0.5−*y*, −0.5+*z*	2.461	0.95	3.287	144.96

Table A5.4 Hydrogen bonds of bis(2,2,2-trinitroethyl) imidodicarboxylate (**5**).

D–H···A			sym. of A	H···A	D–H	D···A	angle, DHA
C2	H1	O1	1.25−*x*, 0.25+*y*, 0.25+*z*	2.633	0.985	3.467	142.53
C2	H2	O7	1−*x*, 0.5−*y*, −0.5+*z*	2.908	0986	3.775	147.23
C2	H2	O8	1−*x*, 0.5−*y*, −0.5+*z*	2.608	0.986	3.550	159.98
N1	H3	O5	1.25−*x*, 0.25+*y*, 0.25+*z*	2.470	0.879	3.129	132.10
N1	H3	O6	1.25−*x*, 0.25+*y*, 0.25+*z*	2.891	0.879	3.544	132.38

Table A5.5 Further predicted detonation and combustion parameters using EXPLO5 V6.02.

	1	**3**	**4**	**5**	**6**	**7**	**AP**
density RT	1.84	1.73	1.75	1.92	1.63	1.50	1.95
formula	$C_6H_4N_6O_{16}$	$C_7H_6N_6O_{16}$	$C_4H_2N_6O_9$	$C_6H_5N_7O_{16}$	$C_7H_7N_7O_{15}$	$C_4H_3N_7O_9$	NH_4ClO_4
$\Delta H°_f$ [kJ mol^{-1}]	–688.0	–705.2	–170.5	–775.2	–645.7	–271.4	–295.8
$\Delta U°_f$ [kJ kg^{-1}]	–1575.9	–1558.7	–537.3	–1717.5	–1420.7	–845.7	–2623.2
Q_v [kJ kg^{-1}]	–5177	–5839	–5701	–5062	–5371	–5199	–1422
T_{ex} [K]	3943	4262	4394	3936	4028	4219	1735
V_0 [L kg^{-1}]	705	711	707	724	741	745	885
P_{CJ} [kbar]	286	270	280	237	241	189	158
V_{Det} [m s^{-1}]	8275	8071	8223	8675	7703	7213	6368
I_s [s]	240	252	250	240	252	247	157
I_s [s] (5% Al)	246	255	253	246	256	251	198
I_s [s] (10% Al)	248	256	255	249	256	253	224
I_s [s] (15% Al)	250	257	257	250	259	255	235
I_s [s] (20% Al)	251	258	258	252	260	256	244
I_s [s] (25% Al)	251	257	255	252	258	252	247
I_s [s] (30% Al)	249	251	246	249	248	241	247
I_s [s] (5% Al, 14% binder)	243	236	237	237	229	226	250
I_s [s] (10% Al, 14% binder)	250	245	246	245	240	238	257
I_s [s] (15% Al, 14% binder)	256	251	247	252	248	243	261

6 APPENDIX A6

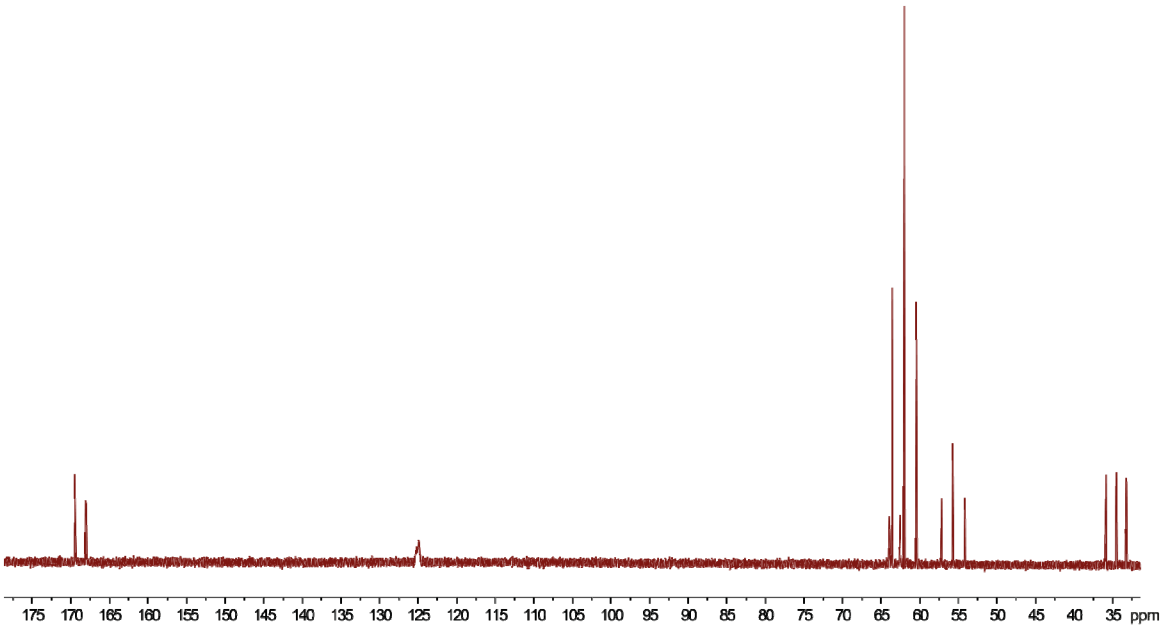

Figure A6.1 ^{1}H coupled ^{13}C NMR spectrum of 2-(nitro(2,2,2-trinitroethyl)amino)-4-oxo-4-(2,2,2-trinitroethoxy)butanoic acid (**8**).

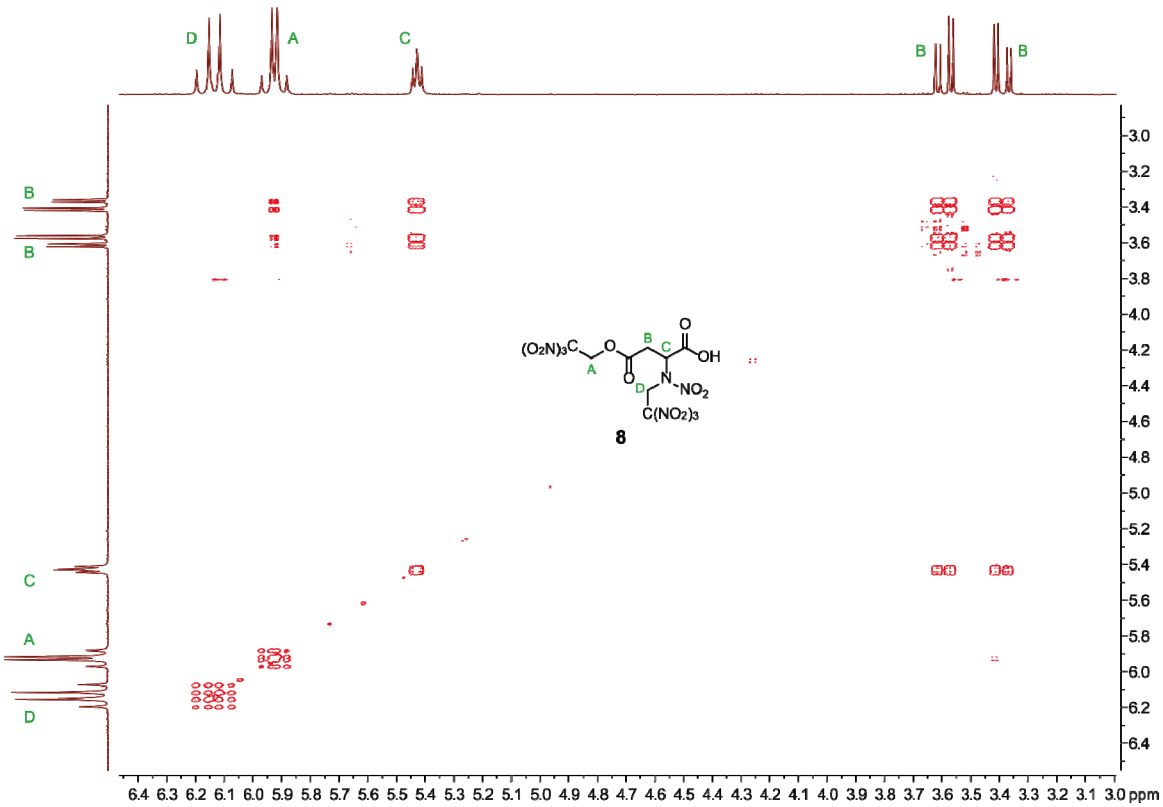

Figure A6.2 $^{1}H,^{1}H$ COSY NMR spectrum of 2-(nitro(2,2,2-trinitroethyl)amino)-4-oxo-4-(2,2,2-trinitroethoxy)butanoic acid (**8**).

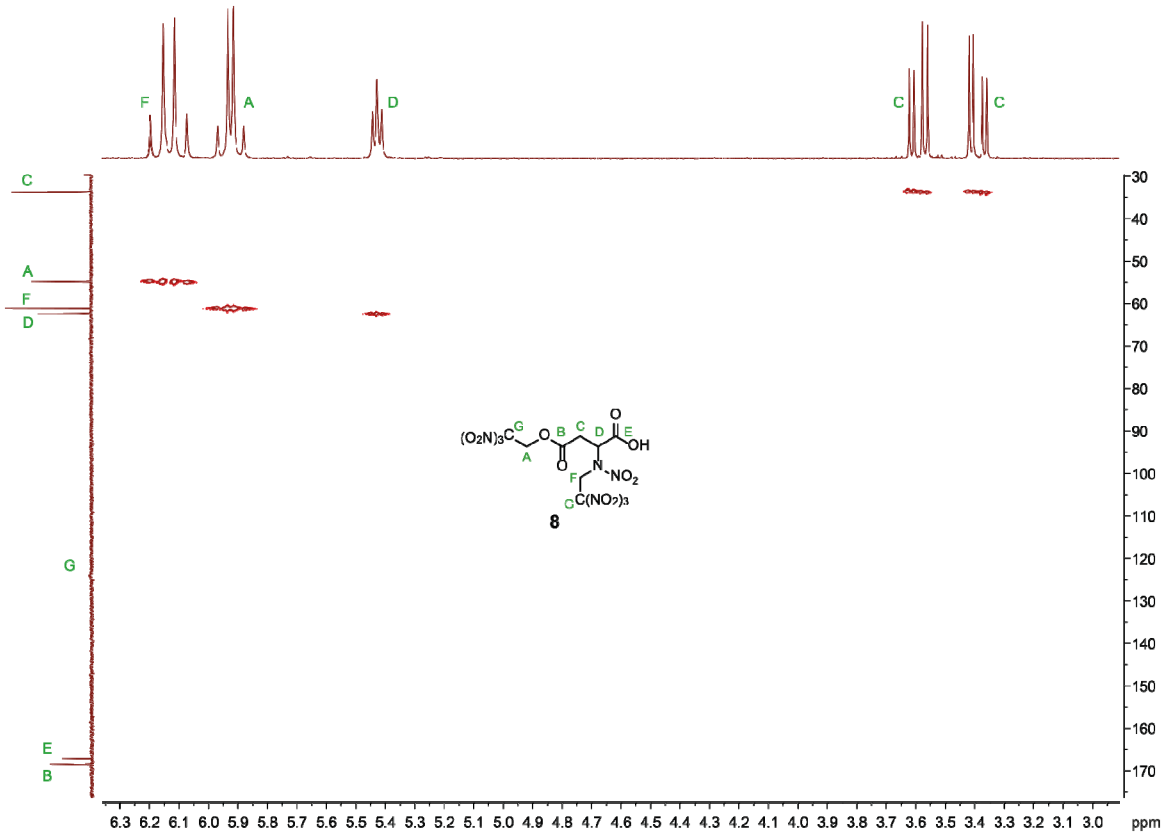

Figure A6.3 $^{1}H,^{13}C$ HMQC NMR spectrum of 2-(nitro(2,2,2-trinitroethyl)amino)-4-oxo-4-(2,2,2-trinitroethoxy)butanoic acid (**8**).

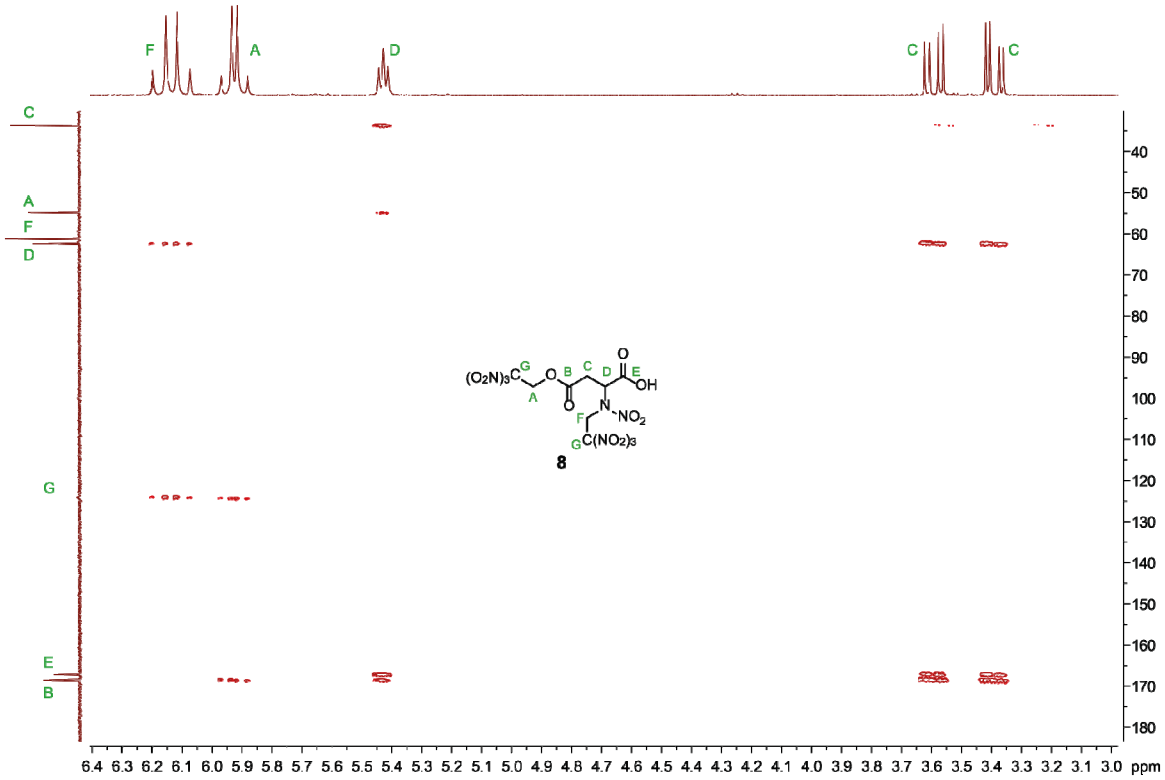

Figure A6.4 $^{1}H,^{13}C$ HMBC NMR spectrum of 2-(nitro(2,2,2-trinitroethyl)amino)-4-oxo-4-(2,2,2-trinitroethoxy)butanoic acid (**8**).

Table A6.1 Hydrogen Crystallographic data and structure refinements of **2** and **4**.

	2	**4**
formula	$C_5H_6N_5O_9Cl$	$C_5H_6N_8O_9$
formula weight [g mol^{-1}]	315.60	322.15
temperature [K]	173	173
crystal system	monoclinic	monoclinic
space group (No.)	*Pc* (7)	$P2_1/n$ (14)
a [Å]	6.1729(3)	12.9530(10)
b [Å]	11.3237(7)	6.7406(5)
c [Å]	17.3554(7)	14.1505(11)
α [°]	90	90
β [°]	90.485(7)	92.699(7)
γ [°]	90	90
V [Å^3]	1213.10(11)	1234.12(16)
Z	4	4
$\rho_{calc.}$ [g cm^{-3}]	1.728	1.734
μ [mm^{-1}]	0.373	0.165
F(000)	640	656
crystal habit	colorless rods	colorless plates
crystal size [mm]	0.32×0.14×0.11	0.39×0.24×0.04
q range [°]	5.00 – 28.55	4.37 – 24.40
index ranges	$-9 \le h \le 8$	$-16 \le h \le 16$
	$-15 \le k \le 16$	$-8 \le k \le 8$
	$-25 \le l \le 25$	$-17 \le l \le 17$
reflections measured	12861	8335
reflections independent	6606	2521
reflections unique	4961	1649
R_{int}	0.0296	0.0601
R_1, wR_2 (2σ data)	0.0417, 0.0665	0.0487, 0.0868
R_1, wR_2 (all data)	0.0788,°0.0685	0.1172, 0.0997
data/restraints/parameters	6606/0/464	2521/0/217
GOOF on F^2	1.021	1.040
residual el. density [e Å^{-3}]	−0.280/0.371	−0.270/0.208
CCDC	1484172	1484173

Table A6.2 Hydrogen bonds of 3-(nitro(2,2,2-trinitroethyl)amino)propanoyl chloride (**2**).

D–H···A			sym. of A	H···A	D–H	D···A	angle, DHA
C2	H1	O7	*x*,–*y*, –0.5+*z*	2.684	0.961	3.548	149.87
C2	H1	O8	*x*, –*y*, –0.5+*z*	2.945	0.961	3.761	143.45
C3	H3	O6	*x*, *y*, *z*	2.694	0.958	3.489	140.84
C3	H3	O13	*x*, –1+*y*, *z*	2.594	0.958	3.337	134.58
C3	H4	O1	–1+*x*, *y* ,*z*	2.376	0.986	3.337	164.58
C4	H5	O1	*x*, *y*, *z*	2.411	0.936	3.077	128.05
C4	H5	O4	–1+*x*, *y*, *z*	2.782	0.936	3.415	125.77
C4	H6	O12	*x*, *y*, *z*	2.385	0.976	3.262	149.22
C7	H8	O18	*x*, 1–*y*, –0.5+*z*	2.572	0.977	3.293	130.62
C8	H9	O5	1+*x*, 1–*y*, –0.5+*z*	2.725	1.010	3.440	127.98
C8	H9	O21	*x*, *y*, *z*	2.538	1.010	3.371	139.58
C8	H10	O10	–1+*x*, *y*, *z*	2.428	0.961	3.339	158.00
C9	H11	O3	–1+*x*, *y*, *z*	2.615	0.915	3.333	135.87
C9	H12	O10	*x*, *y*, *z*	2.330	1.002	4.198	127.41
C9	H12	O16	–1+*x*, *y*, *z*	2.682	1.002	3.314	121.22

Table A6.3 Hydrogen bonds of 3-(nitro-(2,2,2-trinitroethyl)amino)propanoyl azide (**4**).

D–H···A			sym. of A	H···A	D–H	D···A	angle, DHA
C2	H2	O5	0.5+*x*, 0.5–*y*, –0.5+*z*	1.016	2.862	3.514	122.49
C3	H3	O6	*x*, *y*, *z*	0.996	2.342	3.184	120.61
C3	H4	O2	–0.5–*x*, –0.5+*y*, 0.5–*z*	0.957	2.931	3.516	141.71
C4	H6	O1	*x*, y, *z*	0.958	2.381	3.097	131.11
C4	H6	O6	–*x*, 1–*y*, 1–*z*	0.958	2.882	3.735	148.81

Table A6.4 Further predicted detonation and combustion parameters using EXPLO5 V6.02.

	1	**3**	**4**	**5**	**6**	**8**	**AP**
density RT	1.72	1.73	1.70	1.89	1.66	1.65	1.95
formula	$C_5H_7N_5O_{10}$	$C_7H_8N_8O_{16}$	$C_5H_6N_8O_9$	$C_7H_8N_{10}O_{18}$	$C_6H_7N_5O_{12}$	$C_8H_8N_8O_{18}$	NH_4ClO_4
$\Delta H°_f$ [kJ mol^{-1}]	−463.1	−398.4	98.3	−292.8	−824.5	−777.5	−295.8
$\Delta U°_f$ [kJ kg^{-1}]	−1466.9	−779.5	393.5	−477.1	−2329.5	−1458.5	−2623.2
Q_v [kJ kg^{-1}]	−5108	−6110	−5700	−6328	−4502	−5601	−1422
T_{ex} [K]	3610	4315	4059	4355	3399	4152	1735
V_0 [L kg^{-1}]	738	740	761	746	734	735	885
P_{CJ} [kbar]	277	292	291	365	234	247	158
V_{Det} [m s^{-1}]	7987	8300	8285	9083	7515	7801	6368
I_s [s]	247	252	259	250	233	244	155
I_s [s] (10% Al)	255	258	266	257	244	251	219
I_s [s] (15% Al)	258	260	268	259	248	253	232
I_s [s] (20% Al)	260	262	262	261	251	255	240
I_s [s] (10% Al, 14% binder)	235	249	236	255	222	239	253
I_s [s] (11% Al, 14% binder)	237	250	236	256	227	241	254
I_s [s] (12% Al, 14% binder)	237	249	236	257	229	242	254
I_s [s] (13% Al, 14% binder)	237	247	236	257	229	241	255
I_s [s] (14% Al, 14% binder)	236	246	237	253	231	240	256
I_s [s] (15% Al, 14% binder)	235	245	237	249	230	240	256
I_s [s] (20% Al, 14% binder)	233	241	236	243	227	236	258

7 APPENDIX A7

Table A7.1 Hydrogen Crystallographic data and structure refinements of **1**, **3**, and **4**.

	1	**3**	**4**
formula	$C_3H_5N_3O_2$	$C_3H_6N_2O_4$	$C_3H_8N_4O_3$
formula weight [g mol^{-1}]	115.10	134.10	148.13
temperature [K]	123	123	173
crystal system	monoclinic	monoclinic	monoclinic
space group (No.)	$P2_1/c$ (14)	$P2_1/c$ (14)	$P2_1/c$ (14)
a [Å]	6.0991(7)	5.8782(3)	10.8689(12)
b [Å]	16.8867(14)	9.1488(5)	6.0536(5)
c [Å]	5.5884(7)	10.2741(5)	9.7660(8)
α [°]	90	90	90
β [°]	117.146(15)	93.968(4)	100.440(9)
γ [°]	90	90	90
V [Å^3]	512.17(11)	551.20(5)	631.93(10)
Z	4	4	4
$\rho_{calc.}$ [g cm^{-3}]	1.493	1.616	1.557
μ [mm^{-1}]	0.126	0.151	0.136
F(000)	240	280	312
crystal habit	colorless needle	colorless plate	colorless block
crystal size [mm]	0.38×0.05×0.05	0.28×0.23×0.05	0.15×0.14×0.10
q range [°]	4.71 – 31.49	4.55 – 32.14	4.59 – 27.59
index ranges	$-7 \le h \le 6$	$-7 \le h \le 6$	$-13 \le h \le 13$
	$-20 \le k \le 21$	$-11 \le k \le 11$	$-7 \le k \le 6$
	$-6 \le l \le 6$	$-12 \le l \le 12$	$-12 \le l \le 12$
reflections measured	3726	4028	3982
reflections independent	1039	1129	1297
reflections unique	905	997	967
R_{int}	0.0239	0.0208	0.0337
R_1, wR_2 (2σ data)	0.0306, 0.0356	0.0284, 0.0334	0.0385, 0.0585
R_1, wR_2 (all data)	0.0767, 0.0799	0.0726, 0.0758	0.0909, 0.1044
data/restraints/parameters	1039/0/93	1129/0/106	1297/0/123
GOOF on F^2	1.056	1.067	1.072
residual el. density [e Å^{-3}]	–0.247/0.138	–0.184/0.249	–0.230/0.221
CCDC	1490177	1490184	1490178

Table A7.2 Hydrogen Crystallographic data and structure refinements of **6**, **8**, and **9**.

	6	**8**	**9**
formula	$C_3H_5N_5O_3$	$C_3H_5N_2O_3Cl$	$C_6H_{12}N_6O_6$
formula weight [g mol^{-1}]	159.12	153.54	264.22
temperature [K]	173	123	123
crystal system	monoclinic	monoclinic	triclinic
space group (No.)	$P2_1/c$ (14)	$P2_1/n$ (14)	$P\bar{1}$ (2)
a [Å]	11.4947(8)	9.3803(6)	6.3435(4)
b [Å]	5.5082(3)	5.0836(3)	8.6488(8)
c [Å]	10.8210(7)	13.0278(7)	10.5766(9)
α [°]	90	90	99.172(7)
β [°]	105.170(7)	97.423(6)	91.181(6)
γ [°]	90	90	105.107(7)
V [Å^3]	661.26(8)	616.03(6)	551.88(8)
Z	4	4	2
$\rho_{calc.}$ [g cm^{-3}]	1.598	1.645	1.590
μ [mm^{-1}]	0.141	0.553	0.141
F(000)	328	312	276
crystal habit	colorless plate	colorless block	colorless plate
crystal size [mm]	0.19×0.12×0.14	0.40×0.40×0.40	0.25×0.10×0.02
q range [°]	4.72 – 27.98	4.72 – 31.88	4.96 – 31.08
index ranges	$-14 \le h \le 14$	$-11 \le h \le 11$	$-7 \le h \le 7$
	$-6 \le k \le 6$	$-6 \le k \le 5$	$-10 \le k \le 10$
	$-7 \le l \le 13$	$-16 \le l \le 16$	$-13 \le l \le 12$
reflections measured	4040	4529	4196
reflections independent	1287	1262	2233
reflections unique	1028	1123	1725
R_{int}	0.0311	0.0203	0.0286
R_1, wR_2 (2σ data)	0.0392, 0.0521	0.0246, 0.0285	0.0385, 0.0562
R_1, wR_2 (all data)	0.0911, 0.1005	0.0621, 0.0637	0.0894, 0.0996
data/restraints/parameters	1287/0/103	1262/0/102	2233/0/211
GOOF on F^2	1.052	1.082	1.020
residual el. density [e Å^{-3}]	–0.280/0.216	– 0.229/0.269	–0.222/0.258
CCDC	1490179	1490183	1490180

Table A7.3 Hydrogen Crystallographic data and structure refinements of **11**, **12**, and **13**.

	11	**12**	**13**
formula	$C_3H_7N_3O_3$	$C_6H_8N_6O_{11}$	$C_3H_6N_4O_5$
formula weight [g mol^{-1}]	133.12	340.16	178.12
temperature [K]	123	123	100
crystal system	monoclinic	monoclinic	orthorhombic
space group (No.)	$P2_1/n$ (14)	$P2_1/c$ (14)	$Fdd2$ (43)
a [Å]	4.8748(5)	12.6522(12)	18.0701
b [Å]	11.0812(11)	9.2288(5)	31.2233(17)
c [Å]	11.1178(12)	11.6546(8)	4.8664(3)
α [°]	90	90	90
β [°]	96.203(9)	108.379(9)	90
γ [°]	90	90	90
V [Å^3]	597.05(11)	1291.43(18)	2745.7(3)
Z	4	4	16
$\rho_{calc.}$ [g cm^{-3}]	1.481	1.750	1.724
μ [mm^{-1}]	0.131	0.170	0.163
F(000)	280	696	1472
crystal habit	colorless needle	colorless block	colorless rod
crystal size [mm]	0.40×0.18×0.18	0.35×0.30×0.10	0.25×0.20×0.15
q range [°]	4.77 – 31.01	4.51 – 27.76	3.45 – 26.33
index ranges	$-5 \le h \le 6$	$-15 \le h \le 14$	$-22 \le h \le 22$
	$-11 \le k \le 13$	$-10 \le k \le 11$	$-38 \le k \le 35$
	$-13 \le l \le 13$	$-14 \le l \le 13$	$-5 \le l \le 6$
reflections measured	4373	8926	7830
reflections independent	1201	2642	1367
reflections unique	987	1964	1317
R_{int}	0.0288	0.0421	0.0415
R_1, wR$_2$ (2σ data)	0.0347, 0.0452	0.0403, 0.0623	0.0569, 0.0598
R_1, wR$_2$ (all data)	0.0860, 0.0939	0.0890, 0.1021	0.1137, 0.1160
data/restraints/parameters	1201/0/110	2642/0/240	1367/1/123
GOOF on F^2	1.075	1.048	1.105
residual el. density [e Å^{-3}]	–0.254/0.163	–0.253/0.261	–0.567/0.627
CCDC	1490181	1490182	1490185

Table A7.4 Hydrogen bonds of *N*-(cyanomethyl)-*N*-methylnitramide (**1**).

D–H···A			sym. of A	H···A	D–H	D···A	angle, DHA
C2	H2	O2	−1+*x*, *y*, −1+*z*	2.537	0.951	3.206	127.52
C3	H5	O1	−1+*x*, *y*, *z*	2.543	0.947	3.329	140.54
C2	H1	O1	*x*, *y*, −1+*z*	2.399	0.959	3.310	158.78
C3	H3	O2	*x*, *y*, −1+*z*	2.776	0.968	3.426	125.21
C3	H5	O2	*x*, 0.5−*y*, 0.5+*z*	2.799	0.947	3.424	124.31

Table A7.5 Hydrogen bonds of *N*-methyl-*N*-nitroglycine (**3**).

D–H···A			sym. of A	H···A	D–H	D···A	angle, DHA
O1	H6	C3	−1+*x*, *y*, *z*	2.806	0.969	3.699	153.66
C2	H2	O4	−1+*x*, *y*, *z*	2.504	0.944	3.398	157.98
C2	H3	O3	1−*x*, −0.5+*y*, 1.5−*z*	2.448	0.979	3.375	157.87
C3	H4	O3	1−*x*, −0.5+*y*, 1.5−*z*	2.816	0.967	3.675	148.40
O1	H1	O1	1−*x*, 1−*y*, 2−*z*	2.986	0.885	3.669	135.33
O1	H1	O2	1−*x*, 1−*y*, 2−*z*	1.775	0.885	2.659	175.94
C3	H6	O4	*x*, 0.5−*y*, −0.5+*z*	2.699	0.969	3.473	137.25

Table A7.6 Hydrogen bonds of *N*-methyl-*N*-nitroglycinoyl hydrazide (**4**).

D–H···A			sym. of A	H···A	D–H	D···A	angle, DHA
C2	H4	O2	*x*, −1+*y*, *z*	2.607	0.951	3.557	176.64
C3	H6	O2	*x*, −1+*y*, *z*	2.905	1.019	3.848	154.28
C3	H6	O3	*x*, −1+*y* ,*z*	2.515	1.019	3.453	152.80
N2	H2	O1	1−*x*, −*y*, 1−*z*	2.404	0.920	3.203	145.09
N2	H3	O1	1−*x*, 1−*y*, 1−*z*	2.547	0.887	3.200	131.12
N2	H3	O2	1−*x*, 1−*y*, 1−*z*	2.698	0.887	3.322	128.38
C3	H7	O2	*x*, 0.5−*y*, −0.5+*z*	2.870	0.947	3.751	155.09
N1	H1	O1	*x*, 0.5−*y*, −0.5+*z*	2.117	0.817	2.925	169.71
C2	H5	O1	*x*, 0.5−*y*, −0.5+*z*	2.706	0.964	3.519	142.35

Table A7.7 Hydrogen bonds of *N*-methyl-*N*-nitroglycinoyl azide (**6**).

D–H···A			sym. of A	H···A	D–H	D···A	angle, DHA
C2	H1	O2	*x*, −1+*y*, *z*	2.704	0.961	3.471	137.28
C3	H3C	O2	*x*, 0.5+*y*, 0.5−*z*	2.626	0.980	3.326	128.55
C2	H2	O3	*x*, 0.5+*y*, 0.5−*z*	2.603	0.919	3.451	134.09
C3	H3C	O3	1−*x*, −*y*, −*z*	2.707	0.980	2.539	142.92
C3	H3A	O2	*x*, 0.5−*y*, −0.5+*z*	2.764	0.980	3.558	138.63

Table A7.8 Hydrogen bonds of *N*-methyl-*N*-nitroglycinoyl chloride (**8**).

D–H···A			sym. of A	H···A	D–H	D···A	angle, DHA
C2	H1	O1	*x*, −1+*y*, *z*	2.756	0.958	3.699	168.06
C2	H1	O2	*x*, −1+*y*, *z*	2.658	0.958	3.268	122.00
C3	H3	O3	*x*, −1+*y*, *z*	2.684	0.951	3.278	121.08
C3	H4	O1	−0.5-*x*, −0.5+*y*, 0.5−*z*	2.731	1.007	3.386	122.97
C2	H2	O3	0.5−*x*, −0.5+*y*,0.5−*z*	2.542	0.950	3.313	138.42
C3	H3	O2	0.5−*x*, −0.5+*y*, 0.5−*z*	2.808	0.951	3.398	121.05
C3	H5	O3	−*x*, 1−*y*, −*z*	2.568	0.915	3.441	159.83

Table A7.9 Hydrogen bonds of bis(*N*-methyl-*N*-nitroglycinoyl) hydrazide (**9**).

D–H···A			sym. of A	H···A	D–H	D···A	angle, DHA
C2	H2	O3	−1+*x*, *y*, *z*	2.421	0.947	3.198	139.13
C3	H6	O6	−*x*, 1−*y*, −*z*	2.821	0.956	3.624	141.70
C3	H5	O6	1−*x*, 1−*y*, −*z*	2.862	0.911	3.581	136.90
N4	H7	O1	−1+*x*, −1+*y*, *z*	2.013	0.889	2.838	153.80
C5	H8	O1	−1+*x*, −1+*y*, *z*	2.465	0.947	3.272	143.08
C3	H4	O5	−1+*x*, −1+*y*, *z*	2.815	0.982	3.747	158.71
C6	H10	O2	1−*x*, 1−*y*, 1−*z*	2.904	1.023	3.917	170.65
N1	H1	O4	1−*x*, 1−*y*, 1−*z*	1.977	0.871	2.777	152.15
C2	H3	O4	1−*x*, 1−*y*, 1−*z*	2.509	0.929	3.216	133.04
C6	H12	O1	1−*x*, 2−*y*, 1−*z*	2.395	0.958	3.334	166.51
C6	H11	O6	1−*x*, 2−*y*, −*z*	2.799	0.931	3.436	126.53
C5	H9	O4	1−*x*, 2−*y*, 1−*z*	2.597	0.968	3.385	138.67

Table A7.10 Hydrogen bonds of 2,2,2-trinitroethyl (*N*-methyl-*N*-nitroglycyl)carbamate (**12**).

D–H···A			sym. of A	H···A	D–H	D···A	angle, DHA
N3	H6	O3	−*x*, −*y*, −*z*	2.076	0.843	2.886	160.85
C1	H1	O10	−*x*, −*y*, −*z*	2.724	0.971	3.624	154.35
C5	H8	O1	−*x*, 1−*y*, −*z*	2.704	0.964	3.492	139.35
C2	H4	O2	−*x*, 1−*y*, −*z*	2.867	0.944	3.793	166.86
C1	H3	O7	−*x*, 1−*y*, −*z*	2.782	0.906	3.588	148.85
C1	H2	O9	−1+*x*, 0.5−*y*, −0.5+*z*	2.828	0.958	3.725	156.35
C1	H3	O10	−1+*x*, 0.5−*y*, −0.5+*z*	2.811	0.906	3.494	133.28
C2	H5	O1	*x*, 0.5−*y*, −0.5+*z*	2.497	0.954	3.245	135.24
C5	H7	O6	*x*, 0.5−*y*, −0.5+*z*	2.463	0.960	3.379	159.54

Table A7.11 Hydrogen bonds of 2-(methylnitramino)-*N*-nitroacetamide (**13**).

D–H···A			sym. of A	H···A	D–H	D···A	angle, DHA
C2	H2B	O3	*x*, *y*, −1+*z*	2.240	0.996	3.157	152.55
C3	H3A	O1	−*x*, 0.5−*y*, −0.5+*z*	2.802	0.960	3.753	125.32
C3	H3B	O4	−0.25+*x*, 0.25−*y*, −0.25+*z*	2.639	0.960	3.552	159.03
C2	H2A	O5	−0.25+*x*, 0.25−*y*, 0.75+*z*	2.295	0.969	3.036	132.55
N1	H1	O4	−0.25+*x*, 0.25−*y*, 0.75+*z*	2.394	0.811	3.168	159.74
N1	H1	O5	−0.25+*x*, 0.25−*y*, 0.75+*z*	2.555	0.811	3.194	136.68
C3	H3B	O1	−0.5+*x*, *y*, 0.5+*z*	2.806	0.960	3.451	125.32

Table A7.12 Further predicted detonation and combustion parameters using EXPLO5 V6.02.

	1	**3**	**4**	**5**	**6**	**9**	**10**	**11**	**12**	**13**	**AP**
density RT	1.46	1.58	1.53	1.72	1.57	1.55	1.48	1.44	1.71	1.67	1.48
formula	$C_3H_5N_3O_2$	$C_3H_6N_2O_4$	$C_3H_8N_4O_3$	$C_5H_9N_7O_9$	$C_3H_5N_5O_3$	$C_6H_{12}N_6O_6$	$C_5H_7N_5O_{10}$	$C_3H_7N_3O_3$	$C_6H_8N_6O_3$	$C_3H_6N_4O_5$	NH_4ClO_4
$\Delta H°_f$ [kJ mol^{-1}]	73.6	−449.3	−151.8	−137.6	109.4	−317.0	−401.4	−267.8.0	−590.0	−168.7	−295.8
$\Delta U°_f$ [kJ kg^{-1}]	747.4	−3240.1	−899.3	−342.6	788.9	−1087.3	−1259.0	−1890.7	−1643.5	−842.6	−2623.2
Q_v [kJ kg^{-1}]	−4911	−3461	−4111	−5494	−4952	−4257	−5075	−3569	−4616	−5040	−1422
T_{ex} [K]	3092	2455	2604	3660	3366	2794	3810	2423	3408	3358	1735
V_0 [L kg^{-1}]	846	824	912	780	817	841	808	884	738	815	885
P_{CJ} [kbar]	171	168	194	293	213	181	205	142	258	256	158
V_{Det} [m s^{-1}]	7151	6961	7669	8304	7670	7276	7286	6729	7835	8033	6368
I_s [s]	215	185	202	254	221	200	253	190	237	237	157
I_s [s] (5% Al)	230	196	214	262	238	212	259	200	246	249	198
I_s [s] (10% Al)	244	208	230	268	249	229	263	214	253	258	224
I_s [s] (15% Al)	245	225	245	272	248	243	271	233	257	265	235
I_s [s] (20% Al)	242	239	247	269	246	243	266	241	251	262	244
I_s [s] (25% Al)	239	237	243	252	244	239	261	237	244	255	247
I_s [s] (5% Al, 14% binder)	215	187	201	229	220	199	229	189	212	218	250
I_s [s] (10% Al, 14% binder)	231	202	218	244	235	216	240	205	229	234	257
I_s [s] (15% Al, 14% binder)	237	216	234	252	239	232	249	222	242	247	261

8 REFERENCES

[1] A. Bondi, *J. Phys. Chem.* **1964**, *68*, 441–451.

9 BIBLIOGRAPHY

Publications

T. M. Klapötke, B. Krumm, R. Scharf
"From Amino Acids to High-Energy Dense Oxidizers: Polynitro Materials Derived from β-Alanine and L-Aspartic Acid"
Z. Anorg. Allg. Chemie **2016**, *ahead of print* DOI: 10.1002/zaac.201600223.

T. M. Klapötke, B. Krumm, S. F. Rest, R. Scharf, J. Schwabedissen, H.-G. Stammler, N. W. Mitzel
"Carbonyl Diisocyanate $CO(NCO)_2$: Synthesis and Structures in Solid State and Gas Pase"
J.Phys. Chem. A **2016**, *120*, 4534–4541.

T. M. Klapötke, B. Krumm, R. Scharf
"Oxalyl Chloride and Hydrazide Based Energetic Polynitro Derivatives"
Eur. J. Inorg. Chem. **2016**, 3086–3093.

Q. Axthammer, T. M. Klapötke, B. Krumm, R. Scharf
"A Study of the 3,3,3-Trinitropropyl Unit as a Potential Energetic Building Block"
Chem. – Euro. J. **2015**, *21*, 16229–16239.

T. M. Klapötke, M. Q. Kurz, R. Scharf, P. C. Schmid, J. Stierstorfer, M. Sućeska
"5-(1*H*-Tetrazolyl)-2-Hydroxy-Tetrazole: A Selective 2*N*-Monooxidation of Bis(1*H*-Tetrazole)"
ChemPlusChem **2015**, *80*, 97–106.

T. M. Klapötke, B. Krumm, S. F. Rest, M. Reynders, R. Scharf
"(2-Fluoro-2,2-dinitroethyl)-2,2,2-trinitroethylnitramine: A Possible High-Energy Dense Oxidizer"
Eur. J. Inorg. Chem. **2013**, 5871–5878.

D. Izsak, T. M. Klapötke, R. Scharf, J. Stierstorfer
"Energetic Materials Based on the 5-Azido-3-nitro-1,2,4-triazolate Anion"
Z. Anorg. Allg. Chemie **2013**, *639*, 1746–1755.

Poster Presentations

T. M. Klapötke, R. Scharf, J. Stierstorfer

"Aquatic Toxicity Determination of Energetic Materials Using the Luminescent Bacteria Inhibition Test"

17th New Trends in Research of Energetic Materials, Proceedings of the Seminar, Pardubice, Czech Republic **2014**, *2*, 769–773.